

Characterising adaptational dysfunction in age-related macular degeneration

A thesis submitted to Cardiff University for the degree of
Doctor of Philosophy

By

Allannah Jayne Gaffney

School of Optometry and Vision Sciences
Cardiff University

August 2012

Supervised by Dr Alison Binns and Dr Tom Margrain

Summary

Age-related macular degeneration (AMD) is the leading cause of visual impairment in the developed world (Resnikoff et al., 2004). The prevalence of this disease will continue to increase over the coming decades as the average age of the global population rises (United Nations, 2009). There is consequently an urgent need to develop tests that are sensitive to early visual dysfunction, in order to identify individuals that have a high risk of developing AMD, to identify patients that would benefit from treatment, to assess the outcomes of that treatment and to evaluate emerging treatment strategies.

An emerging body of evidence suggests that dark adaptation is a sensitive biomarker for early AMD. Cone dark adaptation is of particular interest to clinicians, as it can identify patients with early AMD in a relatively short recording period. Consequently, this thesis aimed to optimise psychophysical and electrophysiological techniques for the assessment of cone dark adaptation in early AMD, in order to maximise its diagnostic potential.

A range of psychophysical methods were shown to be capable of monitoring the rapid changes in threshold that occur during cone dark adaptation. An optimal psychophysical protocol for the assessment of cone dark adaptation in early AMD was developed based on the results of a systematic evaluation of the effect of stimulus parameters and pre-adapting light intensity on the diagnostic potential of cone dark adaptation in early AMD. When compared to the focal cone ERG photostress test, both techniques were shown to be similarly diagnostic for early AMD. In addition, the time constant of cone recovery was shown to be significantly correlated with age, hence the sensitivity and specificity of cone dark adaptation as a biomarker for early macular disease may be further improved by considering these age-related changes.

In conclusion, this thesis has confirmed that cone dark adaptation is a sensitive functional biomarker for early AMD. However, as cross-sectional studies are unable to determine the true diagnostic potential of a biomarker, longitudinal investigations are needed to explore the long-term potential of cone dark adaptation and other visual functions as biomarkers for early AMD.

Acknowledgements

Having spent a considerable amount of time quite literally ‘in the dark’ during the course of this thesis, I must express my gratitude to those individuals who have helped me along the way.

Firstly, my sincere thanks to my two inspirational supervisors, Dr Alison Binns and Dr Tom Margrain, for all of their advice and encouragement throughout the last few years. I feel extremely lucky to have worked as part of their team and I hope I can continue to do so for some time to come!

Many thanks to all the dedicated participants that spent hours in darkness in order to generate the data presented in this thesis. In hindsight I can’t quite believe all that I put them through, yet without exception, they greeted everything thrown at them with excellent humour and certainly made my job much more enjoyable!

Thank you to the residents of room 2.10, past and present, for their friendship and support - I’m quite sure that the distractions that come with working in a communal office play an integral role in completing a thesis! Thank you also to Sue, Leanne and the many other supportive staff at Maindy Road for making the Optometry department such a pleasant working environment.

A big thank you to the Gaffney family for the constant encouragement they have given me over the years and for conscientiously listening to intricate explanations of the many ‘interesting’ projects that I have pursued!

Last, but by no means least, thank you to Amar for making me smile each day – exactly as I asked.

Contents

Summary	i
Acknowledgements	ii
Contents	iii
List of Figures	x
List of Tables	xiv
List of abbreviations	xvi

Chapter 1. Introduction	1
1.1. The healthy retina	1
1.1.1. Healthy macular anatomy	3
1.1.2. Bruch's membrane	3
1.1.3. The retinal pigment epithelium (RPE)	4
1.1.4. Photoreceptor cells	5
1.1.5. Bipolar cells	7
1.1.6. Horizontal cells	8
1.1.7. Müller cells	8
1.1.8. Amacrine cells	9
1.1.9. Retinal ganglion cells (RGCs)	9
1.1.10. The visual pathway	10
1.2. Age-related macular degeneration (AMD)	11
1.2.1. Incidence and prevalence of AMD	11
1.2.2. Clinical features of AMD	12
1.2.2.1. Drusen	12
1.2.2.2. Pigmentary abnormalities	13
1.2.2.3. Geographic atrophy (GA)	13
1.2.2.4. Neovascular AMD (nAMD)	14
1.2.2.5. Pigment epithelial detachment (PED)	14
1.2.3. Clinical classification of AMD	14
1.2.4. Risk factors for AMD	16

1.2.4.1. Smoking	16
1.2.4.2. Genetics	17
1.2.4.3. Race	17
1.2.4.4. General health	17
1.2.4.5. Diet	18
1.2.4.6. Sunlight	19
1.2.5. Pathogenesis of AMD	19
1.2.5.1. Oxidative stress	19
1.2.5.2. Lipofuscin formation	20
1.2.5.3. Chronic inflammation and the immune response	21
1.2.5.4. Hypoxia and choroidal vascular changes	22
1.2.6. Clinical investigation of AMD	23
1.2.6.1. Fundus photography	23
1.2.6.2. Fundus angiography (FA)	24
1.2.6.3. Fundus autofluorescence (FAF)	24
1.2.6.4. Optical coherence tomography (OCT)	24
1.2.6.5. Visual acuity	25
1.2.6.6. Visual field testing	26
1.2.6.7. Contrast sensitivity	27
1.2.6.8. Temporal sensitivity	27
1.2.6.9. Colour vision	27
1.2.6.10. Dark adaptation	28
1.2.7. Prevention and treatment	28
1.2.7.1. Focal laser photocoagulation	28
1.2.7.2. Verteporfin photodynamic therapy (PDT)	29
1.2.7.3. Anti-VEGF drugs	29
1.2.7.4. Management of dry AMD	31
1.2.7.5. Novel therapies	31
1.3. Visual adaptation	32
1.3.1. Dark adaptation	32
1.3.2. Physiology of dark adaptation: the retinoid cycle	34
1.3.3. The Müller cell hypothesis: An alternative pathway for photopigment regeneration	36
1.3.4. The retinoid cycle and visual threshold during dark adaptation	37

1.3.4.1. The photochemical hypothesis	37
1.3.4.2. The equivalent background hypothesis	38
1.3.5. Adaptational dysfunction	40
1.3.5.1. Dark adaptation and age	40
1.3.5.2. Dark adaptation and retinal disease	41
1.3.5.3. Dark adaptation in AMD	42
1.3.5.4. Photostress recovery in AMD	44
1.4. Visual psychophysics	44
1.4.1. Classical psychophysical methods	45
1.4.1.1. The method of constant stimuli	46
1.4.1.2. The method of limits	46
1.4.1.3. The method of adjustment	46
1.4.1.4. Disadvantages of classical psychophysical methods	47
1.4.2. Adaptive psychophysical methods	47
1.4.2.1. The staircase procedure	48
1.4.2.2. Parameter estimation by sequential testing (PEST)	48
1.4.2.3. Maximum-likelihood procedures	48
1.4.3. Forced-choice psychophysical methods	49
1.4.3.1. Forced-choice methods	50
1.4.3.2. Yes-no methods	50
1.4.4. Psychophysical assessment of dark adaptation	51
1.5. The electroretinogram (ERG)	52
1.5.1. The transient (flash) ERG	52
1.5.1.1. Early receptor potential (ERP)	53
1.5.1.2. a-wave	53
1.5.1.3. b-wave and oscillatory potentials	54
1.5.1.4. Photopic negative response (PhNR)	55
1.5.1.5. Scotopic threshold response (STR)	55
1.5.1.6. c-wave	55
1.5.1.7. d-wave	56
1.5.2. The steady state (flicker) ERG	56
1.5.3. The focal ERG	57
1.5.4. The multifocal ERG (mfERG)	57
1.5.5. The pattern ERG (PERG)	58

1.5.6. Recording the ERG	59
1.5.6.1. Electrodes	59
1.5.6.2. Electrical noise and noise reduction	60
1.5.6. The ERG in AMD	62
1.5.7. Assessment of dark adaptation using the ERG and related techniques	64
1.6. Overview and aims	65

Chapter 2. A comparison of psychophysical methods of monitoring cone dark adaptation

2.1. The repeatability of the Goldmann-Weekers adaptometer for monitoring cone dark adaptation	70
2.1.1. Introduction	70
2.1.2. Aims	71
2.1.3. Methods	71
2.1.4. Results	74
2.1.5. Discussion	77
2.2. A comparison of four psychophysical methods for monitoring cone dark adaptation	78
2.2.1. Introduction	78
2.2.2. Aims	80
2.2.3. Methods	80
2.2.4. Results	84
2.2.5. Discussion	88

Chapter 3. The effect of age on cone dark adaptation in healthy eyes

3.1. Introduction	92
3.2. Aims	94
3.3. Methods	94
3.4. Results	95
3.5. Discussion	99

**Chapter 4. The effect of retinal eccentricity on dark adaptation in 103
healthy eyes and eyes with early AMD**

4.1. A comparison of models of cone and rod dark adaptation in healthy eyes	103
4.1.1. Introduction	103
4.1.2. Aims	106
4.1.3. Methods	106
4.1.4. Results	109
4.1.5. Discussion	113
4.2. The topography of cone and rod dark adaptation in healthy eyes	115
4.2.1. Introduction	115
4.2.2. Aims	116
4.2.3. Methods	116
4.2.4. Results	117
4.2.5. Discussion	120
4.3. The topography of cone dark adaptation deficits in early AMD	122
4.3.1. Introduction	122
4.3.2. Aims	123
4.3.3. Methods	124
4.3.4. Results	127
4.3.5. Discussion	133

**Chapter 5. The effect of bleaching intensity on dark adaptation in 138
early AMD**

5.1. Introduction	138
5.2. Aims	139
5.3. Methods	139
5.4. Results	142
5.5. Discussion	147

Chapter 6. The development of the focal rod ERG photostress 150 test (PST)

6.1. The development and validation of the full field rod ERG PST	150
6.1.1. Introduction	150
6.1.2. Aims	151
6.1.3. General ERG methods	151
6.1.4. Methods	153
6.1.5. Results	154
6.1.6. Discussion	155
6.2. The development of the focal rod ERG PST	156
6.2.1. Introduction	156
6.2.2. Aims	158
6.2.3. Determination of the optimal stimulus frequency	158
6.2.3.1. Background/aims	158
6.2.3.2. Methods	159
6.2.3.3. Results	159
6.2.3.4. Discussion	161
6.2.4. Determination of the optimal stimulus intensity	162
6.2.4.1. Background/aims	162
6.2.4.2. Methods	162
6.2.4.3. Results	163
6.2.4.4. Discussion	164
6.2.5. Development and validation of a recording protocol for the focal rod ERG PST	165
6.2.5.1. Background/aims	165
6.2.5.2. Methods	165
6.2.5.3. Results	167
6.2.5.4. Discussion	170

Chapter 7. A comparison of psychophysical and electrophysiological techniques for monitoring dark adaptation in early AMD 172

7.1. Introduction 172
7.2. Aims 173
7.3. Methods 173
7.4. Results 176
7.5. Discussion 181

Chapter 8. General discussion, conclusions and future directions 184

8.1. Discussion 184
8.2. Future directions 188
 8.2.1. Risk profiling for the development of wet AMD 189
 8.2.2. Investigation of risk factors for the development of early AMD ... 190
 8.2.3. Development of a portable dark adaptometer 191

References 193

Appendix I. Calibration of the Goldmann-Weekers adaptometer 243

Appendix II. Matlab code for dark adaptation programs 245

Appendix III. Peer reviewed papers and supporting publications 267

List of Figures

	Page
1.1. A cross-section of the human eye	2
1.2. A schematic diagram of a vertical section through the human retina	2
1.3. Diagrammatic representation of the anatomical regions of the human macula	3
1.4. The structure of human photoreceptor cells	6
1.5. Bipolar cell types in the human retina	7
1.6. Horizontal cell types in the human retina	8
1.7. P- and M- ganglion cell types in the human retina	10
1.8. Fundusoscopic appearance of hard and soft drusen	12
1.9. The proposed role of inflammation and the immune response in the pathogenesis of AMD	22
1.10. OCT images of soft drusen, geographic atrophy and CNV	25
1.11. Mean change in best-corrected visual acuity by month, with administration of monthly Ranibizumab injections	30
1.12. Dark adaptation functions recorded after exposure to adapting lights of increasing intensity	33
1.13. Dark adaptation functions recorded using a 2° stimulus placed at different retinal eccentricities and a centrally fixated stimulus of increasing size	34
1.14. The retinoid cycle of vision	35
1.15. Dark adaptation functions and increment threshold functions recorded in response to a range of stimuli	39
1.16. Rod dark adaptation recorded from one elderly adult in good retinal health and three patients with different stages of AMD	42
1.17. A typical psychometric function	45
1.18. Theoretical probability distribution functions of signal and noise (SN) and background noise alone (N)	50
1.19. The three ‘fundamental’ processes of the ERG	52
1.20. The a- and b-waves of the dark adapted ERG	54
1.21. The d-wave of the photopic ERG	56
1.22. A steady state ERG recorded in response to a 41Hz flickering stimuli	57

1.23.	The multifocal ERG	58
1.24.	The pattern ERG waveform	59
1.25.	Standard full field ERG responses as defined by ISCEV	60
1.26.	The recovery of the a-wave amplitude of the full field scotopic ERG plotted as a function of time after a near-total bleach of photopigment	64
2.1.	Schematic diagram of the Maxwellian view optical system	71
2.2.	The Goldmann-Weekers adaptometer	72
2.3.	The logarithmic paper used by the Goldmann-Weekers adaptometer	73
2.4.	Example cone dark adaptation data recorded using the Goldmann-Weekers adaptometer	74
2.5.	Bland-Altman plots for cone τ , initial threshold and final threshold recorded using the Goldmann-Weekers adaptometer on two occasions	76
2.6.	CRT display used by the computer based dark adaptation procedures	82
2.7.	Example cone dark adaptation data recorded using four psychophysical methods	85
2.8.	Bland-Altman plots for cone τ measured using four psychophysical methods on two occasions	86
2.9.	Bland-Altman plots for initial cone threshold measured using four psychophysical methods on two occasions	87
2.10.	Bland-Altman plots for final cone threshold measured using four psychophysical methods on two occasions	89
3.1.	Example cone dark adaptation data for participants aged 23, 45, 65, and 83 years	97
3.2.	Cone dark adaptation data plotted as a function of age	98
4.1.	Dark adaptation data obtained from an albino rat	104
4.2.	Diagrammatic representation of spot stimulus and four annular stimuli superimposed on the macular of a healthy participant	108
4.3.	Example cone dark adaptation data recorded at five retinal locations	110
4.4.	Example dark adaptation data recorded at four retinal locations	111
4.5.	Example dark adaptation curves recorded from three participants at five retinal locations	117
4.6.	Mean cone τ at five retinal locations for AB, AG and TM	118
4.7.	Mean cone final threshold at five retinal locations for AB, AG and TM	118

4.8.	Mean rate of 2 nd component of rod recovery at four retinal locations for AB, AG and TM	119
4.9.	Mean 25 minute rod thresholds at four retinal locations for AB, AG and TM	119
4.10.	Mean time to RCB at four retinal locations for AB, AG and TM	119
4.11.	Human photoreceptor density in the temporal retina	121
4.12.	Predicted threshold recovery of 1, 5 and 10 rods, described by the rate-limited model	122
4.13.	Diagrammatic representaion of spot stimulus and three annular stimuli superimposed on the macular of a healthy participant	126
4.14.	Dark adaptation data recorded in response to four stimulus sizes for a typical control participant and a participant with early AMD	130
4.15.	Mean dark adaptation parameters at four retinal locations for early AMD and control groups	131
4.16.	ROC curves for cone τ at 2°, 7° and 12°, and time to RCB at 12°	132
5.1.	Viewing aperture of Maxwellian view optical system during photopigment bleaching	141
5.2.	Dark adaptation data recorded after three pre-adapting light intensities for a typical control participant and a participant with early AMD	143
5.3.	Mean dark adaptation parameters after three pre-adapting light intensities for early AMD and control groups	145
5.4.	ROC curves for cone τ and time to RCB at three pre-adapting light intensities	146
6.1.	Medelec Synergy evoked potential monitoring system and miniature Ganzfeld LED stimulator	152
6.2.	Miniature Ganzfeld LED stimulator positioned within a desensitizing surround for recording focal cone and rod ERGs	152
6.3.	Raw full field rod ERG waveform and the fourier analysed waveform	154
6.4.	Recovery of the b-wave of the full field rod mediated ERG for two healthy participants	155
6.5.	Dark adapted full field ERG responses for two healthy participants in response to a blue flash of increasing frequency	160
6.6.	The amplitude of the full field, dark adapted ERG b-wave plotted as a function of stimulus frequency for two healthy participants	160

6.7.	Dark adapted focal ERG responses for two healthy participants in response to a blue flash presented at 0.5 and 2Hz	161
6.8.	Cone contribution to dark adapted full field ERG responses recorded from two healthy participants in response to a blue flash of increasing intensity	163
6.9.	Cone contribution to dark adapted focal ERG responses recorded from two healthy participants in response to a blue flash of increasing intensity	164
6.10.	The amplitude of the b-wave of the focal rod ERG plotted as a function of time, in the absence of a photopigment bleach for two healthy participants	167
6.11.	Recovery of the b-wave of the focal rod mediated ERG for two healthy participants	168
6.12.	The amplitude of the b-wave of the focal rod ERG plotted as a function of time for six ERG naïve participants	169
7.1.	Raw full field cone ERG waveform and the fourier analysed waveform	175
7.2.	Dark adaptation data recorded from a typical control participant and a participant with early AMD using the optimal psychophysical protocol and the focal cone ERG PST	179
7.3.	ROC curves for cone τ recorded using the focal cone ERG PST and the psychophysical protocol, and psychophysical time to RCB	180

List of Tables

	Page
1.1. AREDS Grading System for AMD	15
1.2. International Classification and Grading System for AMD	16
2.1. Cone τ , initial cone threshold and final cone threshold for all participants	75
2.2. Mean (+/- standard deviation) of dark adaptation parameters assessed by the Goldmann-Weekers adaptometer at visit one and two	77
2.3. Decision criteria used by the hybrid adaptive procedure to determine stimulus luminance	83
2.4. Mean (+/- standard deviation) of dark adaptation parameters at visit one and two for the four psychophysical methods of dark adaptation measurement	86
3.1. Cone τ , initial cone threshold and final cone threshold for all participants	96
3.2. Summary of studies that have examined the relationship between cone dark adaptation and age in healthy participants	100
4.1. Mean RMS error (+/- standard deviation) of the exponential and rate-limited models of cone dark adaptation at five retinal locations	112
4.2. Mean AIC value (+/- standard deviation) of the exponential and rate-limited models of cone dark adaptation at five retinal locations	112
4.3. Mean RMS error (+/- standard deviation) of the exponential-linear and double exponential models of dark adaptation at four retinal locations	113
4.4. Mean AIC value (+/- standard deviation) of the exponential-linear and double exponential models of dark adaptation at four retinal locations	113
4.5. Mean (+/- standard deviation) dark adaptation parameters at five retinal locations in all participants	120
4.6. Visual acuity and fundus appearance in the early AMD group	128
4.7. Cone τ , final cone threshold and time to RCB given by the best fitting exponential-linear model for all participants	129
4.8. Comparison of mean (+/- standard deviation) dark adaptation parameters in the control and early AMD groups	131
4.9. Comparison of mean (+/- standard deviation) dark adaptation parameters obtained during the first and second test within a single recording session	133

5.1.	Percentages of cone photopigment and rhodopsin bleached at the three adapting intensities	140
5.2.	Visual acuity and fundus appearance in the early AMD group	142
5.3.	Cone τ , final cone threshold and time to RCB given by the best fitting exponential-linear model for all participants	144
5.4.	Comparison of mean (+/- standard deviation) dark adaptation parameters in the control and early AMD groups	145
5.5.	Sensitivity and specificity of the dark adaptation parameters that differed significantly on univariate analysis, calculated according to the optimal cut-off value given by the ROC curve	147
6.1.	Characteristics of the ERG naïve participants	168
7.1.	Visual acuity and fundus appearance in the early AMD group	177
7.2.	Dark adaptation data measured using the focal cone ERG PST and a psychophysical method for all participants	178
7.3.	Comparison of mean (+/- standard deviation) dark adaptation parameters in the control and early AMD groups assessed using the optimal psychophysical protocol and the focal cone ERG PST	180

Abbreviations

AIC	Akaike Criterion
AMD	Age-related macular degeneration
ANOVA	Analysis of variance
AREDS	Age-related eye disease study
ARMS2 gene	Age-related maculopathy susceptibility gene
AUC	Area under the curve
BMI	Body mass index
CFH gene	Complement factor H gene
CoR	Co-efficient of repeatability
CRALBP	Cellular retinaldehyde binding protein
CRBP	Cellular retinol binding protein
CRP	C-reactive protein
CRT	Cathode ray tube
DHA	Docosahexaenoic acid
DTL	Dawson-Trick-Litzkov
EMS	Eger macular stressometer
ERG	Electroretinogram
ERP	Early receptor potential
FAF	Fundus autofluorescence
FFA	Fundus fluorescein angiography
GA	Geographic atrophy
HIF	Hypoxia inducible factor
IPBP	Inter-photoreceptor binding protein
IPM	Inter-photoreceptor matrix
ISCEV	International Society for Clinical Electrophysiology of Vision
LED	Light emitting diode
LGN	Lateral geniculate nucleus
logMAR	Logarithm of the minimum angle of resolution
LRAT	Lecithin retinol acyl transferase
mfERG	Multifocal electroretinogram

N	Noise distribution
nAMD	Neovascular AMD
ND	Neutral density
NICE	National Institute for Clinical Excellence
NSAID	Non-steroidal anti-inflammatory drug
OCT	Optical coherence tomography
OP	Oscillatory potential
Ops-trans ROL	Opsin-all-trans retinol
PDT	Photodynamic therapy
PED	Pigment epithelial detachment
PEDF	Pigment epithelial derived factor
PERG	Pattern electroretinogram
PEST	Parameter estimation by sequential testing
PhNR	Photopic negative response
PSR	Photostress recovery
PSRT	Photostress recovery time
QUEST	Quick estimate by sequential testing
RCB	Rod-cone-break
RDH	All-trans retinol dehydrogenase
RGC	Retinal ganglion cell
RMS error	Root mean square error
RNFL	Retinal nerve fibre layer
ROC	Receiver operating characteristic (curve)
ROI	Reactive oxygen intermediate
RPE	Retinal pigment epithelium
SITA	Swedish interactive threshold algorithm
SN	Signal & noise distribution
SNR	Signal-noise-ratio
STR	Scotopic threshold response
TSD	Theory of signal detection
VA	Visual acuity
VEGF	Vascular endothelial growth factor
VEP	Visual evoked potential
ZEST	Zippy estimate of sequential testing

11-cis retinal	11-cis retinaldehyde
τ	Time constant of recovery/tau
γ	Gamma

1. Introduction

Age-related macular degeneration (AMD) is a degenerative disease of the central retina that typically presents after 55 years of age. Although treatments for this prevalent disease are limited at present, they are advancing rapidly, which means that there is currently an urgent need to develop tests that are sensitive to subtle functional abnormalities in AMD, in order to facilitate early diagnosis and effective monitoring of treatment outcomes.

The overall objective of this PhD is to investigate the potential of dark adaptation assessment as a test for early AMD. This introductory chapter begins by providing an overview of the structure of the healthy retina, before describing the aetiology, classification, investigation and treatment of AMD. This is followed by a comprehensive review of an emerging body of evidence which suggests that dark adaptation is a sensitive functional biomarker for early AMD. The latter part of the chapter provides an overview of psychophysical and electrophysiological investigative techniques for the assessment of dark adaptation, with a particular emphasis on their use in AMD. Finally, the specific aims of the PhD are outlined.

1.1. The healthy retina

The retina is the first stage of visual processing. It is located between the choroid and the vitreous humour and extends from the optic nerve head to the ora serrata, just posterior to the ciliary body (Figure 1.1.). Light energy focused on the retina is converted to nervous impulses via phototransduction. These impulses are transferred through the retinal layers and ultimately exit the eye at the optic nerve head. The human retina comprises a series of well-defined layers (Figure 1.2.), including an outer pigmented layer, three layers of neuronal cell bodies and two plexiform layers that contain synaptic connections.

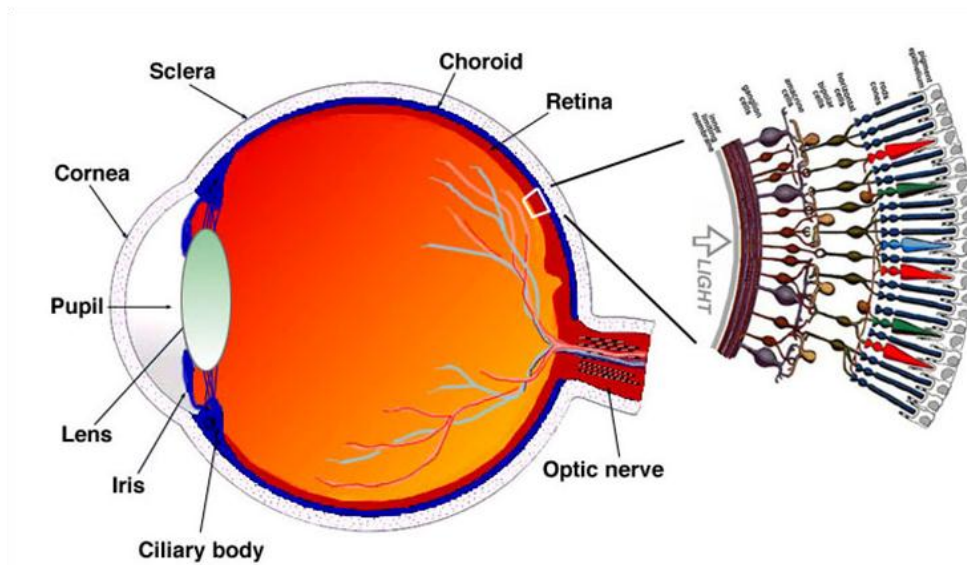


Figure 1.1. A cross-section of the human eye, including a schematic enlargement of the retina (Kolb, 2003a).

The blood supply to the retina consists of two separate circulatory systems that originate from the ophthalmic artery. The inner retinal layers are supplied by the central retinal artery. It enters the eye through the optic nerve head where it bifurcates into inferior and superior branches, before further dividing into additional nasal and temporal branches. In contrast, the outer retinal layers, including the photoreceptor layer, receive their blood supply from the choriocapillaris, the densely branching capillary network of the choroidal circulation. The choriocapillaris is the only blood supply to the avascular region of the macula (Hendrickson, 2005).

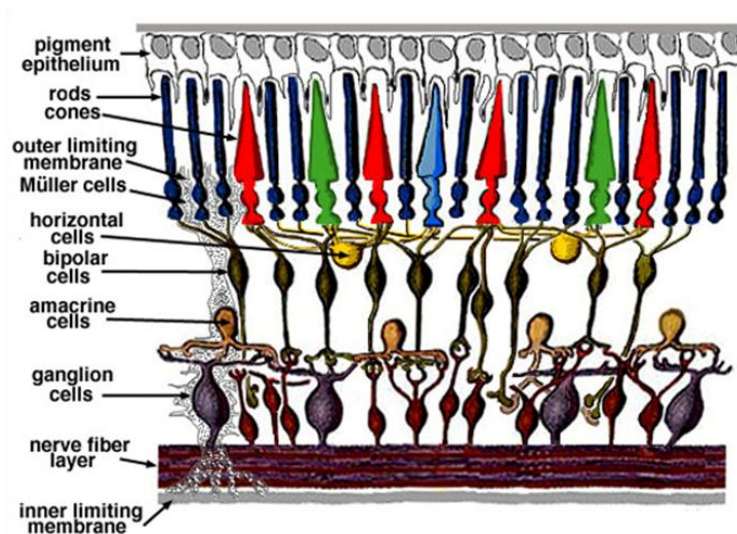


Figure 1.2. A schematic diagram of a vertical section through the human retina, including the major retinal cell types (Kolb, 2003a).

1.1.1. Healthy macular anatomy

Unique to primates, the macula is a highly specialised retinal region that is responsible for high resolution visual acuity (VA). Anatomically, it is defined as the area of the posterior retina that contains xanthophyll, a carotenoid, and more than one layer of retinal ganglion cells. Located within the vascular arcades, the macula is 5-6mm in diameter, or 15-20° of visual angle (Figure 1.3) (Hendrickson, 2005). It is centred on the fovea; a 1.5mm diameter area, located 4mm temporally and 0.8mm inferiorly to the optic nerve head. The 0.35mm foveola, visible ophthalmoscopically as the foveal light reflex, is a thin central depression in the fovea and is composed entirely of cones. The neural components of the inner retina are displaced away from this area, allowing the photoreceptors unobstructed access to the incident light. These anatomical features facilitate high resolution visual acuity.

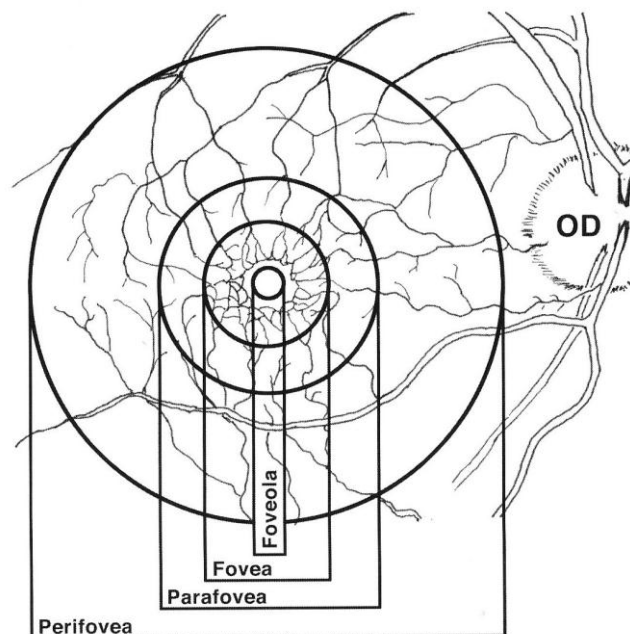


Figure 1.3. Diagrammatic representation of the anatomical regions of the human macula (Hendrickson, 2005).

1.1.2. Bruch's membrane

Bruch's membrane is a thin, semi-permeable structure composed of collagen and elastic fibres, located between the retinal pigment epithelium (RPE) and the choriocapillaris. Although it is not actually considered part of the retina, Bruch's membrane is closely associated with the basement membrane of the RPE. It may be divided into 5 layers: the basement membrane of the RPE, the inner collagenous layer, the elastin layer, the outer

collagenous layer and the basement membrane of the choriocapillaris (Guymer et al., 1999; Booij et al., 2010). Bruch's membrane is considered to have three primary functions (Guymer et al., 1999; Booij et al., 2010):

- regulation of the diffusion of biomolecules between the retina and the choroidal circulation
- provision of physical support for the RPE
- and restriction of cell migration.

Bruch's membrane is approximately 2µm thick in young human eyes, but thickens with age to approximately 4.7µm in the 10th decade of life (Ramrattan et al., 1994). This is accompanied by changes in the elastic and collagenous fibres and an accumulation of waste material within the membrane (Feeneyburns and Ellersieck, 1985; Bird, 1992). These changes cause a reduction in the elasticity of the membrane, increased hydrophobicity and an increased resistance to diffusion, thus generating a barrier to normal metabolic exchange (Bird, 1992).

1.1.3. The retinal pigment epithelium (RPE)

The retinal pigment epithelium is located between the photoreceptor outer segments and the choroidal blood supply. It consists of a single layer of hexagonal cells, connected by tight junctions (zonulae occludens), which contain pigment granules and organelles for the digestion of photoreceptor outer segments. The highly specialised apical surface of the RPE comprises multiple long microvilli that project into the inter-photoreceptor matrix (IPM) and surround the tips of the photoreceptor outer segments. Several comprehensive reviews of the RPE have identified its key functions (Bok, 1993; Boulton & Dayhaw-Barker, 2001; Strauss, 2005). These include:

- stray light absorption
- epithelial transport (of ions, water and metabolic end products from the subretinal space to the bloodstream, and of nutrients from the bloodstream to the photoreceptors)
- spatial ion buffering
- recycling of retinoid during the visual cycle
- phagocytosis of photoreceptor outer segments
- secretion of growth factors

- and immune modulation.

Clearly, the failure of one or more of these functions may cause retinal degeneration and subsequent loss of visual function (Stauss, 2005).

1.1.4. Photoreceptor cells

The human retina contains two photoreceptor subsystems that operate optimally under different viewing conditions (Young, 1970). The cones of the photopic system are dominant at high retinal illuminance levels and are responsible for high acuity vision and colour perception. In contrast, the rod based scotopic system is monochromatic. It functions best at low illuminances as it is extremely sensitive to light, but is insensitive to spatial detail. A degree of overlap between the systems occurs across intermediary mesopic retinal illuminances.

The density of the photoreceptors varies with retinal location. Cone density is maximal at the fovea (200,000 cells/mm²) (Curcio et al., 1990) and then decreases rapidly with increasing eccentricity (Figure 4.11, Page 119). In contrast, rod photoreceptors first appear in the parafovea and increase to a maximum density of 150,000 cells/mm² at 12-18° from fixation (Curcio et al., 1990).

The rods and cones comprise several specialized compartments (Figure 1.4). The outer segment, adjacent to the RPE, is devoted to light absorption, while the inner segment houses the organelles of the cell (Young, 1970). A nerve fibre, containing the cell nucleus, extends from the inner segment and culminates in a synaptic terminal to which other cells connect. The photoreceptor outer segment consists of a series of membranous discs containing visual pigment molecules (Young, 1970). The outer segments of the rods and cones are distinctly different in shape (Figure 1.4). The discs in the rod outer segment maintain a consistent diameter throughout the structure. In contrast, in cones there is a progressive reduction in the diameter of the discs contained within the outer segment with increasing distance from the inner segment. This results in their characteristic conical shape. Protein synthesized in the inner segment of the cell migrates to the outer segment to renew the discs. In cone photoreceptors this protein is distributed diffusely throughout the outer segment to replenish the existing discs, whereas in the rods new discs are formed at

the base of the outer segment and the oldest discs are shed from the tip and phagocytosed by the RPE (Young, 1969).

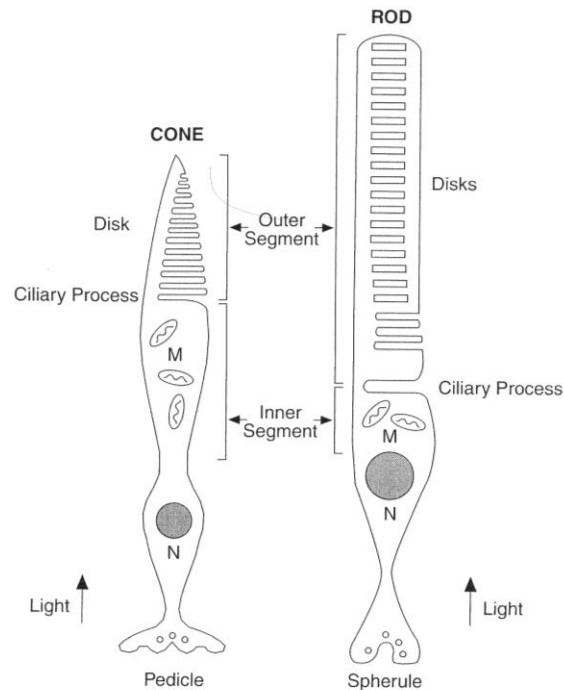


Figure 1.4. The structure of human photoreceptor cells (Schwartz, 2004).

Visual pigment

Human visual pigment comprises 11-cis retinaldehyde (11-cis retinal) and opsin. 11-cis retinal is a light sensitive chromophore molecule derived from vitamin A and opsin is an intracellular membrane protein. The visual pigment present in the rod outer segment is known as rhodopsin and has a peak spectral sensitivity of 507nm. Cone visual pigment is known as iodopsin and there are three types: cyanolabe, chloralabe and erythrolabe, sensitive to short (426nm), medium (530nm) and long (557nm) wavelengths respectively (Gouras, 1984).

The absorption of light quanta by the visual pigment initiates the process that leads to the generation of visual signal. On absorption of a photon the visual pigment molecule becomes transparent, or 'bleached', and is unable to capture further quanta. However, given that there are approximately 120 million rods in the human retina, each of which contain approximately 10^8 rhodopsin molecules, the probability of absorption of quanta is high (Lamb & Pugh, 2004).

1.1.5. Bipolar cells

The bipolar cell bodies are located in the inner nuclear layer of the retina. They convey signals from the photoreceptors in the outer plexiform layer to the amacrine and ganglion cells in the inner plexiform layer. In the human retina, eleven different types of bipolar cell have been identified using Golgi staining (Figure 1.5) (Mariani, 1984; Boycott and Wassle, 1991; Kolb et al., 1992; Kolb, 2001). Only one type of bipolar cell is known to synapse with rod photoreceptors, whilst the remaining ten synapse with cone photoreceptors. Bipolar cells may be differentiated by the shape of their dendrites (Kolb et al., 1992). Cone bipolars have clusters of dendritic terminals in the plane of the cone pedicles, whereas rod bipolars have spiky dendrites that generally extend further, to reach the rod spherules.

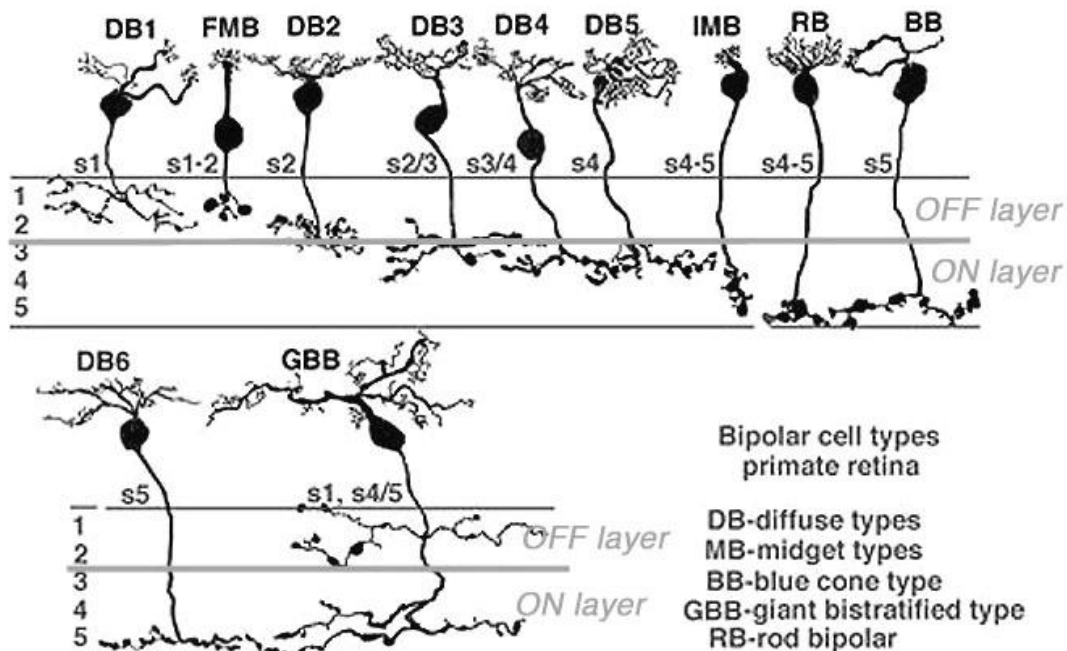


Figure 1.5. Bipolar cell types in the human retina, identified by Golgi staining (Kolb, 2001).

Ten different types of cone bipolar have been identified in the human retina (Figure 1.5). These may be further subdivided into the following categories (Mariani, 1984; Boycott and Wassle, 1991; Kolb et al., 1992):

- diffuse bipolar cells (6 types)
- midget bipolar cells (2 types)
- short wavelength sensitive or blue cone bipolar cells
- and giant bistratified bipolar cells.

The diffuse and giant bistratified bipolar cells converge information from many cone photoreceptors. In contrast, the midget and short wavelength sensitive bipolar cells each synapse with a single cone only, although each cone is in contact with two of these bipolar types (Kolb, 2001). As shown in Figure 1.5, ON-centre (centre depolarising) and OFF-centre (centre hyperpolarising) bipolar cells synapse in different strata of the inner plexiform layer.

1.1.6. Horizontal cells

Horizontal cells are a form of interneuron that convey information laterally within the outer plexiform layer by forming synapses with the photoreceptor and bipolar cells. They therefore provide feedback to the photoreceptor cells and feed forward to bipolar cells, which helps to generate bipolar and ganglion cell receptive field surrounds (Dacey, 1999). Three types of horizontal cell have been identified in the human retina on the basis of dendritic field characteristics and spectral preferences: HI, HII and HIII (Kolb et al., 1992; Kolb et al., 1994; Kolb, 2001) (Figure 1.6).

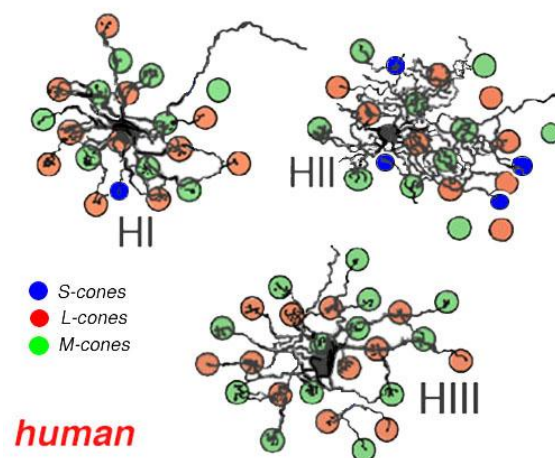


Figure 1.6. Horizontal cell types in the human retina, shown with their spectral preferences (Kolb, 2001).

1.1.7. Müller cells

The Müller cells are the principal glial cell of the retina (Bringmann et al., 2006). Their cell bodies are located in the inner nuclear layer and their processes span the radial thickness of the retina: from the outer limiting membrane to the inner limiting membrane. The Müller cell processes occupy most of the space between the retinal neurones and one

of their main functions is to provide structural and architectural support for the retina. Müller cells are involved in:

- metabolic support and nutrition of neurons
- maintenance of ion and water homeostasis
- protection against oxidative stress
- contribution to neuronal signalling
- recycling of photopigments
- release of neuroactive and vasoactive substances
- transmission of light from retinal surface to photoreceptors (Franze et al., 2007)
- and retinal development.

For an excellent review of the key functions of the Müller cells, the reader is referred to Bringmann et al. (2006).

Recently, the Müller cells have been implicated in an alternative pathway for cone photopigment regeneration (Das et al., 1992; Mata et al., 2002; Wang, & Kefalov, 2009; 2011). This will be discussed further in Section 1.3.3 (Page 36).

1.1.8. Amacrine cells

Amacrine cells are a type of interneuron that facilitate the lateral transfer of information within the inner plexiform layer by synapsing with the bipolar and retinal ganglion cells. At least 25 morphological types of amacrine cell have been identified in the human retina (Mariani, 1990; Kolb et al., 1992). These are classified according to their dendritic tree size and this morphological variation appears to reflect a wide range of functions. AII and A17 amacrine cells are particularly important in the rod pathway because, unlike cone bipolar cells, rod bipolar cells do not make direct contact with retinal ganglion cells (Kolb & Famiglietti, 1974; Kolb, 1994). Rather, they contact AII and A17 amacrine cells, which, in turn, pass the information to the ganglion cells, either directly or via cone bipolar cells.

1.1.9. Retinal ganglion cells (RGCs)

The RGC bodies are located in the ganglion cell layer. Retinal ganglion cells receive information from amacrine and bipolar cells, which they pass along their axons to higher visual processing centres via the optic nerve. Ganglion cell density varies with retinal

location: it peaks 1.5-7° from fixation and declines rapidly at increasingly eccentric retinal locations (Curcio & Allen, 1990).

At least 18 types of RGCs have been identified in the human retina (Kolb et al., 1992). These may be classified according to where their axons terminate in the lateral geniculate nucleus (LGN): P-cells (midget-type morphology) project to the parvocellular layers of the LGN and M-cells (parasol type morphology) project to the magnocellular layers (Figure 1.7) (Perry and Cowey, 1981; 1984; Perry et al., 1984). RGCs may also be classified according to the organisation of their receptive fields. OFF-centre (centre hyperpolarising) RGCs synapse with OFF-centre bipolar cells in sublamina 'a' of the inner plexiform layer, whilst ON-centre (centre depolarising) RGCs synapse with ON-centre bipolar cells in sublamina 'b' of the inner plexiform layer.

The axons of the RGCs form the innermost layer of the retina: the retinal nerve fibre layer (RNFL). In most individuals these axons remain unmyelinated until they exit the retina at the optic nerve head. The nerve fibre layer is thickest at the optic nerve head.

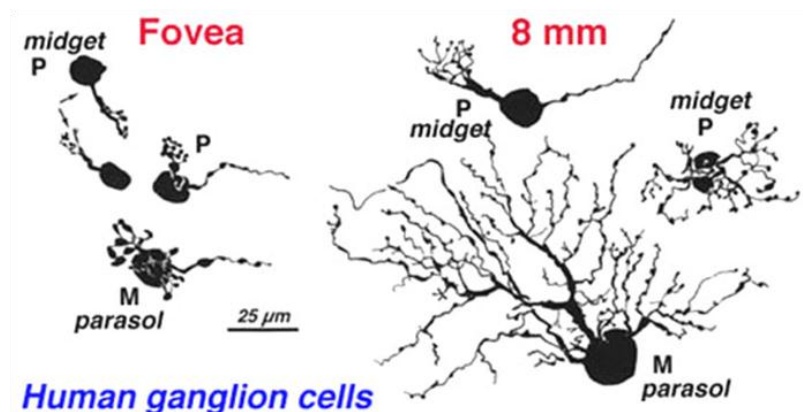


Figure 1.7. P- and M- ganglion cell types in the human retina (Kolb, 2003b).

1.1.10. The visual pathway

After the RGC axons exit the retina they travel along the optic nerve to the chiasm, where those fibres arising from the nasal retina decussate to the opposite side of the brain before entering the optic tracts. From here, approximately 90% of the axons project to the LGN (Perry et al., 1984), while the remaining 10% of axons follow a separate pathway to the superior colliculus and pretectum (Perry & Cowey, 1984). Finally information is relayed from the LGN to the primary visual cortex by the optic radiations. It is beyond the scope of

this thesis to describe the anatomy of the visual cortex, but for the interested reader excellent descriptions are provided by Schmolesky (2007).

1.2. Age-related macular degeneration (AMD)

1.2.1. Incidence and prevalence of AMD

Age-related macular degeneration is the primary cause of visual impairment in the UK (Bunce and Wormald, 2008). The number of registrations of ‘sight impairment’ and ‘severe sight impairment’ as a consequence of AMD increased by 30-40% between 1950 and 1990 (Evans and Wormald, 1996). Recent estimates of visual impairment registrations attributed to AMD stand at 55.9-57.2% in England and Wales (Evans et al., 2004; Bunce and Wormald, 2008) and 44.2% in the Republic of Ireland (Kelliher et al., 2006). Registration of visual impairment in the UK is voluntary and requires validation by an ophthalmologist. It has been estimated that less than 50% of patients that are eligible for registration are actually registered (Robinson et al., 1994), and this means that the true proportion of the population affected by AMD is likely to be significantly higher than these statistics suggest. This suggestion has recently been supported by a Bayesian meta-analysis of 31 population studies with a combined sample size of 57,173, which estimated the prevalence of late stage AMD to be 2.4% in the UK, which means that there are approximately half a million adults in the UK currently living with late stage AMD (Owen et al., 2012). In addition, a recent cross-sectional study of European adults (UK, Norway, Estonia, France, Italy, Greece, and Spain) estimated the prevalence of early AMD to be 36.48% in the population aged over 65 years (Augood et al., 2006).

The prevalence of AMD is closely associated with age (Bamashmus et al., 2004; Owen et al., 2012). The prevalence of late stage AMD in the UK has been estimated as 2.4% in the population aged over 50 years compared to 12.2% in the population aged over 80 years (Owen et al., 2012). The Office for National Statistics has predicted a 32% increase in the population of state pension age from 11.8 million in 2008 to 15.6 million by 2033 and a 100% increase in the population aged over 85 years in the same period (Office for National Statistics, 2009). As a consequence of the ageing population, significant increases in the

prevalence of AMD, and its associated costs, have been predicted (Congdon et al., 2004; Rein et al., 2009).

1.2.2. Clinical features of AMD

1.2.2.1. Drusen

Drusen are deposits of extracellular membranous debris that accumulate between the RPE and the inner collagenous layer of Bruch's membrane. They vary in size, colour, shape, elevation and distinctness. The drusen that are most commonly associated with AMD are known as hard and soft drusen. In addition, reticular drusen have been associated with progression to late AMD (Klein et al., 2008a; Zweifel et al., 2010; Schmitz-Valckenberg et al., 2011).

Hard drusen

Small (< 63µm), round, flat, yellow or white deposits are classified as hard drusen (Figure 1.8.A). They have been reported in 50-80% of the population aged over 30 years and are therefore not considered indicative of AMD when present in isolation (Bressler et al., 1989; Bird et al., 1995; Sarks et al., 1999).



Figure 1.8. Funduscopy appearance of hard (A) and soft (B) drusen. (Hageman et al., 2001).

Soft drusen

Soft drusen are larger than hard drusen. They are grey or yellow in colour and have variable margins (Figure 1.8.B). They may form independently or develop from pre-existing hard drusen (Sarks et al., 1994) and as they enlarge, they may coalesce to form

confluent drusen. The presence of soft drusen is diagnostic for early AMD (Bird et al., 1995) and in large numbers they are associated with a significantly increased risk of progression to advanced disease (Klein et al., 1997).

Reticular drusen

Reticular drusen form an interlacing network of yellow lobular or ribbon like deposits, which tend to appear in the outer macula (Arnold et al., 1995), and are typically associated with pigmentary changes (Zweifel et al., 2010). It has been proposed that the presence of reticular drusen in AMD may have previously been underestimated, due to misclassification as other types of drusen (Sarks et al., 2011). In recent years, reticular drusen have been recognised as an additional distinctive feature of AMD and have been shown to be associated with progression to late stage disease (Klein et al., 2008a; Zweifel et al., 2010; Schmitz-Valckenberg et al., 2011).

1.2.2.2. Pigmentary abnormalities

Focal areas of pigment change within the RPE are another characteristic sign of early AMD (Bird et al., 1995; AREDS, 2001). Focal hyperpigmentation is evident as small areas of pigment clumping, resulting from an increase in the melanin content of RPE cells, or from cell proliferation or migration (Bressler et al., 1994). In contrast, focal hypopigmentation manifests as small patches of mottled pigment, in areas where the melanin content of RPE cells is reduced, potentially due to RPE atrophy or thinning. Focal pigment changes are associated with an increased risk of progression to advanced disease (Klein et al., 1997).

1.2.2.3. Geographic atrophy (GA)

Geographic atrophy represents the end stage of dry AMD (Bird et al., 1995; AREDS, 2001). It is characterised by well demarcated areas of RPE atrophy, a reduction in retinal thickness and increased visibility of the underlying choroidal vasculature (Biarnes et al., 2011). GA progresses slowly over time and is associated with a gradual reduction in VA and the development of scotomas, which can significantly impair visual function (Sunness et al., 2008), although the fovea is typically preserved until relatively late in the disease process (Sunness et al., 2008).

1.2.2.4. Neovascular AMD (nAMD)

In healthy eyes, the choroidal architecture is maintained by a balance between the anti-angiogenic growth factor PEDF (pigment epithelial derived factor), also present in the optically clear cornea and vitreous, and the pro-angiogenic growth factor VEGF (vascular endothelial growth factor). In eyes with advanced AMD, a local imbalance of these growth factors in favour of VEGF induces inward growth of capillaries from the choroid, through Bruch's membrane, into the subretinal space (Roth et al., 2004). Patients may report metamorphopsia and blurring or loss of vision and a green-grey lesion may be visible ophthalmoscopically. As the new vessels are fragile, they are prone to leakage and haemorrhage and are therefore often associated with hard exudate, subretinal or intraretinal haemorrhage and pigment epithelial detachment (PED). Ultimately, the end stage of wet AMD is the formation of a disciform scar, with accompanying absolute scotoma, which leads to devastating central vision loss.

1.2.2.5. Pigment epithelial detachment (PED)

Pigment epithelial detachments occur between the basal lamina of the RPE and the inner collagenous layer of Bruch's membrane. Clinically, this is visible as a well-demarcated round elevation of the retina, usually confined to the macula. PEDs are generally asymptomatic, except when the fovea is affected. There are three types of PED associated with AMD, which may be differentially diagnosed using fluorescein and indocyanine green angiography: serous, fibrovascular and drusenoid (Zayit-Soudry et al., 2007). Although PEDs may spontaneously flatten, there is a risk of tearing and vision loss (Pauleikhoff et al., 2002).

1.2.3. Clinical classification of AMD

Prior to the 1990s, there were no standardized definitions or severity scales for grading of AMD. The development of a standardized system was deemed necessary to enhance the comparability of results between research studies. The 'Wisconsin Age-related Maculopathy Grading System' (Klein et al., 1991a) was initially developed for use in the Beaver Dam and Framingham eye studies (Krueger et al., 1980; Klein et al., 1991b). This formed the basis for the 'International Classification and Grading System' (Bird et al., 1995) and the 'Age-related Eye Disease Study System' (AREDS, 2001; Davis et al., 2005; Ferris et al., 2005).

Table 1.1. Classification of AMD according to the AREDS Grading System (modified from Davis et al., 2005). C-1, C-2, I-2, O-2 and DA (disc area) denote the standard circles used to assess the size of the fundus features (Figure 1, Davis et al., 2005). The final column shows how participants were classified during the investigations included in this thesis. As the AREDS scale was primarily developed to allow monitoring of disease progression, it did not originally include steps 10 and 11 (late AMD).

Step	Drusen area	Increased pigment	Depigmentation-Geographic atrophy		
1	< C-1	0	0	0	Normal ageing
2	\geq C-1, < C-2, < C-1	0 \geq Q	&/or	0 \geq Q, < I-2	Early
3	\geq C-2, < I-2	0		0	Early
4	\geq I-2, < O-2 \geq C-1, < I-2 < C-2	0 \geq Q \geq 0	&/or	0 \geq Q, < I-2 \geq I-2, < 0.5 DA	Early
5	\geq O-2, < 0.5 DA \geq I-2, < O-2 \geq C-2, < I-2	0 \geq Q \geq 0	&/or	0 \geq Q, < I-2 \geq I-2, < 0.5 DA	Early
6	\geq 0.5 DA \geq O-2, < 0.5 DA \geq I-2, < O-2	0 \geq Q \geq 0	&/or	0 \geq Q, < I-2 \geq I-2, < 0.5 DA	Early
7	\geq 0.5 DA \geq O-2, < 0.5 DA	\geq Q \geq 0	&/or	\geq Q, < I-2 \geq I-2, < 0.5 DA	Intermediate
8	\geq 0.5 DA Any	\geq 0 \geq 0		\geq I-2, < 0.5 DA \geq 0.5 DA	Intermediate
9	Any	\geq		Noncentral geographic atrophy	Intermediate
10		Central geographic atrophy			Late
11		Wet AMD			Late

These grading systems are based purely on the morphological changes that occur in the ageing eye; visual acuity is disregarded (Bird et al., 1995). Colour stereoscopic fundus photographs are used to identify key stages of the disease, including early AMD, dry AMD or wet AMD (Bird et al., 1995; AREDS, 2001; Davis et al., 2005; Ferris et al., 2005). Table 1.1 summarises the diagnostic criteria for AMD based on The Age-Related Eye

Disease Study grading scale (AREDS) (AREDS, 2001; Davis et al., 2005). The International Classification and Grading System (Bird et al., 1995) comprises fewer subsections with which to classify the disease (Table 1.2). During this thesis, drusen and pigmentary changes will be defined as ‘early AMD’, while geographic atrophy (GA) and neovascular AMD (nAMD) will be defined as ‘late AMD’.

Table 1.2. Classification of AMD according to the International Classification and Grading System (modified from Bird et al., 1995)

<u>Disease status</u>	<u>Diagnostic criteria</u>
Early AMD	Drusen with or without associated pigment and/or hypopigmentation of the RPE
Late AMD: dry	Geographic atrophy > 175µm in diameter
Late AMD: wet	At least one of the following: subRPE/subretinal neovascular membrane, RPE detachment, hard exudates, subretinal haemorrhage, disciform scar

1.2.4. Risk factors for AMD

Age-related macular degeneration is a disease of the ageing eye and it is widely agreed that increasing age is the most inextricable risk factor for the development and progression of AMD (Evans, 2001; Buch et al., 2005; Coleman et al., 2008). There are however many additional factors that are closely associated with the progression of AMD. For excellent reviews of risk factors for AMD, the reader is referred to Evans (2001), Seddon et al. (2009) and Chakravarthy et al. (2010). A summary of the key risk factors that are strongly associated with the development and progression of AMD is included here.

1.2.4.1. Smoking

Smoking is the most significant modifiable risk factor for AMD (Thornton et al., 2005; Khan et al., 2006; Klein et al., 2008b), most likely as a result of the oxidative damage it induces (Thornton et al., 2005) (see section 1.2.5.1, page 19). The duration and intensity of the smoking have been shown to influence the degree of risk (Khan et al., 2006; Chang et al., 2008) and the risk of developing AMD may increase by up to five times for a current smoker compared an individual that has never smoked (Smith et al., 1996). However, these effects appear to be reversible, as it has been shown that 20 years after ceasing to smoke, an individual’s risk of developing AMD becomes similar to that of a non-smoker (Khan et al., 2006).

1.2.4.2. Genetics

A family history of AMD is associated with an increased risk of disease development (Klein et al., 2001) and correspondingly AMD has been shown to occur more frequently and at a younger age in the first degree relatives of patients with late stage AMD (Klein et al., 2001). Similarly, studies of twins have shown a higher concordance of AMD in monozygotic twins compared to dizygotic twins (Hammond et al., 2002). Attempts to identify the genetic risk factors for AMD are ongoing and recently a number of genetic variants have been shown to be independently associated with an increased prevalence and incidence of AMD (Seddon et al., 2009), in particular, the complement factor H (CFH) gene, the C2 gene, both associated with the complement pathway, and the age-related maculopathy susceptibility (ARMS2) gene (Bergeron-Sawitzke et al., 2009; Farwick et al., 2009; Seddon et al., 2009; Ting et al., 2009).

1.2.4.3. Race

Racial differences in the incidence of AMD have been demonstrated. A higher risk of the development and progression of large drusen and pigmentary abnormalities at the macula, as well as progression to late stage AMD has been demonstrated in white people compared to black people (Klein et al., 2003a; Klein et al., 2006 Chang et al., 2008; Klein, 2011; Klein et al., 2011). It has been suggested that the higher concentration of melanin present in darker skin may help to protect the RPE and outer retina against oxidative damage (Jampol and Tielsch, 1992). The evidence regarding the prevalence of AMD in Hispanics has previously been inconclusive (Klein, 2011). However, recent studies have shown that although the prevalence of early AMD may be similar in Hispanic and white populations, Hispanic people are less likely to develop late AMD (Klein et al., 2006; Varma et al., 2010; Klein, 2011; VanderBeek et al., 2011).

1.2.4.4. General health

A recent systematic review of the literature identified several aspects of a patient's general health that have been consistently associated with the development of late AMD (Chakravarthy et al., 2010). These included cardiovascular disease, in which the risk of late AMD is doubled, hypertension and elevated levels of plasma fibrinogen. In addition, the

risk of late stage disease increased with increasing body mass index (BMI) (Chakravarthy et al., 2010).

1.2.4.5. Diet

The retina is particularly prone to oxidative damage (Beatty et al., 2000) (See Section 1.2.5.1, Page 19). Anti-oxidant enzymes, vitamins and carotenoids have been proposed to minimise this damage and therefore lower the risk of progression to advanced AMD (Evans, 2008). The Age-Related Eye Disease Study (AREDS) Research Group investigated the ability of high-dose antioxidant vitamins (C, E and beta carotene) and zinc to delay the development of advanced AMD (Kassoff et al., 2001; Chew et al., 2009). The 4757 participants were classified on the basis of their fundus appearance, before they were randomly assigned to receive one of four types of oral tablets daily: antioxidants, zinc, antioxidants plus zinc or a placebo. There was a 25% reduction in the risk of progression to advanced AMD in those participants that exhibited signs of AMD (extensive intermediate drusen, large drusen or advanced AMD) on commencing supplementation with the antioxidant vitamin and zinc formulation (Kassoff et al., 2001). Consequently the study concluded that these supplements should be recommended to patients at a high risk of developing advanced disease (Kassoff et al. 2001; Chew et al., 2009).

Docosahexaenoic acid (DHA) is a type of omega-3 fatty acid present in high concentration in the photoreceptor outer segments (Krishnadev et al., 2010). These fatty acids cannot be synthesized by humans and therefore must be obtained wholly from dietary sources. There is an emerging body of evidence to suggest that a diet rich in omega-3 fatty acids is associated with a reduced risk of AMD (SanGiovanni et al., 2009; Tan et al., 2009; Krishnadev et al., 2010; Christen et al., 2011; Ho et al., 2011; Merle et al., 2011). For example, in a large cohort (n=2454) included in a recent epidemiological study, one serving of fish each week was associated with a reduction of the 10-year risk of incident early AMD (Tan et al., 2009). Furthermore, the risk of progression to advanced disease has been shown to be lowest in the proportion of the population with the highest consumption of omega-3 fatty acids (SanGiovanni et al., 2009).

Macular pigment comprises the xanthophylls lutein and zeaxanthin (Bone et al., 1985). These plant pigments selectively accumulate at the macula, although they are present in

lower concentrations throughout the retina (Ahmed et al., 2005). They must be obtained entirely from dietary sources and are abundant in a variety of coloured fruit and vegetables, especially dark green leafy vegetables, and corn products (Sommerburg et al., 1998; Perry et al., 2009). Macular pigment is thought to play a crucial role in limiting light induced damage to the retina (Ahmed et al., 2005) and correspondingly a diet rich in these nutrients has been shown to reduce the risk of AMD (Gale et al., 2003; Delcourt et al., 2006; SanGiovanni et al., 2007; Tan et al., 2008). Two large multi-centre, randomised-control trials are underway to systematically assess the effects of daily oral supplementation with lutein and zeaxanthin, in conjunction with anti-oxidant vitamins (Neelam et al., 2008) and omega-3 fatty acids (AREDS2, 2012), on the progression to advanced AMD.

1.2.4.6. Sunlight

The effect of exposure to sunlight on the development of AMD is less clear. The amount of leisure time spent outside before the age of 40 years has been linked to the development of AMD (Cruickshanks et al., 2001) and a significant association between extended exposure to sunlight and the 10-year incidence of early AMD has been reported (Tomany et al., 2004). However, there is additional evidence to suggest that the effect of sunlight is only significant in individuals with low antioxidant levels (Fletcher et al., 2008).

1.2.5. Pathogenesis of AMD

Age-related macular degeneration is a complex multi-factorial disease, in which a series of overlapping events contribute to abnormalities in the photoreceptors, RPE, Bruch's membrane and choroid.

1.2.5.1. Oxidative stress

Oxygen metabolism during aerobic respiration releases energy from carbohydrates, proteins and lipids. The physiological by-products of this process are reactive oxygen intermediates (ROIs) and comprise free radicals, hydrogen peroxide and singlet oxygen (Beatty et al., 2000). These ROIs cause cellular damage, known as oxidative stress. The retina is particularly prone to oxidative damage because of its high oxygen demands, its life-long exposure to visible light, the high proportion of polyunsaturated fatty acids in the photoreceptor outer segments and RPE phagocytosis (Beatty et al., 2000).

The human body uses antioxidants to neutralise the effect of ROIs (Muller et al., 2007). At the macula, this function is fulfilled by the macular pigments lutein and zeaxanthin. However, with increasing age the quantity of ROIs often exceeds the capacity of these antioxidants, resulting in tissue damage. At the macula this manifests as RPE and photoreceptor cell death, increases in the thickness of Bruch's membrane with a subsequent reduction in its permeability and the up-regulation of VEGF (Kannan et al., 2006).

There is a range of evidence to indicate that oxidative mechanisms contribute to the disease process in AMD. Firstly, smoking, the primary modifiable risk factor for AMD, is known to exacerbate oxidative stress (Thornton et al., 2005; Khan et al., 2006; Klein et al., 2008b). In addition, clinical studies have demonstrated that the risk of developing advanced AMD is reduced by supplementation with antioxidant vitamins and minerals (Kassoff et al., 2001; Chew et al., 2009; Ho et al., 2011). This is consistent with evidence that individuals with high levels of systemic carotenoids are less likely to develop advanced AMD (Sperduto, 1993), and post-mortem studies that have demonstrated that a reduction in the concentration of macular pigments lutein and zeaxanthin is associated with an increased risk of AMD (Bone et al., 2001). Finally, a series of studies have recorded higher level of systemic homocysteine, an amino acid that rapidly oxidises to form ROIs, in patients with AMD compared to controls (Coral et al., 2006; Seddon et al., 2006; Rochtchina et al., 2007).

1.2.5.2. Lipofuscin formation

Incomplete phagocytosis of photoreceptor outer segments by the RPE and prolonged oxidative stress gradually leads to the accumulation of lipofuscin granules in the lysosomal compartments of RPE cells (Wolf, 2003; Roth et al., 2004; Schmitz-Valckenberg et al., 2009). Lipofuscin contains a cytotoxic component which further aggravates oxidative damage and contributes to the impairment of RPE function (Wolf et al., 2003; Roth et al., 2004). This impairment of RPE function is considered to be a critical event in the development of AMD (Nowark, 2006) and may initiate the complement cascade, leading to chronic inflammation at the macula (Zhou et al., 2006).

1.2.5.3. Chronic inflammation and the immune response

There is a growing body of evidence to suggest that inflammatory processes contribute to the pathogenesis of AMD. Inflammatory markers, including elevated levels of plasma fibrinogen (Smith et al., 1998; Chakravarthy et al., 2010) and a high white blood cell count (Klein et al., 2003b; Shankar et al., 2007; Yasuda et al., 2009) are associated with the development of both early and advanced AMD. Proteins that are associated with the immune response have been identified in drusen (Hageman et al., 2001; Rodrigues, 2007; Buschini et al., 2011). These drusen and additional debris trapped between the RPE and Bruch's membrane generate a local pro-inflammatory signal which, in turn, initiates the complement cascade, an innate physiological immune reaction to dead, damaged or foreign cells (Roth et al., 2004).

Genetic polymorphisms in the complement factor H (CFH) gene and other regulatory proteins involved in the complement cascade have also been shown to have a significant role in the development and progression of AMD (Donoso et al., 2006; Fletcher and Chong, 2008; Kanda et al., 2008; Bergeron-Sawitzke et al., 2009; Farwick et al., 2009; Seddon et al., 2009; Ting et al., 2009). These polymorphisms lead to uncontrolled complement activation and alter the cellular response of the RPE to injury (Nowark, 2006).

Most recently, a link between C-reactive protein (CRP) and AMD has been established. CRP is an initiation factor that is bound by CFH during the complement cascade that has previously been identified as a major risk factor for cardiovascular disease (Hong et al., 2011). A recent meta-analysis of the literature demonstrated a significant association between high levels of serum and plasma CRP (greater than 3mg/L) and late stage AMD, although the association with early AMD was weaker (Hong et al., 2011).

It has been proposed that the pathological changes associated with AMD are initially triggered by ageing and oxidative stress and that subsequent cellular damage is amplified by the inflammatory response (Figure 1.9) (Kanda et al., 2008). The clinical presentation of the disease is therefore subject to immense individual variation as it is influenced by polymorphisms in the genes governing the inflammatory process.

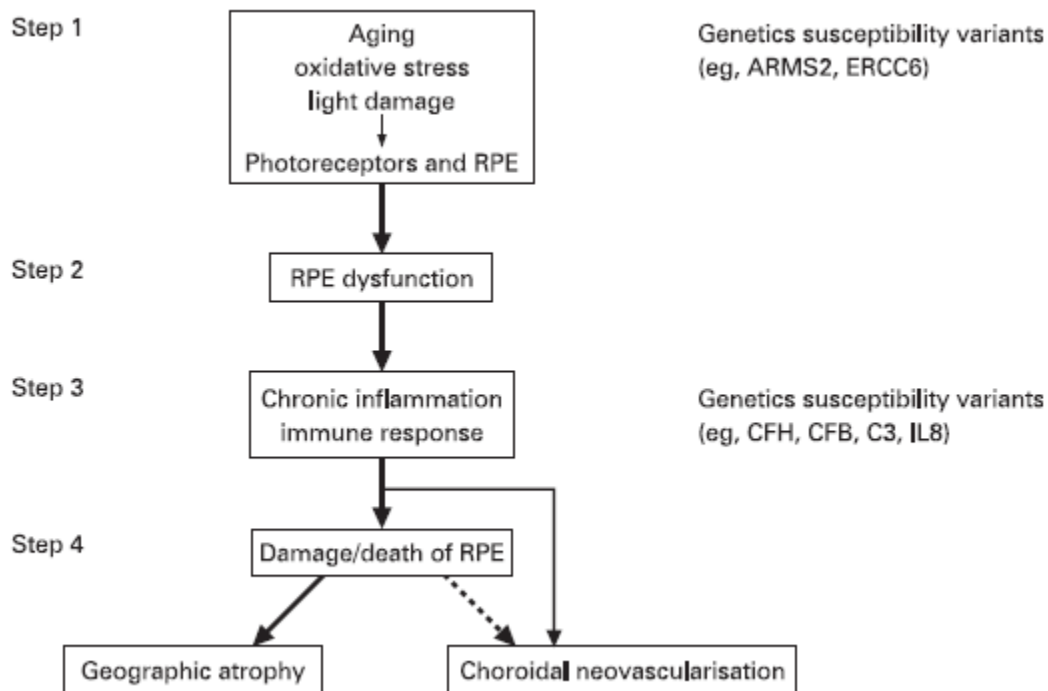


Figure 1.9. The proposed role of inflammation and the immune response in the pathogenesis of AMD (Kanda et al., 2008).

1.2.5.4. Hypoxia and choroidal vascular changes

As described (See Section 1.2.2.4, Page 14), in healthy eyes, the choroidal architecture is maintained by a balance between numerous growth factors, including the anti-angiogenic growth factor PEDF and the pro-angiogenic growth factor VEGF. Hypoxia in retinal cells has been shown to increase VEGF expression (Aiello et al., 1995; Blaauwgeers et al., 1999; Stefánsson et al., 2011), which, in turn, induces the inward growth of blood vessels from the choroid. Support for this relationship between hypoxia, VEGF and angiogenesis has emerged from studies that have identified ‘Hypoxia inducible factor’ (HIF) in the endothelium and macrophages of the choroidal neovascular membrane (CNVM) (Inoue et al., 2007; Sheridan et al., 2009).

In the healthy eye, the choroidal circulation is barely sufficient to meet the metabolic needs of the outer retina, and the partial pressure of oxygen falls to almost zero proximal to the photoreceptor outer segments in the dark adapted eye (Wangsa-Wirawan & Linsenmeier, 2003). The changes to the choroidal circulation and Bruch’s membrane that occur in AMD are therefore hypothesised to result in outer retinal hypoxia (Feigl, 2009; Stefánsson et al.,

2011). In the healthy retina, oxygen diffuses from the choriocapillaris, through Bruch's membrane to the RPE and photoreceptors. However, the reduction in the density of the choriocapillaris that occurs with increasing age and in AMD (Ramrattan et al., 1994) causes delayed choroidal perfusion and decreased choroidal blood flow (Ciulla et al., 2002). This hinders removal of waste from the RPE, exacerbating drusen formation and changes to the RPE and Bruch's membrane (Feigl, 2009). Soft confluent drusen and thickening of Bruch's membrane increase the distance between the choriocapillaris and the retinal cells, which disturbs the delivery of oxygen to the cells, thereby further promoting hypoxia (Stefánsson et al., 2011). Correspondingly increasing drusen size has been shown to be associated with an increased risk of CNV (Solomon et al., 2009). Similarly, retinal elevation, detachment and oedema all effectively thicken the retina, which increase the distance over which the oxygen has to diffuse and increases the risk of hypoxia (Stefánsson et al., 2011). The effect of these hypoxic changes may be exaggerated by vitreoretinal adhesion, which reduces the diffusion of oxygen towards hypoxic retinal locations (Stefánsson et al., 2011). In addition, inflammation is proposed to independently stimulate formation of VEGF (Stefánsson et al., 2011) and chronic sub-RPE inflammation causes local damage to Bruch's membrane, which facilitates the subsequent protrusion of vessels through the membrane (Roth et al., 2004).

1.2.6. Clinical investigation of AMD

Historically, AMD has been evaluated clinically using measures of visual acuity, central visual field testing and fundus photography. However, there are a range of new techniques that may be more sensitive to the changes that occur in early AMD. In particular, psychophysical tests of visual function and advanced imaging techniques may be used to detect subtle changes at the macula before they are visible ophthalmoscopically (Neelam et al., 2009).

1.2.6.1. Fundus photography

Digital retinal photography is the primary method used to image the posterior pole in the clinic and in the absence of more advanced imaging techniques is a useful method for detecting AMD and for monitoring its progression (Jain et al., 2006). It has been suggested that colour fundus photographs should be used in conjunction with optical coherence tomography (OCT) to establish the need for treatment of wet AMD (Hibbs et al., 2011).

Stereoscopic fundus photography is particularly advantageous as it allows appreciation of the height and depth of retinal features. All of the AMD grading systems described in Section 1.2.3 (Page 14) are based solely on the assessment of morphological changes in the eye using colour stereoscopic photographs and templates to aid assessment of lesion size and location (Bird et al., 1995; AREDS, 2001; Davis et al., 2005; Ferris et al., 2005).

1.2.6.2. Fundus angiography (FA)

Prior to the development of OCT imaging, fundus angiography (FA) was the gold standard for evaluating the integrity of the macula (Yannuzzi, 2011). Fluorescein or Indocyanine Green dye is administered via intravenous injection and sequential fundus photos are taken to assess the choroidal and retinal circulation, using filters to excite the molecules within the dye (Lim et al., 2012). Hyperfluorescence caused by leakage of the dye may be indicative of wet AMD and may be classified by location and type (Lim et al., 2012). A classic neovascular lesion is well defined and causes early leakage of dye, whereas an occult lesion is less well defined and does not leak until later.

1.2.6.3. Fundus autofluorescence (FAF)

As discussed (Section 1.2.5.1, Page 19), the prolonged oxidative stress that is associated both with normal ageing and AMD leads to an accumulation of lipofuscin granules in the lysosomal compartments of RPE cells (Wolf, 2003; Roth et al., 2004; Schmitz-Valckenberg et al., 2009). The autofluorescent phosphores within the granules emit a characteristic yellow fluorescence when stimulated with blue light (Heimes et al., 2008; Schmitz-Valckenberg et al., 2009). The development of the confocal scanning laser ophthalmoscope has facilitated the assessment of the distribution of fundus autofluorescence (FAF) in the eye (Midena et al., 2007; Schmitz-Valckenberg et al., 2009). Changes in autofluorescence have been shown to be associated with drusen (vonRuckmann et al., 1997; Delori et al., 2000; Roth et al., 2004), geographic atrophy (vonRuckmann et al., 1997; Holz et al., 2001; 2007), CNVM (vonRuckmann et al., 1997; Spaide, 2003; Silva et al., 2011) and a reduction in visual sensitivity (Midena et al., 2007).

1.2.6.4. Optical coherence tomography (OCT)

Although retinal photography has previously been used to monitor the progression of AMD over time, in the last decade, optical coherence tomography (OCT) has emerged as a

valuable clinical tool for the analysis of retinal microstructure (Yasuno et al., 2009; Chung et al., 2011; Wood et al., 2011a). This non-invasive technique constructs high resolution cross-sectional images of the retina (Figure 1.10) by using low coherence light to measure the backscattered light from within the tissue (Wood et al., 2011a). OCT is now acknowledged as the standard clinical method for the assessment of AMD in hospital ophthalmology clinics (Drexler & Fujimoto, 2008) and recently, novel algorithms have been developed to allow automated volumetric analysis of drusen, which can be used to assess disease progression over time (Gregori et al., 2011; Yehoshua et al., 2011).

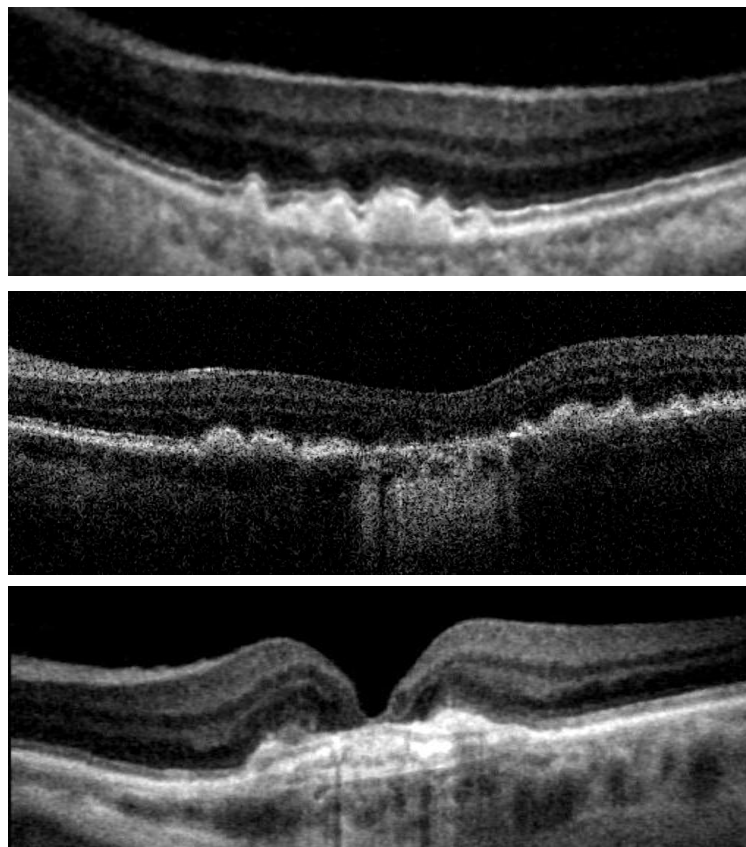


Figure 1.10. OCT images from our laboratory, obtained using a Spectral Domain OCT operating at 1050nm, showing soft drusen (top panel), geographic atrophy (middle panel) and CNV (bottom panel).

1.2.6.5. Visual acuity (VA)

Visual acuity is the standard psychophysical test of visual function in the clinic. However, there is considerable variation in the best corrected VA attained by patients with AMD, most likely as a result of the heterogeneity of the lesions associated with the disease (Beirne et al., 2006, Sunness et al., 2008). Although advanced AMD is associated with a significant reduction in VA, during the earlier stages of the disease process, VA remains

relatively unaffected (Klein et al., 1995). As early AMD is typically characterised by the absence of noticeable vision loss (Bird et al., 1995) and foveal vision often remains intact until relatively late in the disease (Sunness et al., 2008), the measurement of VA in isolation has limited diagnostic potential.

1.2.6.6. Visual field testing

During visual field testing, the sensitivity of the eyes is determined at a range of retinal locations, by presenting stimuli of variable intensity. Generally, lower mean sensitivities in the central field have been reported in patients with AMD compared to healthy controls (Midena et al., 1994; 1997; Owsley et al., 2000) and focal sensitivity losses have been recorded over large soft drusen (Takamine et al., 1998; Midena et al., 1997). However, standard automated perimetry is rarely used in the clinical assessment of AMD.

Conventional visual field testing requires stable foveal fixation and is therefore likely to be inaccurate for the precise evaluation of macular disorders (Rohrschneider et al., 2008). In recent years, microperimetry has been used as an alternative technique to evaluate the central visual field in AMD. Microperimetry is based on integrating fundus images with computerised threshold perimetry, in order to correlate fundus lesions to retinal sensitivity (Rohrschneider et al., 2008). The technique has been used effectively to identify and monitor the progression of geographic atrophy (Rohrschneider et al., 2008; Meleth et al., 2011) and to monitor the accumulation of lipofuscin in the RPE cells (Midena et al., 2007). Furthermore, microperimetry has been shown to be a more sensitive measure of visual outcome after antiVEGF therapy than the assessment of visual acuity (Parravano et al., 2010).

The technique classically used to assess the integrity of the central visual field in macular disease is the Amsler grid (Amsler, 1953). The patient is instructed to fixate the centre of a grid pattern presented monocularly and to report any defects or disturbances to the pattern. The chart may also be used by patients to self-monitor their vision at home. A sudden onset of distortion is considered to indicate incipient wet AMD, requiring urgent ophthalmological assessment.

1.2.6.7. Contrast sensitivity

As discussed (Section 1.2.6.5, Page 25), visual acuity, that is, the highest spatial frequency that may be resolved by the visual system at 100% contrast (Owsley, 2003), is relatively unaffected by early macular disease (Bird et al., 1995; Klein et al., 1995) and there is considerable variation in the best corrected visual acuity attained by patients with advanced AMD (Beirne et al., 2006; Sunness et al., 2008). Consequently the assessment of contrast sensitivity across a range of spatial frequencies has been investigated as a more comprehensive assessment of visual function in AMD.

A range of studies have demonstrated a loss of contrast sensitivity across all spatial frequencies in early AMD, with the most marked reduction at medium and high spatial frequencies (Kleiner et al., 1988; Stangos et al., 1995; Midená et al., 1997; Feigl et al., 2005a; Mei & Leat, 2007; Hahn et al., 2009). This is accompanied by a shift in the peak of the contrast sensitivity function towards lower spatial frequencies (Mei & Leat, 2007). These changes in contrast sensitivity have been shown to correlate with disease severity (Kleiner et al., 1988; Midená et al., 1997).

1.2.6.8. Temporal sensitivity

Temporal vision describes the eye's ability to detect flickering stimuli (Neelam et al., 2009). A reduction in temporal sensitivity across a range of temporal frequencies has been demonstrated in patients with early AMD compared to control patients (Mayer et al., 1992; 1994; Phipps et al., 2003; Dimitrov et al., 2011), especially at low to mid-temporal frequencies (Mayer et al., 1992; 1994). In addition flickering stimuli may be more sensitive to functional changes in AMD than static stimuli because of the increased metabolic demand placed on the retina by the flicker (Kiryu et al., 1995).

1.2.6.9. Colour vision

The majority of studies that have examined the relationship between colour vision and AMD indicate that colour discrimination deteriorates in early AMD, with tritan defects most commonly recorded (Eisner et al., 1991; 1992; Cheng & Vingrys, 1993; Frennesson et al., 1995; Arden & Wolf, 2004; Feigl et al., 2005a). These defects have been shown to progressively worsen in patients at high risk of developing wet AMD (Eisner et al., 1991; 1992; Arden & Wolf, 2004).

1.2.6.10. Dark adaptation

Dark adaptation classically refers to the relatively slow recovery of visual threshold that occurs in the dark following exposure to a bright light (Lamb & Pugh, 2004). Patients with early AMD often report visual difficulties when moving from high to low illumination and there is an emerging body of evidence to suggest that dark adaptation is a sensitive biomarker for the disease (Brown & Lovie-Kitchin, 1983; Eisner et al., 1987a; Collins & Brown, 1989; Eisner et al., 1991; Sandberg & Gaudio, 1995; Midea et al., 1997; Owsley et al., 2001; Phipps et al., 2003; Binns & Margrain, 2007; Owsley et al., 2007; Dimitrov et al., 2008; 2011). That is, it is a characteristic that may be objectively measured and evaluated as an indicator of normal and pathogenic biological processes (Puntmann, 2009). In studies that have measured a range of visual functions in patients with AMD, dark adaptation abnormalities appear to be the most sensitive markers for the condition (Eisner et al., 1991; Phipps et al., 2003; Owsley et al., 2001). For example, Eisner et al. (1991), showed that although colour vision and dark adaptation parameters both provided 100% specificity in AMD, the sensitivity of photopic dark adaptation (65%) was superior to that of the colour matching (48%). A comprehensive discussion of the relationship between dark adaptation and AMD is included later in this chapter (Section 1.3.5.3, Page 42).

1.2.7. Prevention and treatment

The treatment options for AMD have evolved rapidly over recent decades and are constantly advancing. Currently, most treatments target the neovascular form of the disease.

1.2.7.1. Focal laser photocoagulation

The first treatment for wet AMD to be used with some success was laser photocoagulation. This technique uses a laser burn to occlude the leaking blood vessels of the neovascular membrane (Chakravarthy et al., 2006). It has been shown to reduce the rate of vision loss in small well demarcated lesions, although its efficacy for poorly demarcated lesions is less clear (Hawkins and Fine, 1993). However, the laser causes irreversible damage to the overlying retina and the resultant scotoma renders the technique unsuitable for the treatment of subfoveal lesions (Ciulla et al., 1998; Chakravarthy et al., 2006). In addition, high recurrence rates of CNV have been reported (Maguire et al., 1994). A review of

fifteen trials in which laser photocoagulation was used to treat wet AMD concluded that although laser photocoagulation of the CNVM was shown to slow vision loss in wet AMD, in many cases the technique was contraindicated for use in the clinic as a result of the associated scotoma and the risk of laser-induced vision loss (Virgili & Bini, 2007).

1.2.7.2. Verteporfin photodynamic therapy (PDT)

The aim of PDT is to reduce the rate of vision loss in AMD by destruction of the CNVM without damage to the overlying retina. Verteporfin, a benzoporphyrin derivative, is administered via intravitreal injection and shows a selective uptake by active neovascular vessels, providing a targeted therapy for wet AMD (National Institute for Health and Clinical Excellence, 2003). Activation of the Verteporfin using a low powered laser causes the formation of short-lived free radicals that induce major platelet action, thrombosis and subsequent occlusion of the new vessels (Chakravarthy et al., 2006; Cruess et al., 2009). Photodynamic therapy is considered superior to focal laser photocoagulation due to the preservation of the overlying retina. Early multi-centre randomized placebo-controlled trials of patients with subfoveal CNV showed that PDT reduced the risk of vision loss in patients with predominantly ‘classic’ (well-defined) AMD lesions over a 36 month follow up period, but was less effective for minimally classic or ‘occult’ lesions (Bressler, 1999; Blumenkranz et al., 2001; Bressler, 2002; Greve et al., 2005; Cruess et al., 2009). Consequently, the National Institute for Health and Clinical Excellence (NICE) guidelines recommend the use of PDT for the treatment of classic AMD lesions only (National Institute for Health and Clinical Excellence, 2003).

1.2.7.3. Anti-VEGF drugs

As discussed (section 1.2.2.4, page 14), the formation of the neovascular membrane in wet AMD is induced by a local imbalance of soluble growth factors in favour of the pro-angiogenic growth factor VEGF. Consequently, a series of pharmacological agents has been developed to inhibit VEGF. These anti-VEGF drugs are administered by intravenous injection. Ranibizumab (Lucentis; Novartis) is a humanised monoclonal antibody fragment that binds to all human isoforms of VEGF, whereas Pegaptanib (Macugen; Eyetech) is a pegylated modified oligonucleotide that selectively binds the VEGF-165 isoform (Chakravarthy et al., 2006). It is perhaps unsurprising that better visual outcomes have been recorded following treatment with Ranibizumab compared to Pegaptanib, and

therefore Ranibizumab is more commonly used (Ip et al. 2008). Under guidelines issued by the National Institute for Health and Clinical Excellence (NICE) Ranibizumab, but not Pegaptanib, is recommended for the treatment of wet AMD under the NHS in Britain (National Institute for Health and Clinical Excellence, 2008). It is appropriate for all major types of CNVM and is primarily indicated for active subfoveal lesions (Mitchell et al., 2010).

As the first treatment for wet AMD to generate a clinically significant improvement in VA, monthly Ranibizumab injections have proved groundbreaking (Brown et al., 2006; Rosenfeld et al., 2006; Brown et al., 2009). The most significant gain in VA has been shown to occur after the first injection and this level of VA is maintained when Ranibizumab injections are administered monthly (Figure 1.11). The recommended treatment schedule comprises an initial loading phase, in which an injection is administered monthly for the first three months. This is followed by a maintenance phase, in which the patient is monitored on a monthly basis and further injections administered as required (National Institute for Health and Clinical Excellence, 2008; Mitchell et al., 2010).

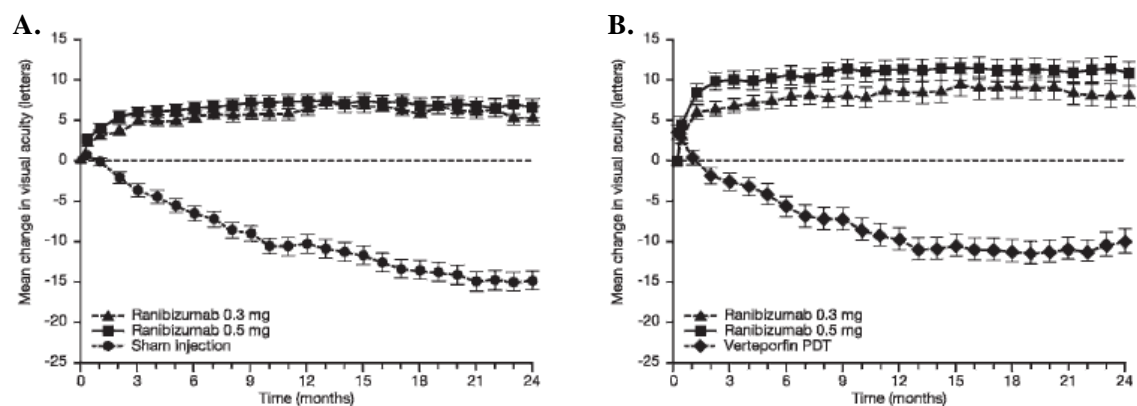


Figure 1.11. Mean change from baseline in best-corrected visual acuity by month, with administration of monthly Ranibizumab injections compared to a) monthly placebo injections (Rosenfeld et al., 2006) and b) monthly verteporfin PDT (Brown et al., 2009).

A third anti-VEGF drug, Bevacizumab (Avastin; Genentech), a full-length monoclonal antibody that binds all human isoforms of VEGF, is not yet licensed for the treatment of AMD (Ip et al., 2008; Martin et al., 2011). However, recent trials have suggested that the effectiveness of Bevacizumab is as high as that of Ranibizumab (Martin et al., 2011) and, given the substantially lower unit cost of Bevacizumab, many advocate further

investigation of its possible use for the treatment of wet AMD (Jackson & Kirkpatrick, 2011; Martin et al., 2011; Mitchell et al., 2011).

1.2.7.4. Management of dry AMD

There is currently no effective treatment for dry AMD. Instead, preventative strategies can be used to reduce the risk of disease development, for example, patients should be advised to stop smoking (Khan et al., 2006) and sunglasses worn to protect the eyes from sunlight induced damage (Fletcher et al., 2008). Nutritional supplements and dietary advice may also be effective (see Section 1.2.4.5, Page 18).

1.2.7.5. Novel therapies

Although anti-VEGF therapy can improve VA in patients with wet AMD (Brown et al., 2006; Rosenfeld et al., 2006; Brown et al., 2009), the monthly follow up appointments that are required to assess the need for retreatment place a huge pressure on limited healthcare resources. Consequently, alternative therapies are constantly being evaluated. A summary of some of the key emerging strategies is included here.

There are some patients that do not respond to treatment with a single anti-VEGF agent (Miller 2010). As a result, combination therapy, in which PDT and/or intravitreal steroids are used in conjunction with an anti-VEGF agent, has been suggested in order to improve visual outcomes and to reduce the frequency of retreatment (Miller 2010; Couch & Bakri, 2011). A recent review of the clinical trials that have assessed the outcomes of this therapy concluded that although favourable visual outcomes were achieved, further investigation is required to determine the optimal combination and dosage administered (Couch & Bakri, 2011).

As described (Section 1.2.5.3, Page 21), inflammation has a key role in the pathogenesis and progression of AMD. Consequently, a range of anti-inflammatory agents have been proposed as an addition or alternative to anti-VEGF therapy, including corticosteroids, nonsteroidal anti-inflammatories (NSAIDS) and immunosuppressive agents (Wang et al., 2011). For an excellent review of the use of anti-inflammatory agents for the treatment of AMD the reader is referred to Wang et al (2011).

Stem cells transplanted into an injured central nervous system secrete neurotrophic factors and inflammatory modulators that provide neuroprotection for the tissue. Exploitation of this property for the treatment of neurodegenerative diseases such as AMD is currently under investigation (Bull & Martin, 2011). Subretinal transplantation of RPE cells aims to preserve photoreceptors, and therefore visual function, by replacing dysfunctional RPE with functional RPE generated from embryonic stem cells (Bull & Martin, 2011). It has been shown to improve retinal function in animal models of photoreceptor degeneration (Pinilla et al., 2007; Lu et al., 2009) and consequently a range of clinical trials to evaluate the technique in patients with AMD are currently planned (Bull & Martin, 2011).

1.3. Visual adaptation

As described previously in this chapter, a range of visual functions are affected by early AMD. In particular, there is an emerging body of evidence to suggest that dark adaptation is a sensitive biomarker for this disease (Brown & Lovie-Kitchin, 1983; Eisner et al., 1987a; Collins & Brown, 1989; Eisner et al., 1991; Sandberg & Gaudio, 1995; Midena et al., 1997; Owsley et al., 2001; Phipps et al., 2003; Binns & Margrain, 2007; Owsley et al., 2007; Dimitrov et al., 2008; 2011). This section outlines the physiology of dark adaptation in the healthy retina, before reviewing the literature regarding the changes to dark adaptation that occur in AMD.

1.3.1. Dark adaptation

The human visual system functions over a vast light intensity range and generally adapts rapidly to changes in the ambient illumination. However, after exposure to a prolonged or intense adapting light source, the visual pigment becomes deactivated or 'bleached' and can take many minutes to recover. The slow recovery of visual sensitivity that occurs over time in the dark following exposure to an adapting light source is known as dark adaptation (Lamb and Pugh, 2004).

After an intense bleach of visual pigment, the recovery of visual sensitivity follows a biphasic course (Figure 1.12), in which the visual threshold reduces (and correspondingly visual sensitivity increases) by approximately 5 log units during a 35-40 minute period of darkness (Hecht et al., 1937). During the first 10 minutes in the dark there is a rapid

reduction of visual threshold, followed by a period over which threshold remains stable, known as the cone plateau. The end of the plateau is marked by the rod-cone-break (RCB), after which threshold continues to reduce at a slower pace. The initial rapid reduction in visual threshold is mediated by the cones, while the slower threshold reduction that follows is governed by the rods (Hecht et al., 1937). The visual threshold at any given moment during dark adaptation is determined by the most sensitive photoreceptor system at that time and the RCB indicates the change in the dominant system.

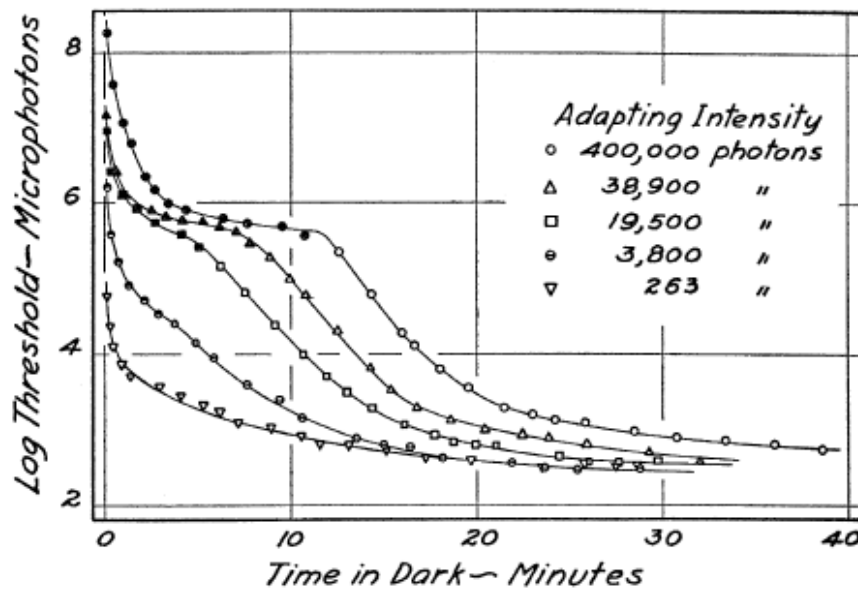


Figure 1.12. Dark adaptation functions for a normal observer recorded after exposure to adapting lights of increasing intensity (Hecht et al., 1937).

The configuration of the dark adaptation function is affected by the characteristics of the adapting light. The full biphasic function is only evident at high adapting intensities (Hecht et al., 1937). As the intensity of the adapting light decreases, a lower proportion of photopigment is bleached and consequently the cone-mediated portion is less prominent (Figure 1.12).

In addition, the shape of the dark adaptation curve is altered by variations in the parameters of the stimulus, including its retinal location, size and wavelength. Rod photoreceptor density increases with increasing retinal eccentricity (Curcio et al., 1990). Consequently, the rod portion of the curve becomes progressively more prominent as the position of the stimulus moves from the central to the peripheral retina (Figure 1.13) (Hecht et al., 1935). Similarly, as the size of the stimulus increases, exciting increasingly peripheral retinal

locations at which rod density is higher, as well as increasing the effect of spatial summation, the rod portion is accentuated and absolute threshold is reduced (Figure 1.13) (Hecht et al., 1935; Wolf & Zigler, 1950). Finally, short wavelength stimuli, to which the rods are maximally sensitive, induce a prominent rod portion (Hecht, 1937).

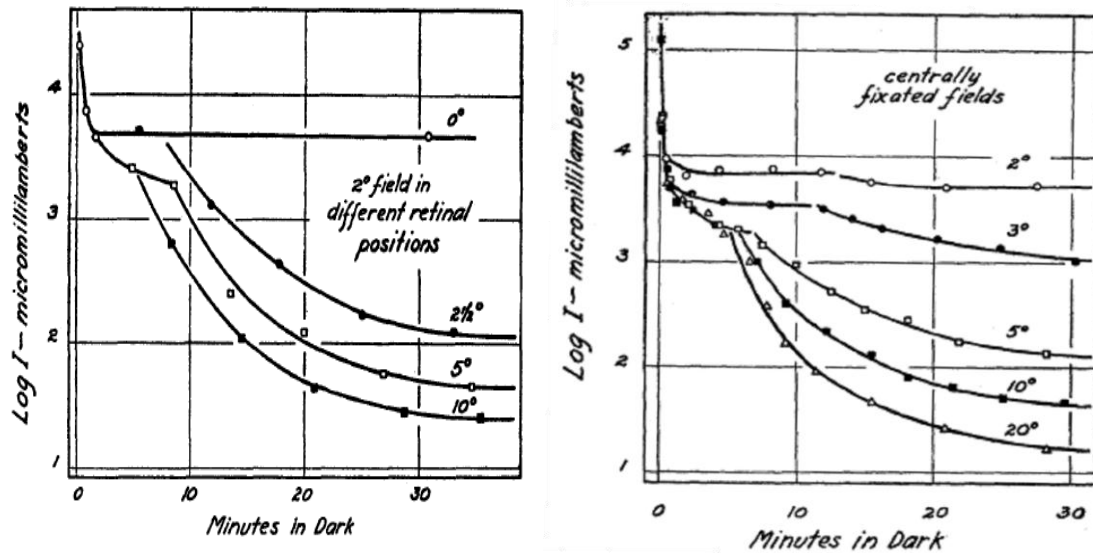


Figure 1.13. Dark adaptation functions recorded using a 2° stimulus placed at different retinal eccentricities (left panel) and a centrally fixated stimulus of increasing size (right panel) (Hecht et al., 1935).

1.3.2. Physiology of dark adaptation: the retinoid cycle

The series of events, initiated by photon capture, which leads to the generation of visual signal, is known as phototransduction (Burns & Baylor, 2001). In the initial stages, the 11-cis retinal chromophore is isomerised to all-trans retinal and the molecule becomes 'bleached'. Once activated in this way, the molecule is unable to respond to a further photon until the 11-cis retinal has been restored (Lamb & Pugh, 2004). In vertebrates, this process of photopigment bleaching and restoration is governed by a process known as the retinoid cycle (Figure 1.14). For an excellent review of the stages of the retinoid cycle, the reader is referred to Lamb and Pugh (2004), a summary of which appears below.

Stage 1: Photoisomerization

On absorption of a photon, the 11-cis retinal chromophore (in rhodopsin or the cone equivalent) is isomerised to all-trans retinal.

formed by the free retinoid is reduced by RDH in the cytoplasm, forming additional all-trans retinol.

Stage 7: Transportation of all-trans retinol

When the all-trans retinol moves across the IPM, it is chaperoned by the interphotoreceptor binding protein: IPBP, to increase its solubility. Within the RPE, this chaperone is replaced by the cellular retinol binding protein (CRBP). Similar chaperone processes exist throughout the retinoid cycle to ensure the delivery of the retinoid to the next locus of activity without degradation.

Stages 8, 9 and 10: Formation of 11-cis retinal within the RPE

The enzyme lecithin retinol acyl transferase (LRAT) is responsible for the esterification of all-trans retinol. The all-trans retinyl ester that is produced is chaperoned by the protein RPE65. The all-trans retinyl ester is then isomerized to 11-cis retinol by the enzyme retinyl ester isomerohydrolase. The 11-cis retinol then undergoes further oxidation to form 11-cis retinal, which is then chaperoned by the cellular retinaldehyde binding protein (CRALBP).

Stages 11, 12 and 13: Formation of rhodopsin/cone photopigment

The 11-cis retinal diffuses across the IPM to the photoreceptor outer segments. When it reaches the disc membranes in the photoreceptor outer segments, it forms a non-covalent bond with opsin. This is converted to a Schiff-base bond and rhodopsin, or the cone equivalent, is formed.

1.3.3. The Müller cell hypothesis: An alternative pathway for photopigment regeneration

Clearly, the presence of a healthy RPE is fundamental to photopigment renewal, and therefore the recovery of visual sensitivity, during the retinoid cycle. Correspondingly, little rhodopsin regeneration occurs in isolated rod photoreceptors (Goldstein, 1970; Jones et al., 1989). Conversely, there is a body of evidence to suggest that cone photopigment can regenerate in the absence of the RPE (Goldstein, 1970; Hood & Hock, 1973; Das et al., 1992; Mata et al., 2002; Wang, & Kefalov, 2009; 2011). In addition, when RPE65, a protein normally abundantly expressed in the RPE, is deficient, all-trans retinyl ester is not converted to 11-cis retinal and there is no regeneration of rhodopsin (Redmond et al.,

1998). However, regeneration of cone photopigment does occur in the RPE65 deficient retina (Redmond et al., 1998). This implies that the cone photoreceptors have access to an alternative supply of retinoid for photopigment regeneration.

The Müller cells have been strongly implicated in the alternative pathway of cone photopigment regeneration (Das et al., 1992; Mata et al., 2002; Wang, & Kefalov, 2009; 2011). Evidence for this secondary pathway initially emerged from studies of the cone-dominated retina of ground-squirrel and chicken (Das et al., 1992; Mata et al., 2002). More recently, this additional pathway was also shown to exist in the rod-dominated retina of the mouse, primate and human (Wang & Kefalov; 2009). Rod photopigment can only regenerate when provided with 11-cis retinal (Jones et al., 1989). In contrast, cone photopigment will regenerate when provided with an alternative form of retinoid: 11-cis retinol. Müller cells contain all-trans-retinol isomerase and 11-cis-retinyl-ester synthase; catalytic enzymes that enable the Müller cells to take up all-trans retinol and convert it to 11-cis retinol, which is then released into the surrounding media and taken up by the cones (Mata et al., 2002). A third enzyme, 11-cis-retinol dehydrogenase, present in cones but not rods, facilitates the final stages of photopigment regeneration.

While rods and cones must compete for RPE derived 11-cis retinal, this additional pathway provides cones with an exclusive secondary source of retinoid. This facilitates rapid photopigment regeneration, which contributes to sustained visual sensitivity in photopic viewing conditions. It has been suggested that this Müller cell pathway has a critical role in the rod-dominated retina, in which the cones compete with the rods for a limited supply of 11-cis retinal from the RPE (Mata et al., 2002).

1.3.4. The retinoid cycle and visual threshold during dark adaptation

Several theories have explored the close relationship between the retinoid cycle and visual threshold during dark adaptation, namely; the photochemical and equivalent background hypotheses.

1.3.4.1. The photochemical hypothesis

It was originally proposed that the visual threshold during dark adaptation was directly proportional to the amount of unbleached photopigment (Hecht et al., 1937), i.e. a 50%

bleach of photopigment would cause threshold to double. However, this hypothesis was later disproved when retinal densitometry data showed that although both the regeneration of rhodopsin and visual threshold during dark adaptation followed an exponential time course, threshold remained elevated by 3 log units after 90% of rhodopsin had regenerated (Campbell & Rushton, 1955).

Following work in the albino rat (Dowling, 1960) and a rod monochromat (Rushton, 1961), it was proposed that the logarithm of the visual threshold during dark adaptation was proportional to the concentration of bleached rhodopsin. This relationship between threshold and bleached rhodopsin is known as the Dowling-Rushton relationship (Equation 1a) and for many years it was adopted as a comprehensive explanation of dark adaptation. The relationship was later also shown to provide an appropriate description of the regeneration of cone photopigment (Hollins & Alpern, 1973).

Equation 1a.
$$\log(I_t/I_a) = \alpha B$$

where I_t is the visual threshold at a given time, I_a is the final dark adapted threshold, α is a constant and B is the proportion of bleached rhodopsin.

The Dowling-Rushton relationship was subsequently shown to be restricted to the description of dark adaptation under specific conditions only (Lamb, 1990; Lamb & Pugh, 2004). When a low intensity photopigment bleach is administered, the initial threshold recorded is markedly higher than that predicted by the model, whereas at large bleaching intensities, the initial threshold is lower than predicted (Lamb, 1990). In addition, the constant ‘ α ’ included in the model has been shown to vary with the bleaching intensity and is therefore not actually a constant (Pugh, 1975).

1.3.4.2. The equivalent background hypothesis

Stiles and Crawford (1932) proposed that the elevation of threshold at any given time during dark adaptation may be described by an ‘equivalent background’. This theory suggests that sensitivity during dark adaptation is equivalent to that produced by exposure to an adapting light (the so-called ‘equivalent background’) and that this equivalent background has the same effect on vision as a real background light (Stiles & Crawford,

1932). Consequently, dark adaptation is considered to be a unique form of light adaptation, in which the adaptational state is quantified in terms of the intensity of a steady background light that would produce an equal desensitization of the retina. During dark adaptation, the equivalent background gradually fades and correspondingly, threshold decreases. The decay of the equivalent background was proposed to be related to a hypothetical photoproduct of bleaching (Stiles & Crawford, 1932).

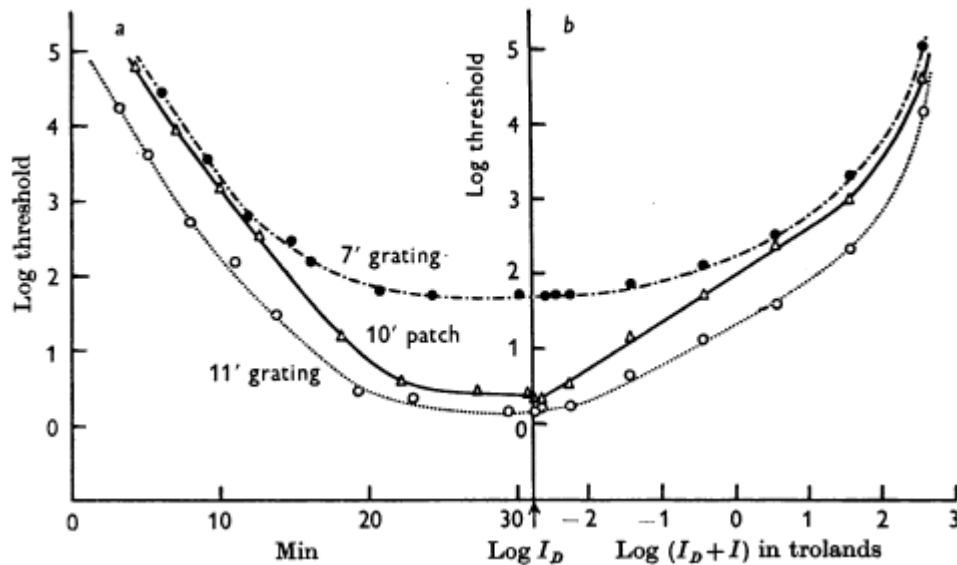


Figure 1.15. Dark adaptation functions (left panel) and increment threshold functions (right panel), recorded in response to a range of stimuli. Threshold at any given time in the dark may be described in terms of the adapting background that produces the same increment threshold as that recorded in the dark (Blakemore and Rushton, 1965).

The equivalent background hypothesis states that threshold elevation, spatial resolution and temporal resolution measured at any given time during dark adaptation should be equivalent to those measured in the presence of a real background light. This was demonstrated by Blakemore and Rushton (1965). Dark adaptation and increment threshold functions were recorded using a range of stimuli, in a rod monochromat, (Figure 1.15). Although the shape of the dark adaptation curve and increment threshold function were different, for all stimuli the threshold at any given time in the dark was equivalent to that measured on a steady background. However, there is evidence to suggest that the equivalent background hypothesis breaks down under certain conditions, for example when the temporal modulation threshold is measured after exposure to a long, dim adapting light (Hayhoe & Chen, 1986).

Researchers have proposed that the photoproduct responsible for generating the equivalent background (and therefore threshold elevation) during dark adaptation is likely to be a metarhodopsin photoproduct, such as free-opsin or all-trans retinal (Lamb & Pugh, 2004). In the 1960s, threshold elevation was shown to be associated with the presence of metarhodopsin photoproducts (Donner & Reuter, 1967). Some years later, when rod dark adaptation data were collected at a range of bleaching intensities, the recovery of the logarithm of visual threshold was accurately described by three straight lines with recovery constants of 5, 100 and 400 seconds (Lamb, 1981). It was proposed that these distinct components were generated by the presence of metarhodopsin photoproducts (Lamb, 1981). Additional evidence for the relationship between metarhodopsin photoproducts and visual threshold elevation emerged from work with the inorganic compound hydroxylamine (Leibrock et al., 1998). When added to rod photoreceptors hydroxylamine was shown to expedite threshold recovery during dark adaptation (Leibrock et al., 1998). As hydroxylamine is known to destroy metarhodopsin, this strongly implied that metarhodopsin photoproducts contribute to the elevation of visual threshold.

As discussed (Section 1.3.2, Page 34), regeneration of visual pigment during dark adaptation requires the recombination of 11-cis retinal with free-opsin. The free-opsin formed when metarhodopsin is hydrolysed has been proposed to be responsible for threshold elevation during dark adaptation, particularly during the second component of rod recovery (Lamb & Pugh, 2004). The time course of threshold recovery during the second component of rod dark adaptation is therefore determined by the removal of opsin as it recombines with 11-cis retinal.

1.3.5. Adaptational dysfunction

1.3.5.1. Dark adaptation and age

Visual difficulties in low illumination are often reported by elderly adults in the absence of ocular pathology (Kline et al., 1992; McGregor & Chaparro, 2005) and, correspondingly, a reduction in photopic and scotopic sensitivity with increasing age has been reported (Robertson & Yudkin, 1944; Steven 1946; Birren et al., 1948; Birren & Shock 1950; Eisner et al., 1987b; Sturr et al., 1997; Jackson et al., 1998). For example, scotopic sensitivity has been shown to decline by 0.51 log units between the ages of 20 and 80 years

(Jackson et al., 1998). The reduction in visual sensitivity that occurs with age may be partially explained by age-related changes to pre-retinal structures that restrict the amount of light reaching the retina, such as age-related pupillary miosis (Birren et al., 1950) and increases in the density of the ocular media (Bron et al., 2000). In addition, retinal changes, including the loss of RPE and photoreceptor cells, are also likely to contribute to diminishing visual sensitivity (Dorey et al., 1989; Gao & Hollyfield, 1992; Curcio et al., 1993). However, differences between the topographical distribution of rod photoreceptor loss and the loci of scotopic sensitivity loss (Curcio et al., 1993; Jackson et al., 1998) imply that additional retinal factors may also contribute to the changes in visual sensitivity.

Although increases in rod thresholds have consistently been reported with increasing age, the dynamics of rod dark adaptation were initially shown to be independent of age (Birren & Shock, 1950). However, contemporary investigations have since reported an age-related slowing of rod dark adaptation (Holopigian et al., 1997; Jackson et al., 2006a), with increases in the time constant of rod recovery of 20.4 seconds/decade (Jackson et al., 1999). The evidence regarding the relationship between age and cone dark adaptation also varies between investigations. Early studies of cone dark adaptation found it to be independent of age (Birren & Shock, 1950; Eisner et al., 1987b). However, more recently the time constant of cone recovery has been reported to increase by 16.4 seconds/decade (Coile & Baker, 1992). The differences in the outcomes of these studies may, in part, be attributed to methodological differences in the study design and will be discussed in detail in Chapter 3.

1.3.5.2. Dark adaptation and retinal disease

As discussed (Section 1.3.2, Page 34), recovery of visual sensitivity in the dark is dependent on the regeneration of visual pigment via the retinoid cycle. This process relies on the integrity of the photoreceptors, RPE, choriocapillaris and Bruch's membrane (Lamb & Pugh, 2004). Consequently, diseases that affect these outer retinal structures are likely to prolong dark adaptation in rods and cones (Midena et al., 1997). Abnormal dark adaptation kinetics have been reported in a range of conditions including retinitis pigmentosa (Moore et al., 1992; Sandberg et al., 1999), congenital stationary night blindness (Petzold & Plant, 2006), Sorsby's fundus dystrophy (Cideciyan et al., 1997), vitamin A deficiency (Kemp et al., 1988, Cideciyan et al., 1997), diabetic retinopathy (Phipps et al., 2006; Newsome &

Negreiro, 2009) and AMD (Steinmetz et al., 1993; Owsley et al., 2001; Phipps et al., 2003; Binns & Margrain, 2007; Owsley et al., 2007; Dimitrov et al., 2008; 2011).

1.3.5.3. Dark adaptation in AMD

As AMD may be considered to be a pathological extension of normal retinal ageing (Zarbin, 2004), it is perhaps unsurprising that abnormal dark adaptation has been reported in AMD (Brown & Lovie-Kitchin, 1983; Eisner et al., 1987a; Collins & Brown, 1989; Eisner et al., 1991; Sandberg & Gaudio 1995; Midená et al., 1997; Owsley et al., 2001; Phipps et al., 2003; Binns & Margrain, 2007; Owsley et al., 2007; Dimitrov et al., 2008; 2011). One of the earliest studies to explore dark adaptation in AMD reported elevated rod and cone thresholds, an increase in the time to RCB (which may be due to a change in cone final threshold or delayed rod adaptation) and slower dark adaptation in participants with AMD (Brown & Lovie-Kitchin, 1983). A myriad of evidence has since emerged regarding the relative adaptational dysfunction of rods and cones in AMD.

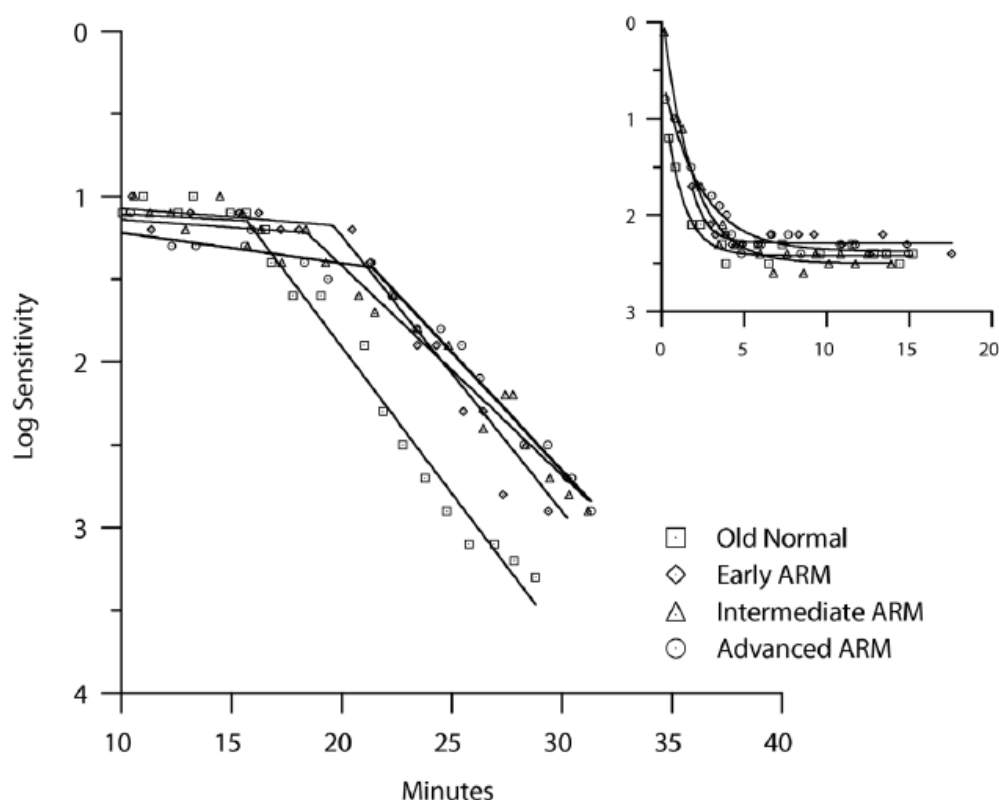


Figure 1.16. Rod dark adaptation (main figure) recorded from one elderly adult in good retinal health and three patients with different stages of AMD. The inset shows the cone dark adaptation data for the same patients (Owsley et al., 2007).

There is a clear consensus within the literature that rod dark adaptation is delayed in early AMD (Brown & Lovie-Kitchin, 1983; Brown et al., 1986a; Owsley et al., 2001; Owsley et al., 2007; Dimitrov et al., 2008; 2011). For example, Owsley et al. (2007) identified significant abnormalities in rod-mediated parameters of dark adaptation, including the time to RCB, rod recovery rate and rod sensitivity in participants with AMD compared to age-matched control participants. Moreover, the extent of the rod recovery deficit in AMD was found to worsen with increasing disease severity (Figure 1.16).

The evidence for abnormal cone dark adaptation in AMD however, is equivocal. In their 2007 study, Owsley et al. reported that cone-mediated parameters of dark adaptation were unaffected by AMD, even during the later stages of the disease. This is consistent with histological evidence to show that rod photoreceptors exhibit the earliest signs of degeneration in AMD, while cones may remain unaffected until later in the disease process (Curcio, 2001). In contrast, there is an emerging body of evidence to indicate that cone-mediated parameters of dark adaptation are highly sensitive to early AMD (Phipps et al., 2003; Dimitrov et al., 2008; 2011). In addition, photostress or ‘glare’ recovery (see Section 1.3.5.4, Page 44) is prolonged in AMD (Smiddy and Fine, 1984; Collins & Brown, 1989; Wu et al., 1990; Sandberg and Gaudio, 1995; Midena et al., 1997; Sandberg et al. 1998; Binns and Margrain, 2007; Newsome & Negreiro, 2009). This discrepancy may relate to the difficulty of accurately monitoring the rapid threshold changes that occur during the initial stages of cone dark adaptation.

When measured alongside other visual functions, such as colour vision and static thresholds, rod and cone dark adaptation appears to be the single most sensitive marker for AMD (Eisner et al., 1991, Owsley et al., 2001; Phipps et al., 2003). It has proved a more sensitive predictor of the disease than conventional clinical tests, including VA, contrast sensitivity and Amsler testing (Midena et al., 1997; Sandberg et al., 1998) and has been identified as an independent risk factor for wet AMD (Sandberg et al., 1998). This has important clinical implications for the early detection of AMD, the management of patients at a high risk of developing the disease and the evaluation of treatment outcomes.

1.3.5.4. Photostress recovery in AMD

‘Photostress recovery’ may also be used as a measure of retinal cone function in AMD (Glaser et al., 1977). During conventional dark adaptation measurement, visual threshold is monitored over time in the dark. In contrast, during photostress testing the eye is exposed to an intense light from an ophthalmoscope or pen torch and the time taken for a particular aspect of visual function, such as VA or contrast sensitivity, to return to a predetermined level is monitored. Prolonged photostress recovery has been reported in AMD (Glaser et al., 1977; Collins & Brown, 1989; Wu et al., 1990; Cheng & Vingrys, 1993; Sandberg & Gaudio, 1995; Midena et al., 1997; Bartlett et al., 2004; Newsome & Negreiro, 2009). The delay in photostress recovery appears to parallel disease progression, as longer recovery times have been recorded in advanced disease (Cheng & Vingrys, 1993; Midena et al., 1997). There is also evidence to suggest that the photostress test has the potential to identify eyes at risk of development of CNV (Sandberg & Gaudio, 1995; Sandberg et al., 1998).

The psychophysical photostress test is little used by clinicians due to the absence of a standardized protocol for the technique (Margrain & Thomson, 2002). The Eger Macular Stressometer (EMS) was developed to address this issue in order to provide a standardized clinical tool to monitor photostress recovery (Neelam et al., 2009). Initially, significant differences in photostress recovery times between participants with AMD and healthy controls were measured using the device (Bartlett et al., 2004). However, later evidence failed to identify a difference between the two groups, possibly due to the use of an insufficient pre-adapting light source (Wolffsohn et al., 2006). Recently, a new commercially available clinical tool for measuring photostress recovery has been developed. Preliminary data using the Macular Degeneration Detection Device (MDD-2) were favourable (Newsome & Negreiro, 2009); however the diagnostic/prognostic potential remains unexplored.

1.4. Visual psychophysics

Chapter 2 describes the evaluation of four psychophysical methods of measuring threshold during dark adaptation. The measurement of psychophysical thresholds is often problematic but during dark adaptation the challenge is even greater because of the rate at

which threshold changes, particularly during the early stages of cone recovery. To acquaint the reader with the range of psychophysical methods available and some of the associated challenges, this section describes some of the key psychophysical methods that may be used to quantify dark adaptation.

1.4.1. Classical psychophysical methods

Psychophysics is the scientific study of the relationships between physical stimuli and perceptual sensations (Gescheider, 1997). It is based around the concept of threshold testing. Sensory events must exceed a critical strength, known as a sensory threshold, in order to enter conscious awareness. ‘Absolute threshold’ describes the smallest amount of stimulus energy required to produce a sensation. In visual psychophysics, this is the fully dark adapted threshold. When operating in the range above absolute threshold, many aspects of vision may be assessed by recording thresholds, for example, acuity, contrast, colour and flicker thresholds. A ‘difference threshold’ is defined as the smallest change in stimulus energy required to produce a ‘just noticeable difference’ in sensation. Weber’s law states that the difference threshold is dependent on the starting energy of the stimulus and that it remains a constant fraction of that starting energy i.e. at high stimulus energies, a larger difference must exist between two stimuli for perception of a difference threshold (Green & Swets, 1966).

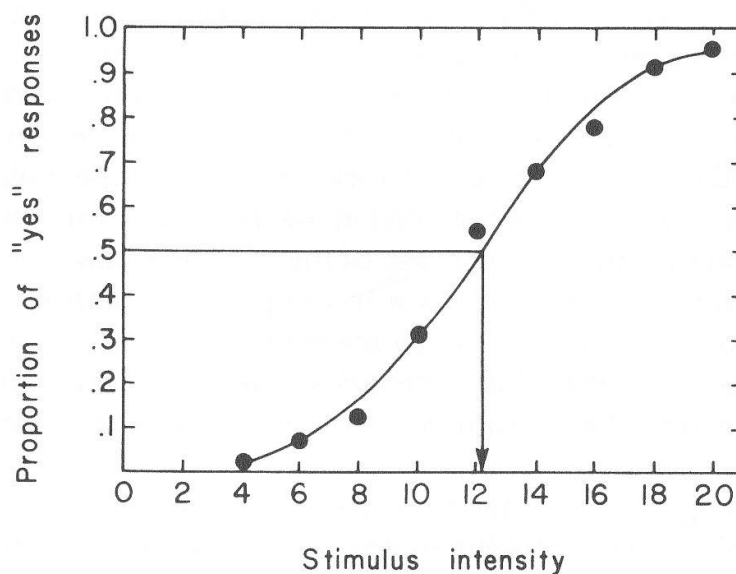


Figure 1.17. A typical psychometric function (Gescheider, 1997). Threshold is the stimulus intensity that would be detected 50% of the time.

As biological systems are subject to variation in their response patterns, psychophysical thresholds are liable to vary. Fundamental to this concept is the psychometric function, which plots the probability of a correct response at a range of stimulus intensities (Figure 1.17). At high stimulus intensities, above the observer's threshold, the stimulus is correctly detected on every trial. Conversely, at low stimulus intensities, which are well below the observer's threshold, the stimulus remains undetected on every trial. Threshold is typically taken as the stimulus level that corresponds to an intermediary level of performance, such as 50% detection rate (Gescheider, 1997).

In 1860, Fechner described three methods of threshold measurement, which have since been widely used (Treutwein, 1995):

- the method of constant stimuli
- the method of limits
- and the method of adjustment.

1.4.1.1. The method of constant stimuli

The method of constant stimuli involves the repeated presentation of a fixed collection of stimulus levels, in a random order, throughout the experiment. The cumulative responses are used to plot a psychometric response function to illustrate the rate of detection as a function of stimulus intensity (Figure 1.17). Threshold is usually defined as the stimulus level that corresponds to a 50% detection rate.

1.4.1.2. The method of limits

During the methods of limits, stimuli are presented in ascending or descending steps until the observer first reports the appearance or disappearance of the stimulus. The procedure is repeated several times and threshold is calculated as the average of the threshold points estimated by several ascending and descending series.

1.4.1.3. The method of adjustment

The observer is responsible for altering the level of the stimulus during the method of adjustment. A number of ascending and descending series are completed and threshold is calculated by averaging the responses.

1.4.1.4. Disadvantages of classical psychophysical methods

Humans are not perfect observers. Given that classical psychophysical methods are reliant on subjective feedback from the observer, they are often subject to degradation by a series of inconsistencies (Kalloniatis & Luu, 2011). Habituation errors manifest as a tendency by the observer to repeatedly give the same response on consecutive trials. Conversely, anticipation errors occur when the observer reports seeing the stimulus before their true threshold has been reached. These errors result in false threshold points being recorded. The randomisation of the order in which the stimuli are presented during the method of constant stimuli helps to minimise these errors of habituation and anticipation.

Classical psychophysical methods have also been criticised for their time consuming nature, the lack of justification for certain aspects of the procedures, redundant data collection at stimulus levels far from threshold and the lack of control over the observer's decision criterion (Treutwein, 1995).

1.4.2. Adaptive psychophysical methods

In contrast to the classical psychophysical methods described, adaptive procedures are performance dependent, that is, the stimulus presented on any one trial is determined by one, several or all of the preceding responses given by the participant (Hall, 1981). Adaptive procedures aim to improve the efficiency of testing by concentrating stimulus presentations at or near the presumed threshold, thereby minimising redundant presentations (Treutwein, 1995).

Adaptive psychophysical methods should clearly specify the following conditions (Treutwein, 1995):

- when to change the testing level and what the next testing level should be
- when to terminate the test sequence
- and how to determine the estimate of final threshold.

A summary of several of the key adaptive psychophysical procedures is included here. However, for a comprehensive review of adaptive methods the reader is referred to Treutwein (1995).

1.4.2.1. The staircase procedure

The staircase procedure is based on the method of limits and was developed in order to improve the efficiency of testing (Cornsweet, 1962). Stimuli are first presented in an ascending or descending series until the observer reports the appearance or disappearance of the stimulus. The direction of stimulus presentation is then reversed and a second series completed. Additional series, starting progressively closer to threshold, are implemented each time the appearance or disappearance of the stimulus is reported. Threshold is then calculated as the average of the reversal values. This method eliminates largely redundant presentations, which increases the efficiency of the procedure.

1.4.2.2. Parameter estimation by sequential testing (PEST)

The PEST procedure was designed to address the problem of determining the optimal starting stimulus level and change in stimulus level with each presentation (Taylor & Creelman, 1967). The initial stimulus level is set by the investigator and the aim is to determine, in as few trials as possible, whether the testing level is above or below threshold. The testing level is then progressively modified in order to move closer to threshold. The session begins with large step sizes, which become progressively smaller as threshold approaches (Taylor & Creelman, 1967). Threshold is recorded as the final testing level.

1.4.2.3. Maximum-likelihood procedures

During a maximum-likelihood procedure, the stimulus level presented at each trial is determined by a statistical estimation of threshold based on all of the observer's responses throughout the session (Hall, 1981). After each trial, a new threshold estimate is calculated and the stimulus level is adjusted accordingly. The final threshold is reached after a predetermined number of trials or when there is minimal change in the stimulus level between trials.

The maximum-likelihood method has formed the basis for techniques such as QUEST (quick estimate by sequential testing), ZEST (zippy estimate of sequential testing), SITA (Swedish interactive threshold algorithm) (Kalloniatis & Luu, 2011) and the 'hybrid-adaptive procedure' (Friedburg et al., 1998). During these procedures, prior knowledge about the distribution of threshold for a given stimulus, from published data or pilot

studies, is used to construct a probability distribution function. On the basis of this information a stimulus is presented that is most likely to be at the observer's threshold. The observer's response is used to modify the probability distribution function before the next stimulus is presented. The observer's threshold is defined as the point at which the stimulus intensity becomes stable.

1.4.3. Forced-choice psychophysical methods

Forced choice psychophysical methods, based on the theory of signal detection (TSD) (Tanner & Swets, 1954), were developed to minimise the effects of noise and changes in the observer's criterion on the results obtained; therefore improving the reliability of psychophysical data.

Signals generated by a stimulus occur against a background of randomly occurring noise. Two overlapping probability distribution functions are formed (Figure 1.18): SN, which comprises the signal and the noise, and N, which comprises the noise only (Tanner & Swets, 1954). These two distributions are assumed to be Gaussian and of equal variance. The observer must decide, on the basis of neural activity, whether a particular sensation may be attributed to the signal or is evoked by noise alone. When the signal is small, there is a higher degree of overlap between the two distributions (Figure 1.18), which makes it increasingly difficult for the observer to differentiate between the distributions.

The theory of signal detection assumes that the observer designates a response criterion on which to base their judgements (Tanner & Swets, 1954). The signal must exceed the observer's criterion for detection to occur. Consequently, the performance during a psychophysical task is dependent on the degree of overlap between the SN and N distributions, as well as the observer's criterion level. The outcomes of a psychophysical procedure become biased if the observer fails to maintain a consistent response criterion throughout the procedure. A range of psychophysical procedures based on the principles of TSD have developed to minimise the effect of changes in the observer's criterion on the results obtained.

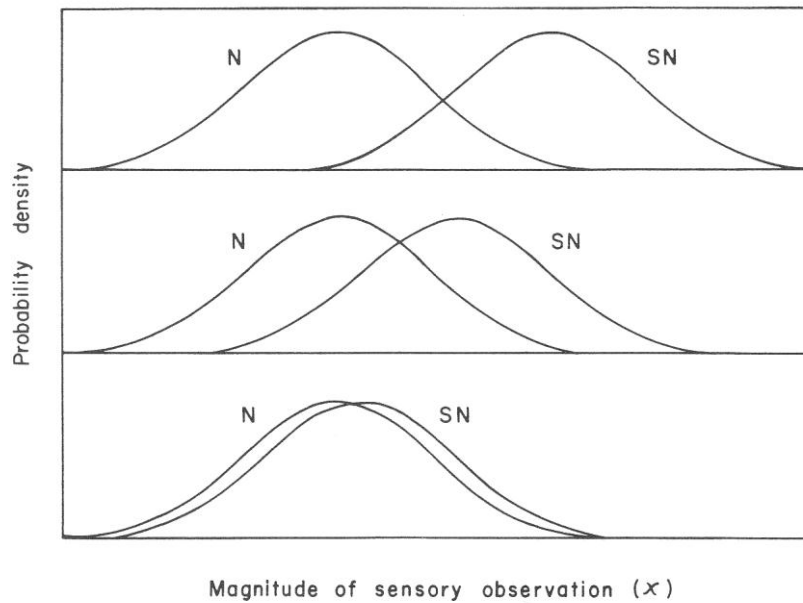


Figure 1.18. Theoretical probability distribution functions of signal and noise (SN) and background noise alone (N) for three different values of signal strength. The top panel shows the strongest signal while the second and third panels show progressively smaller signals (Gescheider, 1997).

1.4.3.1. Forced choice methods

During a forced-choice procedure, the observer is required to select one of a number of presented options on every trial. In the absence of a response bias, the observer should select the option that contains the largest sensory signal (Green & Swets, 1966). As the number of options available to the observer increases, the probability of a correct response due to chance alone declines (Gescheider, 1997). Forced-choice methods have been shown to consistently produce lower and more accurate threshold estimates compared to unforced subjective procedures because the measurements are criterion free (Sekuler & Blake, 2006).

1.4.3.2. Yes-No methods

During a Yes-No procedure, the observer is required to judge the presence or absence of a signal (Green & Swets, 1966). A designated proportion of trials contain a signal, while the remainder contain noise alone. Presentation cues, such as light or sound, are used to signal the start of the trial.

1.4.4. Psychophysical assessment of dark adaptation

The fundamental difficulty associated with measuring visual thresholds during dark adaptation is the speed with which threshold changes. This is especially problematic when monitoring cone dark adaptation, in which threshold falls by approximately 2 log units during the initial 10 minutes in the dark (Hecht et al., 1937, Hollins & Alpern, 1973). Clearly, rapid psychophysical methods capable of obtaining robust and repeatable threshold measurements are necessary, and consequently many of the more robust techniques, such as forced-choice methods, have been rejected in favour of faster techniques.

Early work by Hecht et al (1935; 1937) used a custom made dark adaptometer and the method of adjustment to explore dark adaptation. Many other investigators have since developed custom-made dark adaptometers in order to record dark adaptation data during their experiments (Hecht & Shlaer, 1938; Goldstein, 1975; Henson & Allen, 1977; Friedburg et al., 1998; Jackson et al., 1999). However, there are currently only a small number of commercially available instruments for the clinical assessment of dark adaptation, including LKC Technologies' SST-1 (Peters et al., 2000; Jackson et al., 2006b) and Apeliotus Vision Science's AdaptDx (Jackson & Edwards, 2008).

The Goldmann-Weekers adaptometer was considered the 'gold standard' method for measurement of dark adaptation for many decades. It used an operator controlled 'method of ascending limits' to determine the visual threshold, which was recorded directly onto logarithmic paper (Dieterle & Gordon, 1956). This 'method of limits' has formed the basis for many custom-made dark adaptometers that implement simple computer controlled staircases, similar to those used in visual field testing equipment (Jackson et al., 1999, Owsley et al., 2001, Owsley et al., 2007; Jackson & Edwards' 2008)

The increasing sophistication of computer technology has enabled the implementation of increasingly complex algorithms that present stimuli according to adaptive psychophysical principles, such as the hybrid adaptive procedure described by Friedburg et al. (1998). This procedure uses a set of three decision criteria to determine the luminance of the stimulus on the basis of all of the participant's previous responses during the session, and a maximum-likelihood computation to calculate threshold (Friedburg et al., 1998). Despite

their theoretical advantages, forced choice procedures have not, thus far, been used to track threshold during dark adaptation.

1.5. The electroretinogram (ERG)

The electroretinogram (ERG) is an objective, non-invasive method of assessing the integrity of the retina (Berrow et al., 2010). Measured at the cornea, the ERG is the summed potential arising from the retinal cells in response to light stimulation (Robson & Frishman, 1999). As discussed in a recent review (Berrow et al., 2010) the ERG has been used to investigate retinal function in AMD and therefore this section aims to provide the reader with an overview of common ERG techniques.

1.5.1. The transient (flash) ERG

Recorded in response to a single flash stimulus, the transient ERG is a highly repeatable waveform comprising distinct features that represent the electrical activity of different groups of retinal cells. Granit's classic 1933 analysis of the scotopic transient ERG in the cat retina showed that the signal was the result of three distinct underlying physiological processes (Figure 1.19). These three independent processes dominate the ERG at different times following light stimulation: PI is a slow positive component, PII a moderately fast positive component and PIII is a negative component comprising fast and slow portions (Granit, 1933). The three processes combine to form the subcomponents of the ERG waveform and so are inseparable in the standard flash ERG.

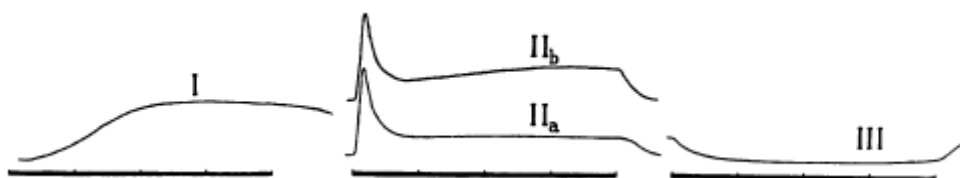


Figure 1.19. The three ‘fundamental’ processes of the ERG (After Granit, 1933).

The subcomponents of the ERG are formed by the summation of the active retinal elements at any given moment after the offset of the stimulus. Several methods have been used in experimental animals to identify the cellular origins of these components (Robson

& Frishman, 1999). During current source-density analysis microelectrodes are used to identify the retinal layer from which the electrical signals originate (Penn & Hagins, 1969; Witkovsky et al., 1973). Alternatively, pharmacological agents may be used to block synapses between the retinal layers to isolate the origin of the signal (Sillman et al., 1969; Wakabayashi et al., 1988; Stockton & Slaughter, 1989; Bush & Sieving, 1994; Viswanathan et al., 1999; Xu & Karwoski, 1994; Lei & Perlman, 1999). In humans, the effect of diseases known to affect specific populations of retinal neurons on the ERG subcomponents provides further evidence for their origin, as does the change in the ERG waveform under different adaptational and stimulus conditions (Robson & Frishman, 1999).

1.5.1.1. Early receptor potential (ERP)

First identified in 1964, the ERP is only recorded when the eye is exposed to a very bright flash of less than 1ms duration (Brown & Murakami, 1964; Galloway, 1967). It is a biphasic waveform, comprising a small positive phase followed by a larger negative phase. The ERP is the fastest occurring waveform of the ERG and is thought to originate from the photoreceptor cells (Fain, 2006).

1.5.1.2. a-wave

Dominated by Granit's 'fast PIII' process, the a-wave is a negative potential that occurs within 25 msec of the flash offset (Figure 1.20) (Robson & Frishman, 1999). The amplitude and latency of the a-wave are dependent on the adaptational state of the eye. In both photopic and scotopic conditions the a-wave is truncated by the rising edge of the b-wave (Frishman, 2006). The early portion of the a-wave is generally considered to reflect photoreceptor activity (Penn & Hagins, 1969; Sillman et al., 1969; Wakabayashi et al., 1988). Current source density analysis has demonstrated that the a-wave follows a similar time course to the light-evoked extracellular current of the photoreceptors (Penn & Hagins, 1969). In addition, the a-wave is not extinguished by the administration of sodium aspartate, a glutamate agonist that prevents the transmission of signal from the photoreceptors to the bipolar cells (Sillman et al., 1969; Wakabayashi et al., 1988). More recently, Bush and Sieving (1994) used more specific glutamate agonists and antagonists to demonstrate that there is also an inner retinal contribution to the a-wave of the photopic ERG, which is more dominant at low stimulus intensities (Bush & Sieving, 1994).

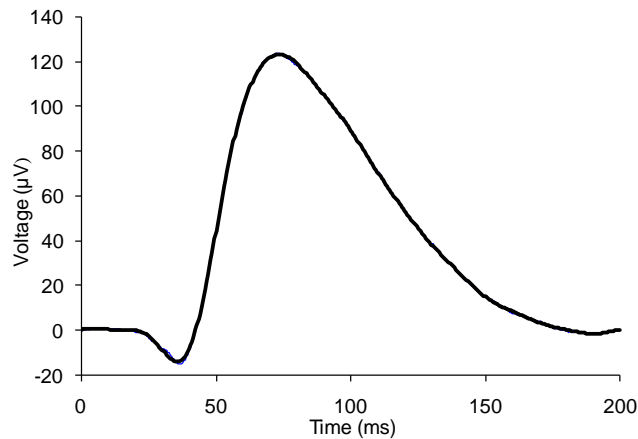


Figure 1.20. A dark-adapted ERG recorded from our own laboratory. The initial negative component is the a-wave. This is followed by a large positive component: the b-wave.

1.5.1.3. b-wave and oscillatory potentials (OPs)

The b-wave is a positive potential, which occurs after the a-wave, and is dependent on the underlying PII process (Figure 1.20) (Frishman, 2006). PII has been shown to originate from ON-bipolar activity, but intracellular recordings from the mudpuppy retina and current source density analysis in the monkey retina initially also implicated the Müller cells in the generation of the b-wave (Miller & Dowling, 1970; Heynen & van Norren, 1985). However, later evidence showed that the b-wave was relatively unaffected when barium ions were administered to block Müller cell activity in the frog and rabbit retina (Xu & Karwoski, 1994; Lei & Perlman, 1999). In contrast, administration of 2-amino-4-phosphonobutyrate, a glutamate known to eliminate the ON-bipolar cell response, was shown to extinguish the b-wave in the mudpuppy and salamander (Stockton & Slaughter, 1989). Therefore, although Müller cell activity may contribute to the b-wave, it is now generally accepted that the b-wave directly reflects the activity of the ON-bipolar cells (Xu & Karwoski, 1994; Stockton & Slaughter, 1989).

Exposure to a bright flash evokes a series of small wavelets, known as oscillatory potentials, superimposed on the rising edge of the b-wave (Lachapelle, 2006). This low voltage, high frequency component of the ERG may be isolated using a bandpass filter, where the low-frequency cut-off is set at 70-100Hz and the high-frequency cut-off is set to at least 300Hz (Marmor et al., 2009). Although the exact origin of the oscillatory potentials is unconfirmed, they are believed to be postreceptoral in origin, and there is evidence to suggest input from both the retinal ganglion and amacrine cells (Lachapelle, 2006).

1.5.1.4. Photopic negative response (PhNR)

The PhNR is a negative wave that follows the b-wave under photopic conditions and is most clearly visible when the ERG is recorded in response to a red stimulus presented on a blue background (Frishman, 2006). There is a range of evidence to suggest that it originates in the RGCs (Viswanathan et al., 1999; Drasdo et al., 2001; Viswanathan et al., 2001; Tamada et al., 2010). When tetrodotoxin, a neurotoxin, was used to block ganglion cell action potentials in monkeys, the PhNR was eliminated (Viswanathan et al., 1999). In addition, the PhNR was also extinguished when experimental glaucoma was induced in the monkeys (Viswanathan et al., 1999). In humans, a reduction in the amplitude of the PhNR has been linked to retinal ganglion cell loss in primary open angle glaucoma (Drasdo et al., 2001; Viswanathan et al., 2001; Tamada et al., 2010).

1.5.1.5. Scotopic threshold response (STR)

This negative potential is only evident when an extremely dim flash is presented to the dark-adapted eye (Sieving et al., 1986; Sieving & Nino, 1988; Wakabayashi et al., 1988). As the intensity of the stimulus increases, it is obscured by the much larger b-wave. Unlike the a-wave, the STR is eliminated by the administration of sodium aspartate, which implies that it is postreceptoral in origin (Wakabayashi et al., 1988), and it is generally considered to originate from the amacrine or ganglion cells of the rod pathway (Sieving & Nino, 1988; Wakabayashi et al., 1988).

1.5.1.6. c-wave

When a bright flash is presented to the dark adapted eye, the b-wave is followed by a slow positive phase, known as the c-wave. It is largely dependent on rod photoreceptor cell activity and is therefore most distinct in dark adapted conditions. The c-wave is generally considered to be the sum of positive PI and slow negative PIII (Frishman, 2006). The positive process contributing to the c-wave has been attributed to the RPE, as it is abolished by intravenous injection of sodium iodate, which is poisonous to RPE cells (Noell, 1953) and by removing the RPE in the frog retina (Sillman et al., 1969). In contrast, intraretinal recordings have indicated that the slow negative contribution to the c-wave originates from a cell that spans the whole retina, such as the Müller cell (Witkovsky et al., 1973). There is evidence that both of the processes contributing to the c-wave are

generated by the reduction in extracellular potassium concentration in the subretinal space that occurs in response to light (Oakley & Green, 1976; Bolnick et al., 1979; Hu & Marmor, 1984).

1.5.1.7. d-wave

The positive d-wave occurs when a long duration stimulus is presented under photopic conditions (Figure 1.21). It is eliminated by pharmacological suppression of the OFF-bipolar cells and is proposed to reflect the fluctuation in potassium ions caused by depolarization of the OFF-bipolar cells at the light offset (Stockton & Slaughter, 1989).

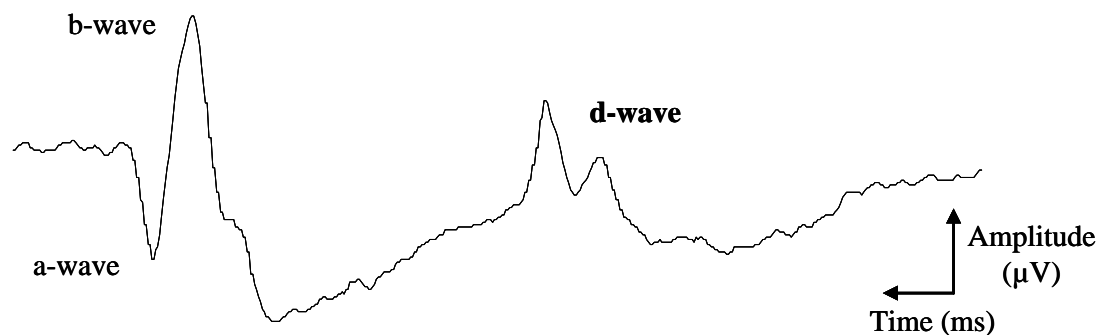


Figure 1.21. The d-wave of the photopic ERG recorded in our own laboratory.

1.5.2. The steady state (flicker) ERG

When stimuli are presented to the eye in quick succession, the responses to successive stimuli are likely to overlap. Consequently, ERGs recorded in response to a flickering stimulus form a sinusoidal waveform that matches the frequency of the stimulus, known as a 'steady state' response (Figure 1.22). At stimulus frequencies greater than 15Hz the steady state response is an isolated cone photoreceptor response, as rod photoreceptors are unable to detect higher temporal frequencies due to their poor temporal resolution (Hecht & Schlaer, 1936; Sharpe et al., 1989). Pharmacological suppression of the postreceptoral contribution to the response has been shown to virtually eliminate the flicker ERG (Bush & Sieving, 1996; Kondo & Sieving, 2002). This major postreceptoral contribution to the flicker ERG has primarily been attributed to the bipolar cells (Bush & Sieving, 1996; Kondo & Sieving, 2002).

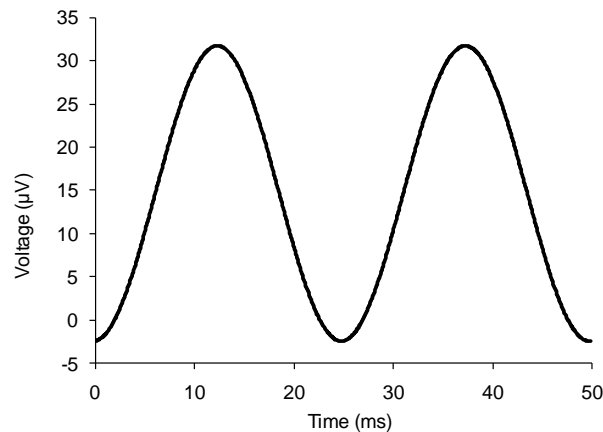


Figure 1.22. A steady state ERG recorded in response to a 41Hz flickering stimulus in our own laboratory.

1.5.3. The focal ERG

As described (Section 1.5, Page 52), the full field ERG is a summed response from all of the retinal cells in response to light stimulation (Robson & Frishman, 1999). Consequently, it is relatively insensitive to the functional changes that occur in diseases such as AMD, which affect a much smaller retinal area (Sunness et al., 1985; Holopigian et al., 1997; Jackson et al., 2004). In contrast, the focal ERG allows selective stimulation of a discrete retinal locus to facilitate identification of localised defects. In order to avoid stimulation of the peripheral retina by scattered light during focal ERG recording, a desensitising surround or background should be used. This is particularly important when recording rod-dominated focal ERGs, as rods lack directional sensitivity and so are particularly prone to stimulation by scattered light, which causes the formation of a double b-wave, making the focal rod response difficult to interpret (Fry & Bartley, 1935; Sandberg et al., 1996; Hood et al., 1998). The application of the desensitising surround, as well as several other approaches that have been used to eliminate the scattered light response during focal ERG recording, will be described in Section 6.2.1 (Page 157).

1.5.4. The multifocal ERG (mfERG)

The multifocal ERG (mfERG) allows simultaneous assessment of numerous discrete locations within the central retina. It is usually a cone-specific response, recorded under light-adapted conditions from the central 20-30° of the retina (Hood et al., 2011). The stimulus comprises an array of hexagonal elements (Figure 1.23), usually 61 or 103, which are scaled to produce responses of equal amplitude at all locations (in a control subject)

(Sutter & Tran, 1992). During the recording period, each hexagon flickers in a pseudo-random sequence of black and white presentations. The local ERG signal is then calculated by correlating the continuous signal with the on- and off- responses at each retinal location (Hood et al., 2011). The resultant mfERG waveform obtained at each retinal location consists of three components (Figure 1.23): two negative peaks (N1 and N2) and a positive peak (P1) (Hood & Birch, 2006). Pharmacological evidence has shown that the mfERG is primarily dependent on bipolar cell activity, with smaller contributions from the photoreceptor and inner retinal cells (Hood et al., 2002). Adapted mfERG protocols have been developed to assess rod pathway function (Hood et al., 1998; Chen et al., 2004).

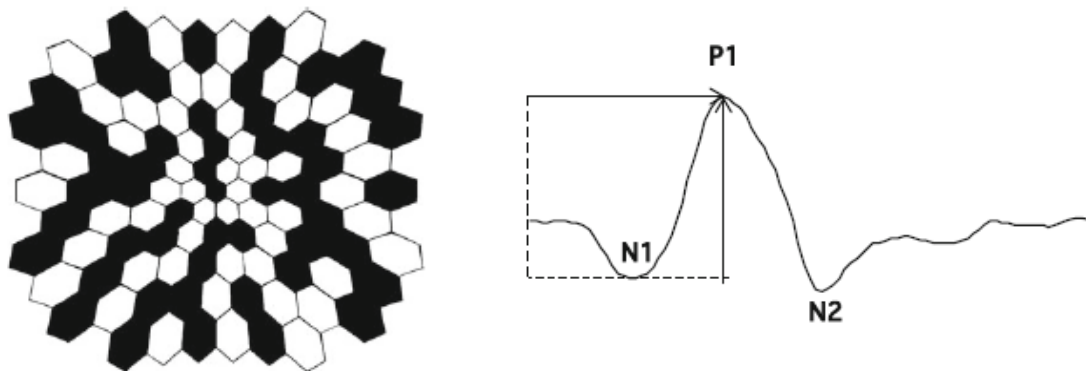


Figure 1.23. The multifocal ERG (mfERG). The left panel illustrates a typical array of 103 hexagons used to elicit a retinal response (right panel) at each retinal location (adapted from Hood et al., 2011).

1.5.5. The pattern ERG (PERG)

The pattern ERG (PERG) is evoked by stimulating the central retina with a reversing black-white square checkerboard or grating stimulus of constant mean luminance (Holder et al., 2007). The transient PERG consists of three components (Figure 1.24): a small negative component at 35msecs (N35), a positive component at 45-60msecs (P50), and a larger negative component at 95-100msecs (N95) (Holder et al., 2007).

There is evidence to suggest that the PERG originates from the inner retina, specifically the RGCs (Maffei & Fiorentini, 1981; Maffei et al., 1985). For example the PERG was extinguished after the optic nerve was sectioned in the cat and primate retina (Maffei & Fiorentini, 1981; Maffei et al., 1985). More recently, when tetrodotoxin was used to block ganglion cell action potentials in the monkey, the P50 component of the response was markedly reduced and N95 was completely extinguished (Viswanathan et al., 2000). The P50 component appears to be less reliant on RGC activity, for example, it shows less

spatial tuning than N95 (Berninger & Schuurmans, 1985). A reduced N95:P50 amplitude ratio is therefore thought to be indicative of RGC disease (Holder et al., 1999).

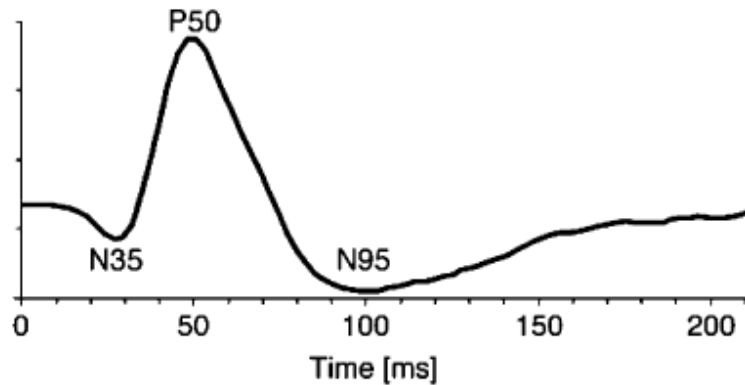


Figure 1.24. The pattern ERG waveform (Holder et al., 2007).

1.5.6. Recording the ERG

The International Society for Clinical Electrophysiology of Vision (ISCEV) has published standardized protocols to allow comparable full field ERGs to be recorded worldwide (Marmor et al., 2009). These are regularly reviewed to keep pace with advances in knowledge and technology. Five standard responses are outlined (Figure 1.25a) and an additional two dark adapted ERGs recorded in response to high intensity flashes are recommended (Figure 1.25b). The use of a modifiable stimulus is advised, in order to allow adjustment of stimulus intensity, frequency and wavelength. In addition, the guidelines recommend maximal pupil dilation and pre-adaptation to the ambient light levels prior to ERG recording. However, there are currently no published standards for the recording of focal ERGs.

1.5.6.1. Electrodes

Active, reference and ground electrodes are required to record an ERG. The active electrode should maintain contact with the cornea or bulbar conjunctiva, while the corresponding reference electrode should be proximal to or contacting the eye. Ideally, the active and reference electrodes should be of the same metallic type to ensure that the potential difference between the two is zero (Coupland, 2006). A third electrode, the ground, is usually placed on the forehead or the ear.

The amplitude of the ERG is dependent on the contact between the active electrode and the cornea (Marmor et al., 2009). Corneal contact lens electrodes are considered the ‘gold standard’, but are uncomfortable, require topical anaesthetic and impair vision when in place. The Dawson-Trick-Litzkov (DTL) electrode, a low mass silver impregnated nylon fibre that is draped in the lower fornix, was developed in order to overcome these problems (Dawson et al., 1979). The signal obtained when a DTL electrode is used is of similar quality as that obtained using a contact electrode, (Dawson et al., 1979), although smaller in amplitude (McCulloch et al., 1997).

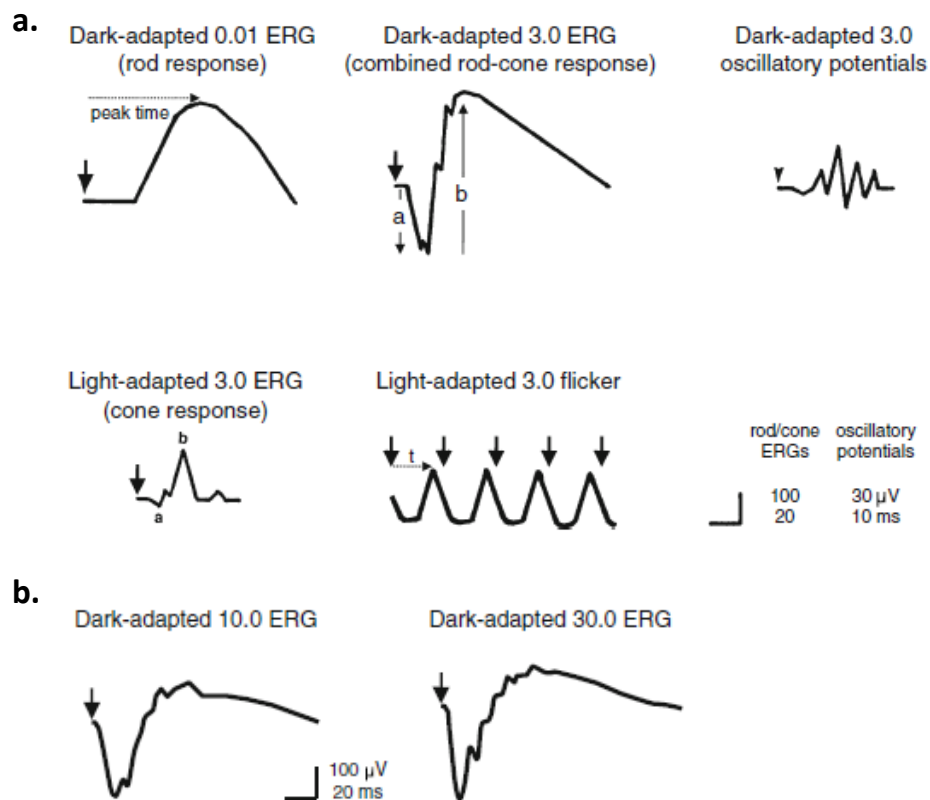


Figure 1.25. Standard full field ERG responses as defined by ISCEV (Marmor et al., 2009). The five responses shown in the top panel (a) should be recorded as standard. The additional dark adapted responses shown in the bottom panel (b) are also recommended. The large arrow heads indicate the stimulus flash.

1.5.6.2. Electrical noise and noise reduction

Evoked potentials within the visual system are extremely small and are therefore easily affected by electrical noise. This may include mains interference (50Hz in the UK), randomly occurring electrical noise (internal and external) and unwanted biological noise, such as muscle activity. A high signal-to-noise ratio (SNR) is necessary to obtain a high

quality signal and, consequently, a range of techniques has emerged to minimise the effect of electrical noise on ERG recording.

The electrical activity recorded by the active electrode comprises both signal and background noise, whereas the reference electrode records noise alone. Differential amplification, where the electrical activity recorded by the reference electrode is subtracted from that recorded by the active electrode, may be used to isolate the true retinal signal (Weisinger et al., 1996).

An evoked potential is time locked to the stimulus, whereas electrical noise is spontaneous and occurs randomly. Consequently, the averaging of multiple ERG traces, or recordings, reinforces the signal but cancels out the noise. This is particularly important when recording low amplitude ERGs (Marmor et al., 2009). However, as recording multiple ERG traces can be time consuming, it is important to select a level of averaging that reinforces the signal but does not require a disproportionately long recording session.

Blinks and eye movements are examples of biological artefacts that generate relatively high voltages that distort the ERG signal. Prior to ERG recording, the acquisition system may be programmed to reject any electrical signals of an amplitude that falls above a preset value. Traces containing components that are greater than this 'artefact reject' setting are excluded from the averaging process (Hogg & Nusinowitz, 2006).

The majority of transient and flicker ERG waveforms fall within the limited frequency range of 1 to 100Hz. Electronic filters may be applied to reduce the amount of redundant data that is collected (Hogg & Nusinowitz, 2006). The application of a high pass filter eliminates frequencies that fall below the range of interest. Conversely, the application of a low pass filter eliminates those frequencies that fall above the range. Alternatively, bandpass filters may be used to reject frequencies outside of a given range. At specific frequencies for which noise is particularly problematic, for example the mains interference that occurs at 50Hz, a notch filter may be applied to remove the frequencies within a given range. However, as these electronic filters do not have a sharp cut off at any given frequency, they may distort the waveform of the ERG (Hogg & Nusinowitz, 2006).

1.5.7. The ERG in AMD

There is currently no electrophysiological technique that is considered to be the ‘gold standard’ method for the investigation of retinal dysfunction in AMD (Gerth, 2009). Consequently, a variety of techniques have previously been used to investigate AMD.

The full field ERG is a summed response generated by the whole retina and it is therefore unsurprising that some investigations have shown it to be insensitive to the subtle, localised dysfunction that occurs in early AMD (Sunness et al., 1985; Holopigian et al., 1997; Jackson et al., 2004). For example, the a-wave amplitude of the full field rod mediated ERG has been shown to be similar in participants with early AMD and healthy controls (Jackson et al., 2004). However, a reduction in the a-wave amplitude was later demonstrated in participants with advanced AMD (Jackson et al., 2006a). In addition, a reduction in the amplitude of the a- and b-waves of the photopic ERG has been recorded in patients with established AMD (Walter et al., 1999). This indicates that although full field ERGs may be useful to monitor the progression of advanced AMD, they are likely to be less valuable for the diagnosis of early AMD.

Multifocal ERGs (mfERG) allow the electrical activity from a number of specific retinal locations to be recorded in isolation. Reductions in photopic (Huang et al., 2000; Li et al., 2001; Chen et al., 2004) and scotopic (Chen et al., 2004; Feigl et al., 2005b; 2006) mfERG amplitudes have been recorded in patients with AMD compared to healthy control participants. While the reduction in the amplitude of the photopic mfERG was shown to be independent of retinal eccentricity, the reduction in the amplitude of the scotopic mfERG was maximal at approximately 5° from fixation (Chen et al., 2004). This is consistent with histological evidence to suggest that rod loss in AMD is maximal in the parafovea (Curcio et al., 1996). However, although the photopic mfERG is widely used, the scotopic mfERG is more difficult to record and therefore not suitable for use in all patients (Hood et al., 1998). The reader is referred to Berrow et al. (2010) for a comprehensive review of the use of the mfERG for the assessment of AMD.

Similarly, focal ERGs may be used to isolate the electrical signal from a discrete retinal location, for example the macula. There is evidence to suggest that focal ERGs recorded at the macula are affected by AMD (Seiple et al., 1986; Sandberg et al., 1993; Remulla et al.,

1995; Sandberg et al., 1998; Falsini et al., 1999; Binns & Margrain 2007; Piccardi et al., 2009; Wood et al., 2011b). For example, extended implicit times of the a- and b-waves of the photopic focal ERG have been recorded in participants with early AMD (Binns & Margrain, 2007). In addition, a reduction in the amplitude of the focal cone flicker ERG has also been reported in participants with AMD (Falsini et al., 1999; Binns & Margrain, 2007; Piccardi et al., 2009). The extent of the amplitude reduction appears to parallel the disease progression, with the greatest reduction in flicker ERG amplitude reported in people with advanced AMD (Falsini et al., 1999). As a whole, this literature indicates that the focal cone flicker ERG may be a valuable diagnostic and prognostic tool in early AMD.

The focal cone flicker ERG has also been used as an objective measure of photostress recovery after a photopigment bleach in participants with early AMD (Binns & Margrain, 2005; 2007). The technique monitors the recovery of the amplitude of the first harmonic of the focal cone ERG after a photopigment bleach. The recovery of the foveal flicker ERG amplitude was shown to be significantly slower in people with early AMD compared to control participants (Binns & Margrain, 2007). Clearly, focal ERG techniques are sensitive to the localised retinal dysfunction that occurs in early AMD. However, the small signal obtained from specific retinal regions is susceptible to interference from electrical noise, which leads to the degradation of the signal quality (Gerth, 2009).

The potential of electrophysiological techniques as a means of monitoring treatment outcomes in patients with AMD has also been explored (Oner et al., 2005; Maturi et al., 2006; Mackay et al., 2008). For example, the pattern ERG has been used successfully to monitor retinal function after PDT (Oner et al., 2005). There is also evidence that the mfERG may be used to predict the outcomes of PDT treatment (Mackay et al., 2008) and to monitor retinal function during antiVEGF therapy (Maturi et al., 2006). However, the outcomes of these investigations have often been considered unreliable as a result of insufficient follow up intervals, small sample sizes or the inhomogeneous disease characteristics of the participants (Gerth et al., 2009).

1.5.8. Assessment of dark adaptation using the ERG and related techniques

The a- and b-waves of the full field scotopic ERG are initially completely extinguished after a near-total bleach of visual pigment, before the amplitude gradually recovers to the pre-bleach level during a 30-40 minute period in darkness (Thomas & Lamb, 1999; Cameron et al., 2006; 2008). When plotted as a function of time after the photopigment bleach, the recovery of the scotopic b-wave amplitude was shown to follow an ‘S-shaped’ configuration (Cameron et al., 2006; 2008). The b-wave was unrecordable for the initial 10 minutes after the bleach and half recovery occurred at 23 minutes. Similar recovery curves have been recorded for the scotopic a-wave amplitude (Thomas & Lamb., 1999). After a substantial photopigment bleach, the a-wave was extinguished for the first 5 minutes of recording, half recovery occurred at 14-17 minutes and pre-bleach amplitude was regained within 30 minutes in the dark. The S-shaped curve was shown to accurately describe the recovery of the a-wave amplitude after a photopigment bleach of 40% or greater (Figure 1.26) (Thomas and Lamb., 1999).

Previous electrophysiological assessments of cone dark adaptation have measured the recovery of the a-wave of the photopic ERG after a photopigment bleach (Paupoo et al., 2000; Mahroo & Lamb, 2004). After a substantial bleach of photopigment, Paupoo et al. (2000) found the recovery of the a-wave amplitude was well described by an exponential function with a time constant of 1.5 minutes and full recovery of the a-wave amplitude occurred within 6 minutes. The reduction in the a-wave amplitude is more marked at higher pre-adapting intensities (Mahroo & Lamb, 2004).

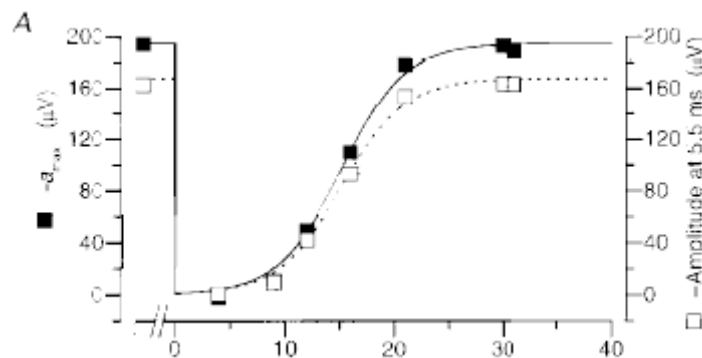


Figure 1.26. The recovery of the a-wave amplitude of the full field scotopic ERG plotted as a function of time after a near-total bleach of photopigment (Thomas & Lamb., 1999).

The visual evoked potential (VEP) has been used as an objective measure of photostress recovery (Lovasik, 1983; Parisi & Bucci, 1992; Parisi et al, 1994; 1998; 2002). During this technique, the amplitude of the PI component of the VEP response was recorded at regular intervals after a photopigment bleach. PI was significantly reduced immediately after the bleach and gradually recovered during the time in the dark (Lovasik, 1983). In healthy participants, full recovery of the VEP was shown to occur within one minute (Lovasik, 1983; Parisi & Bucci, 1992). In addition, as discussed (Section 1.5.7, Page 62) the focal cone flicker ERG has also been used as an objective measure of photostress recovery in healthy participants and those with early AMD, by monitoring the recovery of the amplitude of the first harmonic of the focal cone ERG after a photopigment bleach (Binns & Margrain, 2005; 2007).

1.6. Overview and aims

Age-related macular degeneration is the leading cause of visual impairment in the UK and developed world (Bunce and Wormald, 2008; Resnikoff et al., 2004). Treatment options for this disease are evolving rapidly and the development of anti-VEGF agents, such as Ranibizumab, have for the first time enabled doctors to generate clinically significant improvements in VA in patients with wet AMD (Brown et al., 2006; Rosenfeld et al., 2006; Brown et al., 2009), although at a substantial on-going cost to the NHS (National Institute for Health and Clinical Excellence, 2008). However, there is as yet no effective treatment for dry AMD. Given that the average age of the population is predicted to increase in the UK and across the world during the coming decades (Office for National Statistics, 2009; United Nations, 2009), the prevalence of AMD and associated vision loss will rise. There is consequently an urgent need for the development of new treatments for dry AMD, and of more economically viable interventions for wet AMD. This necessitates the identification of functional markers that are sensitive to early visual dysfunction in order to:

- identify patients who are at an increased risk of developing early AMD
- identify patients who are at risk of progression to late AMD
- identify patients that are suitable for treatment
- assess treatment outcomes
- and evaluate emerging treatment strategies.

There is an emerging body of evidence to suggest that dark adaptation is a highly sensitive functional biomarker for early AMD (Brown & Lovie-Kitchin, 1983; Brown et al., 1986a; Eisner et al., 1987a, Eisner et al., 1991; Owsley et al., 2001; Phipps et al., 2003; Binns & Margrain, 2007; Owsley et al., 2007; Dimitrov et al., 2008; 2011). In particular, cone dark adaptation may be useful clinically, as it can identify patients with early AMD in a relatively short recording period (Phipps et al., 2003, Dimitrov et al., 2008; 2011). However, at present, dark adaptation is an underexploited clinical tool, most likely as a result of the lack of standardised instrumentation and protocols for monitoring the rapid changes in visual threshold that occur during dark adaptation and ambiguity surrounding the extent to which cone photoreceptors are affected by early AMD (Brown et al., 1986b; Phipps et al., 2003; Binns & Margrain, 2007; Owsley et al., 2007; Dimitrov et al., 2008; 2011).

The primary aim of this series of studies was therefore to optimise psychophysical and electrophysiological techniques for the assessment of dark adaptation in AMD, with an emphasis on cone dark adaptation, in order to maximise its diagnostic potential for detection of the disease. The specific aims were:

- 1) To identify the most robust, clinically applicable psychophysical technique for the measurement of visual threshold during cone dark adaptation, by assessing the repeatability and agreement of three computer-based psychophysical methods and the Goldmann-Weekers adaptometer.

Hypothesis: The repeatability of the data obtained using the Goldmann-Weekers adaptometer will be inferior to that obtained using computer based techniques because operator error will introduce an additional source of variability to the threshold measurements. However, there will be no significant difference in the time constant of cone recovery (τ) (the time required for threshold to recover to approximately 63% of the dark adapted value) between the techniques, because cone τ should be independent of differences in variability between techniques.

- 2) To assess the effect of age on the dynamics of cone dark adaptation in a cohort of healthy adults.

Hypothesis: Given the changes that occur to the retina with increasing age, including the thickening of Bruch's membrane, accumulation of lipofuscin in the RPE and photoreceptor loss (Zarbin, 2004), and the subjective reports by elderly adults of visual difficulties adjusting to low illumination (Kline et al., 1992; McGregor & Chaparro, 2005), cone dark adaptation is predicted to become slower with increasing age in healthy adults.

- 3) To assess the dynamics of dark adaptation as a function of retinal eccentricity in healthy participants.

Hypothesis: In light of the heterogeneity of the retinal mosaic, dark adaptation is expected to vary as a function of retinal location.

- 4) To identify the most appropriate mathematical model to describe cone and rod recovery during dark adaptation.

Hypothesis: A rate-limited model will provide the best fit to recovery data as this most accurately represents the current understanding of recovery in the dark being limited by the presence of metarhodopsin photoproducts.

- 5) To quantify differences in cone dark adaptation between participants with early AMD and healthy controls at different retinal locations and to determine the diagnostic potential of cone dark adaptation and the time to RCB at each retinal location.

Hypothesis: Cone dark adaptation and the time to RCB will be significantly delayed in participants with early AMD. The current literature implies that this difference is likely to be most marked within the central 4° for cone-mediated recovery parameters (Dimitrov et al., 2008) and at 12° from fixation for the time to RCB (Owsley et al., 2007).

- 6) To quantify the diagnostic potential of cone dark adaptation in discriminating between participants with early AMD and healthy controls at a range of pre-adapting light intensities.

Hypothesis: Cone dark adaptation and the time to RCB will be significantly delayed in participants with early AMD at all pre-adapting intensities. However,

the most distinct separation in the recovery parameters between participants with early AMD and healthy controls is expected occur at the highest pre-adapting intensity, as this will place the greatest metabolic demand on the retina.

- 7) To develop a focal ERG technique for the assessment of macular rod dark adaptation within a clinically viable timeframe, in order to expand the range of objective techniques available for dark adaptation measurement.

Hypothesis: The b-wave amplitude of the full field rod ERG is initially markedly reduced by photopigment bleaching, before slowly returning to the pre-bleach amplitude over time in the dark (Thomas & Lamb, 1999; Cameron et al., 2006; 2008). It is anticipated that the b-wave of the focal rod ERG will be affected in the same way by exposure to a pre-adapting light and therefore measuring the b-wave amplitude at pre-specified intervals in the dark will enable the objective assessment of rod dark adaptation.

- 8) To compare the diagnostic potential of the optimal psychophysical and electrophysiological protocols for the assessment of dark adaptation for the detection of early AMD.

Hypothesis: Rod and cone dark adaptation will be significantly delayed in participants with early AMD when measured using both psychophysical and electrophysiological methods. However, psychophysical data are based on the subjective responses of the participant, and may therefore be degraded by human inconsistencies such as expectation and habituation errors (Treutwein, 1995). Therefore the diagnostic potential of these techniques may be inferior to that of objective electrophysiological methods.

2. A comparison of psychophysical methods of monitoring cone dark adaptation

Investigators have used psychophysical methods to quantify the process of dark adaptation for eight decades (Hecht et al., 1935; Windsor and Clark, 1936; Hecht et al., 1937; Wald & Clark, 1937; Hecht & Schlaer, 1938; Haig et al., 1938; Haig, 1941; Dieterle & Gordon, 1956; Goldstein, 1975; Henson & Allen, 1977; Friedburg et al., 1998; Jackson et al., 1999; Peters et al., 2000; Lamb & Pugh, 2004; Jackson et al., 2006b; Jackson and Edwards, 2008). The measurement of dark adaptation has played an important role in the diagnosis of a range of conditions, including retinitis pigmentosa (Moore et al., 1992; Sandberg et al., 1999), congenital stationary night blindness (Petzold & Plant, 2006), Sorsby's fundus dystrophy (Cideciyan et al., 1997), vitamin A deficiency (Kemp et al., 1988; Cideciyan et al., 1997), diabetic retinopathy (Phipps et al., 2006; Newsome & Negreiro, 2009) and AMD (Steinmetz et al., 1993; Owsley et al., 2001; Phipps et al., 2003; Binns & Margrain, 2007; Owsley et al., 2007; Dimitrov et al., 2008; 2011). The clinical significance of dark adaptation measurement is growing because of emerging evidence to suggest that it is a sensitive biomarker in AMD (Brown & Lovie-Kitchin, 1983; Eisner et al., 1987a; Eisner et al., 1991; Owsley et al., 2001; Phipps et al., 2003; Binns & Margrain, 2007; Owsley et al., 2007; Dimitrov et al., 2008; 2011), the primary cause of blindness in the developed world. Recently there has been particular interest in the measurement of cone dark adaptation because of its ability to identify people with early AMD in a relatively short recording period (Phipps et al., 2003; Dimitrov et al., 2008; 2011). However, although dark adaptation is clearly an important diagnostic tool, there is little published literature regarding the most robust psychophysical technique for the assessment of the change in visual threshold over time in the dark. This chapter will explore the repeatability of a range of psychophysical methods for monitoring cone dark adaptation.

2.1. The repeatability of the Goldmann-Weekers adaptometer for monitoring cone dark adaptation

2.1.1. Introduction

The Goldmann-Weekers adaptometer was once a commercially available instrument that was considered the ‘gold standard’ method for measurement of dark adaptation for many decades. It uses an operator controlled ‘method of ascending limits’ to determine the visual threshold, which is recorded directly onto logarithmic paper (Dieterle & Gordon, 1956). Despite its widespread use, there is little information about the performance of this device and no published data regarding its repeatability for the assessment of the kinetics of dark adaptation.

Dark adaptation data have also been recorded using custom made dark adaptometers (Hecht & Shlaer, 1938; Goldstein, 1975; Henson & Allen, 1977; Friedburg et al., 1998; Jackson et al., 1999) and several commercially available instruments, including LKC Technologies’ SST-1 (Peters et al., 2000; Jackson et al., 2006b) and Apeliotus Vision Science’s AdaptDx (Jackson & Edwards, 2008). Given the increasing prevalence of disorders like AMD (Minassian et al., 2011; Owen et al., 2012), in which the kinetics of dark adaptation are impaired, it seems likely that the range of contemporary dark adaptometers will expand. Knowledge of the performance of these devices, in particular their repeatability, will be important. Ideally, the repeatability of emerging techniques should be superior to that obtained with existing clinical devices. It is, therefore, useful to obtain repeatability data from the Goldman-Weekers device as a comparison measure. The data presented in this section have been published in a peer-reviewed journal (see Gaffney et al., 2011a in Appendix III).

2.1.2. Aims

The aim of this study was to assess the inter-session repeatability of the Goldmann-Weekers adaptometer for the measurement of cone dark adaptation in a population of healthy participants, in order to obtain data that may be used as a benchmark for the performance of future comparisons.

2.1.3. Methods

Participants

Thirty-one healthy adults, aged 19-30 years (mean = 21.5 +/- 2.5 years) were recruited to the study from the staff and students at the School of Optometry and Vision Sciences, Cardiff University. All participants had a corrected visual acuity of 6/6 or better in the test eye, clear ocular media (\leq Grade 3, LOCS-III) (Chylack et al., 1993), and a normal retinal appearance, in the absence of any history of ocular or systemic disease known to affect visual function. The study was approved by the School's Research Ethics Committee and all procedures adhered to the tenets of the Declaration of Helsinki. All participants provided informed written consent prior to participation.

Calibration

The Goldmann-Weekers adaptometer recorded luminance in units of log microapostilbs, rather than the more contemporary unit of luminance, log cd/m². In order to ensure that the values recorded by the Goldmann-Weekers adaptometer were accurately converted to log cd/m², the luminance of the stimulus was calibrated using a photometer (LS-110; Konica Minolta, Osaka, Japan) (Appendix I).

Experimental procedure

All participants attended the laboratory on two days within a two week period. Baseline data, including best corrected visual acuity and assessment of fundus appearance, were obtained at the start of the first session. At each session, participant's pupils were dilated with one drop of 1.0% Tropicamide in each eye. After a short familiarisation trial, dark adaptation was monitored in the right eye of all participants (the left eye was occluded). Refractive correction was worn as required.

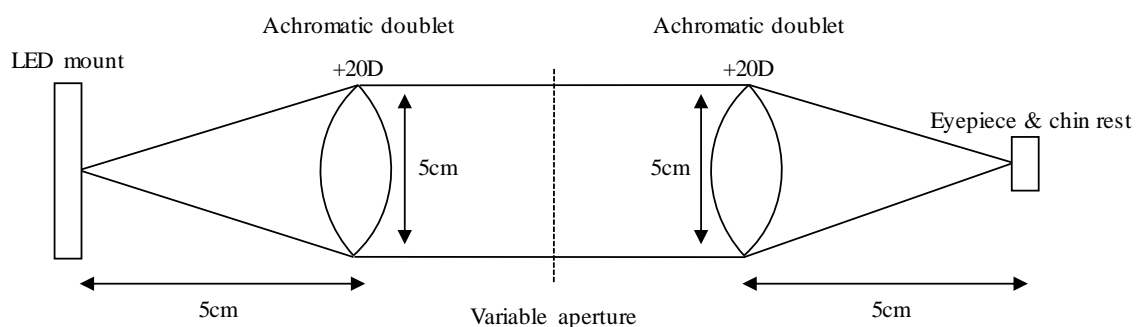


Figure 2.1. A schematic diagram of the Maxwellian view optical system

In order to obtain precise control of photopigment bleaching, a Maxwellian view optical system was used instead of the Goldmann-Weeker's integrated bleaching light (Figure 2.1). A 95% bleach (5.78 log phot.Td for 60s) of cone photopigment (Hollins & Alpern, 1973) was administered to the central 43.6° of the test eye.



Figure 2.2. The Goldmann-Weekers adaptometer. The participant positioned their chin on the rest at the front of the device and fixated the stimulus at the back of the bowl, the luminance of which was manually adjusted by the investigator using the controls at the rear of the device.

Upon cessation of the bleach, the participant turned to fixate the stimulus in the bowl of the Goldmann-Weekers adaptometer within 3 seconds and recording commenced immediately (Figure 2.2). Cone dark adaptation was monitored continuously for 5 minutes. The stimulus was a 4° diameter achromatic spot viewed centrally and was presented for 1 second every 2 seconds (i.e. 0.5Hz). The luminance of the stimulus was under direct control of the investigator, who used a method of ascending limits to record the dark adaptation function. That is, the examiner manually increased the intensity of the stimulus until the participant reported that it was just seen. Threshold was recorded by marking the

recording paper (Figure 2.3), before the stimulus intensity was reduced and the procedure repeated. This continued throughout the recording period. Subsequently, the marks on the recording paper were digitised (DigitizeIt Ver 1.5) and transferred to a spreadsheet for analysis.

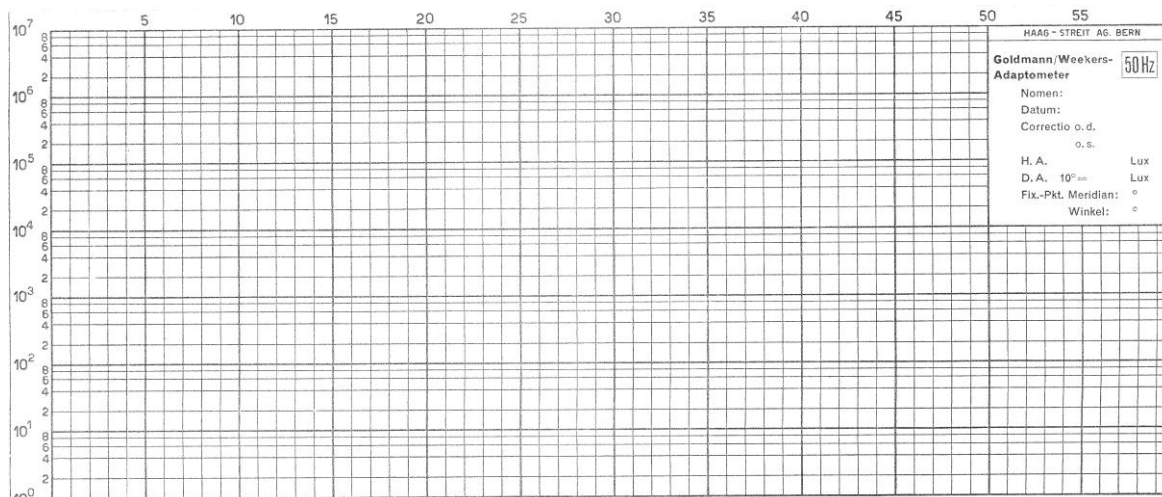


Figure 2.3. The logarithmic recording paper used by the Goldmann-Weekers adaptometer to record visual threshold.

Statistical analysis

The time constant of cone recovery (τ) was determined by fitting a single exponential function (Equation 2a), on a least squares basis, to the threshold recovery data recorded from each participant, using Microsoft Excel (2003).

$$\text{Equation 2a.} \quad T(t) = a + (b \cdot \exp^{-t/\tau})$$

where T is the threshold at time t after the bleach, a is the final cone threshold, b is the change in cone threshold from $t = 0$ and τ is the time constant of cone recovery (McGwin et al., 1999). The final cone threshold and the change in cone threshold were added together to calculate the initial cone threshold.

The repeatability of cone τ , initial cone threshold and final cone threshold of the best fitting models was assessed using established statistical techniques (Bland & Altman, 1986), including by calculating the coefficient of repeatability (CoR). The CoR is calculated as 1.96 multiplied by the standard deviation of differences between visits one and two. A paired t-test was used to determine whether parameters of adaptation differed significantly

between visits. This would indicate a systematic difference between the two visits e.g. due to a learning effect.

2.1.4. Results

Cone dark adaptation data were recorded from all 31 participants, on two occasions, using the Goldmann-Weekers adaptometer. The cone τ , initial cone threshold and final cone threshold given by the best fitting exponential model are shown for each participant in Table 2.1. An example of the dark adaptation data obtained from a typical participant (SH) at the two visits are shown in Figure 2.4, with the best fitting exponential model for each visit.

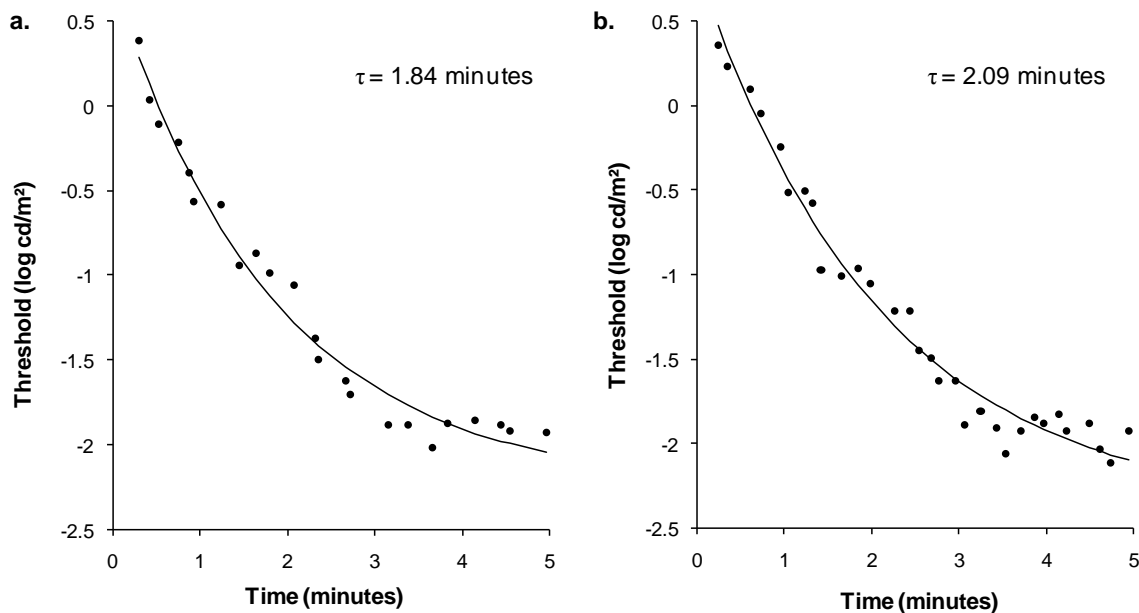


Figure 2.4. Cone dark adaptation data and best fitting exponential model for SH, recorded using the Goldmann-Weekers adaptometer at visit 1 (a) and visit 2 (b), shown with the time constant of cone recovery (τ) in minutes.

The difference in cone τ recorded at the first and second visit is plotted as a function of the mean cone τ for all 31 participants in the Bland and Altman plot shown in Figure 2.5a. Similar plots for the initial and final cone thresholds are shown in Figure 2.5b and 2.5c. In each plot, the solid horizontal line represents the bias i.e. the mean difference observed between visits, and the dashed horizontal lines indicate the limits of agreement i.e. the mean difference \pm the coefficient of repeatability (CoR). The CoR for cone τ was 1.32 minutes, for the initial threshold 0.71 log cd/m² and for the final threshold 0.58 log cd/m².

Table 2.1. Cone τ , initial cone threshold and final cone threshold for all participants

Participant	Cone τ (minutes)		Initial cone threshold (log cd/m ²)		Final cone threshold (log cd/m ²)	
	Visit 1	Visit 2	Visit 1	Visit 2	Visit 1	Visit 2
AG	1.53	2.25	0.52	0.12	-1.79	-1.90
AH	1.92	2.41	0.93	0.58	-2.08	-2.07
AW	1.69	2.36	0.65	0.41	-1.79	-2.23
BP	2.48	1.55	0.95	1.2	-1.75	-1.60
CD	1.94	2.15	0.84	0.56	-1.72	-2.21
CL	1.32	1.15	0.63	0.88	-1.91	-2.71
CP	1.17	2.12	0.81	0.68	-1.34	-2.06
CW	2.33	1.59	0.41	0.97	-2.09	-2.00
EB	3.53	2.26	0.78	0.88	-2.27	-1.77
EBA	1.74	2.04	0.65	0.37	-1.91	-2.02
EC	2.37	1.91	0.07	1.11	-1.70	-1.82
FD	1.46	1.49	1.26	0.67	-1.67	-1.87
GN	2.25	2.32	1.22	0.57	-2.05	-2.45
HD	1.76	1.87	0.74	0.60	-2.06	-2.25
HH	2.05	1.62	0.72	0.77	-2.00	-2.03
HS	2.46	2.79	0.3	0.42	-2.22	-2.36
JH	1.94	3.06	0.93	0.51	-2.28	-2.37
JAH	2.30	1.95	0.55	0.61	-2.32	-1.85
KK	1.90	1.41	0.75	0.32	-1.83	-1.83
KM	2.49	1.68	0.68	0.78	-1.96	-1.61
LF	1.40	1.55	0.88	0.46	-1.94	-1.69
LS	1.30	1.77	0.81	0.29	-1.81	-2.14
MC	2.43	1.58	0.35	0.55	-2.10	-1.52
PG	2.65	2.10	1.06	1.00	-2.29	-1.39
PH	4.10	3.61	0.78	0.73	-2.25	-1.49
PJ	2.52	2.66	0.62	0.92	-2.57	-2.52
RE	1.09	1.99	0.79	0.79	-1.79	-1.89
SM	2.37	1.51	0.45	0.63	-2.07	-1.78
SH	1.84	2.09	0.74	0.82	-2.25	-2.40
ST	2.02	0.92	0.96	0.75	-2.09	-1.78
SW	2.09	2.19	0.74	1.05	-2.84	-1.89

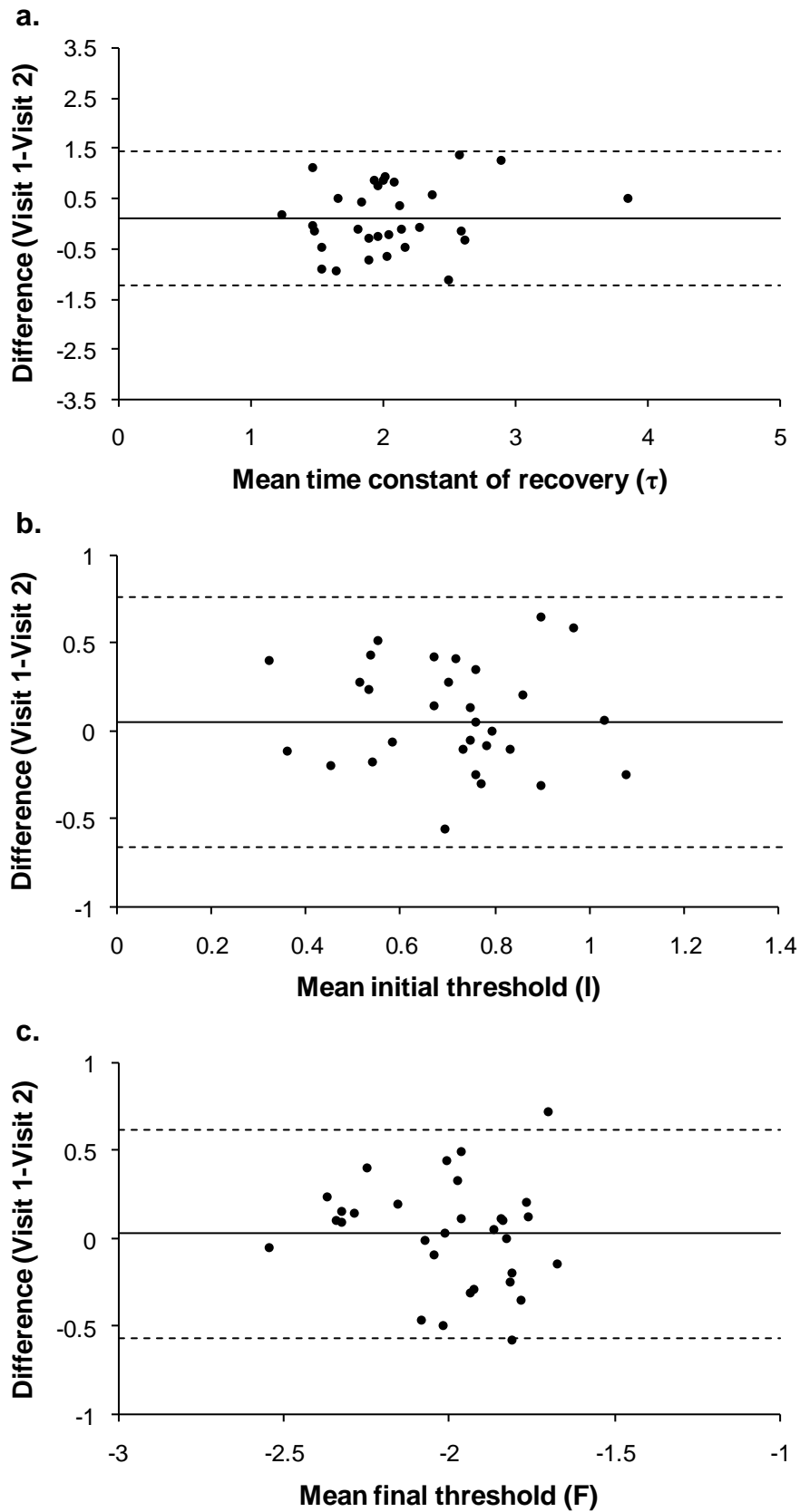


Figure 2.5. Bland-Altman plots for cone τ (a), initial threshold (b) and final threshold (c). The difference between the value recorded at visit 1 and visit 2 is plotted as a function of the mean value for all 31 participants and is shown with the bias (solid line) and 95% limits of agreement (dashed lines).

The mean (+/- standard deviation) cone τ , initial cone threshold and final cone threshold are shown in Table 2.2, for visit one and visit two. There were no statistically significant differences in any of these parameters between the two visits ($p > 0.05$), which indicate that there was no significant learning effect within the dataset.

Table 2.2. Mean (+/- standard deviation) of dark adaptation parameters assessed at visit one and visit two

	Mean (+/- standard deviation)		p-value (paired t-test)
	Visit 1	Visit 2	
Cone τ (minutes)	2.11 (+/-0.67)	2.00 (+/-0.55)	0.376
Initial threshold (log cd/m ²)	0.73 (+/-0.25)	0.68 (+/-0.25)	0.443
Final threshold (log cd/m ²)	-1.99 (+/-0.25)	-2.02 (+/-0.29)	0.652

2.1.5. Discussion

The Goldmann-Weekers adaptometer was capable of monitoring the rapid changes in threshold that occur during dark adaptation, and cone dark adaptation data were successfully recorded from all of the participants on each of the trials. Despite being the default clinical instrument for the measurement of dark adaptation for a number of decades, there has, until now, been no published data on the repeatability of the Goldmann-Weekers adaptometer for measurement of the kinetics of dark adaptation. The repeatability data collated in this study may be used as a benchmark with which to compare other contemporary adaptometers, such as LKC Technologies' SST-1 (Peters et al., 2000; Jackson et al., 2006b) and Apeliotus Vision Science's AdaptDx (Jackson & Edwards, 2008).

When a technique is evaluated for clinical use, it is important to consider the CoR, as it indicates the extent of inherent variability, and therefore the smallest change that may be considered to be clinically significant (Bland & Altman, 1986). In order for a change in dark adaptation between visits to be considered clinically significant, a difference that is equal to or greater than the CoR must be measured. Relative to the mean cone τ recorded at the two visits (2.11 +/- 0.67 and 2.00 +/- 0.55 minutes at the first and second visits respectively) the CoR (1.32 +/- 0.25 minutes) is large, i.e. the adaptometer is not capable of identifying individual differences in cone τ of less than 1.32 minutes. Consequently, small

to moderate changes in dark adaptation may go undetected. This is important as recently, cone τ has been shown to be diagnostic for conditions such as AMD (Phipps et al., 2003; Binns & Margrain, 2007; Dimitrov et al., 2008; 2011) and may therefore be a useful clinical measure if assessed appropriately.

As described in the methodology, this study used a Maxwellian view optical system to deliver a standardised bleach of known intensity prior to dark adaptation. In the clinic, the Goldmann-Weekers' integrated light source may be used to deliver a continuous background bleach. However, the bleach delivered is not consistent between instruments, because it is dependent on the wattage of the bulb used. Consequently, the repeatability may differ between units, but it is unlikely that the performance of the device will be better than that reported here, where results were obtained under optimal control of bleach conditions. It may therefore be useful to evaluate the repeatability of each instrument before clinical use.

In summary, the results of this study suggest that the Goldmann-Weekers adaptometer is insensitive to small to moderate changes in dark adaptation. This data may be used as a benchmark for future comparison with new modalities of dark adaptation assessment.

2.2. A comparison of four psychophysical methods for measurement of cone dark adaptation

2.2.1. Introduction

The 'method of limits' employed by the Goldmann-Weekers adaptometer has been used by other dark adaptometers, for example, by implementing simple computer controlled staircases, similar to those used in visual field testing equipment (Jackson et al., 1999, Owsley et al., 2001, Owsley et al., 2007; Jackson & Edwards' 2008). However, although it is fast, the psychophysical method of limits is prone to errors that may result from changes in the observer's criterion (Treutwein, 1995), i.e. the rationale used by an observer to determine the presence or absence of a stimulus. In addition, non-automated devices, such as the Goldmann-Weekers adaptometer, are affected by changes in the performance of the operator too, for example, the rate at which the luminance of the stimulus is increased.

Adaptive staircases were developed to overcome the limitations of classical psychophysical procedures, such as the method of limits used by the Goldmann-Weekers adaptometer (Treutwein, 1995). Threshold is estimated by fitting psychometric functions to a series of threshold estimations. The psychometric function plots the probability of a correct response for a range of stimulus levels (see Figure 1.17, Page 44). Threshold is taken as the stimulus level that corresponds to a preselected level of performance. Adaptive procedures aim to improve the efficiency of testing by concentrating stimulus presentations at or near the presumed threshold, thus minimising redundant presentations (Treutwein, 1995). Unlike classical psychophysical methods, during which stimuli are presented at fixed intervals, adaptive procedures are performance dependent, that is, the stimulus presented on any one trial is determined by one, several or all of the preceding responses given by the participant (Hall, 1981).

Although adaptive techniques allow increasingly robust measurement of dark adaptation, they are not entirely free from the effects of changes in the observer's criterion. Consequently, forced choice methods may be considered preferable. During a forced choice procedure, the observer is required to respond by selecting one of a number of presented options on each trial. The greater the number of options presented, the smaller the probability of the observer obtaining a correct response due to chance alone (Gescheider, 1997). However, despite their advantages, as forced choice procedures tend to be time consuming, they have not, thus far, been used to track threshold during dark adaptation.

Cone dark adaptation is particularly attractive to clinicians as a diagnostic tool because of its sensitivity to early AMD (Phipps et al., 2003; Dimitrov et al., 2008; 2011) and the relative speed with which it can be recorded. However, the fundamental difficulty associated with measuring visual thresholds during dark adaptation is the speed with which threshold changes. This is most problematic when monitoring cone adaptation, in which the threshold decreases by approximately 2 log units during the initial 10 minutes in the dark (Hecht et al., 1937, Hollins & Alpern, 1973). Clearly, rapid psychophysical methods capable of obtaining robust and repeatable threshold measurements are desirable.

2.2.2. Aims

In order to identify the most robust, clinically applicable technique for the measurement of visual threshold during cone dark adaptation, the repeatability and agreement of three computer based methods and the Goldmann-Weekers adaptometer were assessed. The computer based methods evaluated were: a hybrid adaptive stimulus presentation combined with a maximum likelihood calculation (Friedburg et al., 1998), a modified staircase procedure based on a method previously used with the Humphrey Visual Field Analyser (Jackson et al., 1999) and a novel 10-alternative forced choice procedure. The analysis of the CoR concentrated on cone τ , as this parameter appears to be most affected by early AMD (Phipps et al., 2003; Binns & Margrain, 2007; Dimitrov et al., 2008; 2011).

Three hypotheses were proposed:

1. The repeatability of the data obtained using the Goldmann-Weekers adaptometer would be inferior to that obtained using the computer based techniques because operator error would introduce an additional source of variability to the threshold measurements.
2. The estimates of final cone threshold would be lower for the 10-alternative forced choice and hybrid adaptive techniques than for the method of limits because these techniques should provide a genuine estimate of the observer's threshold (Friedburg et al., 1998; Sekuler & Blake, 2006).
3. Finally, there would be no significant difference in the time constant of cone recovery (τ) between techniques, because cone τ should be independent of the expected translation of the data up or down the vertical axis and, to some extent, differences in variability between techniques.

2.2.3. Methods

Participants

A new cohort of thirty-one healthy adults, aged 20-31 years (mean age 21.6 +/- 2.5 years) were recruited to the study from the staff and students at the School of Optometry and Vision Sciences, Cardiff University. The inclusion criteria were similar to that of the preceding investigation: a corrected visual acuity of 6/6 or better in the test eye, clear ocular media (\leq Grade 3, LOCS-III) (Chylack et al., 1993), a normal retinal appearance and no history of ocular or systemic disease. The study was approved by the School's Research Ethics Committee and all procedures conformed to the tenets of the Declaration

of Helsinki. Informed written consent was provided by all participants prior to participation.

Psychophysical methods

As described (Section 2.1.3, Page 72), the Goldmann-Weekers adaptometer used the method of ascending limits to record the dark adaptation function directly onto logarithmic paper. The luminance of the 4° diameter achromatic spot stimulus was under direct control of the investigator, who manually increased the intensity of the stimulus until it was just seen. Threshold was recorded by marking the recording paper, before the stimulus intensity was reduced and the procedure repeated. This continued throughout the recording period. Subsequently, the marks on the recording paper were digitised (DigitizeIt Ver 1.5) and transferred to a spreadsheet for analysis.

The remaining three methods were computer based and all stimuli were presented on a calibrated high resolution CRT monitor (Iiyama LS 902UT) driven by an 8-bit graphics board (nVIDIA Geforce 9) under software control (Matlab, R2009a, The MathWorks Inc.). The luminance output of the monitor was γ -corrected (Metha et al., 1993; Brainard et al., 2001) and modified by neutral density filters mounted on the screen to expose the full range of visual recovery. The background luminance of the CRT ($-0.85 \log \text{ cd/m}^2$) was attenuated by a 1.2 ND filter in place throughout recordings. As the lower end of the luminance range approached, additional filters were added to further attenuate the luminance. This ensured that only 2.1 log units of the linear range of the γ -corrected monitor was used during testing.

The 4° diameter achromatic stimulus was presented at the centre of the screen, indicated by four fixation markers (Figure 2.6). The hybrid adaptive and modified staircase procedures used spot stimuli, whilst numeric stimuli were presented during the forced choice paradigm. The participant was instructed to fixate the centre of the screen and to indicate perception of the stimulus via the computer keyboard, or to report the number seen in the case of the forced choice program. The three computer programs are shown in Appendix II.

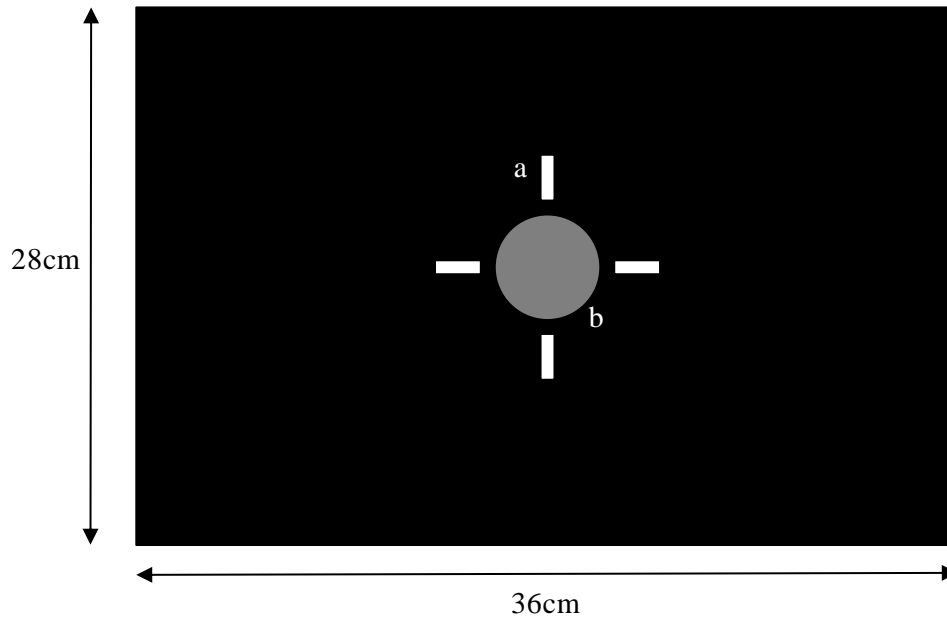


Figure 2.6. CRT display used by the computer based dark adaptation procedures; at a viewing distance of 55cm. Participants were instructed to fixate the centre of the screen indicated by four $1^\circ \times 0.5^\circ$ fixation markers (a), where a 4° diameter achromatic spot or numeric stimulus was presented (b).

The hybrid adaptive procedure has previously been described by Friedburg et al. (1998). On each trial, the luminance of the stimulus was determined by a set of three decision criteria, based on the participant's previous responses (Table 2.3). A visual threshold estimate was recorded when a maximum of twelve trials were exceeded or five consecutive reversals ('seen to not seen', or vice versa) occurred. A maximum likelihood computation was employed to determine threshold by estimating values of the midpoint and spread of the psychometric function on the basis of the distribution of all of the participant's previous responses to the stimuli presented (Hall, 1981).

The modified staircase procedure was based on a method previously implemented using a Humphrey perimeter (Jackson et al., 1999). The stimulus was presented for 200 msec, followed by a 600 msec response window and then a randomly determined interstimulus delay of 0.9 – 2.4 seconds. If the participant reported perception of the stimulus within the 600 msec response window, the luminance was reduced by 0.3 log units for the next presentation. Conversely, if the participant took longer than 600 msec to respond to the stimulus, or failed to respond at all, the intensity was increased by 0.1 log units on the following presentation. Threshold was recorded when the stimulus first became visible on an ascending staircase.

Table 2.3. Decision criteria used by the hybrid adaptive procedure to determine the stimulus luminance (Friedburg et al., 1998).

<u>Response sequence</u>	<u>Target luminance</u>
Response ‘changes from ‘seen’ to ‘not seen’ or vice versa	Reversal of step direction and step size reduced by 60%
Response consistent for 2 trials	Step size and direction remain unchanged
Response consistent for 3 trials	Step size doubled but step direction remains unchanged

The 10-alternative forced choice program presented numeric stimuli, from zero to nine. Participants were instructed to report the number shown after every stimulus presentation, irrespective of their level of confidence, and the investigator entered the response via the computer keyboard. After each correct response the stimulus luminance was reduced by 0.3 log units on the subsequent presentation, and for each incorrect response it was increased by 0.1 log units. Similarly to the modified staircase procedure, threshold was recorded when the stimulus first became visible on an ascending staircase.

Experimental procedure

Participants attended the laboratory on two days within a two week period. Baseline data, including best corrected visual acuity and assessment of fundus appearance, were obtained at the start of the first session. At each session, participant’s pupils were dilated with one drop of 1.0% Tropicamide in each eye. Dark adaptation was assessed in the right eye of all participants (the left eye was occluded) and refractive correction was worn as required.

At the start of each session, the procedures involved were explained to the participant and a 5 minute practice trial was provided. This was extended at the investigator’s discretion, until the participant appeared to be competent with the procedures.

A Maxwellian view optical system was used to administer a 95% bleach (5.78 log phot.Td for 60s) of cone photopigment (Hollins & Alpern, 1973) to the central 43.6° of the test eye. Upon cessation of the bleach, participants turned to fixate the test stimulus within 3 seconds and recording commenced immediately. Cone dark adaptation was monitored continuously for 5 minutes, in response to a 4° diameter achromatic stimulus centred on the

fovea, using one of the four psychophysical techniques, selected at random. This procedure was repeated for each of the remaining psychophysical methods. A 10 minute ‘wash out’ period was interleaved between successive photopigment bleaches to avoid carry-over effects. In conjunction with the wash-out period, the use of a long duration ‘equilibrium’ bleaching light would ensure the same baseline level of adaptation on each trial. The same protocol was followed at the second visit, excluding the collection of baseline data.

Statistical analysis

The time constant of cone recovery (τ), initial cone threshold and final cone threshold were determined by fitting a single exponential function (Equation 2a), on a least squares basis, to all threshold recovery data using Microsoft Excel (2003).

The repeatability of the four methods was assessed by evaluating the data from each of the sessions using established statistical techniques (Bland & Altman, 1986), including by calculating the coefficient of repeatability (CoR). Paired t-tests were completed to determine any significant differences between cone τ between visit one and two, which may be indicative of a learning effect. A repeated measures analysis of variance (ANOVA) was carried out to look for significant order effects. A repeated measures ANOVA was then used to compare the mean cone τ , initial cone threshold and final cone threshold obtained using the four psychophysical methods, and a posthoc analysis (including Bonferroni correction) was used to determine which techniques differed significantly from each other.

2.2.4. Results

Cone dark adaptation data were recorded from all 31 participants, on both occasions, using each of the methods described. The dark adaptation data recorded from a typical participant (JF) at the first visit are shown in Figure 2.7, with the best fitting exponential model for each method. Threshold estimates were obtained approximately every 15 seconds using the hybrid adaptive procedure, approximately every 10 seconds using the Goldmann-Weekers adaptometer and 10-alternative forced choice procedures and approximately every 7 seconds using the modified staircase procedure.

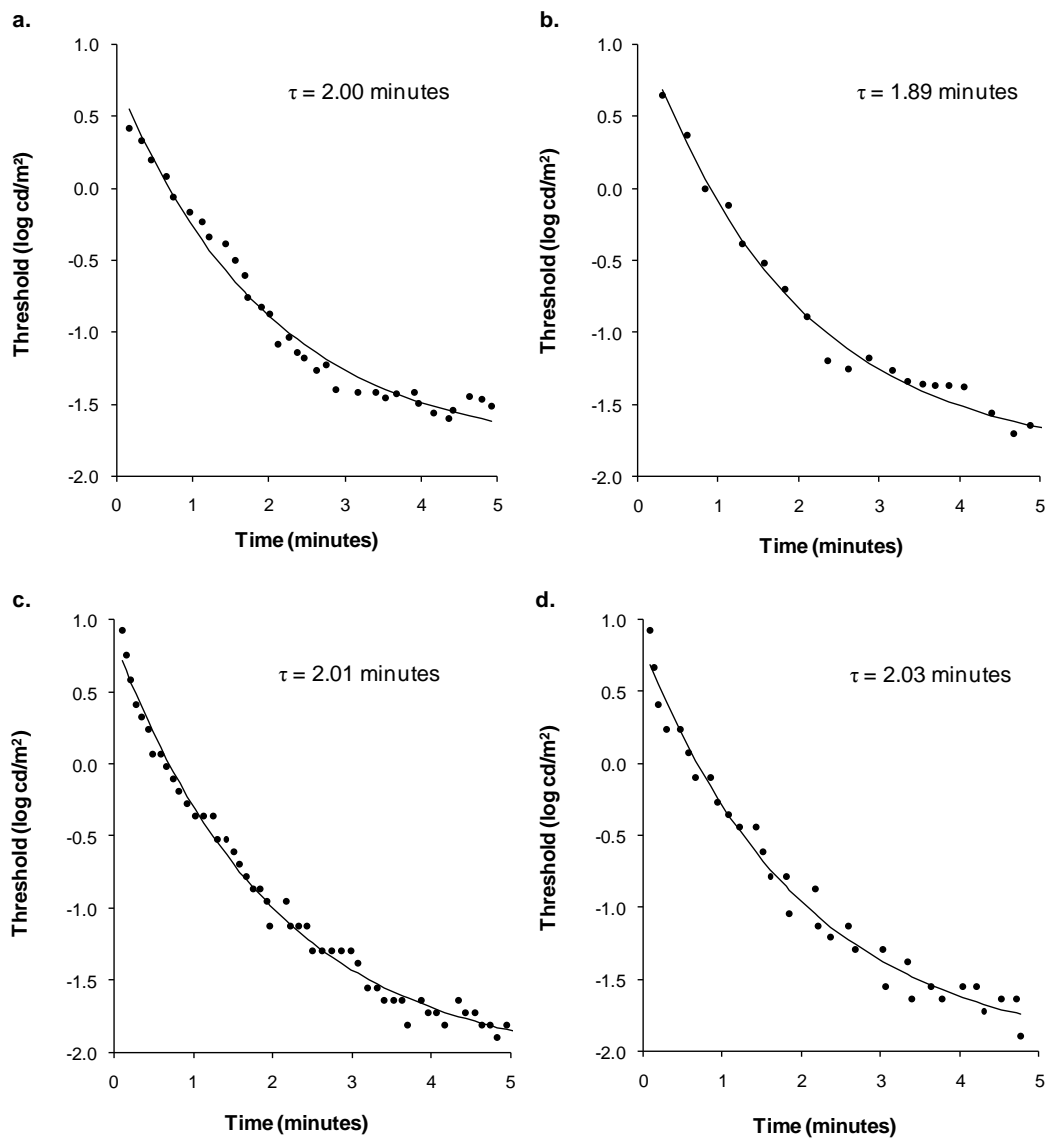


Figure 2.7. Cone dark adaptation data and best fitting exponential model for JF, recorded at visit 1 using the Goldmann-Weekers adaptometer (a), the hybrid adaptive procedure (b), the modified staircase procedure (c) and a novel 10-alternative forced choice procedure (d). All shown with the time constant of cone recovery (τ) in minutes.

The mean (\pm standard deviation) cone τ , initial cone threshold and final cone threshold for each of the psychophysical methods, are shown in Table 2.4. There were no statistically significant differences in mean cone τ between the four methods of dark adaptation measurement ($p = 0.488$). However, there was a statistically significant difference in the initial threshold estimates generated by the four methods ($p < 0.005$). Post-hoc analysis showed that the initial threshold given by the Goldmann-Weekers adaptometer was significantly lower than those given by the computer based techniques. There was also a significant difference in the final cone threshold measured by the four methods ($p < 0.005$). More specifically, post-hoc analysis showed that the final cone threshold given by the

Goldmann-Weekers adaptometer was significantly higher than the final threshold obtained using the hybrid adaptive and 10-alternative forced choice methods.

Table 2.4. Mean cone τ , initial cone threshold and final cone threshold for all participants at visit 1 and visit 2 for the four psychophysical methods of dark adaptation measurement.

	Goldmann-Weekers adaptometer	Hybrid adaptive procedure	Modified staircase procedure	10-AFC procedure	p-value
Cone τ (minutes)	2.11 (0.45)	2.05 (0.48)	1.99 (0.42)	2.09 (0.60)	= 0.488
Initial threshold (cd/m ²)	0.67 (0.12)	0.89 (0.21)	0.82 (0.16)	0.80 (0.15)	< 0.0005
Final threshold (cd/m ²)	-1.81 (0.21)	-2.13 (0.33)	-2.05 (0.62)	-2.20 (0.33)	< 0.0005

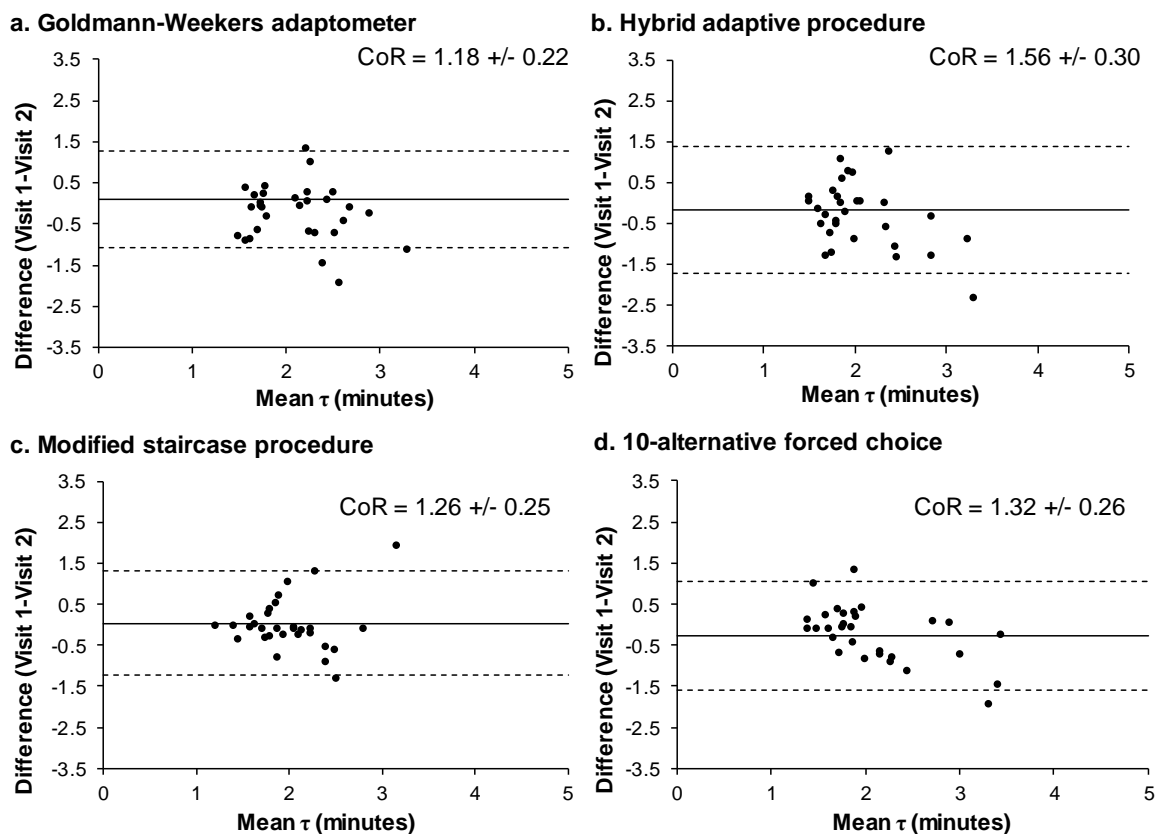


Figure 2.8. Bland-Altman plots for cone τ measured using the Goldmann-Weekers adaptometer (a), the hybrid adaptive procedure (b), the modified staircase procedure (c) and a novel 10-alternative forced choice procedure (d), with the CoR for each technique displayed in minutes. The solid line represents the bias and the dashed lines indicate the 95% limits of agreement.

The difference in cone τ recorded at the first and second visit is plotted as a function of the mean cone τ for each psychophysical method in the Bland and Altman plot shown in Figure 2.8. Similar plots for initial cone threshold and final cone threshold are presented in Figure 2.9 and 2.10. In each plot, the solid horizontal line represents the bias i.e. the mean difference observed between visits, and the dashed horizontal lines indicate the limits of agreement i.e. the mean difference \pm the coefficient of repeatability (CoR). The data from one participant was excluded from all analyses as the mean cone τ obtained for this participant using the hybrid adaptive procedure fell beyond three standard deviations from the mean difference for that psychophysical method. The four psychophysical methods demonstrated a similar level of intersession repeatability for measurement of cone τ and final cone threshold, with overlapping 95% confidence intervals for the CoR. However, with regard to initial cone threshold, the hybrid adaptive procedure was the least repeatable method for the measurement of this parameter.

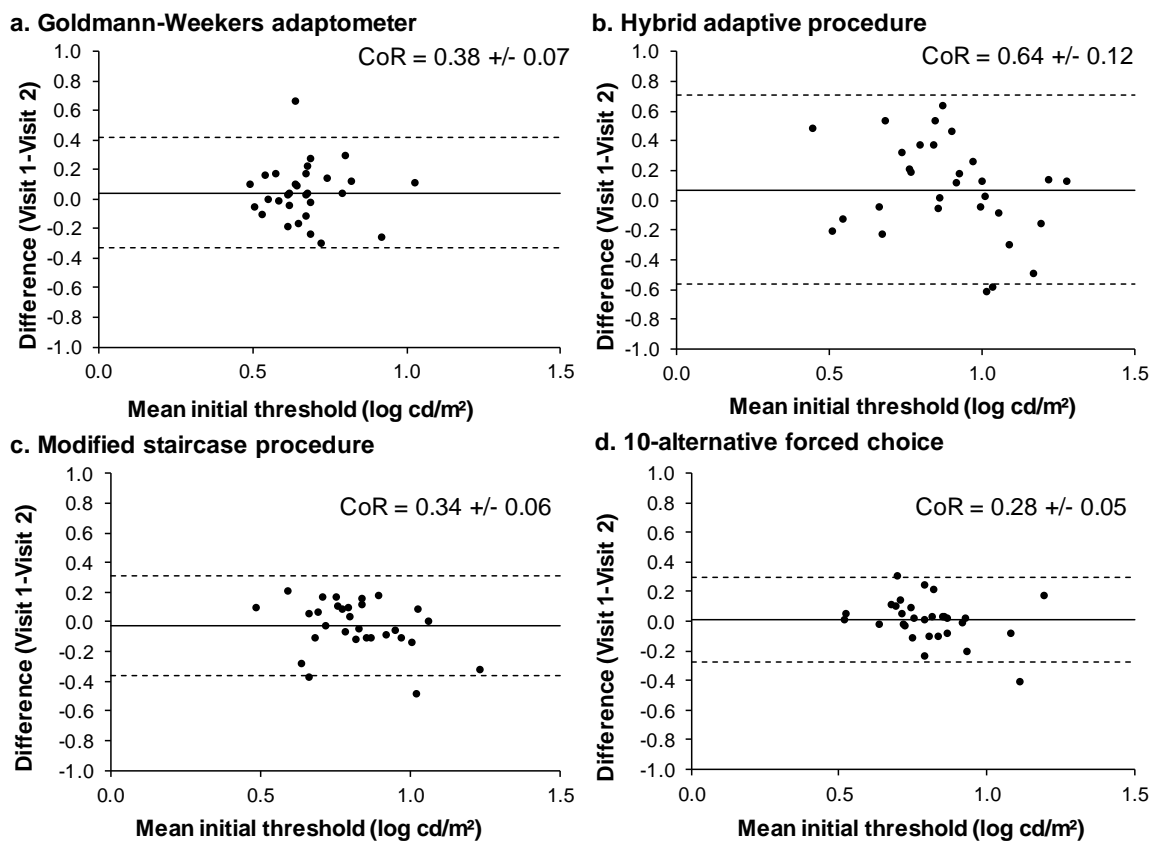


Figure 2.9. Bland-Altman plots for initial cone threshold measured using the Goldmann-Weekers adaptometer (a), the hybrid adaptive procedure (b), the modified staircase procedure (c) and a novel 10-alternative forced choice procedure (d), with the CoR for each technique displayed in minutes. The solid line represents the bias and the dashed lines indicate the 95% limits of agreement.

There were no statistically significant differences in mean cone τ recorded at the first and second visit for any of the psychophysical methods studied ($p > 0.05$). Similarly, an assessment of the order in which each psychophysical technique was used within a single recording session showed no statistically significant differences in mean cone τ for test order ($p > 0.05$). This analysis indicates that there were no learning, fatigue or bleach carry-over effects within the dataset.

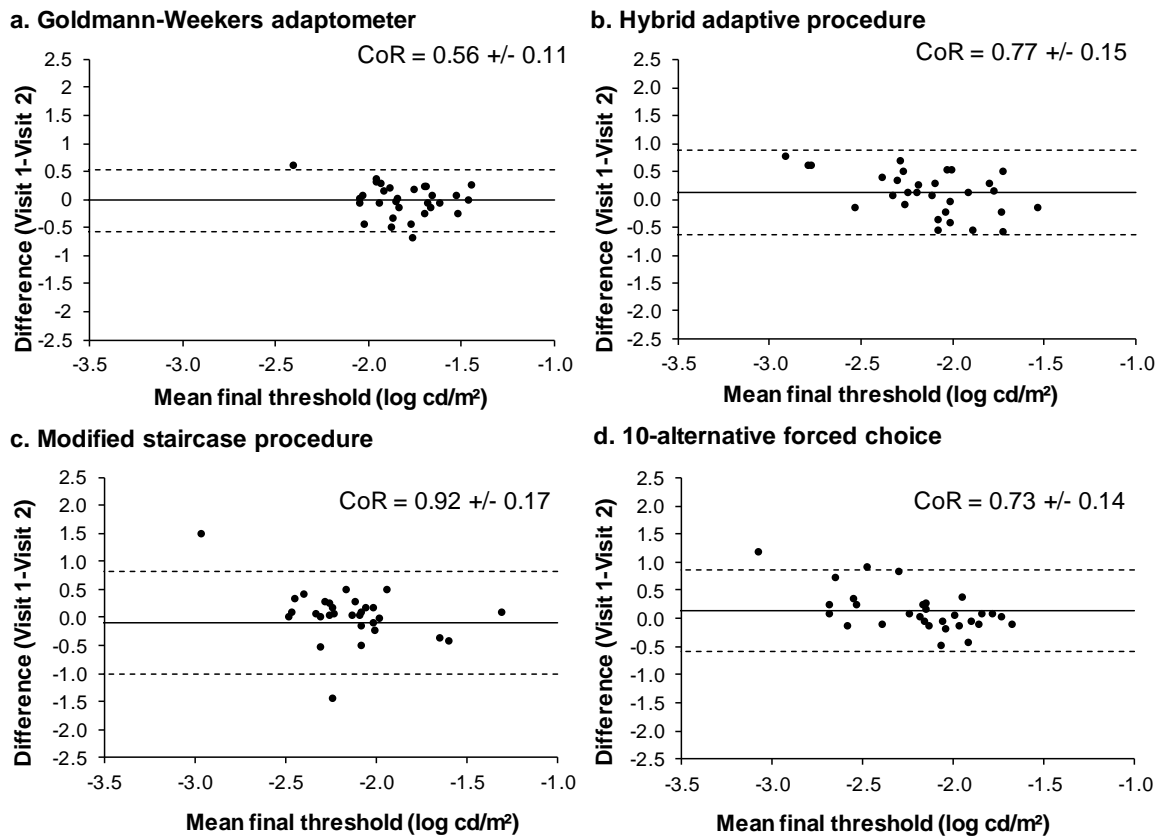


Figure 2.10. Bland-Altman plots for final cone threshold measured using the Goldmann-Weekers adaptometer (a), the hybrid adaptive procedure (b), the modified staircase procedure (c) and a novel 10-alternative forced choice procedure (d), with the CoR for each technique displayed in minutes. The solid line represents the bias and the dashed lines indicate the 95% limits of agreement

2.2.5. Discussion

The major challenge encountered when monitoring cone dark adaptation is that of obtaining robust visual threshold estimations in the limited timeframe imposed by the rate at which cone threshold changes. All four of the techniques used in this study were capable of monitoring the rapid changes in visual threshold that occurred during cone dark adaptation. As predicted, there were no significant differences between cone τ obtained using the different methods. This is reassuring as the parameters of dark adaptation are

determined by the physiology of the visual system and therefore should be independent of the measurement technique.

As discussed (Section 2.1.5, Page 78) the CoR indicates the smallest change in a parameter such as cone τ that may be considered clinically significant. For the methods evaluated here, a change of more than 1.18-1.56 minutes in cone τ between visits can be considered clinically meaningful. The CoR can only really be interpreted in the context of previous experimental data. When a similar computer based technique was used to compare cone τ within the central retina between participants with early AMD and healthy controls, differences of 2.85-8.01 minutes in mean cone τ between the groups were reported (See Chapter 4 and Gaffney et al., 2011b). These differences are clearly greater than the CoRs reported here, suggesting that the psychophysical methods are capable of producing results which can reliably distinguish individuals with early AMD from healthy controls.

The CoR obtained for cone τ measured using the Goldmann-Weekers adaptometer (1.18 +/- 0.22 minutes) is consistent with that obtained in the preceding section of the study (1.32 +/- 0.25 minutes) (Section 2.1.4; Gaffney et al., 2011a). Contrary to expectations, the repeatability of the Goldmann-Weekers adaptometer was equivalent to the computer based methods. This occurred despite differences in the way in which the stimuli were presented: unlike the computer based methods, the stimuli presented by the Goldmann-Weekers adaptometer were controlled by an operator. It is important to acknowledge that the investigator was highly trained in the operation of the Goldmann-Weekers adaptometer and therefore the CoR reported here was based on data obtained under optimal recording conditions. Consequently, the repeatability of the device may be poorer when under the control of a less experienced operator.

As expected, the lowest estimates of final cone threshold were generated by the hybrid adaptive and 10-alternative forced choice methods. The hybrid adaptive procedure was developed in order to provide a fully automated method of dark adaptation measurement aimed at minimising the effects of subjective bias on the data (Friedburg et al., 1998). When it was first described, the technique was shown to produce lower final threshold estimates than the ascending staircase procedure employed by the Goldmann-Weekers adaptometer (Friedburg et al., 1998), a finding that was replicated in the current dataset. This may be explained by the way in which the procedure computes estimates of threshold

using the psychometric frequency of seeing curve. After the data is collected, threshold is estimated as the target luminance that corresponds to a 50% detection rate. This is likely to be lower than when traditional staircase procedures are used, because the subjective decision criterion erroneously raises threshold.

With regard to the repeatability of cone τ , the hybrid adaptive procedure had no advantage over the other techniques. In fact, the repeatability was actually the lowest of all of the methods (CoR = 1.56 +/- 0.30). In addition, this technique also exhibited the poorest repeatability for the measurement of initial cone threshold (CoR = 0.64 +/- 0.12). This is likely to result from the complex 'decision criteria' used to determine threshold, which meant that the procedure only recoded a threshold approximately every 15 seconds, the least frequently of all of the methods. This implies that a more accurate and reliable description of the changes in threshold that occur during cone dark adaptation may be obtained using methods that are capable of producing more frequent threshold estimates, such as the staircase procedure. The hybrid adaptive procedure may be more appropriate for measurement of rod dark adaptation, in which changes in visual threshold occur more slowly.

Forced choice methods have been shown to consistently produce lower and more accurate threshold estimations compared to unforced subjective procedures because the measurements are criterion free (Sekuler & Blake, 2006). As predicted, the 10-alternative forced choice method produced a significantly lower mean final threshold relative to that attained with the Goldmann-Weekers adaptometer, although it was not significantly different to the other computer based methods. However, it is inappropriate to compare this technique directly to the other methods as the 10-alternative forced choice procedure employed numeric stimuli, which was arguably a more demanding recognition task than the identification of the spot stimuli used by the other methods.

The initial cone threshold measured by the Goldmann-Weekers adaptometer was significantly lower than those generated by the computer based techniques. This may be explained by differences in the available luminance range between the adaptometer and the computer. The Goldmann-Weekers adaptometer presented a maximum stimulus intensity of 0.4 log cd/m², compared to the maximum stimulus intensity of 0.8 log cd/m² presented

by the computer. Consequently, the computer based methods were able to collect a greater number of data points during the earliest stages of dark adaptation to anchor the exponential model fit. Removal of these early data points generated by the computer based methods reduces the difference in the initial threshold between the techniques.

In summary, the performance of the Goldmann-Weekers adaptometer was compared to three automated computer methods of measuring cone dark adaptation and the mean cone τ and CoR for each were reported. Contrary to our initial expectations, there were no significant differences in the repeatability between the techniques. As expected, the time constant of cone dark adaptation was also not significantly different between techniques. Despite the theoretical advantages of the criterion free forced choice and hybrid adaptive procedures, these results indicate that any of these psychophysical techniques may be used to measure cone dark adaptation in clinical practice. As our future investigations are primarily concerned with the changes in cone dark adaptation that occur in early AMD, we will continue to use the staircase procedure to collect data, as its simple algorithm facilitates rapid threshold measurement: a necessity for the assessment of cone dark adaptation.

3. The effect of age on cone dark adaptation in healthy eyes

Age-related macular degeneration may be considered a pathological extension of the normal ageing process (Zarbin, 2004). Many features of the ageing retina are present to an elevated extent in eyes with AMD, for example, the thickening of Bruchs membrane, accumulation of lipofuscin in the RPE and photoreceptor loss. This suggests that ageing changes contribute, but do not inevitably lead, to AMD. Consequently, prior to considering the way in which dark adaptation is affected by AMD, it is important to examine the relationship between dark adaptation and age in a population of healthy eyes.

3.1. Introduction

Globally, the average age of the population is forecast to increase during the coming decades (United Nations, 2009). The UK is no exception, with a 32% increase in the population of state pension age predicted by 2033 and a doubling of the population aged over 85 years expected in the same period (Office for National Statistics, 2009). This will, in turn, increase the demand for healthcare services. In order to ensure that the provision of services is sufficient to meet this increased demand, it is important to understand how our biological systems are affected by the ageing process. Furthermore, in the development of clinical tests for AMD, it is important to characterise the effect of normal ageing on visual function, in order to identify disease-specific changes to these parameters.

Age-related changes are evident in many ocular structures (Weale, 1963; Salvi et al., 2006). These include changes in corneal curvature (Topuz et al., 2004; Asano et al., 2005), pupillary miosis (Birren et al., 1950), nuclear sclerosis of the crystalline lens (Bron et al., 2000), liquefaction of the vitreous (Le Goff & Bishop, 2008) and retinal changes (Zarbin, 2004), including reduced choriocapillary density and blood flow, and thickening and increased deposition of Bruch's membrane (Ramrattan et al., 1994; Stefánsson et al., 2011). Correspondingly, changes in many aspects of visual function have been reported with increasing age, for example, a reduction in visual acuity (Klein et al., 1996; West et al., 1997; van der Pols et al., 2000), contrast sensitivity (Nomura et al., 2003; Hohberger et

al., 2007) and photopic and scotopic sensitivity (Robertson & Yudkin, 1944; Steven 1946; Birren et al., 1948; Birren & Shock 1950; Eisner et al., 1987b; Sturr et al., 1997; Jackson et al., 1998), as well as changes in colour vision (Mantjarvi, 2001), stereopsis (Salvi et al., 2006) and dark adaptation (Coile & Baker, 1992; Jackson et al., 1999).

Visual difficulties in low illumination are often reported by elderly adults in the absence of ocular pathology (Kline et al., 1992; McGregor & Chaparro, 2005) and have been identified as a cause of trips and falls in these individuals (McMurdo & Gaskell, 1991). These visual problems are associated with a reduction in photopic and scotopic sensitivity (Robertson & Yudkin, 1944; Steven 1946; Birren et al., 1948; Birren & Shock 1950; Eisner et al., 1987b; Sturr et al., 1997; Jackson et al., 1998). In part, this may be attributed to age-related changes to the pre-retinal ocular structures, which restrict the amount of light reaching the retina (Birren et al., 1950; Bron et al., 2000). Age-related pupillary miosis causes a reduction in the amount of light entering the eye (Birren et al., 1950), while an increase in the density of the ocular media causes an increase in pre-retinal light absorption (Bron et al., 2000). However, the retinal changes that occur with age, for example the loss of RPE and rod photoreceptor cells, are also likely to contribute to diminishing visual sensitivity (Dorey et al., 1989; Gao & Hollyfield, 1992; Curcio et al., 1993).

In addition to the decline in photopic and scotopic sensitivity with increasing age, contemporary investigations have demonstrated an age-related decline in the rates of rod dark adaptation (Holopigian et al., 1997; Jackson et al., 1999; Jackson et al., 2006a). However, data regarding the relationship between age and cone dark adaptation is sparse. Prolonged photostress or ‘glare recovery’ with increasing age has been reported (Collins 1989; Elliott & Whitaker 1991; Margrain & Thomson 2002; Bartlett et al., 2004; Newsome & Negreiro 2009; Wood et al., 2011b). However, only three studies have specifically examined the changes in cone adaptation dynamics that occur with increasing age (Birren & Shock, 1950; Eisner et al., 1987b; Coile & Baker; 1992). Eisner et al. (1987b), found the rate of dark adaptation, measured using a two-channel Maxwellian view device, to be independent of age in 122 participants aged between 60 and 90 years. This finding was supported by earlier work, using the Hecht-Shlaer adaptometer, in 91 male participants aged between 40 and 83 years (Birren & Shock, 1950). In contrast, Coile and Baker (1992) demonstrated a reduction in the rate of cone dark adaptation with increasing age in a cohort of 58 participants aged between 10 and 78 years, using a modified retinal densitometer.

The data presented in this chapter have been accepted for publication in a peer-reviewed journal (see Gaffney et al., 2012 in Appendix III).

3.2. Aims

In light of the limited and apparently contradictory evidence regarding the relationship between age and the dynamics of cone dark adaptation, this study aimed to re-evaluate the effect of age on cone dark adaptation in a cohort of healthy adults.

3.3. Methods

Participants

Forty-one healthy adults, aged 20-83 years, were recruited to the study from the staff, students and patients at the School of Optometry and Vision Sciences, Cardiff University. All participants had a corrected visual acuity of 6/6 or better in the test eye, clear ocular media (\leq Grade 3, LOCS-III) (Chylack et al., 1993), a normal retinal appearance and no history of ocular or systemic disease known to affect visual function. The study was approved by the South East Wales Research Ethics Committee and all procedures adhered to the tenets of the Declaration of Helsinki. Informed written consent was obtained from all participants prior to participation.

All stimuli were presented on a calibrated, high resolution computer monitor (Iiyama LS 902UT) driven by an 8-bit graphics board (nVIDIA Geforce 9) under software control (Matlab, R2009a, The MathWorks Inc.). As described in Chapter 2 (Section 2.2.3, Page 81) the luminance output of the monitor was γ -corrected (Metha et al., 1993; Brainard et al. 2001) and modified using a 1.2 log ND filter mounted on the screen to expose the full range of cone recovery. Dark adaptation was monitored using a modified staircase psychophysical procedure previously implemented by Jackson et al. (1999) (see Section 2.2.3, Page 81).

Experimental procedure

Patient history and baseline data were obtained at the start of the examination. These included Snellen visual acuity, media opacity grading (Chylack et al., 1993) and a binocular indirect fundus examination. Prior to dark adaptation, participants' pupils were dilated with one drop of 1.0% Tropicamide in each eye. A short familiarisation trial was

undertaken until the investigator considered the participant to be competent in the use of the dark adaptation program. Dark adaptation was monitored in the right eye of all participants (the left eye was occluded) and refractive correction was worn as required for a viewing distance of 55cm.

A 95% bleach (5.78 log phot.Td for 60s) of cone photopigment (Hollins & Alpern, 1973) was delivered to the central 43.6° of the test eye using a Maxwellian view optical system. Upon cessation of the bleach, participants placed their chin on the rest in front of the computer screen and recording commenced immediately. Cone dark adaptation was monitored continuously by the computer program for 5 minutes. Thresholds were recorded in response to a 4° diameter achromatic spot presented to the fovea for a duration of 0.2 seconds. Participants were instructed to fixate the centre of the computer monitor, marked by a fixation cross and to indicate perception of the stimulus using the computer keyboard.

Statistical analysis

The time constant of cone recovery (τ) was determined by fitting a single exponential function (Equation 2a, Section 2.1.3), on a least squares basis, to the threshold recovery data recorded from each participant, using Microsoft Excel (2003). Initial and final cone thresholds were also determined from the parameters of the best fitting model. Linear regression analysis was performed to assess the relationship between age and the parameters of cone dark adaptation (Altman, 1991).

3.4. Results

Cone dark adaptation data were recorded from all 41 participants. The cone τ , initial cone threshold and final cone threshold given by the best fitting exponential model are shown in Table 3.1 for each participant. Figure 3.1 illustrates the dark adaptation data obtained from four typical participants, aged 23, 45, 65 and 83 years. Although thresholds remained relatively stable, a general trend towards slower dark adaptation with increasing age was evident.

Table 3.1. Cone τ , initial cone threshold and final cone threshold for all participants

Age (years)	Cone τ (seconds)	Initial threshold (log cd/m ²)	Final threshold (log cd/m ²)
20	117.07	0.73	-2.29
21	79.43	1.01	-2.13
21	72.95	0.89	-1.95
23	98.88	1.06	-2.21
30	84.51	0.82	-2.03
31	45.76	1.51	-1.95
32	77.68	0.97	-2.03
33	85.09	0.77	-2.10
33	125.64	0.82	-2.03
36	91.98	0.80	-2.02
39	55.08	1.33	-1.89
42	128.77	0.75	-2.26
43	122.72	0.86	-2.2
43	60.22	0.76	-1.87
44	106.34	0.72	-2.13
45	99.99	1.01	-2.06
45	100.96	1.00	-2.18
45	90.30	1.19	-1.72
46	112.24	1.11	-2.11
47	108.55	0.83	-2.22
47	91.51	1.22	-2.08
50	130.13	0.86	-2.17
53	92.21	0.81	-2.05
53	127.26	1.04	-2.16
54	77.87	0.76	-1.97
55	97.34	1.13	-2.09
55	125.68	1.03	-2.04
61	136.85	0.67	-2.35
63	163.51	0.69	-2.20
65	135.12	1.00	-2.20
65	128.29	0.99	-1.98
66	153.00	0.80	-2.61
67	127.33	0.92	-2.19
71	108.42	0.88	-2.04
71	202.27	1.00	-2.42
73	210.66	1.04	-2.41
75	234.53	0.98	-1.87
76	121.24	1.11	-1.92
76	152.02	1.14	-1.05
77	170.70	0.43	-2.33
83	153.43	1.10	-2.30

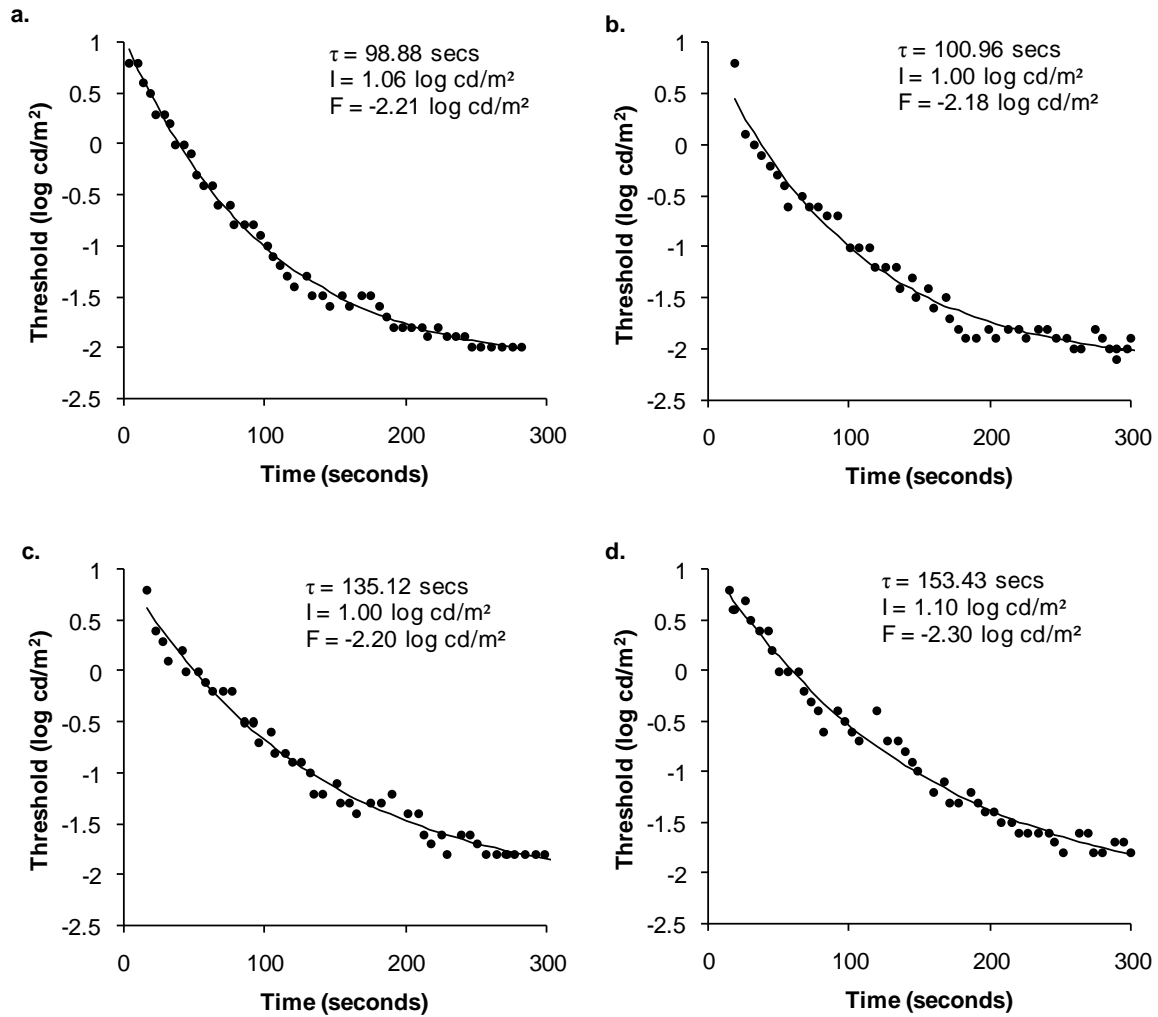


Figure 3.1. Cone dark adaptation data for typical participants aged 23 (a), 45 (b), 65 (c), and 83 (d) years. Each plot is shown with the time constant of cone recovery (τ), initial cone threshold (I) and final cone threshold (F).

A linear regression analysis was used to assess the change in the parameters of cone dark adaptation with increasing age (Figure 3.2). Cone τ increased by 16.35 seconds/decade of life, indicating a progressive slowing of dark adaptation with advancing age (Figure 3.2c). This change in cone τ with increasing age was significant ($p < 0.0005$). There was, however, no significant relationship between increasing age and initial threshold ($p = 0.84$) or final threshold ($p = 0.82$). Remarkably, these data suggest that approximately half of the variation in cone τ may be explained by age alone ($R^2 = 0.50$).

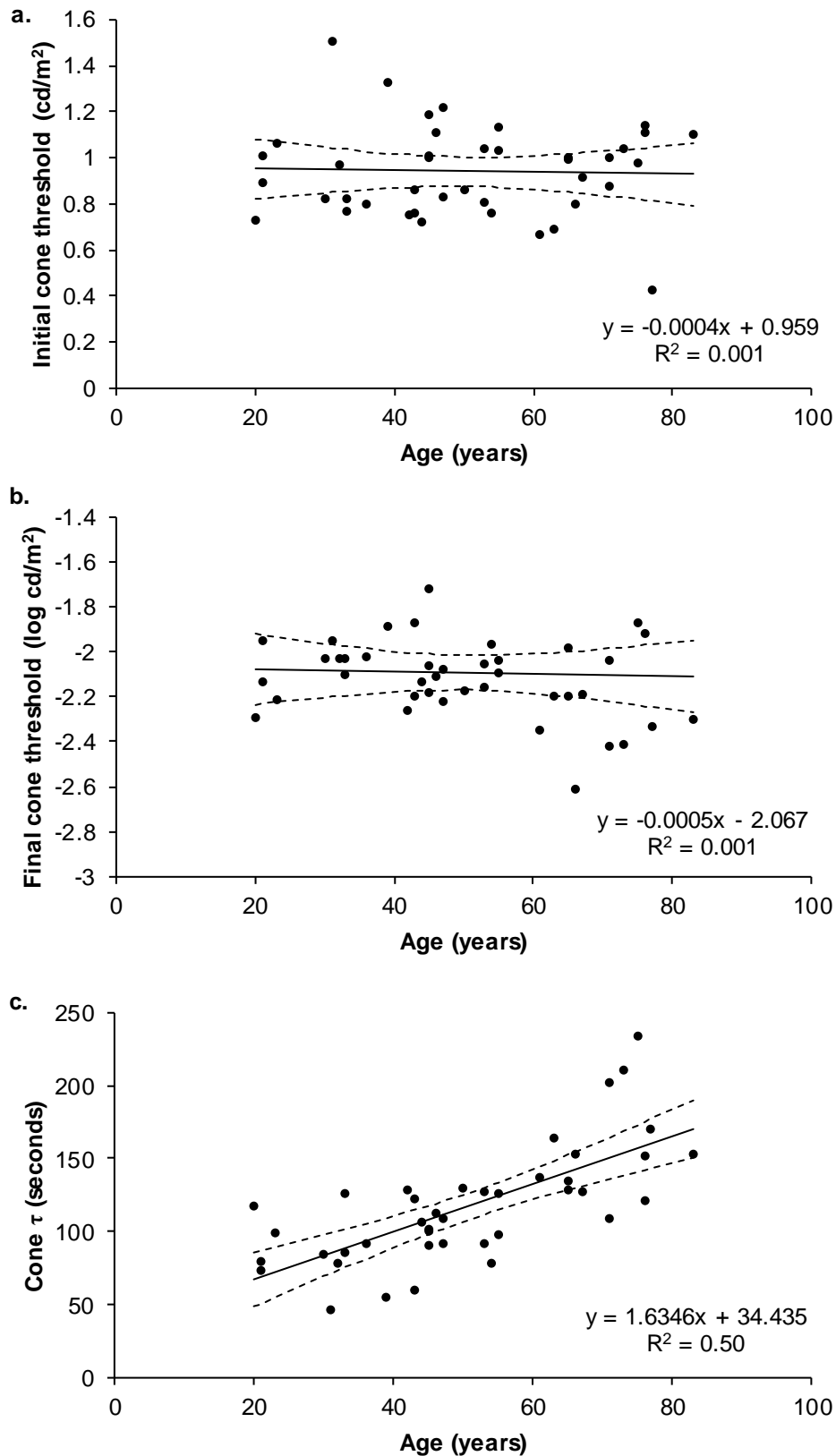


Figure 3.2. Cone dark adaptation as a function of age for initial threshold (a), final threshold (b) and cone τ (c). In each case the solid line is the regression line and the dashed lines indicate the 95% confidence interval for the regression line. The equation for the regression line is displayed on each plot.

3.5. Discussion

These results demonstrate that cone dark adaptation kinetics become progressively slower throughout adulthood. An approximate doubling of cone τ occurred between the ages of 20 and 80 years, which indicates that older adults require substantially more time to adjust to darkness than younger adults. These findings suggest that the performance of older individuals may be impaired during routine visual tasks, particularly those in which a rapid recovery of visual sensitivity is desirable, for example, the recovery of vision following exposure to oncoming headlights when driving at night.

The increase in cone τ of 16.35 seconds/decade of life reported here is comparable to the 12.6 seconds/decade increase reported by Coile & Baker (1992) for cone τ measured using a foveal stimulus in participants aged between 10 and 78 years. The differences between these results and those of earlier work, in which no association between cone dark adaptation and age was reported (Birren & Shock, 1950; Eisner et al. 1987b), are likely to result from methodological differences. The key methodological differences between these studies are shown in Table 3.2. Notably, Eisner et al. (1987) measured cone dark adaptation after exposure to a pre-adapting light of markedly lower intensity than that used by the other investigators, which may have contributed to the variability in their data. Although the use of a relatively modest bleach should not influence the measured exponential time constant, it does reduce the extent to which threshold is raised initially, which may make modelling of an individual's recovery data more challenging (Hollins & Alpern, 1973). In addition, the effects of low intensity pre-adapting lights on the fraction of pigment bleached are more dependent on media changes than more substantial ones. For example, early media changes that reduce the retinal illuminance by a factor of 2 from 20,000 to 10,000 phot.td would reduce the percentage of photopigment bleached from 37% to just 22%, a 15% reduction. In contrast, in this study the same media change would have reduced the percentage of photopigment bleach from 95% to 91%, a 4% reduction. Perhaps just as importantly, Eisner et al (1987) only studied older adults with a limited age range. That is, of the 122 subjects studied all but 5 were in their 60s and 70s. Therefore, it is possible that over the limited age range studied, any effects of age were masked by variability in the dataset.

Table 3.2. Summary of the methodology of previous studies that have examined the relationship between cone dark adaptation and age in healthy participants. The final column shows the characteristics of the methodology employed in the current study.

Parameter	Birren & Shock (1950)	Eisner et al. (1987)	Coile & Baker (1992)	Gaffney et al. (2012)
Participants	91	122	58	41
Age range	40-83 years	60-90 years	10-78 years	20-83 years
Bleach intensity	5.5 log.Td	3.4 log.Td	5.8 log.Td	5.78 log.Td
Bleach duration	3 mins	3 mins	1 min	1 min
Stimulus size	3° Ø	3° Ø	1° Ø	4° Ø
Stimulus location	7.5° nasal to fixation	Fovea	Fovea	Fovea
Stimulus λ	< 460 nm	660 nm	589 nm	White
Psychophysical equipment	Hecht-Shlaer adaptometer	Two channel Maxwellian view	Modified photon counting retinal densitometer	Maxwellian view
Psychophysical method	Method of limits	Method of limits	Method of adjustment	Modified staircase
Threshold interval	1 min for initial 10 mins & 2 mins thereafter	Variable	10 secs for initial 4 mins & 1 min thereafter	Variable (~ every 10 secs)

The violet ($\lambda < 460\text{nm}$) stimulus used to measure dark adaptation by Birren & Shock (1950) makes it possible that visual sensitivity during cone dark adaptation would have been mediated by the S-cones. The data presented in Figure 1 of Birren & Shock (1950) show that no distinct cone plateau occurs before the rods begin to mediate threshold approximately 10 minutes after the bleach offset. This suggests that S-cones dark adapt more slowly than other cone types. The effect of age on S-cone adaptation is unknown, and may differ from that of L- and M-cones. In addition, the participants did not undergo screening for ocular pathologies or general health problems. The lack of standardisation of these characteristics is likely to have increased variability in the results obtained.

There was no evidence of a relationship between age and final cone threshold. This contrasts with previous work in which modest changes in absolute cone threshold with increasing age (0.09-0.37 log cd/m²/decade) have been reported (Birren & Shock., 1950; Eisner et al., 1987b; Coile & Baker; 1992). However, unlike the current study, in which only participants classified as having ‘clear’ ocular media (grade 3 or lower, LOCS-III, Chylack et al., 1993) were included in the sample, these studies did not use such criteria. Consequently, the changes in visual threshold reported previously may be attributed to age-related changes in the density of the ocular media that lead to increased pre-retinal light absorption (Bron et al., 2000). Histological evidence has shown that there is a reduction in rod photoreceptor density throughout life (Curcio et al., 1993), and a corresponding reduction in scotopic sensitivity has previously been reported (Jackson et al., 1998). In contrast, foveal cone density remains relatively stable throughout life (Curcio et al., 1993) and consequently there is no histological premise for a change in cone thresholds with advancing age.

The methodology employed in this study minimised the impact of pre-retinal factors on the results. In addition to all participants having clear ocular media in order to minimise pre-retinal light absorption, pupillary dilation and a Maxwellian view optical system were used to reduce the effect of age-related pupillary miosis on light transmission. Refractive correction was worn if required by the participant to avoid optical blur and ensure that accurate thresholds were obtained. Consequently, the change in the kinetics of cone dark adaptation that occurred with age may be attributed to retinal factors and associated structures alone. Reduced density of the choriocapillaris and reduced choroidal perfusion (Stefánsson et al., 2011), thickening and a reduction in hydraulic conductivity of Bruch’s membrane (Feeneyburns and Ellersieck, 1985; Bird, 1992; Moore et al., 1995), RPE cell loss (Dorey et al., 1989; Gao & Hollyfield, 1992), photoreceptor cell loss (Curcio et al., 1993) and the accumulation of lipofuscin in the RPE (Roth et al., 2004) have been reported to occur with increasing age. These changes are likely to impair photopigment regeneration and will therefore contribute to delays in cone dark adaptation.

Knowledge about the relationship between cone dark adaptation and age is clinically important because cone τ is a potential biomarker for early macular disease (Phipps et al., 2003; Dimitrov et al., 2008; 2011). Our observation that approximately half of the variance in cone τ may be attributed to age alone ($R^2 = 0.50$) suggests that the sensitivity and

specificity of this biomarker could be improved by taking into account the significant age-related decline.

In conclusion, this study has examined the relationship between age and the time course of cone dark adaptation in healthy adults. The results provide compelling evidence in support of an age-related slowing of cone dark adaptation in adults who are free from ocular disease. Therefore we propose that the sensitivity and specificity of cone τ as a biomarker for early age-related macular disease could be improved by taking into account the significant age-related decline in this parameter.

4. The effect of retinal eccentricity on dark adaptation in healthy eyes and eyes with early AMD

Despite widespread agreement that dark adaptation is abnormal in early AMD (Brown et al., 1986a; Collins & Brown, 1989; Steinmetz et al., 1993; Midea et al., 1997; Owsley et al., 2001; Phipps et al., 2003; Binns & Margrain, 2007; Owsley et al., 2007; Dimitrov et al., 2008; 2011), the optimal retinal location for detection of this deficit is unclear. Before examining the changes in dark adaptation that occur across the retina in a disease such as AMD, it is necessary to consider the way in which dark adaptation alters as a function of retinal eccentricity in the healthy retina. Previous investigators have summarised the continuous change in threshold that occurs during cone and rod dark adaptation using several mathematical expressions (models). Therefore, this chapter begins by considering the most appropriate model for characterising experimental dark adaptation data in cones and rods.

4.1. A comparison of models of cone and rod dark adaptation in healthy eyes

4.1.1. Introduction

Originally, visual threshold during dark adaptation was thought to be directly related to the concentration of unbleached photopigment (Hecht et al., 1937). However, this theory was later rejected on the basis of retinal densitometry data that showed that threshold remained significantly elevated after over 90% of photopigment had regenerated. Subsequently, following work in the albino rat (Dowling, 1960) and a rod monochromat (Rushton, 1961), the Dowling-Rushton relationship was adopted as a comprehensive explanation of threshold elevation during rod dark adaptation (Equation 1a, Page 38). This proposed that the logarithm of the visual threshold during dark adaptation was proportional to the concentration of bleached rhodopsin (Figure 4.1). For a comprehensive overview of theories regarding the relationship between visual threshold during dark adaptation and the retinoid cycle, the reader is referred to Section 1.3.4 (Page 37).

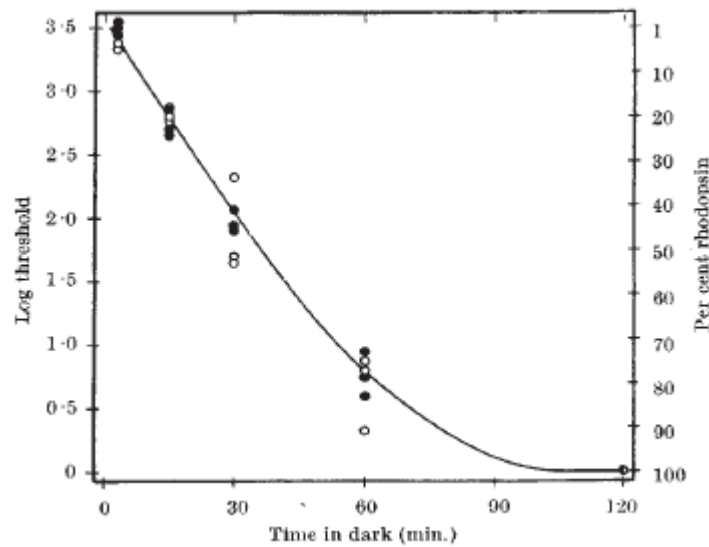


Figure 4.1. Dark adaptation data obtained from an albino rat (Dowling, 1960). The logarithm of visual threshold and the concentration of bleached rhodopsin follow the same exponential time course.

At high adapting intensities, the dark adaptation function is biphasic (Hecht et al., 1937). The rapid recovery of threshold that occurs initially is mediated by the cone photoreceptors and the slower recovery of threshold that follows is mediated by the rod photoreceptors. Dark adaptation data have previously been described using a range of mathematical models based on the physiology of the visual cycle. If photopigment regeneration is considered a ‘first-order’ process, in which recovery of threshold is proportional to the concentration of particular photochemical, it is appropriate to summarise dark adaptation data using an exponential function. Alternatively, should photopigment regeneration be ‘rate-limited’, that is limited by the availability of a particular photochemical or by the presence of a photoproduct of bleaching, a linear model is more applicable.

Models of cone dark adaptation

The Dowling-Rushton relation was shown to provide an appropriate description of the regeneration of cone photopigment (Hollins & Alpern, 1973). Consequently, cone photopigment regeneration was initially thought to proceed as a first-order process and has typically been described using an exponential model (Rushton & Henry, 1968; Hollins & Alpern, 1973; Coile & Baker, 1992), such as the single exponential function given in Equation 4a. However, more recently the exponential time constant of cone recovery (τ) has been shown to vary with bleaching intensity and duration (Paupoo et al., 2000; Mahroo

& Lamb, 2004). This behaviour is inconsistent with a first-order process. Therefore, Mahroo & Lamb (2004) have suggested that the delivery of 11-cis retinal to the photoreceptor outer segment is a rate-limiting step during dark adaptation, and consequently threshold recovery is better described by a rate-limited function (Equation 4b).

$$\text{Equation 4a.} \quad T(t) = a + (b \cdot \exp^{-t/\tau})$$

where T is the threshold at time t after the bleach, a is the final cone threshold, b is the change in cone threshold from $t = 0$ and τ is the time constant of cone recovery (McGwin et al., 1999). The pre-bleach threshold may be calculated by adding together the final cone threshold and the change in cone threshold.

$$\text{Equation 4b.} \quad T(t) = a [1 - K_m \cdot W \{B/K_m \cdot \exp^{(B/K_m)} \cdot \exp^{-r(1+K_m)/K_m} \cdot t\}]$$

where T is the threshold at time t after the bleach, a is the pre-bleach threshold, K_m is the Michaelis constant, W is the ‘Lambert W function’, B is the initial bleach and r is the maximum rate of recovery (Paupoo et al., 2000; Mahroo & Lamb, 2004; Binns & Margrain, 2005).

Models of rod dark adaptation

Traditionally, in accordance with the Dowling-Rushton relation, rod dark adaptation data have been described using exponential models. Equation 4c shows a typical double exponential function, in which the initial exponential component describes the reduction in threshold attributed to cones and the second exponential component describes the rod threshold recovery data.

$$\text{Equation 4c.} \quad T(t) = [a_c + (b_c \cdot \exp^{-t/\tau_c})] + [\min(0, a_r + (b_r \cdot \exp^{-t/\tau_r}))]$$

where T is the threshold at time t after the bleach, a_c is the final dark adapted cone threshold, b_c is the change in cone threshold from $t = 0$, τ_c is the time constant of cone recovery, \min is a logic statement a_r is the final dark adapted rod threshold, b_r is the change in rod threshold from $t = 0$, and τ_r is the time constant of cone recovery (McGwin et al., 1999).

However, the Dowling-Rushton relation was subsequently shown to apply only to rod photopigment regeneration following a near-total bleach of rhodopsin (Pugh, 1975; Lamb, 1981). A linear relationship between elevation of rod threshold and intermediary ‘photoproducts’ produced by the bleach has been proposed as a more appropriate model for a range of bleach intensities (Lamb, 1981). Consequently, rod recovery may be more accurately described by a rate-limited model consisting of several separate components with different rates of recovery (Lamb, 1981), such as that given by the second and third parts of Equation 4d (the initial exponential component of the equation models cone recovery only).

Equation 4d.
$$T(t) = [a + (b.exp^{(-t/\tau)})] + [c.(max(t - rcb, 0))] + [d.(max(t - rrb, 0))]$$

where T is the threshold (log cd/m²) at time t after cessation of the bleach, a is the final cone threshold, b is the change in cone threshold from $t = 0$, τ is the time constant of cone recovery, c is the slope of the second component of rod recovery, max is a logic statement, rcb denotes the time from bleach offset to the RCB, d is the slope of the final component of rod recovery and rrb denotes the time from bleach offset to the transition between the second and final components of rod recovery (McGwin et al., 1999).

4.1.2. Aims

Given the range of models proposed to describe cone and rod recovery data after a photopigment bleach, the first aim of the study was to compare exponential and rate-limited models of cone and rod recovery in a small group of healthy observers. The ability of the respective models to describe cone and rod threshold recovery data were evaluated in order to determine whether the additional parameters included in the rate-limited model are justified by a better fit to the threshold recovery data.

4.1.3. Methods

Participants

Three experienced observers (AB, AG and TM) participated in the study. All participants had a corrected visual acuity of 6/6 or better in the test eye, clear ocular media (\leq Grade 3, LOCS-III) (Chylack et al., 1993), normal retinal appearance and no history of ocular or systemic disease known to affect visual function. The participants provided their informed

written consent prior to participation and all procedures adhered to the tenets of the Declaration of Helsinki.

Apparatus

All stimuli were presented on a calibrated, high resolution CRT monitor (Iiyama LS 902UT) driven by an 8-bit graphics board (nVIDIA Geforce 9) under software control (Matlab, R2009a, The MathWorks Inc). As described in Chapter 2 (Section 2.2.3) the luminance output of the monitor was γ -corrected (Metha et al., 1993; Brainard et al. 2001) and modified by neutral density filters mounted on the screen to expose the full range of retinal recovery. Dark adaptation was monitored using a modified staircase psychophysical method based on a procedure previously implemented by Jackson et al. (1999) (Section 2.2.3). The Matlab code for this procedure is shown in Appendix II ('retinal eccentricity procedure').

Experimental procedure

Prior to dark adaptation, participants were dilated with one drop of 1.0% Tropicamide in each eye. The right eye was tested in all participants and the left eye was occluded. Refractive correction was worn if required.

On each dark adaptation trial, a Maxwellian view optical system was used to bleach 95% of cone photopigment ($5.78 \log \text{phot.Td}$ for 60s) (Hollins & Alpern, 1973) in the central 43.6° of the test eye. Upon cessation of the bleach, participants placed their chin on the rest in front of the computer screen and the dark adaptation program commenced immediately. Participants stared at the centre of the screen, indicated by a fixation cross and signalled perception of the stimulus via the computer keyboard. Dark adaptation was monitored continuously for 25 minutes for each stimulus with the exception of the smallest, when recovery was monitored for 10 minutes.

Thresholds were recorded in response to a foveal spot (radius 0.5°) and four achromatic annuli (1, 2, 4 and 8° in radius), all 0.5° wide, centred on the fovea (Figure 4.2). Data were obtained three times with each stimulus. Consequently, each participant completed a total of 12 dark adaptation trials spread over four occasions within a one month period. When more than one dark adaptation measurement was completed in a single session, a washout period of an hour was interleaved between successive bleaches.

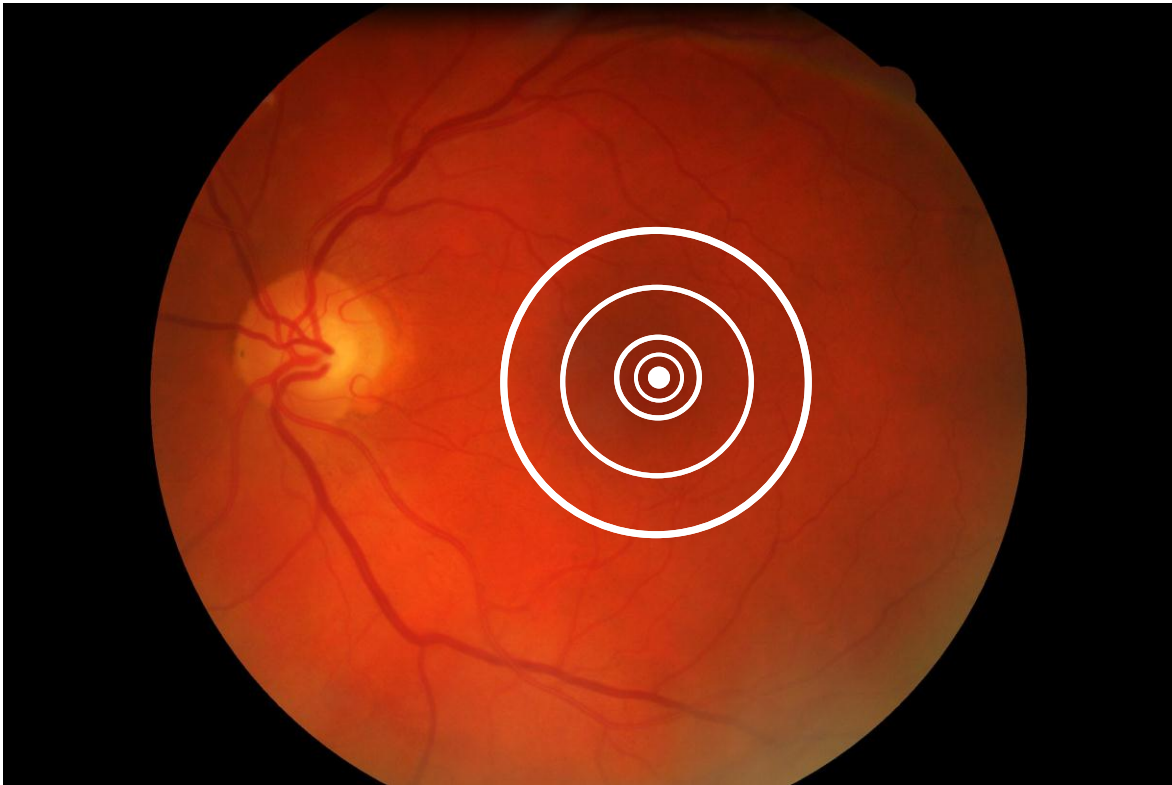


Figure 4.2. Diagrammatic representation of the spot stimulus and the four annular stimuli, superimposed on the macula of a healthy participant. In order of increasing size, the radii of the stimuli were 0.5, 1, 2, 4 and 8°. Each annulus was 0.5° wide.

Models of cone dark adaptation

All cone threshold recovery data were modelled with a single exponential function (Equation 4a), and with a rate-limited function based on Michaelis-Menton kinetics (Equation 4b), on a least-squares basis, using the solver function in Microsoft Excel (2003).

Models of rod dark adaptation

Subsequently, to compare models of rod dark adaptation, all threshold recovery data were modelled using a double exponential function (Equation 4c) and with a single exponential - two linear function (Equation 4d), on a least-squares basis, using the solver function in Microsoft Excel (2003). The initial exponential component of each model, which described the reduction in threshold attributed to cones, was identical. The second component of the model (exponential or linear) was fitted to the rod threshold recovery data. This approach was used to ensure objective identification of the RCB. Given that the cone data were

modelled in the same way for each dataset, any differences in the accuracy of the overall model fit could be attributed to the rod component.

Statistical analysis

The fit of each model was evaluated at each of the five retinal locations tested. The root mean square error (RMS error) was first calculated as a measure of the ‘goodness-of-fit’ the models. A lower RMS error indicated a better model fit to the data. The Akaike criterion (AIC) (Equation 4e) was then calculated in order to determine if the greater number of parameters in the rate-limited models was warranted based on their ability to improve the description of the data. The most appropriate model has the lowest AIC value (Akaike, 1974). Minimising the number of free parameters is desirable to ensure the lowest possible variance during model fitting.

Equation 4e.
$$AIC = [n.Ln(SSr)] + [2.p]$$

where n is the number of data points, SSr is the residual sum of squares adjusted for the measurement error and p is the number of free parameters.

4.1.4. Results

Cone dark adaptation data recorded from participant AB at 0.5, 1, 2, 4 and 8° from fixation are shown in Figure 4.3, with the best fitting exponential and rate-limited models of recovery at each retinal location. On visual inspection, both the exponential and the rate-limited models provided a good fit to the data at all retinal locations and the two models were virtually superimposable. The two models of cone recovery also described the dark adaptation data obtained from the other two participants equally well. Figure 4.4 shows the rod dark adaptation data from the same individual, assessed 1, 2, 4 and 8° from fixation, with the best fitting exponential and rate-limited models. The two models looked extremely similar and both described the data equally well. This was also the case for the rod data collected from the other two participants.

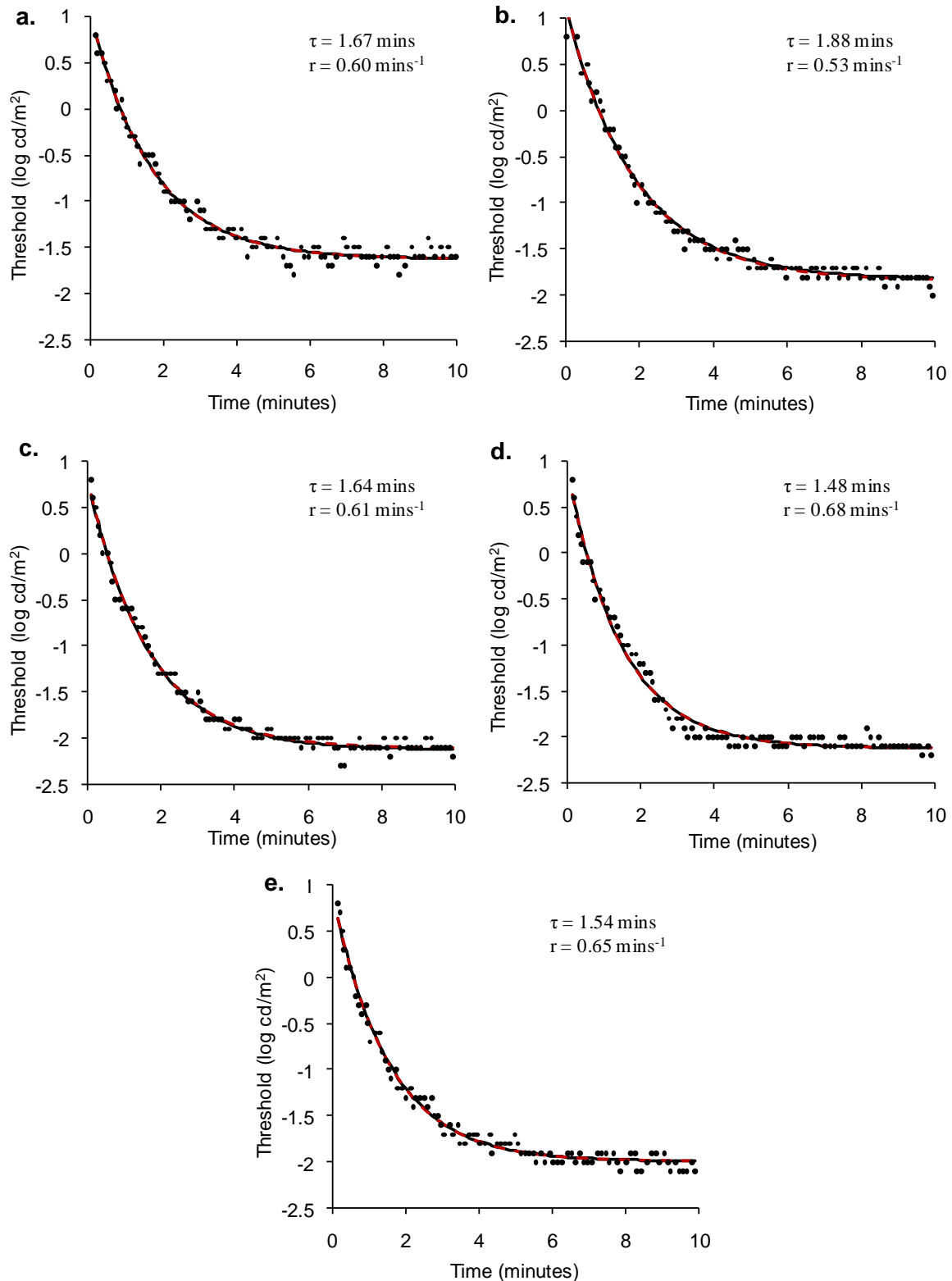


Figure 4.3. Cone dark adaptation curves recorded from AB, at the first visit, at 0.5 (a), 1 (b), 2 (c), 4 (d) and 8° (e) from fixation. For each retinal location the best fitting exponential model is shown by the black line and the best fitting rate-limited model is shown by the red line. These two lines are almost identical and therefore overlap considerably. The time constant of cone recovery (τ) and the maximum rate of cone recovery (r) given by the models are also shown.

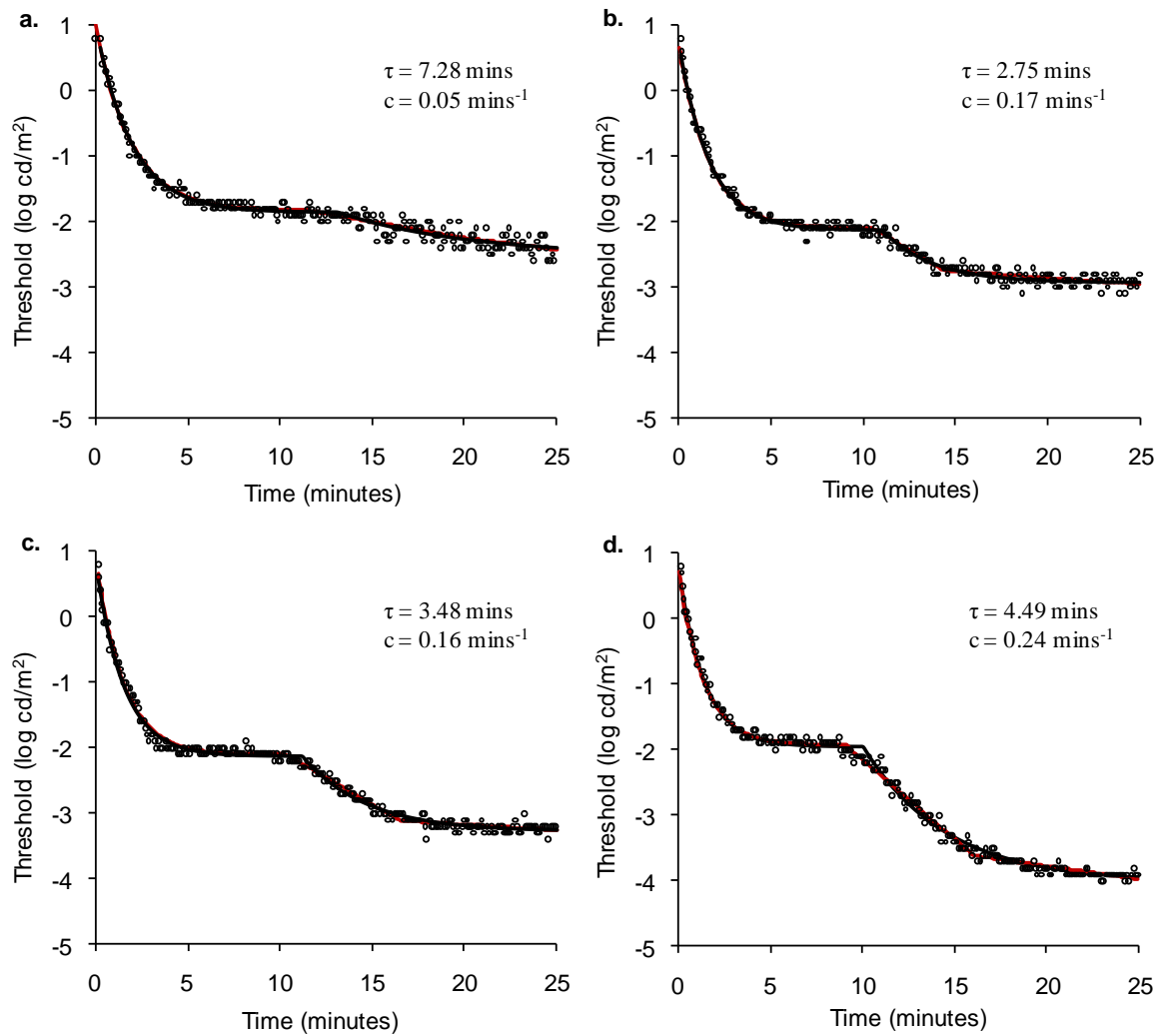


Figure 4.4. Dark adaptation curves recorded from AB, at the first visit, at 1 (a), 2 (b), 4 (c) and 8° (d) from fixation. For each retinal location the cone data is fitted using an exponential model. The rod data is shown with the best fitting exponential model (black line) and the best fitting rate-limited model (red line). There is marked overlap of these two lines as the two models provide extremely similar descriptions of the rod dark adaptation data. The exponential time constant of rod recovery (τ) and the slope of the second component of rod recovery (c) given by the models are also shown.

Table 4.1 shows the mean RMS error for each model of cone dark adaptation at each retinal location. The RMS errors of the exponential and rate-limited models were almost identical at most of the retinal locations tested. Table 4.2 shows the mean AIC values for the two models at the five retinal locations. The lowest AIC value indicates the most appropriate model for the data. The exponential model had a marginally lower AIC value compared to the rate-limited model at three of the five retinal locations. However, these differences in AIC values between the models were very small.

Table 4.1. Mean RMS error (+/- standard deviation) of the exponential and rate-limited models of cone dark adaptation for the five retinal locations. (Dark adaptation was monitored three times at each retinal location in all three participants).

	RMSE (log cd/m²)	
	Exponential	Rate-limited
0.5°	0.109 (0.025)	0.109 (0.025)
1°	0.102 (0.023)	0.101 (0.023)
2°	0.097 (0.019)	0.096 (0.020)
4°	0.095 (0.024)	0.096 (0.023)
8°	0.078 (0.028)	0.086 (0.014)
Mean	0.096 (0.012)	0.098 (0.008)

Table 4.2. Mean AIC value (+/- standard deviation) of the exponential and rate-limited models of cone dark adaptation for the five retinal locations.

	AIC	
	Exponential	Rate-limited
0.5°	451.82 (57.86)	453.81 (57.86)
1°	456.96 (69.53)	456.85 (70.21)
2°	447.87 (50.54)	456.66 (50.60)
4°	2438.28 (2897.37)	2447.53 (2908.78)
8°	2512.84 (2932.00)	2519.11 (2929.23)
Mean	1261.56 (1108.55)	1266.79 (1110.82)

Table 4.3 shows the mean RMS error at each retinal location for the two models of rod dark adaptation. The exponential-linear model yielded an RMS error that was almost identical to the double exponential model at all four retinal locations. The mean AIC values for the two models are shown in Table 4.4 for the four retinal locations tested. For the dark adaptation data obtained 1° and 2° from fixation the double exponential had lower AIC values, whereas at the more eccentric retinal locations tested (4° and 8°) the exponential-linear model had lower AIC values.

Table 4.3. Mean RMS error (+/- standard deviation) of the exponential-linear and double exponential models of dark adaptation for the four retinal locations.

	RMSE (log cd/m ²)	
	Exponential – two linear	Double exponential
1°	0.119 (0.020)	0.115 (0.016)
2°	0.104 (0.024)	0.102 (0.019)
4°	0.093 (0.017)	0.103 (0.017)
8°	0.086 (0.013)	0.095 (0.013)
Mean	0.101 (0.014)	0.104 (0.008)

Table 4.4. Mean AIC value (+/- standard deviation) of the exponential-linear and double exponential models of dark adaptation for the four retinal locations.

	AIC	
	Exponential – two linear	Double exponential
1°	1268.41 (133.12)	1258.29 (119.63)
2°	1222.95 (134.82)	1202.21 (107.17)
4°	1407.49 (259.82)	1440.82 (226.52)
8°	1378.67 (173.65)	1414.92 (197.63)
Mean	1319.38 (87.89)	1329.06 (116.85)

4.1.5. Discussion

This section of the study aimed to compare ‘first order’ and ‘rate-limited’ models for describing cone and rod threshold recovery data after a photopigment bleach. In general, the RMS error for all of the models used to describe the cone and rod recovery data was extremely small ($< 0.14 \log \text{ cd/m}^2$). This showed that all four models provided a good description of the threshold recovery data.

There were no conclusive differences in the RMS error or AIC values between the exponential and rate-limited models of cone recovery. This indicates that no additional benefit is gained by using the rate-limited model of cone recovery, which has a greater number of free parameters, over a conventional exponential or ‘first-order’ model of

threshold recovery. An average cone τ of 1-2 minutes was recorded at all retinal locations in all three participants. This is consistent with previous studies in which data were obtained following a near-total bleach of photopigment (Hollins & Alpern, 1973; Coile & Baker, 1992). However, more recently it has been shown that although cone threshold recovery data are well described by an exponential model after a high intensity bleach, a rate-limited model provides a more appropriate description of recovery after bleaches of a lower intensity (Paupoo et al., 2000; Pianta & Kalloniatis, 2000; Mahroo & Lamb, 2004). Therefore, the similarity in the fit of the exponential and rate-limited models in this study may be a function of the high intensity bleach used. Mahroo & Lamb (2004) propose that a limiting step in cone photopigment regeneration arises from the resistance encountered by 11-cis retinal as it diffuses into the photoreceptor outer segments.

Small differences in the ‘goodness of fit’ of the exponential and rate-limited models of rod dark adaptation were evident at 4 and 8° from fixation. At these locations the rate-limited model had a slightly smaller RMS error and AIC value than the exponential model. This indicates that the rate-limited model provides a more accurate representation of the threshold recovery data at these retinal locations. The differences in the fit of the two models at these retinal eccentricities compared to the more central retinal locations tested may, in part, be attributed to the greater exposure of the rod limb of the dark adaptation curve that occurs with increasingly peripheral retinal locations.

The rate-limited model of rod dark adaptation is widely accepted as a good description of the underlying biology of photopigment regeneration (McGwin et al., 1999) and in recent years has been used in many studies of conditions with abnormal dark adaptation parameters, for example AMD (Owsley et al., 2001; Owsley et al., 2007). This consistency in data modelling is extremely valuable as it facilitates meaningful comparison of results between studies.

In conclusion, at high bleaching intensities, there is insufficient evidence to accept the rate-limited model of cone recovery in preference to the conventional exponential model. However, the RMS errors suggest that the rate-limited model of rod recovery provides a more accurate description of dark adaptation data than the exponential model. The use of an ‘exponential-linear’ model at high bleaching intensities will generate a comprehensive

description of cone and rod threshold recovery data, and will be used to model dark adaptation data during the experiments described within the remainder of this thesis.

4.2. The topography of cone and rod dark adaptation in healthy eyes

4.2.1. Introduction

Only a limited number of studies have documented the effect of retinal location on the kinetics of dark adaptation in the healthy retina (Hecht et al., 1935; Wolf & Zigler, 1950; Dimitrov et al., 2008). These have consistently shown that when dark adaptation is monitored at increasingly eccentric retinal locations, the RCB occurs earlier, the rod branch appears more pronounced and a lower final threshold is attained (see left panel of Figure 1.13, Page 32).

Hecht et al. (1935) obtained identical dark adaptation curves for spot stimuli of enlarging diameter centred on the fovea and small, fixed diameter stimuli, presented at an equivalent retinal location to the edge of the central stimulus, for example a 20° diameter centrally located spot and a 2° diameter spot located 10° from the fovea. This implies that threshold during dark adaptation is determined by the most eccentric retinal location stimulated, rather than the size of the stimulus. The likely cause of this variation in dark adaptation with retinal eccentricity is the corresponding variation in photoreceptor density and receptive field size.

The properties of the retinal mosaic vary with retinal location (see Figure 4.11, Page 119). Human cone photoreceptor density peaks at the fovea (200,000cells/mm²) and decreases rapidly with increasing retinal eccentricity, whereas rod photoreceptors first appear in the parafovea and increase to a maximum density of 150,000cells/mm² at 12-18° from fixation (Curcio et al., 1990). Correspondingly, cone photopigment density is highest at the fovea (Tornow et al., 1997; Bone et al., 2007) and rod photopigment density is maximal approximately 11° from fixation (Tornow et al., 1997; Tornow & Stilling, 1998).

Approximately 50% of retinal ganglion cells are located in the central 16° of the retina and at the fovea there is a favourable ratio of 2-3 ganglion cells to every cone photoreceptor

(Curcio & Allen, 1990). Ganglion cell density peaks 1.5-7° from fixation and declines rapidly at increasingly eccentric retinal locations. Correspondingly, the dendritic field size, and therefore receptive field size, of human retinal ganglion cells increases with increasing eccentricity (Dacey & Petersen, 1992). This leads to an increase in spatial summation with increasing distance from the fovea.

Generally, the density of other types of retinal cells decreases with increasing eccentricity. For example, RPE cell density is maximal at the fovea and declines with increasing eccentricity (Panda-Jonas et al., 1996; Harman et al., 1997). Similarly, Müller cell density decreases when moving from the fovea to the peripheral retina (Nishikawa & Tamai, 2001). This may also have an effect on the rate of adaptation across the retina.

4.2.2. Aims

In light of the heterogeneity of the retinal mosaic, dark adaptation may be expected to vary as a function of retinal location. Consequently, the second aim of this study was to assess the dynamics of dark adaptation as a function of retinal eccentricity in a small group of healthy participants.

4.2.3. Methods

The dark adaptation data obtained in Section 4.1.3 from three experienced observers, at five retinal locations: 0.5, 1, 2, 4 and 8° from fixation, after a 95% bleach of cone photopigment (5.78 log phot.Td for 60s) (Hollins & Alpern, 1973) were used for all analyses.

Statistical analysis

On the basis of the modelling analysis presented previously (section 4.1), all threshold recovery data were fitted with an exponential-two linear model of dark adaptation (Equation 4d, Section 4.1.1) (McGwin et al., 1999). This was implemented, on a least squares basis, using the solver function in Microsoft Excel (2003). Cone threshold recovery was summarised by the exponential component and rod threshold recovery by the linear components.

The parameters of interest were cone τ , final cone threshold, time to RCB, rate of the second component of rod recovery and rod threshold at 25 minutes (taken as the mean of

the final three data points). The mean (\pm standard deviation) was calculated for each parameter in order to make comparisons between the five retinal locations tested.

4.2.4. Results

Typical recovery data obtained from the three experienced observers at 0.5, 1, 2, 4 and 8° from fixation are shown in Figure 4.5. In all participants, as the eccentricity of the stimulus increased, cone adaptation proceeded more rapidly, the rod branch of the dark adaptation curve became increasingly prominent and a lower final rod threshold was attained.

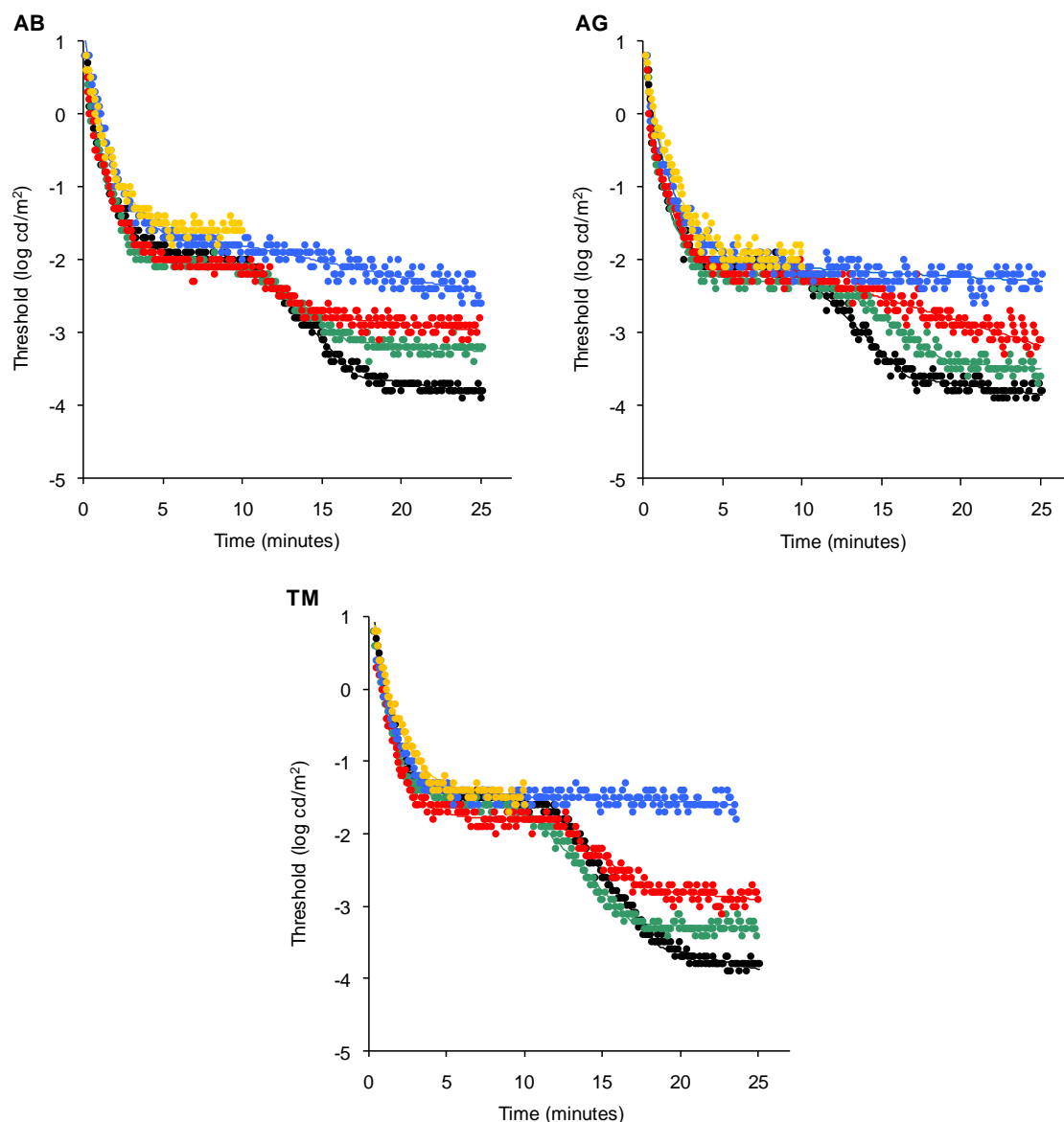


Figure 4.5. Examples of dark adaptation curves recorded from the first trial of all three participants (AB, AG and TM) in response to all five stimulus sizes: 0.5° (yellow), 1° (blue), 2° (red), 4° (green) and 8° (black). For each stimulus size the raw data are shown with the best fitting model of dark adaptation given by equation 4d.

Figure 4.6 shows mean cone τ data for all participants, plotted as a function of retinal eccentricity. As the distance from the fovea increased, cone τ decreased. This indicates that recovery of visual sensitivity was slowest at the fovea. In addition, inspection of Figure 4.7 shows that cone final threshold was higher in at the fovea compared to more eccentric retinal locations.

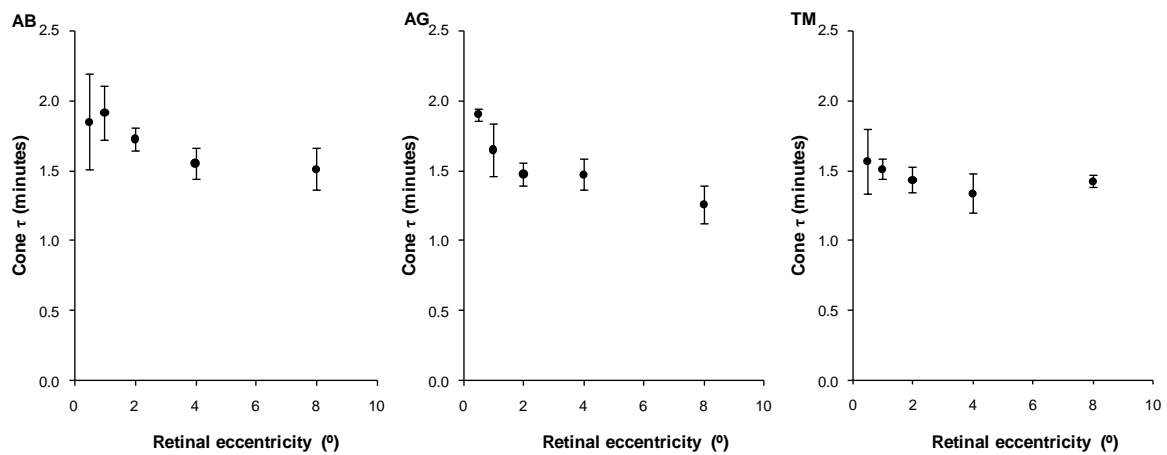


Figure 4.6. Mean cone τ at each retinal eccentricity for AB, AG and TM, shown with 95% confidence intervals.

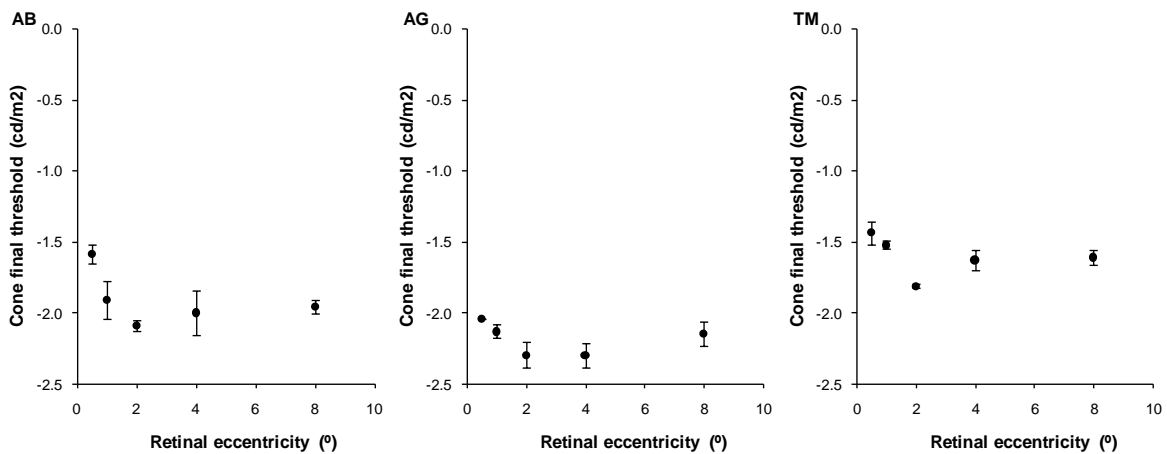


Figure 4.7. Mean cone final threshold at each retinal eccentricity for AB, AG and TM, shown with 95% confidence intervals.

A marked increase in the rate of the second component of rod recovery with increased eccentricity is demonstrated in Figure 4.8. This was accompanied by progressively lower rod thresholds (at 25 minutes) with increasing eccentricity (Figure 4.9). In contrast, no systematic variation in the time to RCB occurred as a function of retinal eccentricity (Figure 4.10).

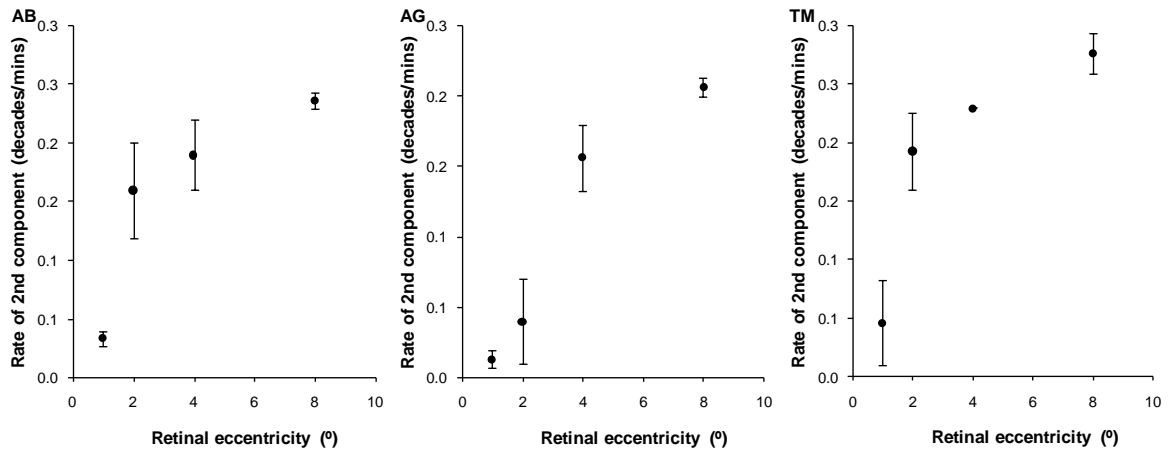


Figure 4.8. Mean rate of 2nd component of rod recovery at 1, 2, 4 and 8° from fixation for AB, AG and TM, shown with 95% confidence intervals.

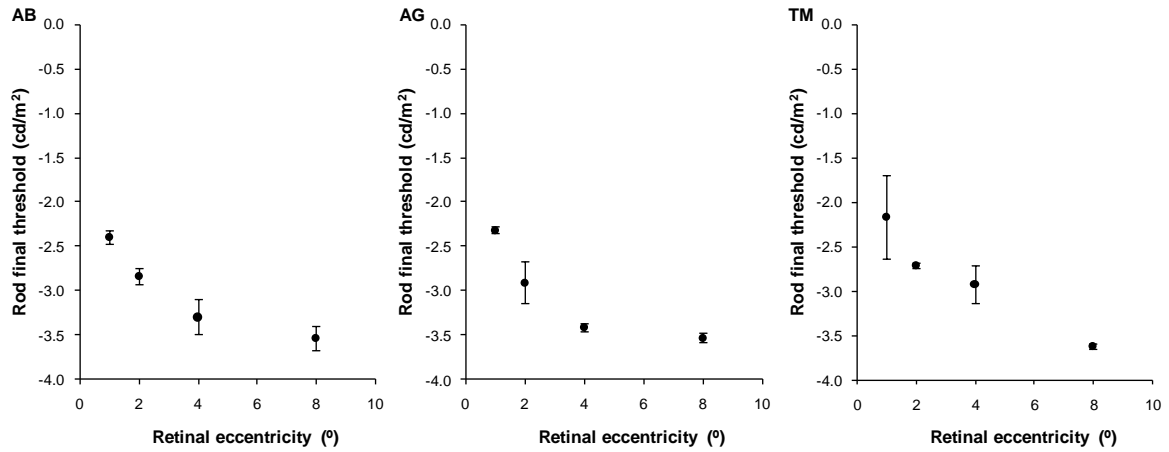


Figure 4.9. Mean 25 minute rod thresholds at 1, 2, 4 and 8° from fixation for AB, AG and TM, shown with 95% confidence intervals.

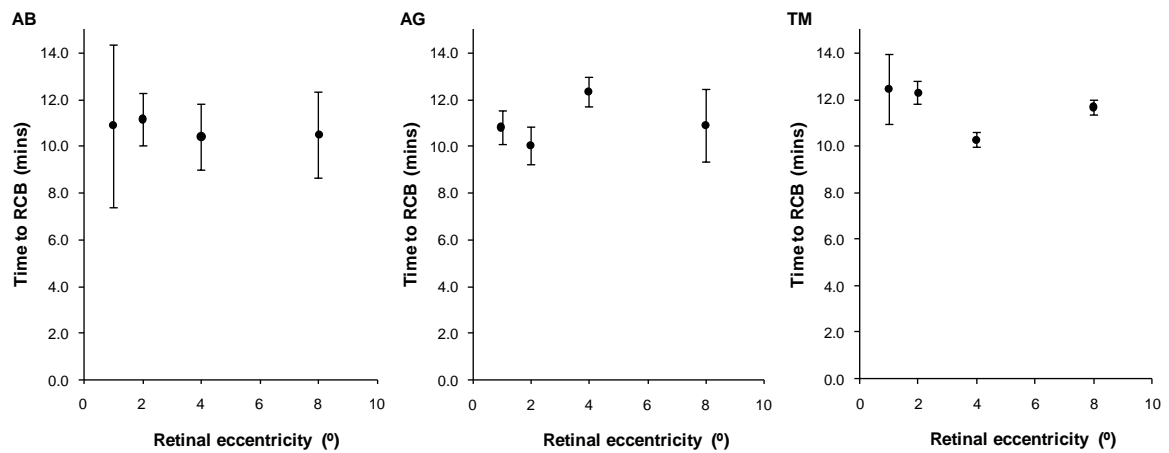


Figure 4.10. Mean time to RCB at 1, 2, 4 and 8° from fixation for AB, AG and TM, shown with 95% confidence intervals.

A summary of the mean dark adaptation parameters (+/- standard deviation) for the group of participants is displayed in Table 4.5. This demonstrates that both rod and cone dark adaptation occurred more rapidly as the retinal eccentricity of the stimulus increased.

Table 4.5. Mean (+/- standard deviation) dark adaptation parameters at five retinal locations tested in all participants.

	0.5°	1°	2°	4°	8°
Cone tau (mins)	1.77 (0.18)	1.69 (0.20)	1.55 (0.14)	1.46 (0.12)	1.40 (0.13)
Cone FT (log cd/m²)	-1.69 (0.31)	-1.85 (0.27)	-2.06 (0.22)	-1.97 (0.30)	-1.90 (0.24)
Time to RCB (mins)	-	11.39 (1.88)	11.17 (1.10)	11.02 (1.15)	11.04 (1.12)
Rate of 2nd comp (decades/min)	-	0.03 (0.02)	0.13 (0.07)	0.19 (0.03)	0.24 (0.03)
Rod FT (log cd/m²)	-	-2.29 (0.27)	-2.82 (0.14)	-3.21 (0.35)	-3.56 (0.11)

4.2.5. Discussion

The dark adaptation data collated from the highly experienced observers in this study provides an insight into the relationship between retinal eccentricity and the dynamics of dark adaptation in the healthy retina. Significantly, this is the first study to quantify the parameters of dark adaptation as a function of retinal eccentricity. In agreement with previous work (Hecht et al., 1935; Wolf & Zigler, 1950; Dimitrov et al., 2008), the results showed that as the eccentricity of the stimulus increased, a progressive acceleration of recovery was observed, which resulted in a faster and more prominent second phase of rod recovery. However, in contrast with these previous studies, we did not find a systematic change in the time to RCB with increasing retinal eccentricity.

Cone dark adaptation was slowest at the fovea. This corresponds to the locus of peak cone photoreceptor density (200,000 cells/mm²) (Curcio et al., 1990) (Figure 4.11) and peak cone photopigment density (Tornow et al., 1997; Bone et al., 2007). Competition for the finite supply of available 11-cis retinal is therefore greatest at the fovea and this may explain the relatively slow cone recovery observed at this retinal location. Cone

photoreceptor density declines by almost 75% between the fovea and 0.7° from fixation (Figure 4.11). This leads to a marked reduction in the demand for 11-cis retinal and expedites threshold recovery. Although overall (rod and cone) photoreceptor density gradually increases again to about 150,000 cells/mm² approximately 14° from fixation, this clearly remains less than the high cone density at the fovea and therefore competition for 11-cis retinal is always lower than at the fovea.

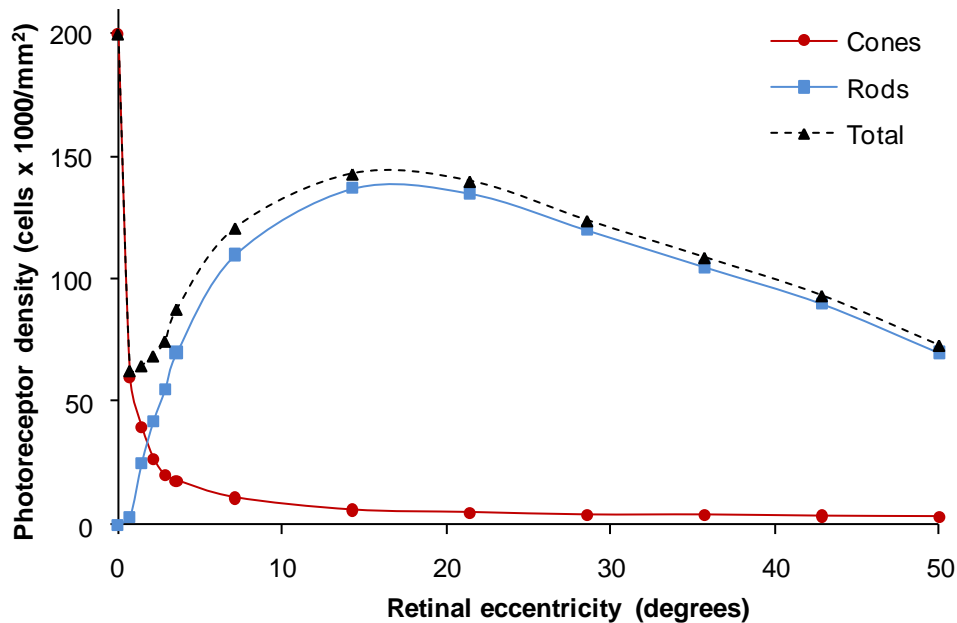


Figure 4.11. Human photoreceptor density in the temporal retina (After Curcio et al., 1990)

A significant increase in the rate of rod recovery with increasing retinal eccentricity was observed between 1 and 8° from fixation. This may initially seem unexpected given the increase in rod density from the rod free fovea to in excess of 110,000 cells/mm² at 8° from fixation (Curcio et al., 1990), which will correspondingly increase competition for 11-cis retinal. However, the increased rate of rod recovery with increased eccentricity was accompanied by the significant lowering of the rod threshold at 25 minutes in all three participants. This is likely to be linked to the increase in receptive field size and spatial summation that occurs between the central and peripheral retina (Dacey & Petersen, 1992). This is exemplified in Figure 4.12, which illustrates the predicted threshold recovery for one, five and ten rods, described by a rate-limited function. Clearly, a reduction in final threshold is closely linked to an apparent increase in the rate of rod recovery. When the rod data of the three observers are re-modelled using an exponential function, the time constant

of rod recovery (τ) is independent of the 25 minute rod threshold and also of eccentricity. This implies that it is the effect of spatial summation on final threshold that influences the measured rate of rod recovery described using a rate-limited function. That is, the peripheral rods are not recovering any more rapidly than the central ones, they are just working together to provide a lower final threshold.

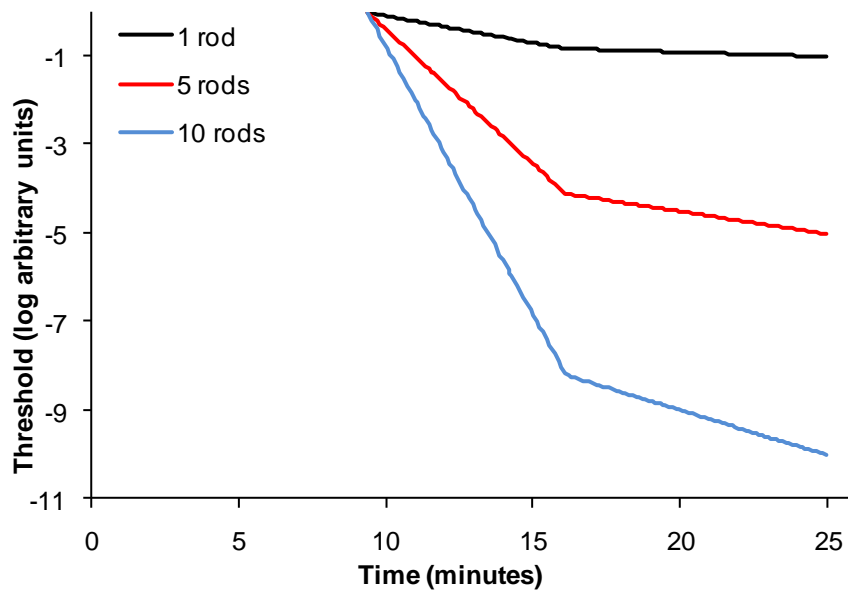


Figure 4.12. The predicted threshold recovery of 1, 5 and 10 rods, described by the rate-limited model. The ‘1 rod’ data was recorded from AB at 8° from fixation. These data were multiplied by the number of rods to obtain the predicted recovery of 5 and 10 rods.

In summary, this study of healthy observers has confirmed that cone dark adaptation occurs more rapidly at increasingly peripheral retinal locations, but while rod dark adaptation appears to proceed at an increased rate with increasing eccentricity, this is likely to be due to changes in final threshold. Knowledge of the way in which dark adaptation is affected by retinal eccentricity in the healthy retina is useful when considering the topography of changes to dark adaptation that occur in a disease such as AMD.

4.3. The topography of cone dark adaptation deficits in early AMD

4.3.1. Introduction

Although many studies have reported dark adaptation deficits in individuals with early AMD, there are inconsistencies within the literature. Delays in rod mediated dark

adaptation have been widely reported (Brown & Lovie-Kitchin, 1983; Brown et al., 1986a, Steinmetz et al., 1993; Owsley et al., 2001; Owsley et al., 2007; Dimitrov et al., 2008; 2011). However, evidence for abnormal cone dark adaptation is equivocal (Brown et al., 1986b; Phipps et al., 2003; Binns & Margrain, 2007; Owsley et al., 2007; Dimitrov et al., 2008; 2011). For example, while Dimitrov et al. (2008) reported significant delays in cone-mediated dark adaptation in people with early AMD, Owsley et al. (2007) found no evidence of changes to cone-mediated dark adaptation in patients with early, intermediate or advanced AMD.

One explanation for the conflicting evidence regarding cone-mediated dark adaptation in early AMD is that the cone dark adaptation deficit in early AMD is dependent on retinal location. The observation that delays in cone adaptation have been reported for stimuli centred on the fovea (Phipps et al., 2003; Binns & Margrain, 2007; Dimitrov et al., 2008; 2011) but not for small spot stimuli presented at more eccentric retinal locations (Owsley et al., 2007) implies that cone dark adaptation deficits in early AMD are greatest for centrally presented stimuli.

The effect of retinal location on rod and cone thresholds in AMD has been examined previously (Brown et al., 1986a; Brown et al., 1986b; Steinmetz et al., 1993; Owsley et al., 2000). These studies have shown elevation of rod and cone thresholds in AMD, most markedly within the macular region. However, only one study has systematically described the topographical variation in dark adaptation kinetics in participants with AMD (Brown et al., 1986b). This study compared cone dark adaptation at four locations within the central 40° of visual field, in six patients with geographic atrophy and six healthy controls. In agreement with previous studies, cone threshold was elevated at all retinal locations in all of the participants with geographic atrophy. However, there were no significant differences in the time course of cone dark adaptation between participants with geographic atrophy and healthy controls at any of the locations studied. It should be noted that the participants in this study all had advanced dry AMD.

4.3.2. Aims

Clearly, there is ambiguity surrounding the extent to which cone dark adaptation is affected by early AMD and the effect, if any, of retinal location on dark adaptation. Consequently, the final part of the study aimed to quantify any differences in cone dark adaptation

between people with early AMD and healthy controls at different retinal locations. The study also sought to determine the diagnostic potential of cone dark adaptation and the time to RCB (the aspect of rod recovery that can be obtained most rapidly in the clinic) at each retinal location. The data presented in this section have been published in a peer-reviewed journal (see Gaffney et al., 2011b in Appendix III).

4.3.3. Methods

Participants

Approximately one hundred people, both those with early AMD and healthy controls, were recruited from the Eye Unit at the University Hospital of Wales, Cardiff, and the Eye Clinic at Cardiff University. These individuals were registered in a secure database from which participants were selected for all of the investigations contained within this thesis. Where possible, new participants were recruited from the database for each of the studies described in the following chapters. However, due to factors such as participant availability, some individuals participated in more than one of the studies.

The power of a study may be defined as the probability that the study will detect a real difference of a given magnitude as statistically significant. A power of 80-90% is generally considered necessary for the results of a study to be considered reliable (Altman, 1991). A nomogram may be used to calculate the sample size required for a study to attain a particular power by considering a measure known as the 'standardised difference', which is obtained by dividing the smallest difference of interest for a test by the standard deviation (Altman, 1991). Based on the data presented in Table 2 of Dimitrov et al. (2008), which reported large differences in mean rod and cone recovery parameters between participants with early AMD and healthy controls, the sample size must be sufficient to detect a standardized difference of 2.27-3.42. For this study 20 participants (10 individuals with early AMD and 10 healthy controls) were recruited from the database, allowing us to detect a standardized difference of 1.2 with 80% power at a 5% significance level, hence this sample size should be sufficient to detect the expected differences between groups. All participants were aged at least 55 years, had a corrected visual acuity of 6/9 or better in the test eye, no history of systemic disease or medication known to affect visual function and no significant media opacity (\leq Grade 3, LOCS-III) (Chylack et al., 1993).

The assessment of fundus status was based on 37° fundus photographs (Canon CR-DGi Camera) obtained at the baseline examination. Participants with AMD were classified according to the Age-Related Eye Disease Study severity scale i.e. early AMD = steps 2-6, intermediate AMD = steps 7-9 and advanced AMD = steps 10 –11 (Davis et al., 2005), in the absence of any co-existing ocular or fundus abnormality. The control group comprised only participants whose fundus appearance was classified as indicative of normal retinal ageing i.e. step 1 of the AREDS scale (Davis et al., 2005).

All participants provided informed written consent prior to participation. The study was approved by the South East Wales Research Ethics Committee and all procedures adhered to the tenets of the Declaration of Helsinki.

Apparatus

All computer equipment and psychophysical methods used were identical to those described in the earlier sections of the study (Section 4.1.3, Page 107).

Experimental procedure

Participants attended the laboratory on two days. Baseline examinations were completed at the start of the first visit. These included patient history, logMAR visual acuity (ETDRS), central visual field screening (C-40, Humphrey Field Analyser), stereoscopic fundus examination, fundus photography (Canon CR-DGi Camera) and media opacity grading (Chylack et al., 1993).

Participants were dilated with one drop of 1.0% Tropicamide in each eye prior to dark adaptation. The eye selected for testing was the eye with early AMD, or the eye with the better visual acuity in bilateral AMD or control participants. The right eye was tested as a default if there was no difference in visual acuity between the two eyes. The contralateral eye was occluded and refractive correction was worn if required.

All participants received instruction on the use of the dark adaptation program, before participating in a 5 minute practice recording session. This was repeated until the participant produced consistent thresholds and the investigator considered the participant to be fully competent with the procedure.



Figure 4.13. Diagrammatic representation of the spot stimulus and the three annular stimuli superimposed on the macula of a healthy participant. In order of increasing size, the radii of the stimuli were 0.5, 2, 7 and 12° from fixation. Each annulus was 0.5° wide.

Thresholds were recorded in response to a foveal spot (radius 0.5°) and three achromatic annuli (2, 7 and 12° in radius), all 0.5° wide, centred on the fovea (Figure 4.13). On each dark adaptation trial, a Maxwellian view optical system was used to bleach 81% of cone photopigment (5.1 log phot.Td for 120s) (Hollins & Alpern, 1973) in the central 43.6° of the test eye. The dark adaptation program commenced immediately after the bleaching light was extinguished. Participants placed their chin on the rest in front of the computer, stared at the centre of the screen, which was indicated by a fixation cross, and signalled perception of the stimulus via the computer keyboard. Dark adaptation was monitored in response to one of the four stimuli, selected at random, until the RCB occurred or for a maximum of 25 minutes. The investigator deemed the RCB to have occurred when threshold fell by at least 1 log unit below the cone plateau. Recovery was only recorded for 10 minutes when the 0.5° stimulus was used, as no rod recovery was expected for this small stimulus. This procedure was repeated for each of the remaining stimuli (the order of which was randomised). Generally, two stimulus sizes were completed at each session, with a washout period of an hour between bleaches. The long duration (120 seconds) adapting light was sufficient to attain an equilibrium bleach, which would ensure that a

consistent level of photopigment was bleached regardless of any small differences in baseline adaptational status.

Statistical analysis

The dynamics of cone recovery and the time to RCB were determined by fitting an exponential-linear model of dark adaptation (McGwin et al. 1999) to the data, on a least squares basis, using Microsoft Excel (2003) (Equation 4f). Cone recovery was described by the exponential component and rod recovery by the linear component. Although the RCB was the only aspect of rod recovery assessed during the analysis, the second component of rod recovery was retained within the model in order to identify the time to RCB.

Equation 4f.
$$T(t) = [a + (b.exp^{(-t/\tau)})] + [c.(max(t - rcb, 0))]$$

where T is the threshold (log cd/m²) at time t after cessation of the bleach, a is the final cone threshold, b is the change in cone threshold from $t = 0$, τ is the time constant of cone recovery, c is the slope of the second component of rod recovery, max is a logic statement, and rcb denotes the time from bleach offset to the RCB, (McGwin et al., 1999).

The parameters of interest were cone τ , final cone threshold and time to RCB. The mean (+/- standard deviation) was calculated for each parameter and independent sample t-tests were used to make comparisons between early AMD and control groups. Receiver operating characteristic (ROC) curves were constructed using statistical software (SPSS, Version 16.0) to assess the diagnostic potential of the parameters that showed a statistically significant difference between groups. A repeated measures ANOVA was completed to determine the effect of test order on the analysis.

4.3.4. Results

The clinical characteristics of the early AMD group are displayed in Table 4.6. Fifty percent of participants in the early AMD group had early AMD in their fellow eye and the remaining 50% had exudative changes in the non-study eye. There were no significant differences in age between early AMD (mean age = 68.3 +/- 7.3 SD years) and control (mean age = 70.0 +/- 4.7 SD years) groups ($p = 0.54$). Similarly, there were no significant differences in logMAR acuity between the test eyes of early AMD and control groups

(mean acuity = 0.09 +/- 0.11 SD logMAR for participants with early AMD and -0.002 +/- 0.10 SD logMAR for control participants; $p = 0.11$).

Table 4.6. Visual acuity and fundus appearance in the early AMD group. AMD status is given according to the Age-Related Eye Disease Study severity scale (Davis et al., 2005) where: normal retinal ageing = step 1, early AMD = steps 2– 6, intermediate AMD = steps 7–9, and advanced AMD = steps 10 –11.

Participant	Age	Gender	Test eye			Fellow eye		
			Eye	logMAR VA	AMD status	Eye	logMAR VA	AMD status
1	80	M	L	0.12	Early	R	0.02	Early
2	65	F	R	0.02	Early	L	0.18	Advanced
3	65	F	L	0.0	Intermed.	R	0.2	Advanced
4	68	F	L	0.0	Early	R	0.02	Early
5	73	M	L	0.24	Early	R	0.26	Advanced
6	67	F	R	-0.1	Intermed.	L	0.06	Advanced
7	57	M	L	0.0	Early	R	0.0	Early
8	59	M	L	0.1	Early	R	0.02	Early
9	75	M	R	0.2	Early	L	0.54	Advanced
10	74	F	R	0.2	Early	L	0.04	Early

Table 4.7 shows the cone τ , final cone threshold and time to RCB given by the best fitting exponential-linear model for each participant, at each retinal location. The time course of dark adaptation at each of the four retinal locations is shown in Figure 4.14a for a typical control participant. An example of the dark adaptation curves for a participant with early AMD is shown in Figure 4.14b. This participant with early AMD had prolonged cone adaptation and only displayed an RCB within 25 minutes for the largest (12°) stimulus.

Table 4.7. Cone τ , final cone threshold and time to RCB given by the best fitting exponential-linear model for all participants, at each retinal location. (* where there was no RCB within the recording time, 25 minutes was given as the time to RCB).

Participant	Cone τ (minutes)				Cone final threshold (log cd/m ²)				Time to RCB (minutes)*		
	0.5°	2°	7°	12°	0.5°	2°	7°	12°	2°	7°	12°
AMD											
1	4.32	5.64	3.20	6.80	-1.02	-1.24	-0.78	-1.34	25.00	25.00	25.00
2	8.74	8.23	9.10	1.93	-2.07	-1.60	-2.20	-1.73	25.00	25.00	25.00
3	6.37	10.36	4.74	5.07	-1.71	-2.50	-2.15	-1.95	25.00	11.73	15.94
4	2.42	0.49	1.85	1.09	-1.94	-2.06	-2.18	-2.07	11.35	12.74	11.26
5	53.57	12.50	3.03	3.07	-2.08	-1.49	-1.75	-1.70	25.00	25.00	15.56
6	11.77	14.98	9.03	5.69	-2.64	-2.97	-2.04	-1.93	25.00	25.00	25.00
7	2.09	1.69	1.00	2.67	-1.63	-2.32	-2.27	-2.76	15.17	12.91	12.49
8	1.95	1.47	1.49	1.60	-2.13	-2.30	-2.40	-2.36	14.59	13.95	13.04
9	6.60	5.25	8.05	5.16	-1.22	-1.42	-2.22	-1.71	12.76	25.00	16.6
10	3.11	3.75	3.24	1.77	-1.28	-1.48	-1.62	-1.64	25.00	25.00	16.87
Control											
11	1.99	1.83	1.33	0.70	-1.41	-2.29	-2.38	-2.49	11.22	15.47	7.01
12	1.46	1.57	0.82	0.36	-1.29	-2.05	-1.98	-1.94	14.57	12.51	8.42
13	1.29	3.21	1.88	0.88	-0.98	-2.06	-1.99	-1.72	25	14.11	11.46
14	1.97	1.41	1.17	0.77	-1.56	-1.52	-1.80	-1.81	9.51	13.80	13.30
15	1.94	2.37	1.16	0.20	-1.44	-1.89	-1.84	-1.66	15.93	13.36	7.52
16	0.42	1.48	0.25	1.38	-1.37	-1.44	-1.37	-1.61	25.00	10.98	8.23
17	3.86	3.66	3.01	0.98	-1.86	-2.27	-2.30	-1.97	25.00	21.67	10.32
18	1.64	1.66	1.59	0.18	-1.4	-2.00	-2.16	-1.82	13.92	11.67	6.38
19	1.41	1.20	0.53	0.46	-1.95	-2.21	-1.82	-1.67	12.99	12.22	8.88
20	4.79	2.26	1.06	0.50	-1.44	-1.43	-1.64	-1.33	16.85	14.53	8.99

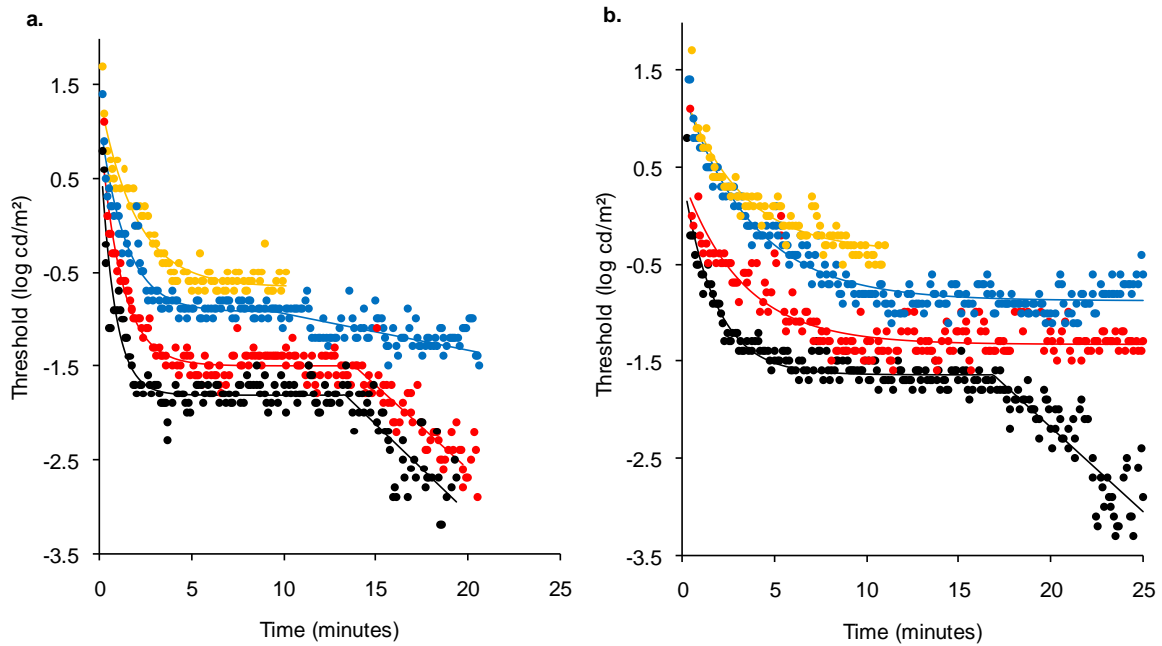


Figure 4.14. Dark adaptation curves recorded for a typical control participant (a) and a participant with early AMD (b) in response to all four stimulus sizes: 0.5° (yellow), 2° (blue), 7° (red) and 12° (black). For each stimulus size the raw data are shown with the best fitting model of dark adaptation given by equation 4f. The 12° data are correctly placed with respect to the y-axis. All other data are displaced upwards by an additional 0.3 log units from the previous (larger) stimulus to aid visualisation.

The mean dark adaptation parameters for the two groups are given in Table 4.8. Where there was no RCB within the 25 minute recording period, it was given as 25 minutes. This means that a conservative estimate of the delay in rod adaptation was included in all statistics. Significant differences in the cone time constant of recovery (τ) between groups were evident for stimuli located 2° , 7° and 12° from fixation (all $p < 0.05$). In addition, there was a significant difference in the time to RCB at 12° ($p < 0.001$). The mean τ , final cone threshold and time to RCB at each retinal location for control and early AMD groups are summarized in Figure 4.15. Although the greatest absolute difference in cone recovery time (Figure 4.15a) between those with early AMD and healthy controls was observed for the central stimulus, this difference failed to reach significance because of the variability in the data obtained at this location. Instead, the most significant difference between groups was observed for the stimulus located at 12° where the variability in the data set was minimal. There were no significant differences in final cone threshold between control and early AMD groups for any of the locations studied (Figure 4.15b).

Table 4.8. Comparison of mean (+/- standard deviation) dark adaptation parameters in control and early AMD groups. (* where there was no RCB within the recording time, 25 minutes was given as the time to RCB).

		Control	AMD	Univariate comparison
Cone τ (mins)	0.5°	2.08 (1.29)	10.09 (15.61)	p = 0.123
	2°	2.07 (0.81)	6.44 (4.95)	p = 0.021
	7°	1.28 (0.77)	4.47 (3.13)	p = 0.011
	12°	0.64 (0.38)	3.49 (2.02)	p = 0.002
Final cone threshold (log cd/m²)	0.5°	-1.47 (0.28)	-1.77 (0.50)	p = 0.111
	2°	-1.92 (0.34)	-1.94 (0.57)	p = 0.918
	7°	-1.93 (0.30)	-1.96 (0.48)	p = 0.856
	12°	-1.78 (0.30)	-1.92 (0.40)	p = 0.400
Time to RCB (mins) *	2°	16.99 (5.91)	20.39 (6.04)	p = 0.221
	7°	14.03 (3.01)	18.76 (6.62)	p = 0.061
	12°	9.05 (2.11)	17.68 (5.37)	p = 0.001

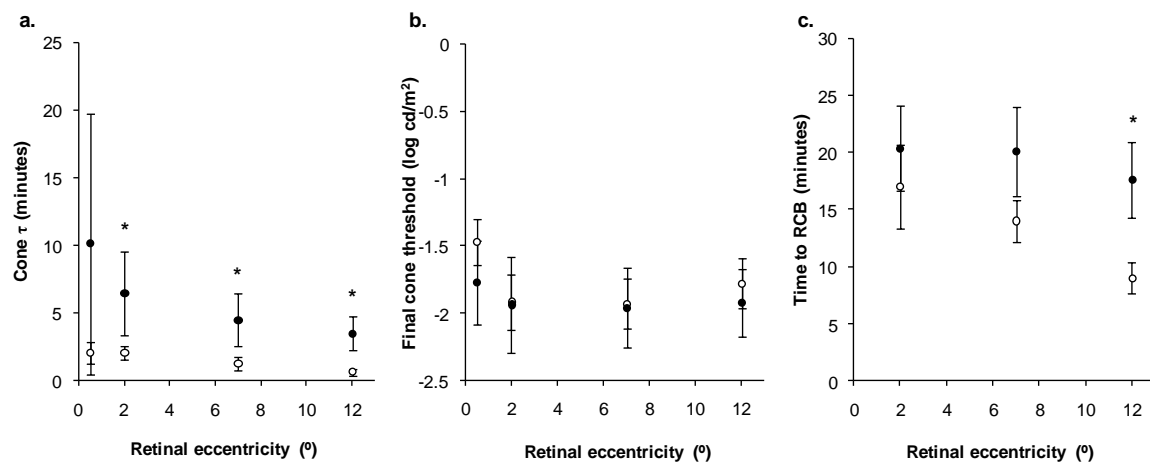


Figure 4.15. Summary of mean cone τ (a), cone final threshold (b) and time to RCB (c) at each retinal eccentricity, shown with 95% confidence intervals. Filled symbols represent the early AMD group and open symbols the control group. * indicates the parameters that demonstrate a significant difference between groups (all p < 0.05).

Receiver operating characteristic curves for all the parameters that differed significantly between groups on univariate analysis are shown in Figure 4.16. The area under the curve (AUC) is used to express the diagnostic capacity of each parameter. An AUC of 1 indicates 100% sensitivity and specificity, whilst an AUC of 0.5 suggests that the parameter is no

better than chance alone at discriminating between healthy and affected participants (Altman & Bland, 1994). The 12° annulus was the best stimulus for discriminating participants with early AMD from healthy controls, yielding an AUC of 0.99 +/- 0.02 for cone τ and 0.96 +/- 0.04 for time to RCB. This equates to 100% sensitivity and 90% specificity for a τ of 1.04 minutes and 90% sensitivity and 90% specificity for a RCB of 11.98 minutes. There was a statistically significant difference in the AUC between cone τ at 12° and at 2° ($z = 2.15$), however there were no statistically significant differences in the AUC of cone τ at 12° and cone τ at 7° or time to RCB at 12° ($z < 1.96$) (Hanley & McNeil, 1982; 1983).

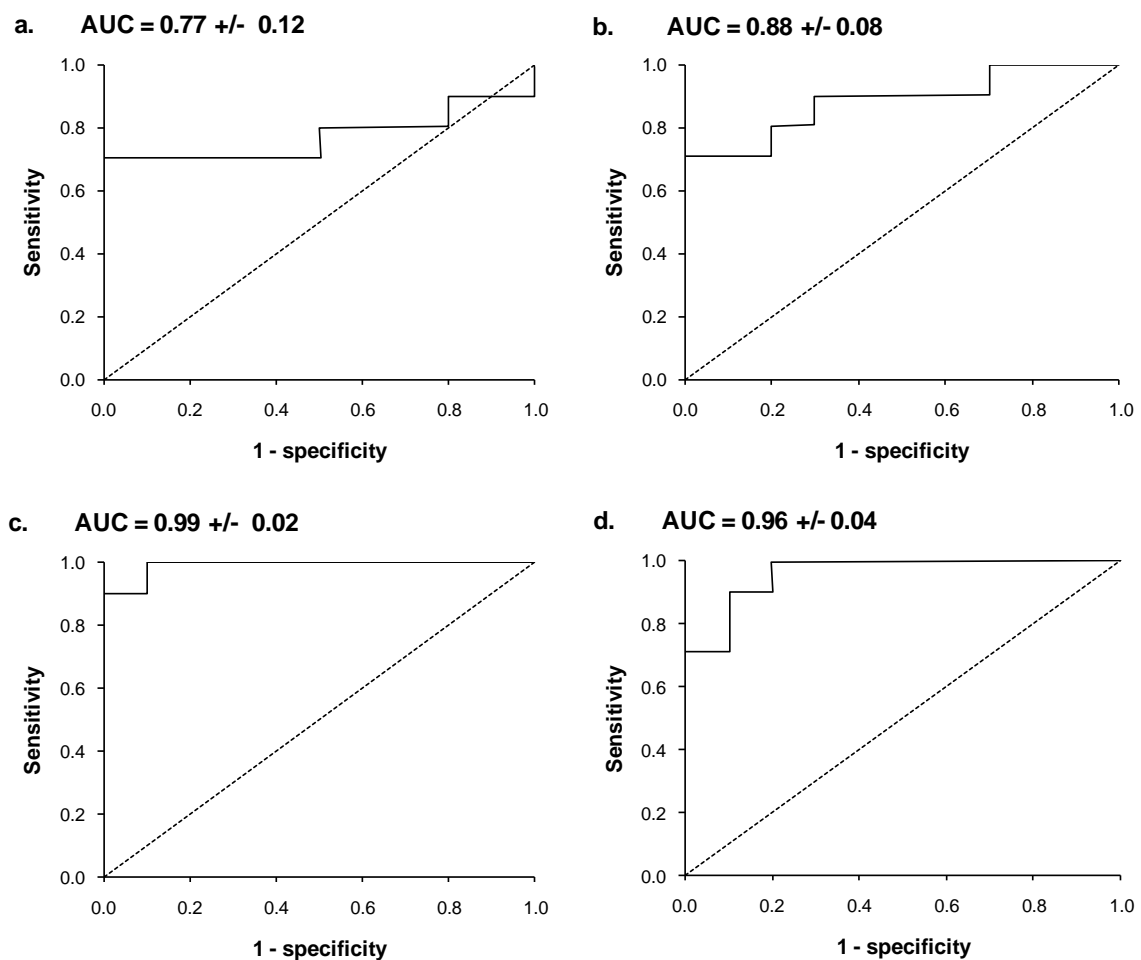


Figure 4.16. ROC curves for cone τ at 2° (a), 7° (b) and 12° (c), and time to RCB at 12° (d) Each plot shows the sensitivity of the parameter to early AMD against the false detection rate (1 – specificity) for all 10 control and 10 early AMD participants.

A separate analysis was undertaken to assess the effect of test order on the dark adaptation results (Table 4.9). There were no significant differences in dark adaptation parameters

recorded for the first and second bleaches within a single session. This indicates that no learning, fatigue or bleach carry-over effects exist within the dataset.

Table 4.9. Comparison of mean (+/- standard deviation) dark adaptation parameters obtained during the first and second test within a single recording session.

		1 st test	2 nd test	Univariate comparison
Cone τ (mins)	0.5°	7.64 (16.23)	4.54 (3.48)	p = 0.586
	2°	3.99 (4.55)	4.51 (3.86)	p = 0.734
	7°	2.63 (2.61)	3.13 (3.02)	p = 0.733
	12°	2.47 (2.40)	1.65 (1.60)	p = 0.350
Final cone threshold (log cd/m ²)	0.5°	-1.48 (0.35)	-1.76 (0.45)	p = 0.065
	2°	-2.03 (0.49)	-1.82 (0.42)	p = 0.367
	7°	-1.97 (0.34)	-1.92 (0.45)	p = 0.814
	12°	-1.76 (0.40)	-1.94 (0.29)	p = 0.329
Time to RCB (mins) *	2°	17.82 (6.40)	19.57 (5.93)	p = 0.174
	7°	16.54 (5.30)	17.62 (6.38)	p = 0.745
	12°	14.37 (6.77)	12.36 (5.15)	p = 0.286

4.3.5. Discussion

The results show that cone τ and time to RCB are highly diagnostic for early AMD for annular stimuli located 12° from the fovea. At this location, cone τ was able to distinguish participants with early AMD from healthy controls with 100% sensitivity and 90% specificity. To a lesser extent, cone τ was also diagnostic for early AMD for stimuli located at 2° and 7°. The greatest absolute difference in mean cone τ between early AMD and control groups was observed at the fovea. This is consistent with previous reports of changes in foveal cone τ in early AMD (Phipps et al., 2003; Dimitrov et al., 2008; 2011). However, this difference failed to reach significance as a result of the variability of the data at this retinal location (illustrated by the large 95% CI in Figure 4.15a). Therefore, with regards to diagnostic potential, the functional deficit 12° from fixation provides the best separation between the two groups.

Although impaired dark adaptation has previously been reported at 12° in AMD (Owsley et al., 2007), it was thought to affect rods exclusively. In contrast, this study has shown that

cone dark adaptation is also highly abnormal at 12° in early AMD. This has significant clinical implications because in the clinic ‘time is of the essence’ and cone dark adaptation may generally be assessed in less time than rod adaptation. An alternative protocol has been described in which rod dark adaptation may be assessed in as little as 20 minutes (Jackson & Edwards, 2008). However, the results presented here show that cone τ may be quantified in as little as 10 minutes and is also highly diagnostic for early AMD.

There are three potential explanations for the discrepancies between the results presented here and those of previous studies, which failed to find a significant effect of early AMD on cone adaptation (Brown et al., 1986b; Owsley et al., 2007). These related explanations are based on the well established rate-limiting step in dark adaptation: the local availability of 11-cis retinal (Lamb & Pugh, 2004).

The initial explanation stems from the bleaching method used (photoflash vs. steady state bleach) and its effect on the rate of cone dark adaptation in people with early AMD. Rods and cones both need 11-cis retinal to regenerate visual pigment. Although rods can only obtain that supply from the RPE, there is a body of evidence to suggest that cones have access to a secondary supply, via a pathway that involves the retinal Müller cells (Das et al., 1992; Mata et al., 2002; Wang, & Kefalov, 2009; 2011). Evidence for this secondary pathway was initially obtained from the cone-dominated retina of ground-squirrel and chicken (Das et al., 1992; Mata et al., 2002). More recently, this additional pathway was also shown to exist in the rod-dominated retina of the mouse, primate and human (Wang & Kefalov; 2009). The Müller cells contain all-trans-retinol isomerase and 11-cis-retinyl-ester synthase; catalytic enzymes that enable the Müller cells to take up all-trans retinol and convert it to 11-cis retinol, which is then released into the surrounding media and taken up by the cones (Mata et al., 2002). A third enzyme, 11-cis-retinol dehydrogenase, present in cones but not rods, facilitates the final stages of photopigment regeneration. While rods and cones must compete for RPE derived 11-cis retinal, this additional pathway provides cones with an exclusive secondary source that helps them regenerate photopigment much more rapidly than rods.

Unlike photoflashes, a long duration (‘steady state’) bleach, such as that used in the current study, involves sustained phototransduction and activation of the visual cycle. If this sustained metabolic activity were to adversely affect the alternative retinoid recycling

pathway, cone photopigment regeneration following a long duration bleach would be relatively more dependent on RPE derived 11-cis retinal. Any impairment to cone-mediated dark adaptation would therefore be more likely to manifest under the bleaching conditions used in the current study than following the 11ms photoflash used previously (Owsley et al., 2007).

This leads logically to the second explanation for the cone dark adaptation deficit at 12°. As described, after a long duration adapting light, the rods and cones may become equally reliant on the RPE for regeneration of 11-cis retinal. It therefore follows that any disturbance to RPE function or the local supply of retinoid will affect both rod and cone dark adaptation. Rod adaptation is known to be significantly impaired 12° from the fovea (Owsley et al., 2001; Owsley et al., 2007). This is also the retinal eccentricity at which human rod photoreceptor density approaches a peak of approximately 150,000 cells/mm² (Curcio et al., 1990), so direct competition between the rods and cones for the same finite supply of retinoid is great at this location. In circumstances where the cones' intraretinal supply of 11-cis retinal may be deficient, such as after a long duration bleach, cone recovery at this location would also be expected to be abnormal. Therefore, the important topographical parameter affecting dark adaptation in AMD is the local availability of 11-cis retinal, upon which rods and cones are dependent.

Cone dark adaptation was particularly slow at the fovea in participants with early AMD, which might be expected given that cone density peaks at this location (200,000 cells/mm²) (Curcio et al., 1990), so competition for 11-cis retinal will be high. The fact that this difference failed to reach statistical significance due to high variability may be explained by stimulus size. The small spot stimulus used at the fovea sampled a precise retinal location. AMD is a heterogeneous disease characterised by localised retinal abnormalities, so the results obtained using small spots are influenced by chance, that is, the chance that the stimulus is located on a healthy or unhealthy area of retina. In contrast, thresholds obtained in response to large annuli will be determined by the most healthy functional area of the retina, because small areas of abnormality will not contribute to the threshold measured. Therefore, large annuli might be expected to produce relatively consistent results based on the functional ability of the retina at a particular eccentricity and the data obtained using spot stimuli are likely to be more variable based on their 'hit or miss' sampling of heterogeneous retina.

The effect of stimulus size on the variability of the data is evident in Table 4.8, in which the standard deviations reported for the early AMD group become smaller as the annuli increase in size. When the largest annulus was used to sample the retina at 12° the standard deviation was only 0.57 times the size of the mean recovery time. This contrasts starkly with the data reported by Owsley et al. (2007) who sampled the retina at the same eccentricity (12° in the inferior field) but used a spot stimulus. The standard deviations reported when this stimulus was used were more than twice the value of the mean cone τ for their ‘intermediate’ AMD group.

The heterogeneity hypothesis appears to explain the relatively increased variability observed for the 0.5° data reported in the current study, as well as providing a rationale for the variability observed in previous studies that used relatively small spot stimuli (Owsley et al., 2001; Owsley et al., 2007). It may also explain why Dimitrov et al. (2008) found cone dark adaptation to be highly diagnostic for early AMD (AUC = 0.98) using a 4° diameter spot stimulus centred on the fovea and reported relatively little variability in their dataset (the standard deviation of their recovery rate was only 0.35 of the mean value). The large area of the stimulus (12.6 deg²) would have been relatively unaffected by focal abnormalities. When considered in conjunction with the current findings, this suggests that the size of the stimulus may be equally important as its retinal location, because larger stimuli are associated with reduced variability and hence better diagnostic ability.

The only previous study that measured cone dark adaptation at more than one retinal location reported no differences in the dynamics of cone dark adaptation within the central 40° of visual field between control participants and those with geographic atrophy (Brown et al., 1986b). However, that patient group had end stage AMD and were very different to those included in the current study.

Eight of the participants with early AMD failed to reach the RCB within the 25 minute recording period for one or more of the experimental stimuli. All five of the participants with a diagnosis of exudative disease in their contralateral eye fell within this group. A higher incidence of choroidal neovascularisation in the fellow eye of patients with unilateral exudative AMD has been widely reported (Klaver et al., 2001; Mitchell et al., 2002; Klein et al., 2007). Therefore, the results support evidence to suggest that dark

adaptation is more severely impaired in eyes with an increased risk of exudative changes (Eisner et al., 1991; Sandberg et al., 1998).

The primary interest of this study was to distinguish those with early AMD from healthy controls i.e. to detect clinically significant differences, rather than to identify small differences in mean values. Although the sample size was relatively modest ($n = 20$), there was a marked separation of participants with early AMD and control participants in both the cone recovery and RCB data.

In conclusion, this study has demonstrated the diagnostic potential of cone dark adaptation in the detection of early AMD and the marked effect of the retinal location at which dark adaptation is measured. The results provide compelling evidence in support of the use of cone dark adaptation and the use of large annular stimuli at 12° in the diagnosis of early AMD.

5. The effect of pre-adapting intensity on dark adaptation in early AMD

In order to fully utilise the diagnostic potential of dark adaptation in the detection of early AMD, it is necessary to identify the characteristics of both the stimulus and the pre-adapting ‘bleaching’ light that provide maximal discrimination between the healthy retina and a retina with early AMD. In the previous chapter, an annulus of 12° radius, centred on the fovea, was identified as the optimal stimulus for assessment of dark adaptation in early AMD. In order to further refine the dark adaptation protocol, this chapter will examine dark adaptation in early AMD as a function of the pre-adapting light intensity.

5.1. Introduction

The time course of sensitivity recovery during dark adaptation is determined by the intensity and duration of the pre-adapting light exposure (Winsor & Clark, 1936; Hecht et al., 1937; Wald & Clark, 1937; Haig, 1941; Mote & Ripoele, 1950; Wolf & Zigler, 1954). The familiar biphasic dark adaptation function only occurs at high pre-adapting light intensities. As the intensity of the adapting light decreases, a lower proportion of photopigment is bleached. Consequently, the resultant cone component is less prominent (see Figure 1.12, Page 31) and the entire dark adaptation function undergoes a lateral shift towards the y-axis. This means that any given visual threshold is attained more rapidly at lower pre-adapting intensities.

The implementation of a low pre-adapting intensity for measurement of dark adaptation is attractive clinically as it would help to expedite data collection. However, it is vital that any reduction in the intensity of the adapting light, and subsequent recording time, does not compromise the diagnostic capacity of the threshold recovery data. Sufficient recovery data must be obtained to allow an accurate model fit, furthermore the ‘demand’ placed on the retina, RPE and choroid must be sufficient to ensure a distinct separation in the recovery parameters between participants with early AMD and healthy controls. Although the relationship between the pre-adapting light exposure and dark adaptation is well established in healthy individuals (Winsor & Clark, 1936; Hecht et al., 1937; Wald &

Clark, 1937; Haig, 1941; Mote & Ripoele, 1950; Wolf & Zigler, 1954; Dimitrov et al., 2008), there is currently no published data regarding the effect of the pre-adapting light intensity on dark adaptation in participants with early AMD.

5.2. Aims

This study aimed to quantify the differences in cone dark adaptation between people with early AMD and healthy controls at a range of pre-adapting light intensities. The diagnostic potential of cone dark adaptation and time to RCB were determined as a function of pre-adapting light intensity.

5.3. Methods

Participants

Ten participants with early AMD were recruited from the database. All of these participants had a diagnosis of early or intermediate AMD in at least one eye, according to the Age-Related Eye Disease Study severity scale (Davis et al., 2005), in the absence of any co-existing ocular or fundus abnormality. The diagnosis was confirmed using 37° fundus photographs (Canon CR-DGi Camera) obtained at the baseline examination. Ten age-matched control participants, with a normal retinal appearance in both eyes, were also recruited from the database. All participants were aged 55 years and over, with a corrected visual acuity of 6/9 or better in the test eye, no significant media opacity (\leq Grade 3, LOCS-III) (Chylack et al., 1993), and no history of systemic disease or medication known to affect visual function.

All participants provided informed written consent prior to participation. The study was approved by the South East Wales Research Ethics Committee and all procedures adhered to the tenets of the Declaration of Helsinki.

Apparatus

Thresholds were recorded in response to a 12° radius amber annulus ($\lambda = 595\text{nm}$), 0.5° wide, 200 msec duration, centred on the fovea. An amber stimulus and adapting light were selected in order to generate similar percentage bleach of cone and rod photopigments across a range of pre-adapting light intensities (Wyszecki & Stiles, 1982) and to minimise the effects of pre-retinal light absorption and scatter. The stimulus was presented on a calibrated, high resolution CRT monitor (Iiyama LS 902UT) driven by an 8-bit graphics

board (nVIDIA Geforce 9) under software control (Matlab, R2009a, The MathWorks Inc.). As described in Chapter 2 (Section 2.2.3) the luminance output of the monitor was γ -corrected (Metha et al., 1993; Brainard et al. 2001) and modified by neutral density filters mounted on the screen to expose the full range of retinal recovery. Dark adaptation was monitored using a psychophysical method based on the modified staircase procedure previously described in Section 2.2.3. The Matlab code for this procedure is shown in Appendix II.

A Maxwellian view optical system, incorporating an amber filter (LEE filters HT 015 ‘deep straw’), was used to deliver all photopigment bleaches to the central 43.6° of the test eye (Figure 5.1). Table 5.1 describes the retinal illuminance and proportion of rod and cone photopigment bleached with the 120 second exposure used in this investigation. The system was calibrated at the highest intensity and additional 0.3 ND filters were placed in front of the adapting light source to attenuate the luminance sufficiently in order to attain the two lower adapting intensities.

Table 5.1. Percentages of cone photopigment (Hollins & Alpern, 1973) and rhodopsin (Thomas & Lamb, 1999) bleached at the three adapting intensities.

Exposure	Retinal Illuminance (log phot.Td)	% cone photopigment bleach	% rhodopsin bleach
1	4.90	71	51
2	5.20	84	74
3	5.50	91	90

Experimental procedure

Participants attended the laboratory on two days. Baseline examinations were completed at the start of the first visit. These included patient history, logMAR visual acuity (ETDRS), central visual field screening (C-40, Humphrey Field Analyser), stereoscopic fundus examination, fundus photography (Canon CR-DGi Camera) and media opacity grading (Chylack et al., 1993).

Participants were dilated with one drop of 1.0% Tropicamide in each eye prior to dark adaptation. The eye selected for testing was the eye with early AMD, or the eye with the better visual acuity in bilateral AMD or control participants. The right eye was tested as a default if there was no difference in visual acuity between the two eyes. The contralateral

eye was occluded and refractive correction was worn if required for a viewing distance of 55cm.

All participants were instructed how to use the dark adaptation program, before participating in a 5 minute practice recording session. This was extended at the examiner's discretion, until the participant produced consistent thresholds and was considered competent with the procedure.

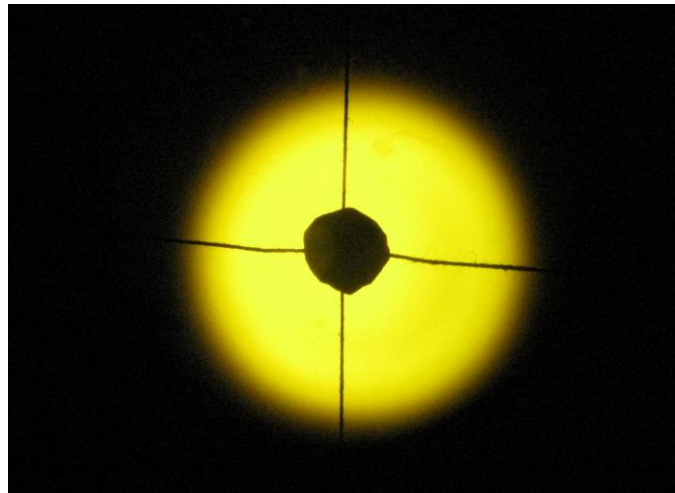


Figure 5.1. Viewing aperture of the Maxwellian view optical system during photopigment bleaching. The fovea was spared from photopigment bleaching by the spot in the centre of the crosshair.

Dark adaptation was monitored for 30 minutes after a photopigment bleach at one of the three pre-adapting intensities, selected at random (Figure 5.1). After cessation of the bleach, the participant placed their chin on the rest in front of the computer and the dark adaptation program commenced immediately. Participants were instructed to fixate the cross at the centre of the screen and to indicate perception of the stimulus using the computer keyboard. At the second visit, the two remaining adapting intensities were completed, following the same procedure and separated by a washout period of an hour. The equilibrium bleach produced by the long duration adapting light (Hollins & Alpern, 1973) ensured that all participants reached the same level of photopigment bleach regardless of any small differences in pre-bleach adaptational status.

Statistical analysis

The dynamics of cone recovery and the time to RCB were determined by fitting an exponential model of dark adaptation to the cone threshold recovery data and a two linear

model to any rod threshold recovery data (McGwin et al. 1999), on a least squares basis, using the solver function in Microsoft Excel (2003) (Equation 4d, Section 4.1.1). Although the RCB was the only aspect of rod recovery assessed during the analysis, rod recovery was modelled in order to identify the time to RCB.

The parameters of interest were cone τ , final cone threshold and time to RCB. The mean (+/- standard deviation) was calculated for each parameter and independent sample t-tests were used to make comparisons between early AMD and control groups. Receiver operating characteristic (ROC) curves were constructed using statistical software (SPSS, Version 16.0) to assess the diagnostic potential of the parameters that showed a statistically significant difference between groups.

5.4. Results

Table 5.2. Visual acuity and fundus appearance in the early AMD group. AMD status is given according to the Age-Related Eye Disease Study severity scale (Davis et al., 2005) where: normal retinal aging = step 1, early AMD = steps 2– 6, intermediate AMD = steps 7–9, and advanced AMD = steps 10 –11.

Participant	Age	Gender	Test eye			Fellow eye		
			Eye	logMAR VA	AMD status	Eye	logMAR VA	AMD status
1	76	F	L	0.2	Intermed.	R	0.7	Advanced
2	72	F	R	-0.1	Early	L	1.0	Advanced
3	66	F	R	0.06	Early	L	0.12	Advanced
4	79	M	R	0.1	Early	L	0.1	Advanced
5	65	M	L	0.1	Early	R	0.8	Advanced
6	76	M	R	0.1	Early	L	0.6	Advanced
7	87	M	L	-0.1	Early	R	0.1	Advanced
8	66	F	L	0.12	Intermed.	R	0.1	Advanced
9	75	F	R	0.1	Early	L	0.3	Early
10	68	F	L	0.04	Early	R	0.04	Early

The clinical characteristics of the early AMD group are shown in Table 5.2. There were no significant differences in age between early AMD (mean age = 73.0 +/- 7.01 SD years) and

control (mean age = 73.3 \pm 4.11 SD years) groups ($p = 0.908$). Similarly, there were no significant differences in logMAR acuity between the test eyes of early AMD and control groups (mean acuity = 0.06 \pm 0.09 SD logMAR for early AMD participants and 0.03 \pm 0.11 SD logMAR for control participants; $p = 0.506$).

Table 5.3 shows the cone τ , final cone threshold and time to RCB given by the best fitting exponential-linear model for each participant, at each pre-adapting intensity. Figure 5.2a shows the time course of dark adaptation for a typical control participant, recorded after a 71, 84 and 91% cone photopigment bleach. As anticipated, the RCB occurred progressively later as the intensity of the adapting light increased. Equivalent dark adaptation curves for a typical participant with early AMD are shown in Figure 5.2b. In comparison to the control data, this participant with early AMD had prolonged cone adaptation, and only displayed a clear RCB within the 30 minute recording period after exposure to the pre-adapting light at the lowest intensity (71% cone photopigment bleach).

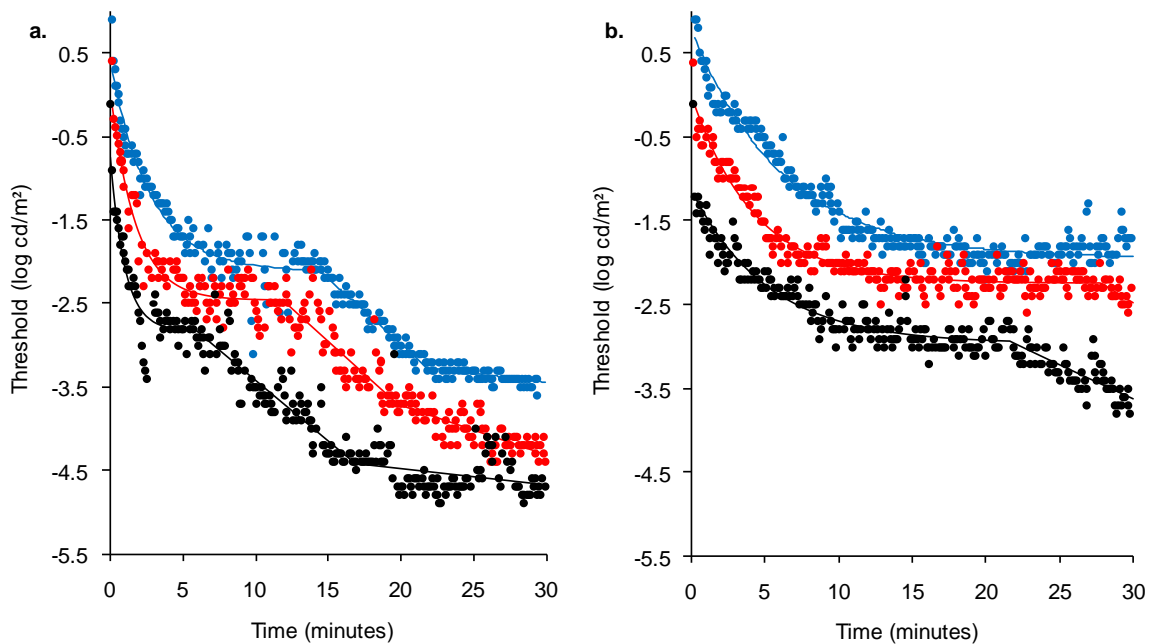


Figure 5.2. Dark adaptation curves recorded for a typical control participant (a) and a participant with early AMD (b) at the three pre-adapting light intensities: 71% (black), 84% (red) and 91% (blue) cone photopigment bleach. For each pre-adapting light intensity the raw data are shown with the best fitting model of dark adaptation given by equation 5a. The 71% data are correctly placed with respect to the y-axis. All other data are displaced upwards by an additional 0.5 log units from the previous (lower intensity bleach) data to aid visualisation.

Table 5.3. Cone τ , final cone threshold and time to RCB given by the best fitting exponential-linear model for all participants, at each pre-adapting light intensity. (* where there was no RCB within the recording time for an individual, 30 minutes was attributed as the time to RCB)

Participant	Cone τ (minutes)			Cone final threshold (log cd/m ²)			Time to RCB (minutes)*		
	71%	84%	91%	71%	84%	91%	71%	84%	91%
AMD									
1	1.85	3.00	4.49	-2.11	-1.85	-2.69	10.67	30.00	30.00
2	5.20	5.30	6.17	-2.97	-2.74	-2.95	21.64	27.83	30.00
3	5.75	6.83	8.27	-2.69	-2.73	-2.99	30.00	30.00	30.00
4	0.70	7.37	4.39	-2.63	-3.06	-3.02	8.46	16.76	19.66
5	0.52	2.62	3.32	-2.55	-2.55	-2.42	26.07	30.00	30.00
6	8.00	8.13	10.17	-2.98	-2.99	-2.96	30.00	30.00	30.00
7	3.27	7.57	10.00	-2.54	-2.78	-2.91	30.00	30.00	30.00
8	1.40	3.35	11.05	-2.77	-2.34	-3.26	12.51	14.03	25.83
9	0.93	1.08	1.09	-2.74	-2.58	-2.72	6.80	7.45	9.41
10	1.84	4.26	2.84	-2.16	-2.24	-2.16	11.66	20.50	30.00
Control									
11	0.56	1.29	1.54	-2.89	-3.02	-2.91	10.11	9.41	14.91
12	0.30	0.97	1.94	-2.55	-2.51	-2.85	6.95	7.37	10.53
13	0.88	1.61	2.63	-2.82	-2.94	-3.10	5.91	11.80	14.37
14	1.94	2.78	2.94	-2.55	-2.76	-2.64	9.76	9.95	17.67
15	0.82	1.67	1.39	-2.34	-2.53	-2.34	3.22	13.85	13.36
16	0.19	1.84	2.15	-2.41	-2.66	-2.65	0.91	10.90	13.35
17	0.18	0.83	0.52	-2.21	-2.63	-2.14	1.10	5.84	7.42
18	0.35	0.96	0.70	-2.71	-2.72	-2.47	4.32	11.61	14.67
19	0.22	0.74	0.82	-2.34	-2.66	-2.47	1.31	4.18	6.46
20	0.88	2.97	1.39	-2.20	-2.77	-2.56	7.76	8.94	10.81

Table 5.4. Comparison of mean (+/- standard deviation) dark adaptation parameters in control and early AMD groups. (* where there was no RCB within the recording time for an individual, 30 minutes was attributed as the time to RCB)

		Control	AMD	Univariate comparison
Cone τ (mins)	71%	0.63 (0.54)	2.95 (2.55)	p = 0.019
	84%	1.57 (0.79)	4.95 (2.44)	p = 0.002
	91%	1.60 (0.81)	6.18 (3.49)	p = 0.002
Final cone threshold (log cd/m ²)	71%	-2.50 (0.24)	-2.61 (0.29)	p = 0.366
	84%	-2.72 (0.16)	-2.59 (0.36)	p = 0.302
	91% ^o	-2.61 (0.28)	-2.81 (0.32)	p = 0.167
Time to RCB (mins) *	71%	5.14 (3.50)	18.78 (9.69)	p = 0.001
	84%	9.39 (2.93)	23.66 (8.38)	p < 0.001
	91%	12.36 (3.51)	26.49 (6.87)	p < 0.001

The mean dark adaptation parameters obtained from participants with early AMD and healthy controls are summarised in Table 5.4. Where there was no RCB within the 30 minute recording period, it was given as 30 minutes. Consequently, a conservative estimate of the delay in rod adaptation was included in all statistics. There were significant differences in cone τ (all $p < 0.05$) and time to RCB (all $p < 0.005$) between groups at all adapting intensities. This distinct separation in mean cone τ and time to RCB between control and early AMD participants is illustrated in Figure 5.3. There were no significant differences in cone final threshold between the two groups at any of the adapting intensities (Table 5.3 and Figure 5.3).

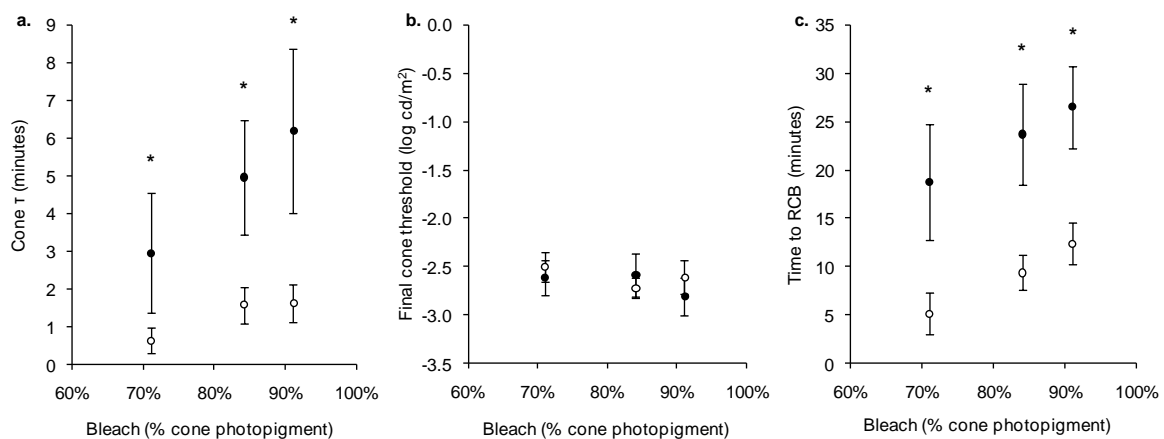


Figure 5.3. Summary of mean cone τ (a), cone final threshold (b) and time to RCB (c) at each bleaching intensity, shown with 95% confidence intervals. Filled symbols represent the early AMD group and open symbols the control group. * indicates those parameters that demonstrate a significant difference between groups.

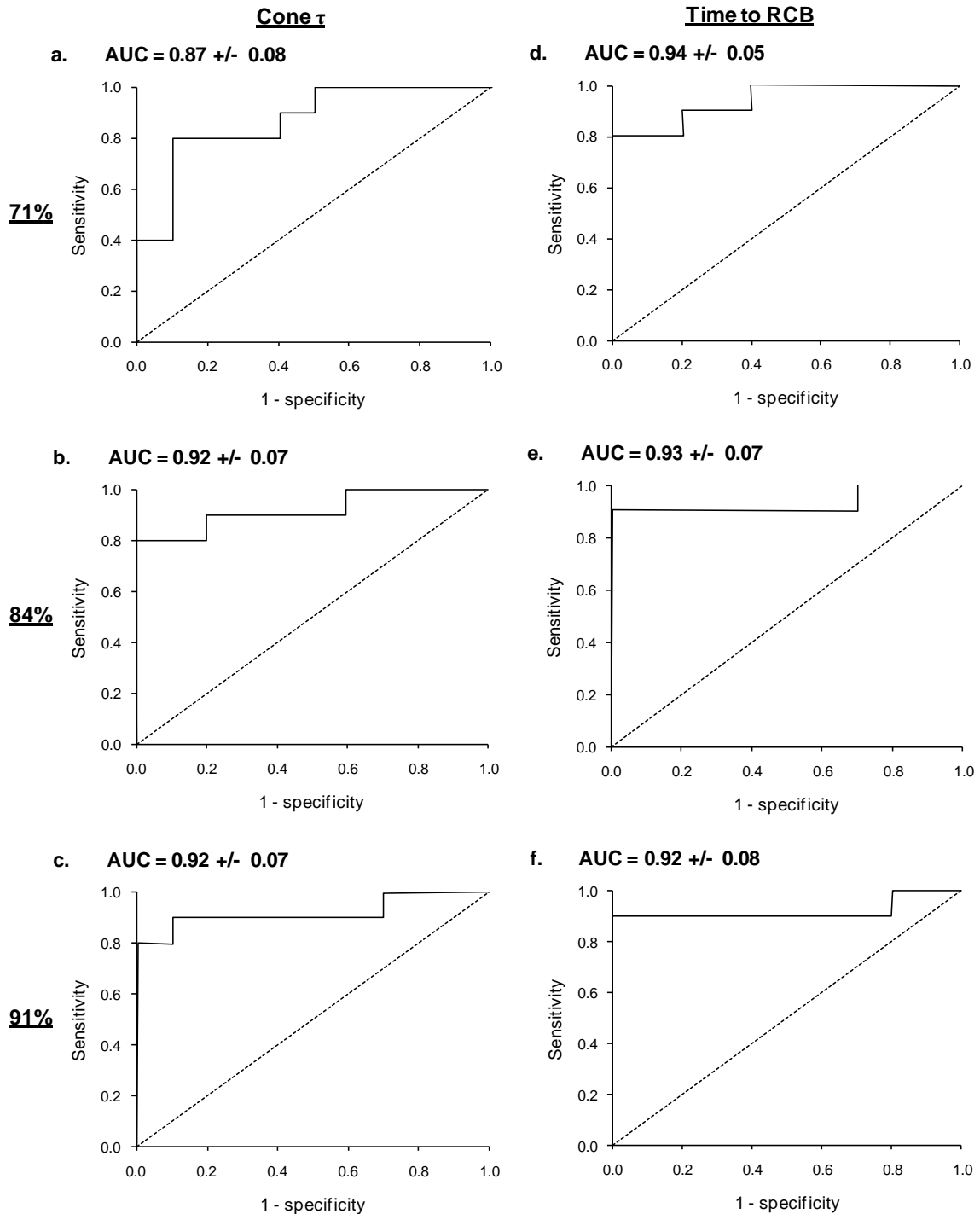


Figure 5.4. ROC curves for cone τ after cone photopigment bleaches of 71% (a), 84% (b) and 91% (c), and time to RCB after 71% (d), 84% (e) and 91% (f). Each plot shows the sensitivity of the parameter to early AMD against the false detection rate (1 – specificity) for all 10 control and 10 early AMD participants.

Figure 5.4 shows ROC curves for all of the dark adaptation parameters that differed significantly between groups on univariate analysis. The area under the curve (AUC) is given to describe the diagnostic capacity of each parameter. At the two higher pre-adapting intensities, 84 and 91% cone photopigment bleach, cone τ was equally capable of

discriminating participants with early AMD from healthy controls, with an AUC of 0.92 +/- 0.07 in both conditions. This was marginally superior to the AUC of 0.87 +/- 0.08 for cone τ after a 71% cone photopigment bleach. The ROC analysis showed that the time to RCB had a high diagnostic capacity for early AMD at all adapting intensities. There were no statistically significant differences in the AUC obtained for cone τ or time to RCB at any of the bleaching intensities ($z < 1.96$) (Hanley & McNeil, 1982; 1983). In addition, sensitivity and specificity values of between 80 and 100% were obtained for optimal cut-off values of cone τ and time to RCB for all pre-adapting intensities, further illustrating their diagnostic potential (Table 5.5).

Table 5.5. Sensitivity and specificity of the dark adaptation parameters that differed significantly on univariate analysis, calculated according to the optimal cut-off value given by the ROC curve.

		Optimal cut-off value (mins)	Sensitivity (%)	Specificity (%)
Cone τ	71%	0.91	80	90
	84%	2.23	90	80
	91%	2.74	90	90
Time to RCB	71%	8.11	90	80
	84%	13.94	90	100
	91%	18.67	90	100

5.5. Discussion

The results show that cone τ and time to RCB are highly diagnostic for early AMD at bleaching intensities between 71% and 91% of cone photopigment. An AUC in excess of 0.87 was obtained at all pre-adapting intensities, and participants with early AMD were discriminated from healthy controls with between 80 and 90% sensitivity and 80 and 100% specificity. Consequently, the two lower pre-adapting intensities, providing 71 and 84% cone photopigment bleach (equivalent to 51 and 74% rhodopsin bleach), may be used to expedite the measurement of dark adaptation in the clinic without compromising the diagnostic value of the data obtained. However, given the speed with which threshold changes during early cone dark adaptation, immediately after bleach offset, the use of an 84% cone photopigment bleach may be considered preferable to the lower pre-adapting

intensity, because at higher intensities a greater number of early data points are obtained with which to anchor the exponential model fit.

With the exception of the lowest pre-adapting intensity, cone τ exhibited a similar diagnostic ability to the time to RCB. This has useful clinical implications as cone dark adaptation may generally be assessed in as little as 10 minutes, thus further expediting data collection. These results provide additional support for the data presented in chapter 4, in which we demonstrated prolonged cone dark adaptation, 12° from fixation, in an independent cohort with early AMD, and reported an area under the ROC curve which was greater than 0.9 (see also Gaffney et al., 2011b).

The relationship between the pre-adapting light exposure and dark adaptation has been extensively explored in healthy individuals (Winsor & Clark, 1936; Hecht et al., 1937; Wald & Clark, 1937; Haig, 1941; Mote & Ripoele, 1950; Wolf & Zigler, 1954). In a recent study, Dimitrov et al. (2008) assessed dark adaptation in a healthy participant at six pre-adapting intensities between 3 and 96% rhodopsin bleach. This formed the basis for a recording protocol in which dark adaptation was measured in participants with early AMD after a 30% rhodopsin bleach. However, this is the first time that the diagnostic power of dark adaptation has been examined at a range of pre-adapting intensities in a cohort with early AMD.

Of the seven participants with early AMD who failed to reach a RCB within the 30 minute recording period during one or more of the experimental conditions, six had a diagnosis of exudative disease in their contralateral eye. An increased incidence of choroidal neovascularisation has previously been reported in this particular patient group (Klaver et al., 2001; Mitchell et al., 2002; Klein et al., 2007) and our findings provide further evidence of an association between impaired dark adaptation and a heightened risk of exudative changes (Eisner et al., 1991; Sandberg et al., 1998).

In conclusion, this study has reinforced the potential importance of rod and cone dark adaptation as a biomarker for early AMD and as a method of monitoring treatment outcomes. Dark adaptation was shown to be diagnostic for early AMD at a range of pre-adapting intensities. Therefore we recommend the use of a pre-adapting bleaching intensity

of 84% of cone photopigment to facilitate the assessment of dark adaptation within a clinically viable timeframe.

6. The development of the focal rod ERG photostress test (PST)

Although psychophysical methods have been widely used to assess dark adaptation, the data are based on the subjective responses of the participant and may therefore be degraded by human inconsistencies, such as expectation and habituation errors (Treutwein, 1995). In contrast, electroretinography provides an objective means of assessing retinal function and so has potential as an alternative technique for evaluating dark adaptation. However, there is currently no ‘gold standard’ electrophysiological technique for the investigation of retinal dysfunction in AMD (Gerth, 2009). Indeed, there are very few standardised protocols for the assessment of dark adaptation at the macula using the ERG. Previous publications have demonstrated that the focal cone ERG may be used to assess cone recovery after a photopigment bleach (Binns & Margrain 2005; Binns & Margrain 2007; Wood et al., 2011b) and that delayed recovery of the ERG amplitude is diagnostic for early AMD (Binns & Margrain 2007). This chapter investigates the use of the full field and focal rod ERG (Binns & Margrain 2006) for the assessment of rod adaptation after a photopigment bleach.

6.1. The development and validation of the full field rod ERG PST

6.1.1. Introduction

The a- and b-waves of the scotopic ERG are initially completely extinguished after a near total bleach of visual pigment, before gradually returning to the pre-bleach amplitude during 35-40 minutes in darkness (Thomas & Lamb, 1999; Cameron et al., 2006; Cameron et al., 2008). By contrast, full recovery of the a-wave of the photopic ERG after a near total photopigment bleach has been shown to occur within 6 minutes (Paupoo et al., 2000). These data were obtained from electrophysiological studies in which ERG data from repeated bleaches were collated over a prolonged recording period. Therefore, although the data illustrate that ERG techniques can be used to monitor dark adaptation, the lengthy protocols clearly render the techniques unsuitable for use in clinical practice.

A procedure in which the ERG is used to monitor cone dark adaptation clinically has previously been described (Binns & Margrain, 2005; 2007). The focal cone ERG PST was developed as an objective technique for the assessment of outer retinal function (Binns & Margrain, 2005). The technique monitors the recovery of the amplitude of the first harmonic of the 41Hz focal cone ERG after a photopigment bleach. The 41Hz focal cone ERG was considered an accurate representation of outer retinal function as it is dominated by bipolar cell activity, which, in turn, is dependent on levels of cone photopigment (Bush & Sieving, 1996; Kondo & Sieving, 2002). Pre-bleach ERGs are recorded as a baseline measure, before post-bleach ERGs are recorded every 20 seconds for 5 minutes. The amplitude of the first harmonic is then plotted as a function of time after the bleach and an exponential model is fitted to the data to generate a time constant of cone recovery. The recovery time constant of the focal cone ERG PST was shown to be significantly longer in participants with early AMD and was able to differentiate participants with early AMD from healthy control participants with high sensitivity and specificity (AUC = 0.74) (Binns & Margrain, 2007). However, there is currently no equivalent technique for the objective assessment of rod dark adaptation.

6.1.2. Aims

In order to expand the range of objective techniques available for dark adaptation measurement the initial aim of this study was to develop a full field ERG technique for the assessment of rod dark adaptation within a clinically viable timeframe.

6.1.3. General ERG methods

A Medelec Synergy evoked potential monitoring system (Oxford Instruments PLC, Old Woking, Surrey, UK) and miniature Ganzfeld LED (light emitting diode) stimulator (CH electronics, Kent, UK) (Figure 6.1) were used to record ERGs throughout all electrophysiological investigations included in this thesis. The stimulator comprised an array of LEDs housed in a 5cm diameter tube, which could be adapted for full field and focal ERG recording. In order to record full field ERGs the stimulator was fitted with a diffuser and held at the eye. In contrast, for focal ERG recordings, the stimulator was positioned within a desensitizing peripheral surround (Figure 6.2) to allow selective stimulation of the central 20° of retina, whilst minimising any response of the peripheral retina to scattered light.

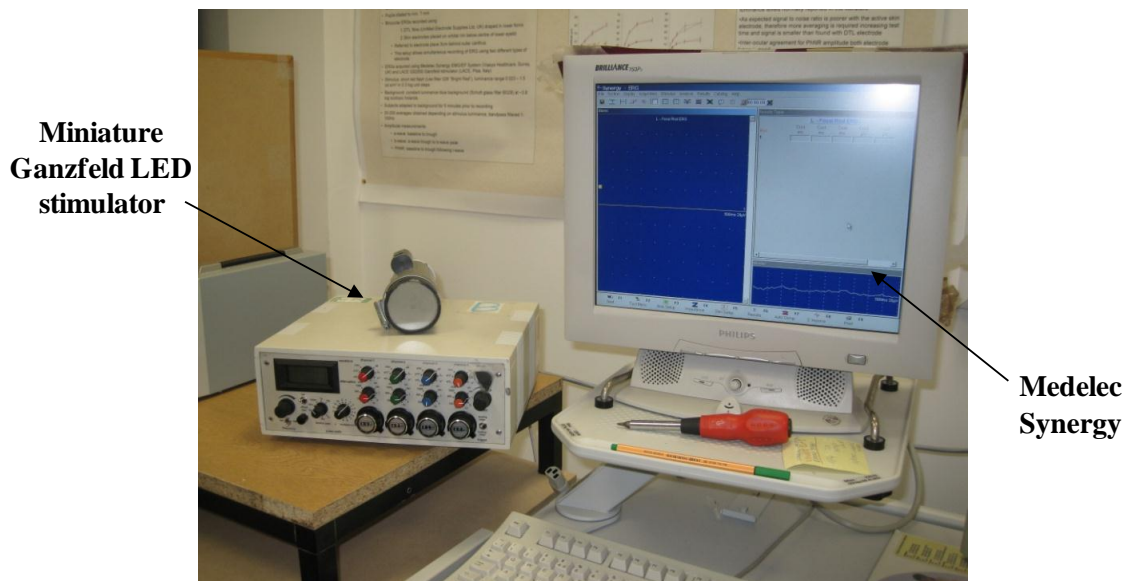


Figure 6.1. Medelec Synergy evoked potential monitoring system (Oxford Instruments PLC, Old Woking, Surrey, UK) and miniature Ganzfeld LED stimulator.

Prior to ERG recording, the participant's pupils were dilated with one drop of 1.0% Tropicamide in each eye. Following skin preparation using an abrasive gel (Nuprep), a silver-silver chloride skin electrode filled with electrolyte gel (TECA) was applied to the mid-frontal position using surgical tape (Blenderm). DTL fibre active and contralateral reference electrodes (Unimed electrode supplies, Surrey, UK) were positioned in the lower fornices. Electoretinograms were recorded monocularly (the contralateral eye was occluded). All ERG responses were digitally averaged and bandpass filtered from 1-100Hz using the Medelec Synergy system. An artefact reject setting was applied to exclude any traces contaminated by blinks or eye movements.

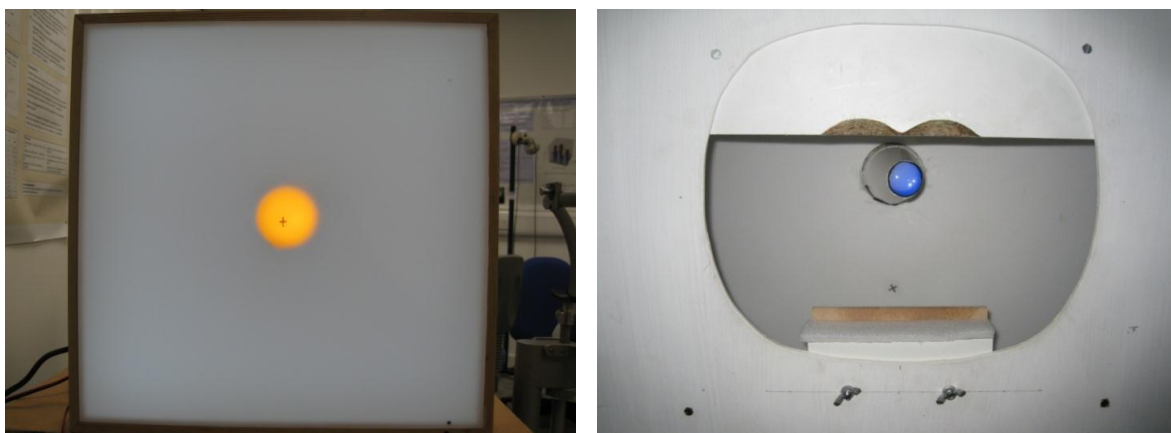


Figure 6.2. Miniature ganzfeld LED stimulator positioned within a desensitizing peripheral surround for recording focal cone (left panel) and rod (right panel) ERGs.

All procedures adhered to the tenets of the Declaration of Helsinki and to the ISCEV guidelines for ERG recording procedures (Marmor et al., 2009). Each participant provided informed written consent prior to their participation.

6.1.4. Methods

Participants

Two experienced observers, AB (34 years) and AG (26 years), participated in the preliminary studies. Both participants had a corrected visual acuity of 6/6 or better in the test eye, clear ocular media (\leq Grade 3, LOCS-III) (Chylack et al., 1993), a normal retinal appearance and no history of ocular or systemic disease known to affect visual function.

Experimental procedure

After pupil dilation and electrode application (see Section 6.1.3), dark adaptation was monitored in the left eye of both participants, using the full field rod ERG PST. Rod ERGs were recorded in response to a full field blue flash stimulus (454nm, half height bandwidth 67nm), duration 5ms, presented at a temporal frequency of 0.5Hz. A stimulus intensity of 5 scot.td.s was used in order to adhere to ISCEV guidelines for recording of isolated rod responses (Marmor et al., 2009). Participants underwent a 2 minute exposure to a Ganzfeld adapting background (7.04 log phot.Td) to produce a near total bleach of photopigment (99% rhodopsin and cone photopigment). On cessation of the bleach, participants directed their gaze to the centre of the test stimulus and recording commenced within 10 seconds. Full field rod ERGs were recorded in the dark every 2 minutes for 35 minutes. Thirty responses were averaged per trace.

Statistical analysis

A drift correction was applied to all ERG responses and Fourier analysis (Stroud, 1986) was used to isolate the first nine harmonics of the signal and to remove high frequency noise ($>45\text{Hz}$) (Figure 6.3). The locations of the a- and b-waves were determined objectively by Microsoft Excel (2003) as the maxima and minima within a given timescale and confirmed using visual inspection. The amplitude of the b-wave was measured from a-wave trough to b-wave peak and plotted as a function of time after the bleach.

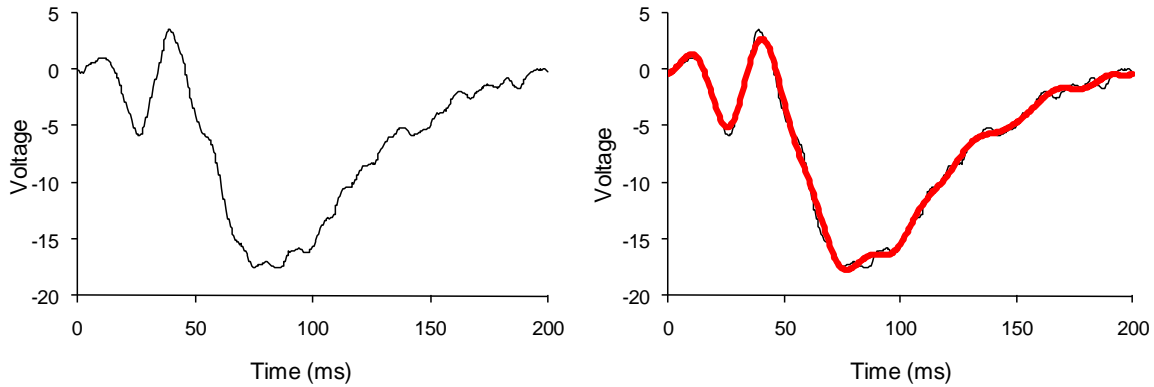


Figure 6.3. Raw full field rod ERG waveform for a healthy participant (left panel) and the Fourier analysed waveform (right panel).

The time constant of recovery (τ) for cones and rods was determined by fitting a single exponential function (Equation 6a) (Thomas & Lamb, 1999), on a least squares basis, to all recovery data, using Microsoft Excel (2003).

Equation 6a.
$$a_{max}(t) = a_{max}(\infty) / (1 + c_a \cdot e^{(-t/\tau)})$$

where a_{max} is the amplitude at time t after the bleach, $a_{max}(\infty)$ is the dark adapted sensitivity, c_a is the reduction in sensitivity immediately after the bleach and τ is the time constant of recovery. The root mean square error (RMS error) was calculated as a measure of ‘goodness-of-fit’ of the model to each dataset. A lower RMS error indicated a better model fit to the data.

6.1.5. Results

The b-wave of the full field rod ERG was extinguished for several minutes immediately after the photopigment bleach in participant AB (Figure 6.4). The amplitude of the b-wave then increased over time, rapidly at first and subsequently more slowly, to recover fully within 35 minutes in darkness, yielding a rod τ of 2.47 minutes. In AG there was a less complete elimination of the b-wave, but the subsequent amplitude recovery followed a slightly slower time course and the resultant rod τ was 4.48 minutes. In both cases the recovery was well described by the exponential model: RMS error = 4.23 for AB and RMS error = 9.13 for AG.

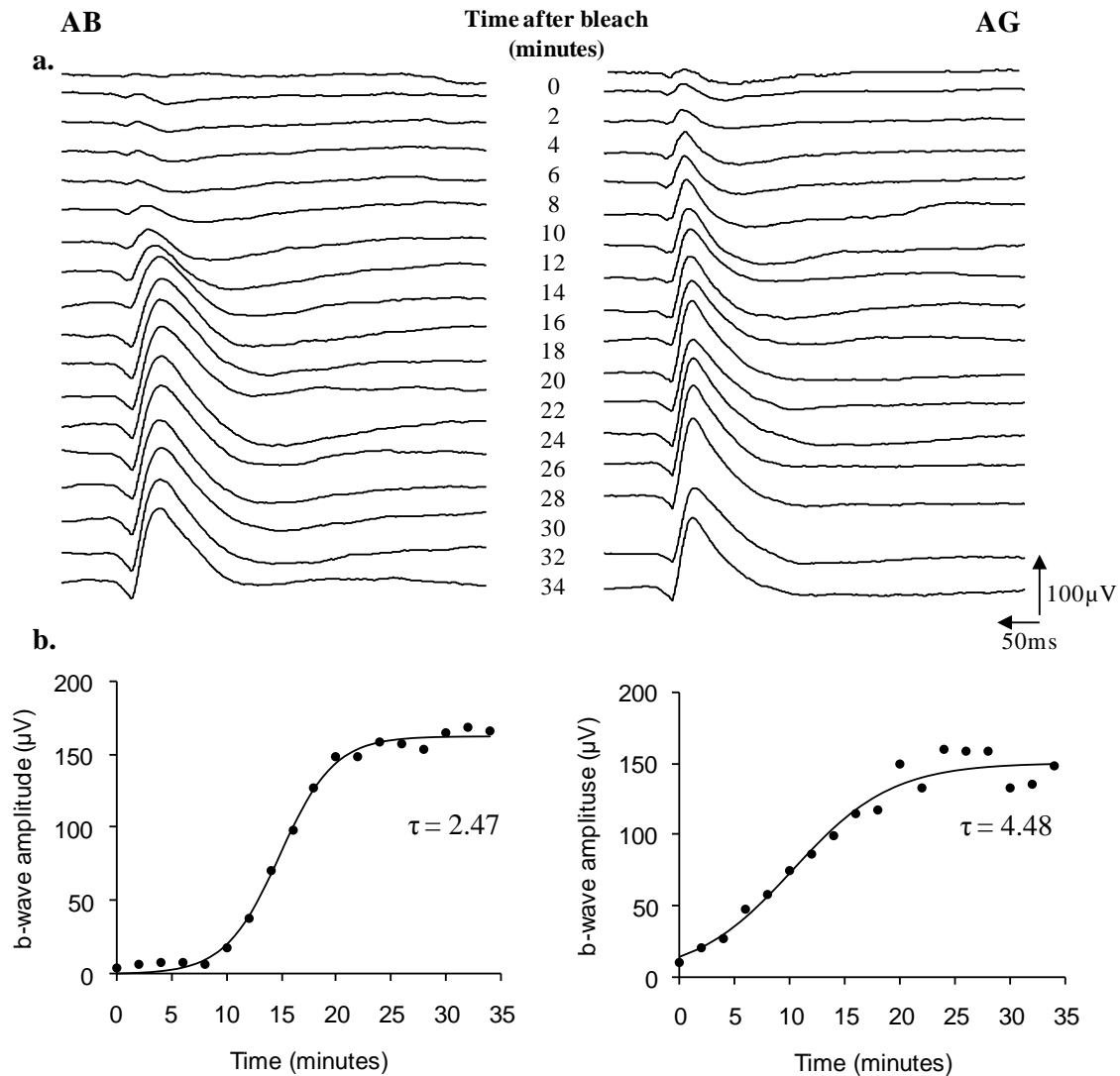


Figure 6.4. Recovery of the b-wave of the full field rod mediated ERG for participants AB and AG. Panel A shows the ERG traces recorded every 2 minutes. The amplitude recovery data are shown in panel B, together with the best fitting exponential function.

6.1.6. Discussion

The aim of this phase of the study was to develop a full field ERG technique for the assessment of rod dark adaptation. The data demonstrate that the full field ERG can be used as a simple, objective means of monitoring rod adaptation. The exponential model, based on the decay of an equivalent background (Thomas & Lamb, 1999), described all threshold recovery data well.

Although rod dominated ERGs are included in the ISCEV clinical protocol guidelines (Marmor et al., 2009), this is the first report of a rod dominated ERG being used in a clinically viable protocol to assess dark adaptation. The b-wave of the scotopic ERG was

initially markedly reduced by the photopigment bleach, before gradually returning to the pre-bleach amplitude during the time in the dark. When the b-wave amplitude was plotted as a function of time after the bleach, an S-shaped recovery curve emerged. This was consistent with previous studies in which the b-wave of the scotopic ERG was recorded at fixed intervals after a bleach (Cameron et al., 2006). The recovery of the scotopic a-wave after a near total bleach of photopigment has been shown to progress in a similar manner (Thomas & Lamb, 1999). This S-shaped recovery curve has been documented after photopigment bleaches of 40% or greater (Thomas & Lamb, 1999).

These previous electrophysiological studies of rod dark adaptation collated data from repeated bleaches (Thomas & Lamb, 1999; Cameron et al., 2006). In contrast, the protocol used in the current study has shown that the ERG can be used to assess dark adaptation in rods and cones within a clinically viable timeframe.

6.2. The development of the focal rod ERG PST

6.2.1. Introduction

In the previous section, the full field ERG was used successfully to monitor rod dark adaptation. However, in AMD, photoreceptor loss and dysfunction is localised to the central retina (Curcio et al., 1996; Curcio, 2001). Correspondingly, functional loss associated with the disease has frequently been reported within the central 25° of the retina (Brown et al., 1986a; Owsley et al., 2000, Owsley et al., 2001, Haimovici et al., 2002; Phipps et al., 2003, Binns & Margrain, 2007; Owsley et al., 2007; Dimitrov et al., 2008, 2011). It has been estimated that 96% of rod photoreceptors are located beyond the macular region (Curcio et al., 1990). As the full field rod ERG is a summed response from rods throughout the whole retina, it remains relatively unaffected by the focal abnormalities that occur in early AMD (Sunness et al., 1985; Holopigian et al., 1997; Jackson et al., 2004). Therefore, although the full field rod ERG is a clinically viable method for the assessment of dark adaptation, it will not necessarily yield clinically useful information in macular disease, as the localised adaptational dysfunction that occurs in early AMD may be masked by the peripheral rod response.

The focal rod ERG

The recording of focal rod responses is complicated by stimulation of the peripheral retina by scattered light. Although the Stiles Crawford effect applies to cones (Stiles & Crawford, 1933), rods lack this same directional sensitivity (Pirene, 1962). Consequently, rod photoreceptors are prone to stimulation by scattered light, which causes the formation of a double b-wave when recording the focal rod ERG (Fry & Bartley, 1935; Sandberg et al., 1996; Hood et al., 1998; Binns & Margrain, 2006). The second b-wave is a slower, larger response generated by the rods located in the peripheral retina, in response to the lower intensity scattered light (Sandberg et al., 1996), and makes the focal rod response difficult to interpret. Several approaches have previously been used to eliminate this scattered light response.

The subtraction technique proposes that the amplitude of the second b-wave of the focal rod ERG may be matched by the amplitude of a full field ERG generated by a stimulus of lower intensity (Sandberg et al., 1996). Subtraction of this matching full field signal from the focal response will eliminate the scattered light component and thereby isolate the focal rod response. However, identification of the appropriate full field stimulus intensity can be time consuming (Binns & Margrain, 2006).

Alternatively, a background adaptation technique has been used to isolate multifocal rod ERGs (Hood et al., 1998) and focal rod ERGs (Binns & Margrain., 2006). That is, the stimulus is positioned within an adapting background to suppress the peripheral rod response to scattered light. As the intensity of the surround increases, the stray light response decreases until it is completely extinguished. The intensity of the surround required to eliminate the stray light response varies between participants (Hood et al., 1998). A protocol has been described for recording focal rod ERGs using this approach (Binns & Margrain, 2006). The focal rod ERG is recorded after 30 minutes of dark adaptation, in response to a 20° diameter blue flash stimulus, presented within a desensitizing surround of 1.67 log.scot.td.s.

An additional method of eliminating the scattered light response is to use a small dim stimulus. The stray light response was demonstrated to be negligible when a 5° diameter stimulus, of low intensity is used (Horiguchi et al., 1991; Choshi et al., 2003). However, the resultant ERG amplitude is extremely small, which leads to a poor signal to noise ratio,

thus rendering the technique insensitive to small changes in retinal function (Binns & Margrain, 2006).

When compared directly, the background adaptation technique proved a more reliable method for obtaining a focal rod ERG response with a measurable a-wave, as well as being less time consuming, than the subtraction technique (Binns & Margrain, 2006). The background adaptation technique may therefore be considered the most clinically applicable technique for eliminating the scattered light response when recording focal rod ERGs. A surround of 1.67 log.scot.td.s has been shown to be effective in most participants (Binns & Margrain, 2006).

6.2.2. Aims

The aim of this second study was to develop an ERG technique for the assessment of rod dark adaptation at the macula using the focal rod ERG. As focal ERG signals are small, they are subject to significant degradation by noise. The effect will be magnified at early times post-bleach, when the signal is substantially reduced in amplitude. Consequently, the initial aim of the study was to evaluate the effect of stimulus frequency and stimulus intensity on signal quality in order to maximise the response amplitude. On establishing an optimal protocol, the second aim of the study was to validate the focal rod PST technique in participants with and without early AMD.

6.2.3. Determination of the optimal stimulus frequency

6.2.3.1. Background/Aims

In scotopic conditions, rod photoreceptors are insensitive to frequencies above 10-15Hz (Conner, 1982). ISCEV standards recommend the use of a stimulus frequency of approximately 0.5Hz for the recording of rod-isolated ERGs to prevent adaptational effects (Marmor et al., 2009). However, at this low stimulus frequency, data collection is slow. In order to improve the SNR of small ERG signals, averaging a large number of responses is beneficial, but during dark adaptation, threshold is constantly changing and there is therefore a limited timeframe in which these averages may be obtained. The use of higher stimulus frequencies facilitates greater averaging within a given time interval. The aim of this phase of the study was to determine the highest stimulus frequency that can be used to

record the dark adapted focal rod ERG without causing significant attenuation of the b-wave.

6.2.3.2. Methods

Participants

Two experienced observers, AB (34 years) and AG (26 years), participated in the study. Both participants had a corrected visual acuity of 6/6 or better in the test eye, clear ocular media (\leq Grade 3, LOCS-III) (Chylack et al., 1993), a normal retinal appearance and no history of ocular or systemic disease known to affect visual function.

Experimental procedure

After pupil dilation and electrode application (see Section 6.1.3), participants were dark adapted for 30 minutes. A series of full field rod ERGs were recorded from each participant, in response to a blue flash stimulus (454nm, half height bandwidth 67nm, intensity 5 scot.td.s), at range of frequencies: 0.5, 1, 2, 5 and 10Hz. The timebase was 500ms, with the exception of the 5Hz and 10Hz stimuli when a 200ms timebase was used in order to display one response cycle. Twenty-five responses were averaged at each stimulus frequency. The locations of the a- and b-waves were determined objectively by Microsoft Excel (2003) and the amplitude of the b-wave was measured from a-wave trough to b-wave peak. The optimal stimulus frequency was identified as the highest frequency that did not cause significant attenuation of the b-wave.

Focal rod ERGs were then recorded at two stimulus frequencies: 0.5Hz and the highest stimulus frequency shown by the full field results to cause no significant attenuation of the b-wave. Participants were instructed to fixate the centre of the 20° diameter blue flash stimulus (454nm, half height bandwidth 67nm, intensity 5 scot.td.s), positioned within a desensitizing surround of 1.67 log.scot.td.s. As the signal was much smaller when this focal stimulus was used, 150 responses were averaged at each stimulus frequency. The a- and b-waves were then identified and the b-wave amplitude measured.

6.2.3.3. Results

The ERG traces showing the effect of stimulus frequency on the b-wave of the dark adapted full field rod ERG are shown in Figure 6.5, for both participants. The b-wave amplitude was similar at 0.5, 1 and 2Hz, however at 5 and 10Hz a marked reduction in

amplitude was evident. Figure 6.6 shows that the b-wave amplitudes recorded between 0.5 and 2Hz fell within a $20\mu\text{V}$ range for AB and a $30\mu\text{V}$ range for AG. However the b-wave amplitude obtained at 5Hz was almost 50% smaller than that obtained at 0.5Hz.

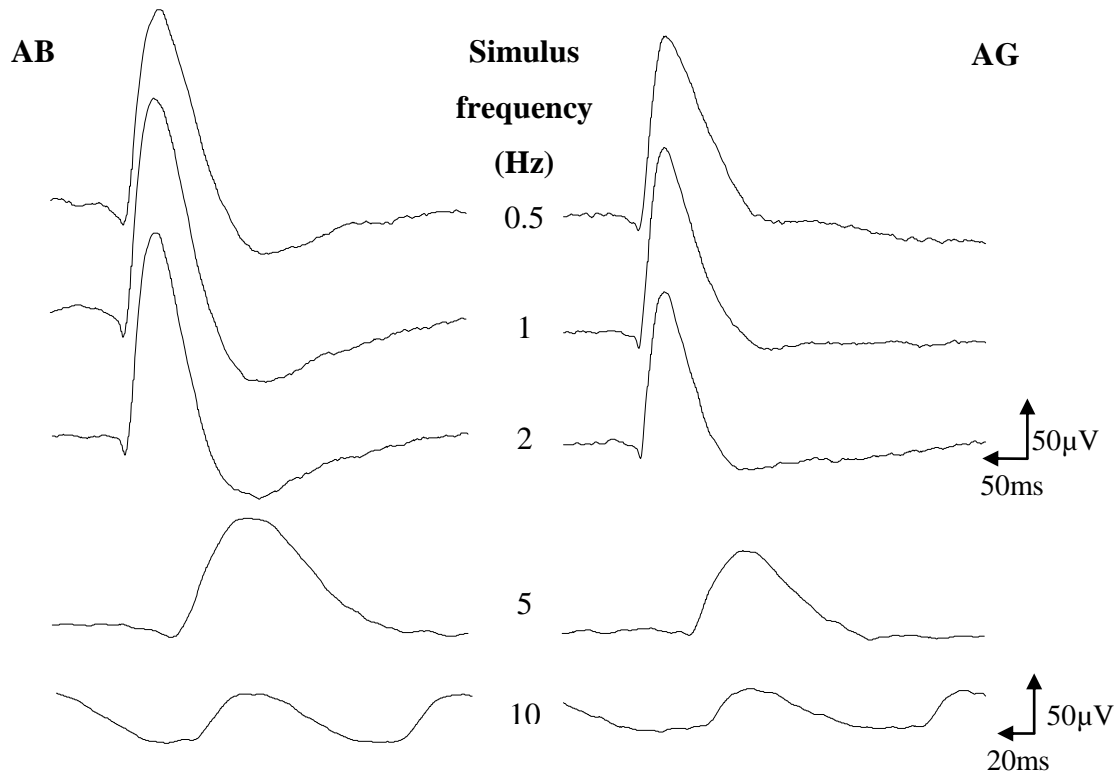


Figure 6.5. Dark adapted full field ERG responses recorded from participants AB and AG in response to a 5 scot.td.s blue flash of increasing frequency: 0.5-10Hz. Twenty-five responses were averaged at each frequency.

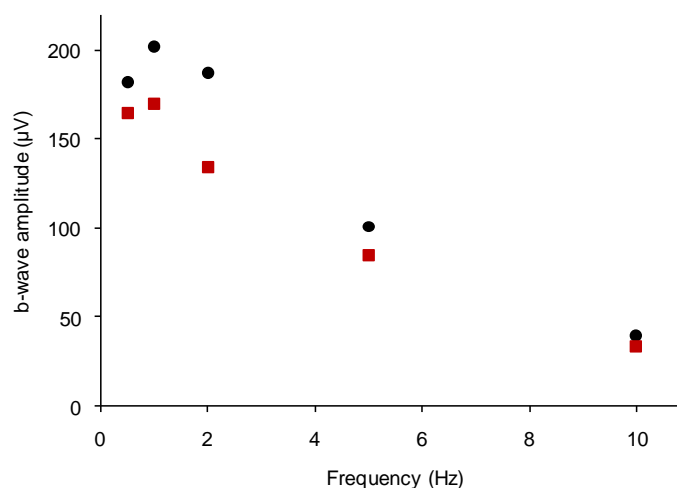


Figure 6.6. The amplitude of the full field, dark adapted ERG b-wave plotted as a function of stimulus frequency for AB (black circles) and AG (red squares).

As 2Hz was the highest stimulus frequency at which there was no marked attenuation of the b-wave of the full field rod ERG, responses at this frequency were compared with those at 0.5Hz for the focal ERG recordings. As expected, at both 0.5 and 2Hz the dark adapted focal ERG b-wave amplitudes were markedly smaller than the equivalent full field b-wave amplitudes (Figure 6.7). There was, however, a negligible difference between the b-wave amplitudes recorded at the two frequencies for each participant.

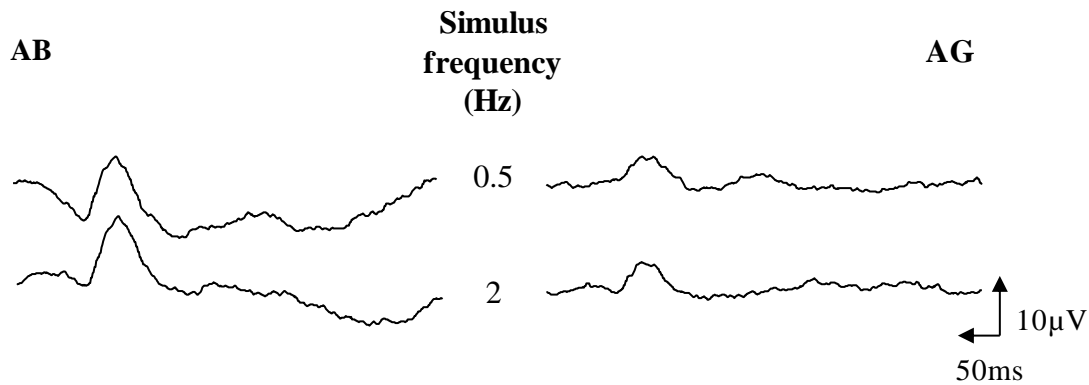


Figure 6.7. Dark adapted focal ERG responses recorded from participants AB and AG in response to a 5 scot.td.s blue flash at 0.5 and 2Hz, presented within a desensitizing surround. One hundred and fifty responses were averaged at each frequency.

6.2.3.4. Discussion

The significant reduction in the b-wave amplitude of the dark adapted focal rod ERG compared to the dark adapted full field ERG emphasises the pressing need to optimise the recording protocol in order to maximise the signal obtained when recording focal rod ERGs. At increased stimulus frequencies, a greater number of averages may be obtained within a given time interval. This results in a strengthening of the resultant signal, but is accompanied by the attenuation of the ERG b-wave at high stimulus frequencies. When full field rod ERGs were recorded, 2Hz was the highest frequency at which there was no significant attenuation of the b-wave. This was therefore selected for further investigation in the recording of the focal rod ERG. The focal recordings revealed a negligible difference in the dark adapted b-wave amplitude at 0.5 and 2Hz. A 2Hz stimulus allows four times as many averages to be recorded in a given time period compared to a 0.5Hz stimulus. Although higher frequencies would increase averaging further, the accompanying b-wave attenuation renders these stimuli impractical for focal recordings. Therefore, a stimulus frequency of 2Hz was selected for all future focal rod ERG recordings.

6.2.4. Determination of the optimal stimulus intensity

6.2.4.1. Background/Aims

The use of relatively high stimulus intensities when recording rod dominated ERGs provides a more accurate estimate of rod photoreceptor activity than the moderate intensity flashes recommended by ISCEV (Marmor et al., 2009), due to the increased amplitude of the response and an improved SNR. However, high intensity stimuli will evoke a response from both the cone and rod pathways (Hood & Birch, 2006). The aim of this phase of the study was to determine the highest stimulus intensity that can be used to record the dark adapted focal rod ERG without cone intrusion, in order to maximise the amplitude of the response obtained.

6.2.4.2. Methods

Participants

The same experienced observers participated in this study. Both participants had a corrected visual acuity of 6/6 or better in the test eye, clear ocular media, a normal retinal appearance and no history of ocular or systemic disease known to affect visual function.

Experimental procedure

After pupil dilation and electrode application (see Section 6.1.3), participants were dark adapted for 30 minutes. A series of full field rod ERGs were recorded from each participant in response to a blue flash stimulus (454nm, half height bandwidth 67nm), presented at a temporal frequency of 2Hz (identified as optimal in the preceding section of the study). In order to identify the stimulus intensity that would elicit a maximal rod response without significant cone intrusion, an approach was used based on a protocol previously advocated by Hood & Birch (1996; 2006). That is, after dark adaptation, full field ERGs were recorded at a range of stimulus intensities: 2.5, 5, 10, 20, 30, 40 and 50 scot.td.s. The same stimuli were then presented against a steady green background (525nm) of 30cd/m² (approximately 3.54 log scot.td.s). An adapting background of this intensity eliminates the rod response, but leave the cone response relatively unaffected (Hood & Birch, 1996; 2006). Sixty responses were averaged at each stimulus intensity. The locations of the a- and b-waves were determined as the minima and maxima within a specified time window (20-70msec post-bleach), and the amplitude of the b-wave was measured from a-wave trough to b-wave peak. The optimal recording intensity for the full

field rod ERG was identified as the highest intensity at which no significant cone response was detected.

Focal rod ERGs were then recorded at the three highest stimulus intensities shown by the full field results to cause minimal cone stimulation, first with and then without the adapting background. Participants were instructed to fixate the centre of the 20° diameter blue flash stimulus (454nm, half height bandwidth 67nm), positioned within a desensitizing surround of 1.67 log.scot.td.s. As the signal was much smaller when this focal stimulus was used, 800 responses were averaged at each stimulus intensity. The a- and b-waves were then identified and the b-wave amplitude recorded.

6.2.4.3. Results

The ERG traces showing the isolated cone contribution to the dark adapted full field ERG response to blue flashes of varying intensity (2.5-50 scot.td.s) are shown in Figure 6.8, for both participants. There was no evidence of a repeatable response recorded from either participant at the lowest two stimulus intensities: 2.5 and 5 scot.td.s. At 10 scot.td.s, AB continued to show no evidence of a repeatable b-wave, however an extremely small b-wave was exhibited by AG (amplitude = 1.6 μ V). As the intensity of the stimulus increased further, the ERG response became larger and more clearly visible in both participants.

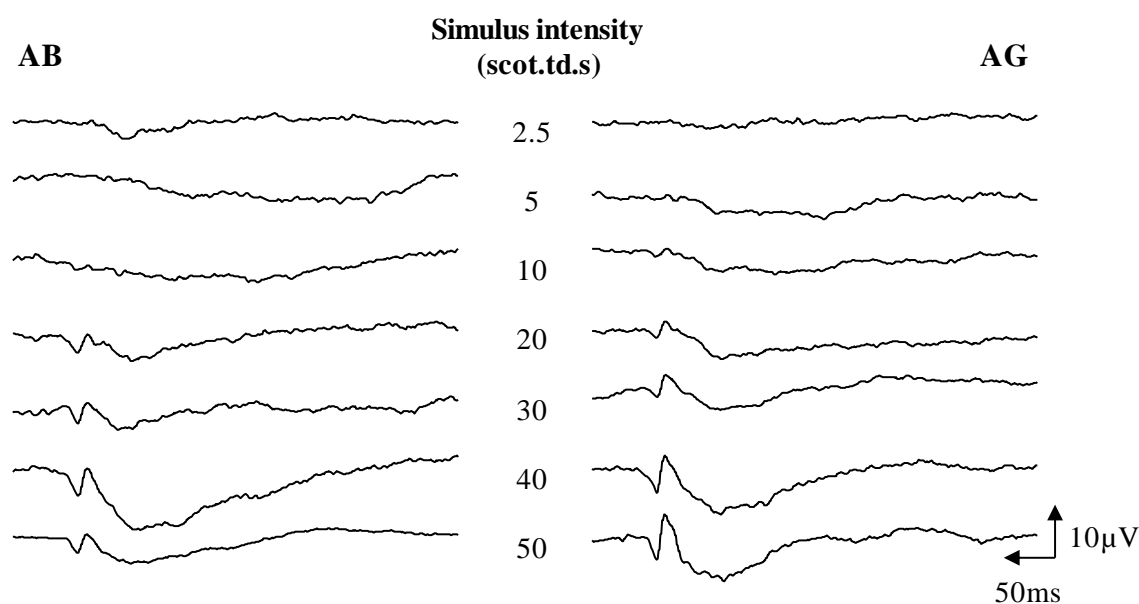


Figure 6.8. Cone contribution to dark adapted full field ERG responses recorded from participants AB and AG in response to a blue flash of increasing intensity: 2.5-50 scot.td.s, presented on a steady field of 30 cd/m².

Having shown a minimal full field cone response at stimulus intensities up to about 20 scot.td.s, the next step was to evaluate focal responses at these intensities. Figure 6.9 shows the dark adapted focal ERG response at 5, 10 and 20 scot.td.s together with the isolated cone response at these intensities. At 5 scot.td.s neither of the participants exhibited a measurable cone contribution to the b-wave. When the stimulus intensity increased to 10 scot.td.s a cone contribution was recorded from AG only. A further increase in the stimulus intensity to 20 scot.td.s evoked a cone contribution from both participants.

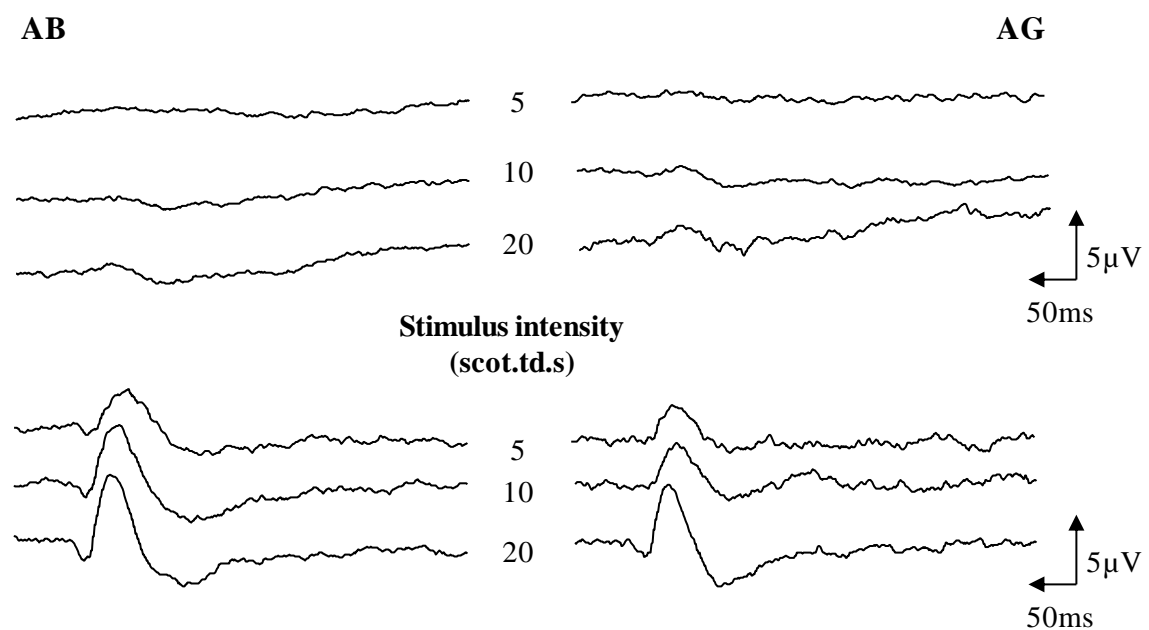


Figure 6.9. Cone contribution to dark adapted focal ERG responses (top panel) recorded from participants AB and AG in response to a blue flash at 5, 10 and 20 scot.td.s, presented on a steady green background of 30 cd/m². The lower panel shows the dark adapted focal ERG responses recorded without the rod saturating background i.e. the combined rod and cone response.

6.2.4.4. Discussion

Although the use of a high intensity stimulus when recording the focal rod ERG ensures that the signal obtained is maximised, there is an increased risk of cone stimulation at these intensities. The full field ERGs recorded here indicate that the cone contribution in response to a flash intensity of 2.5 or 5 scot.td.s is negligible. However, these low intensities are not optimal for recording focal ERGs as many averages are required to obtain a favourable SNR. At 10 scot.td.s a cone contribution was recorded from one

participant only (AG), whilst higher stimulus luminances evoked a cone response from both participants.

Similarly, when focal ERGs were recorded at a stimulus intensity of 20 scot.td.s, the signal comprised a marked cone component in both participants. This intensity was therefore considered too high for the recording of focal rod ERGs. In contrast, at 10 scot.td.s there was no measurable cone response from one participant and only an extremely small cone response from the other participant. Consequently, this stimulus intensity was selected for future focal rod ERG recordings to maximise the amplitude of the signal without inducing a significant cone contribution to the rod data. This stimulus intensity also falls within ISCEV guidelines for recording of isolated rod responses (Marmor et al., 2009).

6.2.5. Development and validation of a recording protocol for the focal rod ERG PST

6.2.5.1. Background/Aims

The preceding investigations in this section have explored the parameters of the stimulus used for recording focal rod ERGs, in order to optimise the resultant ERG signal. A blue flash stimulus presented at a temporal frequency of 2Hz and an intensity of 10 scot.td.s was selected as the ideal stimulus for recording focal rod ERGs during dark adaptation. These parameters ensure that the amplitude of the signal is maximised, so that a sufficient number of responses may be averaged in a limited timeframe and that the resultant signal is free from any significant cone component. The aim of this phase of the study was to describe a protocol for recording the focal rod ERG PST based on these optimal stimulus parameters, and then to validate the protocol in participants with early AMD and age-matched control participants.

6.2.5.2. Methods

Participants

Two experienced observers (AB, 34 years and AG, 26 years), participated in the preliminary testing of the focal rod ERG PST protocol. In order to validate the focal rod ERG PST, three participants with early AMD and three age-matched control participants were recruited from the database. These participants were aged 55 years and over, with a corrected visual acuity of 6/9 or better in the test eye, no significant media opacity (\leq Grade 3, LOCS-III) (Chylack et al., 1993), and no history of systemic disease or

medication known to affect visual function. Those participants with early AMD all had a diagnosis of early or intermediate AMD in at least one eye, according to the Age-Related Eye Disease Study severity scale (Davis et al., 2005), in the absence of any co-existing ocular or fundus abnormality. The diagnosis was confirmed using 37° fundus photographs (Canon CR-DGi Camera) obtained at the baseline examination.

All participants provided informed written consent prior to participation. The study was approved by the South East Wales Research Ethics Committee and all procedures adhered to the tenets of the Declaration of Helsinki.

Experimental procedure

Focal rod ERGs were recorded in response to a 20° diameter blue flash stimulus (454nm, half height bandwidth 67nm), intensity 10 scot.td.s, duration 5ms, presented at a temporal frequency of 2Hz. The stimulus was positioned within a desensitizing surround of 1.67 log.scot.td.s.

In order to assess the effect of adaptation to the stimulus on the amplitude of the b-wave of the focal rod ERG during the 36 minute period over which dark adaptation was measured, a dataset was first recorded from experienced observers AB and AG in the absence of a photopigment bleach. After 30 minutes of dark adaptation, focal rod ERGs were recorded every 3 minutes, for 36 minutes. One hundred responses were averaged on each trace.

The focal rod ERG PST was initially recorded from the two experienced observers. It was then repeated for the three participants with early AMD and the three age-matched control participants. After pupil dilation and electrode application (section 6.1.3), a Maxwellian view optical system was used to bleach 95% of rhodopsin (5.78 log phot.Td for 120s) (Hollins & Alpern, 1973) in the central 43.6° of the test eye. On cessation of the bleach, participants turned to fixate the centre of the test stimulus and recording commenced immediately. Focal rod responses were recorded in the dark, every 3 minutes for 36 minutes. One hundred responses were averaged on each trace, which took approximately 2 minutes, leaving one minute for the patient to relax before the next recording.

All responses were Fourier analysed (Microsoft Excel 2003) and high frequency noise (>45Hz) removed (Stroud, 1986). The locations of the a- and b-waves were determined

objectively by Microsoft Excel (2003) and confirmed using visual inspection. The amplitude of the b-wave was measured from a-wave trough to b-wave peak and plotted as a function of time after the bleach.

Statistical analysis

The time constant of recovery (τ) was determined by fitting a single exponential function (Equation 6a) (Thomas & Lamb, 1999), on a least squares basis, to all recovery data, using Microsoft Excel (2003).

6.2.5.3. Results

The effect of stimulus adaptation on the focal rod ERG PST

Figure 6.10 shows the amplitude of the b-wave of the dark adapted focal rod ERG as a function of time, recorded in response to a 10 scot.td.s blue flash, presented at a temporal frequency of 2Hz, in the absence of a photopigment bleach. The b-wave amplitude fluctuated within a $2\mu\text{V}$ range for each participant, although AB typically produced larger b-wave amplitudes than AG. There was no progressive increase or decrease in the amplitude of the b-wave over time and correspondingly, both datasets were well described by a straight line with a gradient of approximately zero.

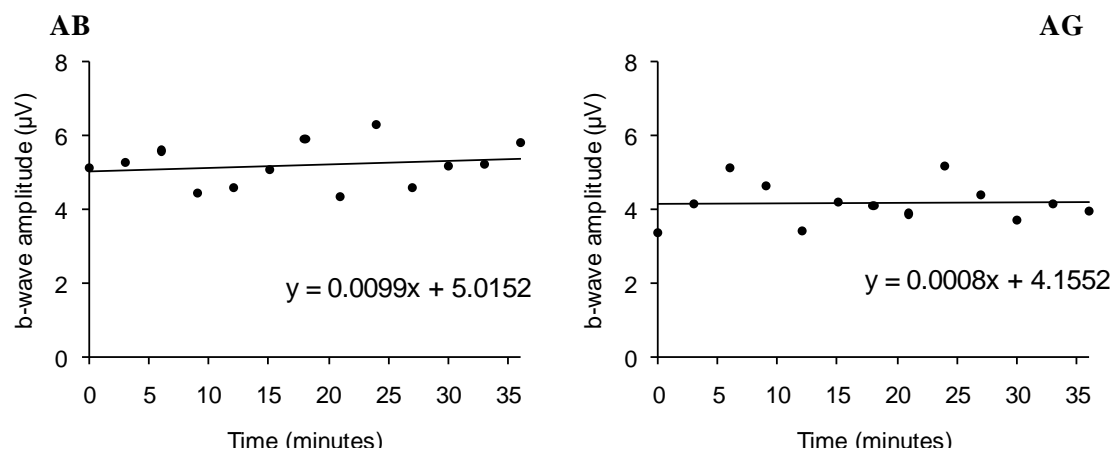


Figure 6.10. The amplitude of the b-wave of the focal rod ERG b-wave plotted as a function of time, recorded in response to a 10 scot.td.s blue flash presented at a temporal frequency of 2Hz, recorded in the absence of a photopigment bleach.

Focal rod ERG PST data from experienced observers

In both experienced observers, the amplitude of the b-wave of the focal rod ERG was markedly reduced immediately after cessation of the photopigment bleach (Figure 6.11).

The amplitude of the b-wave then increased over time, rapidly at first and subsequently more slowly, to recover fully within 36 minutes in darkness. The time constant of rod recovery (τ) for AB was 5.51 minutes and 5.00 minutes for AG. The amplitude recovery in both cases was well described by the exponential model: RMS error = 0.54 for AB and RMS error = 0.35 for AG.

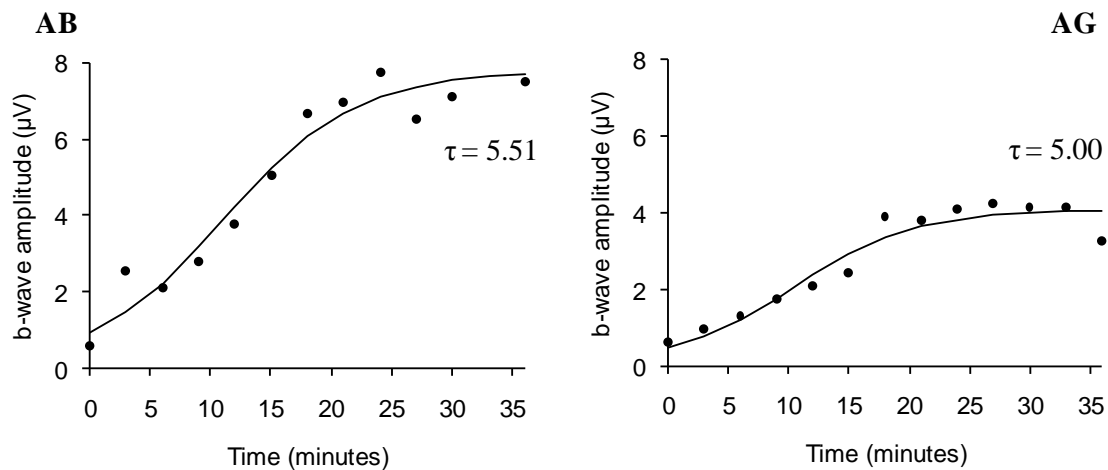


Figure 6.11. Recovery of the b-wave of the focal rod ERG for participants AB and AG. The amplitude recovery data is shown, together with the best fitting exponential function.

Focal rod ERG PST data from participants with early AMD and control participants

Table 6.1. Characteristics of the ‘ERG naive’ participants

Participant	Age (years)	Gender	logMAR VA
Control 1	74	Female	0.0
Control 2	77	Male	-0.08
Control 3	72	Male	0.02
AMD 1	76	Female	0.2
AMD 2	79	Male	0.1
AMD 3	69	Female	0.0

The characteristics of the ‘ERG naive’ participants are shown in Table 6.1 for the early AMD and control groups. These participants were all aged between 69 and 79 years (mean = 74.5 +/- 3.3 years).

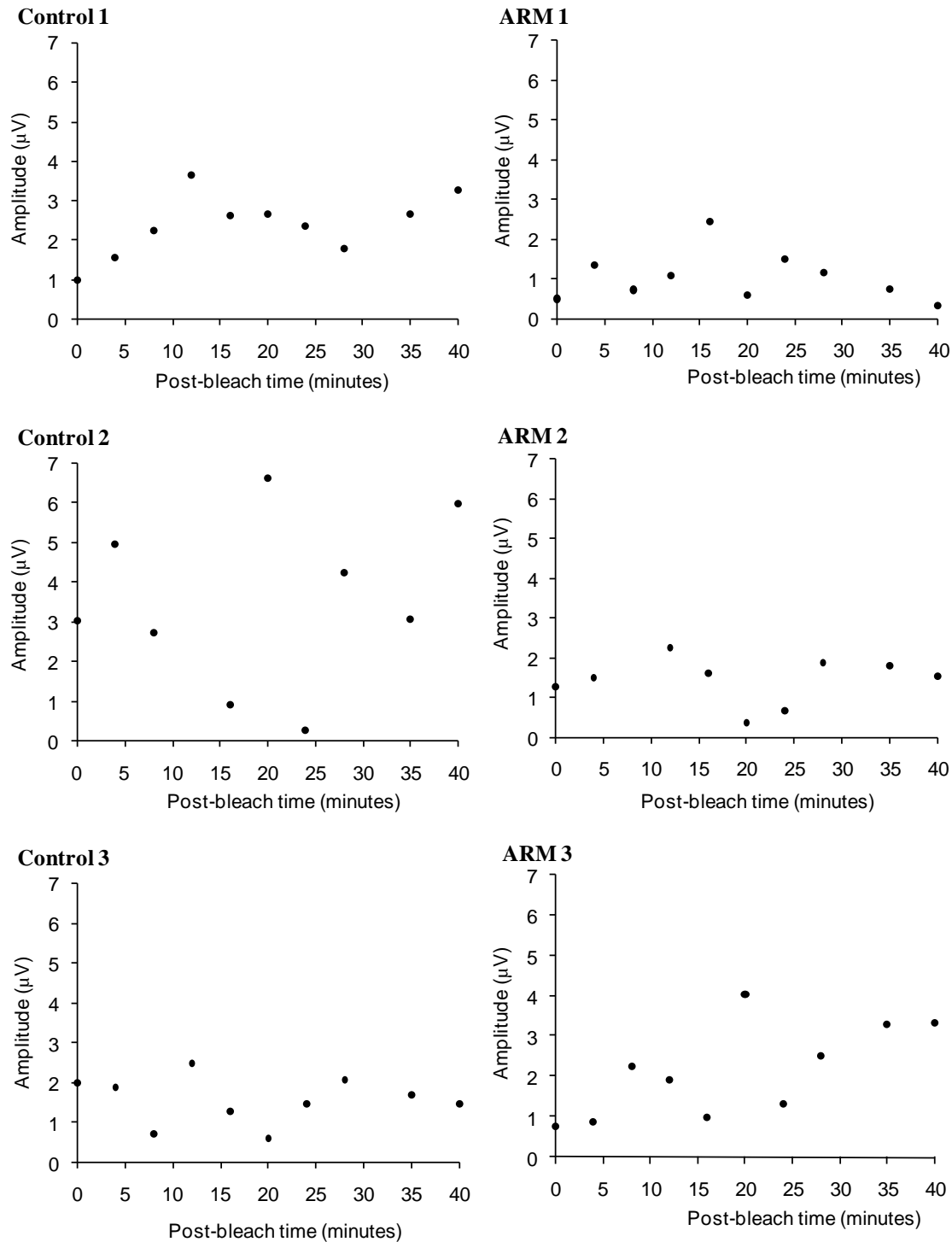


Figure 6.12. Amplitude of the b-wave of the focal rod ERG, plotted as a function of time after a photopigment bleach for six ERG naïve participants. Control data are shown in the left panel and early AMD data in the right panel.

The amplitude recovery data for the b-wave of the focal rod ERG is plotted as a function of time after the photopigment bleach in Figure 6.12, for all six observers. Focal ERG recording was more time consuming in these participants, compared to the experienced

observers, due to numerous responses being rejected by the system as contaminated by artefacts, and consequently, ERG responses were only recorded every 4 minutes in these participants. In addition, for the same reason, the maximum number of averages that could be obtained on each trace ranged from 35 to 80, rather than the full 100 averages proposed in the protocol. Unlike the amplitude recovery data recorded from the experienced observers, these 'ERG naïve' participants showed no evidence of a systematic change in the b-wave amplitude over time in the dark (Figure 6.12). Consequently, when the exponential model was applied to these dataset it failed to generate a meaningful recovery curve for any of the participants.

6.2.5.4. Discussion

In this section of the study a protocol for recording the focal rod ERG PST was described, based on the optimal stimulus parameters identified during the preliminary investigations. The initial data obtained using this technique in two experienced observers suggested that the focal rod ERG PST may be used as an objective means of monitoring rod dark adaptation at the macula. The amplitude of the b-wave of the focal rod ERG was markedly reduced after a near total bleach of rhodopsin and gradually recovered during the 36 minute recording period. The recovery data were well described by an exponential model and the S-shaped recovery curve was consistent with reports of full field scotopic b-wave recovery after a near total bleach of photopigment (Cameron et al., 2006). In addition, there was no progressive reduction in the b-wave amplitude elicited by the focal stimulus during the time in the dark, in the absence of a photopigment bleach. This indicated that neither observer was experiencing any progressive adaptation to the stimulus that would affect the ERG recordings obtained during the focal rod ERG PST.

Although these early results obtained using the focal rod ERG PST were promising, when the same protocol was implemented in an older cohort of participants with and without early AMD, no meaningful recovery of the b-wave in the dark could be observed. As discussed in Chapter 3 (Section 3.1, Page 93), there is an increase in the density of the crystalline lens with increasing age (Bron et al., 2000), which causes an increase in pre-retinal light absorption, particularly at short wavelengths. The reduction in the amount of light reaching the retina results in a diminished ERG signal and therefore a greater number of averages are required to achieve a favourable SNR. Furthermore, the elderly participants struggled with the prolonged recording period, and were prone to blinking and making eye

movements. This generated electrical artefacts, which resulted in automatic rejection of the affected responses. As a result of this, a longer recording period was required to obtain the desired 100 responses averaged on each trace. This degree of averaging is feasible during ERG recordings to assess steady-state retinal functions. However, during dark adaptation the visual threshold is constantly changing, which means that the number of averages that can be obtained is limited by rigorous time constraints.

In summary, the focal rod ERG may be used to assess dark adaptation in young, 'ERG experienced' participants but is an ineffective technique for monitoring dark adaptation in older participants, in whom the SNR is reduced and blinking artefacts are common. Although the full field rod ERG can be used to assess dark adaptation, it was not possible to develop a clinically viable focal protocol for use in elderly patients. Consequently, psychophysical techniques currently remain a more favourable option for monitoring the changes to rod dark adaptation that occur in early AMD.

7. A comparison of psychophysical and electrophysiological techniques for the detection of early AMD

The ERG is a valuable but underused resource for the evaluation of retinal function in early AMD. As discussed in chapter 6, this is most likely due to the absence of a standardised protocol for the investigation of macular function using the ERG (Gerth, 2009). However, the preceding chapters and previous publications (Binns & Margrain, 2005; 2007) have demonstrated that by optimising the methodology, both psychophysical and electrophysiological techniques can be used to assess the changes in cone dark adaptation that occur in early AMD. Given the respective advantages and disadvantages of psychophysical and electrophysiological methods of dark adaptation measurement, this chapter will directly compare the diagnostic potential of the optimal computer based psychophysical procedure for measurement of cone dark adaptation to the focal cone ERG PST (Binns & Margrain, 2007).

7.1. Introduction

Although psychophysical methods have been widely used to assess dark adaptation, the data are based on the subjective responses of the participant and may therefore be degraded by human inconsistencies, such as expectation and habituation errors (Treutwein, 1995). In contrast, ERGs can be used to assess dark adaptation objectively, but require specialist equipment and can be time consuming to set up and record. In addition, focal ERG methods, such as those used to assess macular function are susceptible to the effects of noise because of the relatively small signal obtained (Gerth, 2009).

Psychophysical and electrophysiological dark adaptation data have previously only been compared in healthy participants (Karpe & Tansley, 1948; Fulton & Rushton, 1978). When the recovery of the ERG b-wave amplitude and psychophysical visual threshold were measured simultaneously in a single participant after a photopigment bleach, extremely similar dark adaptation curves were obtained (Karpe & Tansley, 1948). In addition, further evidence showed that the recovery of the ERG b-wave and psychophysical visual threshold

both follow an exponential time course after exposure to an adapting light (Fulton & Rushton, 1978). However, despite the strong resemblance between the ERG and psychophysical dark adaptation curves, quantitative data about the agreement between the two methods has not been published.

7.2. Aims

As both psychophysical and electrophysiological techniques may be used to assess cone dark adaptation in early AMD, the aim of this study was to compare the diagnostic potential of the optimal psychophysical protocol, developed in Chapters 2, 4 and 5, to the focal cone ERG PST, recorded from participants with and without early AMD.

7.3. Methods

Participants

Ten participants with early AMD and ten healthy control participants were recruited from the database. All participants were aged 55 years and over, with a corrected visual acuity of 6/9 or better in the test eye, no significant media opacity (\leq Grade 3, LOCS-III) (Chylack et al., 1993), and no history of systemic disease or medication known to affect visual function. Those participants with early AMD had a diagnosis of early or intermediate AMD in at least one eye, according to the Age-Related Eye Disease Study severity scale (Davis et al., 2005), in the absence of any co-existing ocular or fundus abnormality. The diagnosis was confirmed using 37° fundus photographs (Canon CR-DGi Camera) obtained at the baseline examination.

All participants provided informed written consent prior to participation. The study was approved by the South East Wales Research Ethics Committee and all procedures adhered to the tenets of the Declaration of Helsinki.

Apparatus

All psychophysical stimuli were presented on a calibrated, high resolution CRT monitor (Iiyama LS 902UT) driven by an 8-bit graphics board (nVIDIA Geforce 9) under software control (Matlab, R2009a, The MathWorks Inc.). As described in Chapter 2 (Section 2.2.3) the luminance output of the monitor was γ -corrected (Metha et al., 1993; Brainard et al. 2001) and modified by neutral density filters mounted on the screen to expose the full range of retinal recovery.

ERGs were recorded using a Medelec Synergy evoked potential monitoring system (Oxford Instruments PLC, Old Woking, Surrey, UK) and miniature Ganzfeld LED stimulator (CH electronics, Kent, UK) positioned within a desensitizing peripheral surround, as described previously (Section 6.1.3).

Experimental procedure

Participants attended the laboratory on two days. Baseline examinations were completed at the start of the first visit. These included patient history, logMAR visual acuity (ETDRS), central visual field screening (C-40, Humphrey Field Analyser), stereoscopic fundus examination, fundus photography (Canon CR-DGi Camera) and media opacity grading (Chylack et al., 1993).

Participants were dilated with one drop of 1.0% Tropicamide in each eye prior to dark adaptation. The eye selected for testing was the eye with early AMD, or the eye with the better visual acuity in bilateral AMD or control participants (the right eye was selected as a default when visual acuity was equal in both eyes). The contralateral eye was occluded and refractive correction was worn during psychophysical testing if required.

Prior to dark adaptation, a Maxwellian view optical system, incorporating an amber filter (LEE filters HT 015 ‘deep straw’), was used to bleach 84% of cone photopigment (5.20 log phot.Td for 120s) (Hollins & Alpern, 1973) in the central 43.6° of the test eye. On cessation of the bleach, dark adaptation recording commenced immediately. At the first session, dark adaptation was monitored for 30 minutes using the optimal psychophysical procedure identified by Chapters 2, 4 and 5, and at the second session, cone dark adaptation was assessed using the focal cone ERG PST.

Psychophysical procedure

During psychophysical assessment of dark adaptation, thresholds were recorded in response to a 12° radius amber annulus ($\lambda = 595\text{nm}$), 0.5° wide, 200 msec duration, centred on the fovea. On cessation of the bleach, participants were instructed to fixate the cross at the centre of the computer screen and to indicate perception of the stimulus using the computer keyboard. Dark adaptation was monitored using a modified staircase psychophysical method based on a procedure previously implemented by Jackson et al.

(1999) (Section 2.2.3) and the visual threshold was plotted as a function of time after the bleach. The Matlab code for this procedure is shown in Appendix II ('bleaching intensity procedure').

The focal cone ERG PST

At the second session, cone dark adaptation was monitored using the focal cone ERG PST (Binns & Margrain, 2005). Cone flicker ERGs were recorded in response to an amber (peak output 595nm, half height bandwidth 17nm) square wave stimulus, diameter 20°, presented at a temporal frequency of 41Hz (50% duty cycle, flash duration 12ms), with a time-averaged luminance of 30cd/m². This was set within a white surround which also had a luminance of 30cd/m² (See Figure 6.2, Page 151) A 50msec timebase was used for all cone ERGs and 100 sweeps (each consisting of 2 response cycles) were averaged per trace.

Prior to recording, participants were exposed to the flickering stimulus for 5 minutes to eliminate the effects of flicker adaptation from the subsequent recording period. Eight pre-bleach cone ERGs were recorded to determine the baseline amplitude of the response. The photopigment bleach was then administered to the test eye using the Maxwellian view optical system. On cessation of the bleach, the participant was given 10 seconds to align their gaze to the centre of the test stimulus before recording commenced. Focal cone ERGs were then recorded at 20 second intervals for 5 minutes. Each trace took approximately 5 seconds to record, which allowed 10 to 15 seconds for the participant to relax and blink between successive recordings.

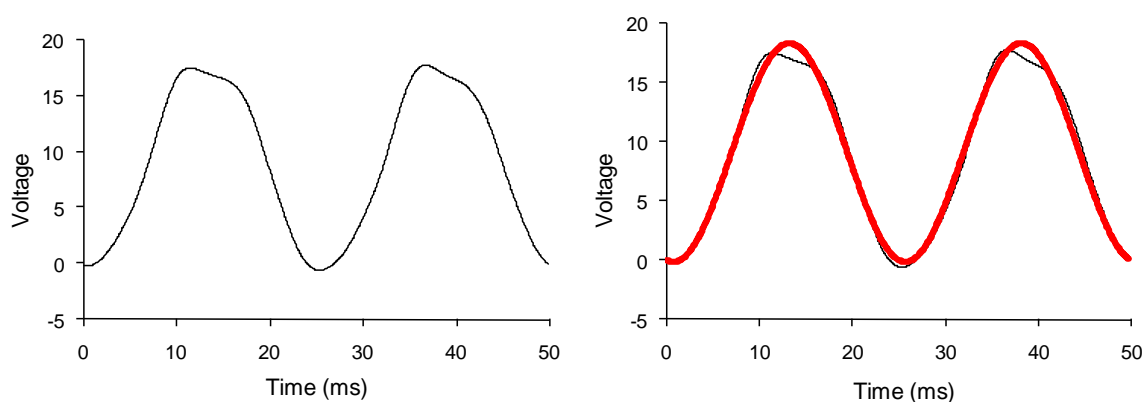


Figure 7.1. Raw full field 41Hz ERG waveform for a healthy participant (left panel) and the Fourier analysed waveform (right panel).

The amplitude of the first harmonic of each trace was determined by Fourier analysis and plotted as a function of time after the bleach (Figure 7.1).

Statistical analysis

The dynamics of cone recovery were determined by fitting an exponential model of dark adaptation to the ERG amplitude recovery data, on a least squares basis, using Microsoft Excel (2003) (Equation 7a).

Equation 7a.
$$T(t) = a + (b.exp^{-t/\tau})$$

where T is the amplitude (μV) of the 41Hz ERG at time t after cessation of the bleach, a is the final amplitude, b is the change in amplitude from $t = 0$, and τ is the time constant of cone recovery.

The psychophysical threshold recovery data were also fitted with an exponential model. Where there was evidence of rod recovery within the recording period, a two linear model (McGwin et al., 1999) was fitted to the rod data (Equation 4d, Page 104). Although the time to RCB was the only aspect of rod recovery assessed during the analysis, rod recovery was modelled in order to objectively identify the RCB, which also allowed identification of the cone-only portion of the data and so facilitated the fitting of the exponential model of cone recovery. The diagnostic potential of the time to RCB was also assessed as a comparative measure reflecting rod recovery

The mean (+/- standard deviation) cone τ was calculated for psychophysical and ERG methods of dark adaptation assessment and independent sample t-tests were used to make comparisons between early AMD and control groups. Receiver operating characteristic (ROC) curves were constructed using statistical software (SPSS, Version 16.0) to assess the diagnostic potential of the techniques.

7.4. Results

The clinical characteristics of the participants with early AMD are summarised in Table 7.1. There were no significant differences in age between early AMD (mean age = 72.1 +/- 8.56 SD years) and control (mean age = 72.6 +/- 4.17 SD years) groups ($p = 0.871$). Similarly, there were no significant differences in logMAR acuity between the test eyes of

early AMD and control groups (mean acuity = 0.02 +/- 0.11 SD logMAR for early AMD participants and 0.2 +/- 0.09 SD logMAR for control participants; $p = 0.949$).

Table 7.1. Visual acuity and fundus appearance in the early AMD group. AMD status is given according to the Age-Related Eye Disease Study severity scale (Davis et al., 2005) where: normal retinal ageing = step 1, early AMD = steps 2– 6, intermediate AMD = steps 7–9, and advanced AMD = steps 10 –11.

Participant	Age	Gender	Test eye			Fellow eye		
			Eye	logMAR VA	AMD status	Eye	logMAR VA	AMD status
1	79	M	R	0.12	Early	L	0.1	Advanced
2	66	F	L	-0.01	Intermed	R	0.2	Advanced
3	76	M	R	0.12	Early	L	0.5	Advanced
4	58	M	L	-0.18	Early	R	-0.1	Early
5	88	M	L	-0.1	Early	R	0.1	Advanced
6	76	F	L	0.2	Intermed	R	0.8	Advanced
7	69	F	L	0.0	Early	R	0.06	Early
8	65	M	L	0.02	Early	R	0.6	Advanced
9	76	M	R	0.06	Early	L	0.1	Early
10	68	F	R	-0.06	Intermed	L	0.9	Advanced

Table 7.2 shows the recovery data for the focal cone ERG PST (pre-bleach ERG amplitude and cone τ) and psychophysical recovery data (cone τ and time to RCB) for each participant. Figure 7.2a illustrates the time course of dark adaptation for a typical control participant, measured using the optimised psychophysical method. The psychophysical dark adaptation data for a typical participant with early AMD are shown in Figure 7.2b. Consistent with dark adaptation data collated in earlier chapters, this participant with early AMD had prolonged cone adaptation in comparison to the control participant, and failed to reach a RCB within the 30 minute recording period. Figures 7.2c & d show the cone dark adaptation data recorded from the same two participants using the focal cone ERG PST. Once again, cone adaptation proceeded more slowly in the participant with AMD.

Table 7.2. Dark adaptation data measured using the focal cone ERG PST and a psychophysical method, for all participants. . (* where there was no evidence of cone recovery using during the 5 minute recording period of the focal cone ERG PST, the cone τ was given as 15 minutes. + where there was no RCB within the recording time for an individual, 30 minutes was attributed as the time to RCB)

Participant	Focal cone ERG PST		Psychophysics	
	Pre-bleach ERG amplitude (μ V)	Cone τ (minutes)*	Cone τ (minutes)	Time to RCB (minutes)+
AMD				
1	1.59	5.38	3.00	30.00
2	0.64	2.02	3.35	14.03
3	1.47	15.00	8.13	30.00
4	3.95	1.08	0.78	8.62
5	1.78	15.00	7.57	30.00
6	2.12	15.00	2.62	30.00
7	3.09	1.44	1.08	7.45
8	1.17	15.00	7.37	16.76
9	1.15	3.90	1.14	21.34
10	1.98	9.55	6.47	30.00
Control				
11	1.66	2.82	0.97	7.37
12	1.31	2.28	2.97	8.94
13	1.95	2.26	1.61	11.80
14	3.09	3.78	1.84	10.90
15	1.46	2.99	0.83	5.84
16	3.35	1.75	2.17	13.07
17	2.90	2.11	0.86	4.18
18	3.58	1.99	1.06	7.96
19	1.81	2.47	0.54	2.37
20	1.83	2.30	1.29	9.41

The mean dark adaptation parameters for early AMD and control groups are summarised in Table 7.3. Where there was no RCB within the 30 minute recording period, it was given

as 30 minutes. Consequently, a conservative estimate of the delay in rod adaptation was included in all statistics. Recordable pre-bleach focal cone ERGs were obtained from all participants and there were no significant differences in baseline ERG amplitude between early AMD and control groups. There were significant differences in cone τ between groups when dark adaptation was assessed psychophysically ($p = 0.017$) and using the focal cone ERG PST ($p = 0.017$). In addition there were significant differences in the time to RCB ($p = 0.001$) between groups.

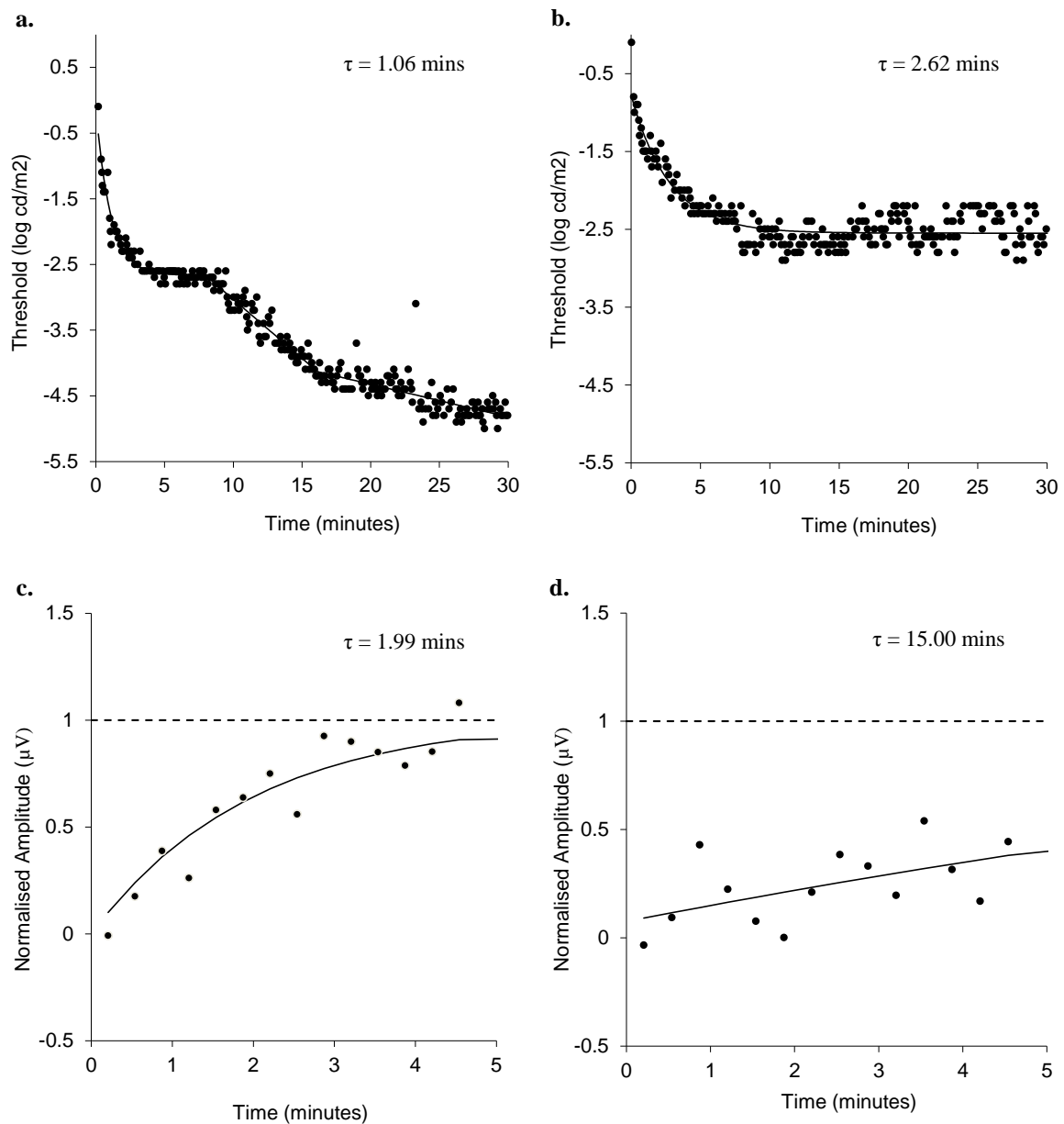


Figure 7.2. Dark adaptation data for a typical control participant (left panel) and a participant with early AMD (right panel), recorded using the optimal psychophysical protocol (a & b) and the focal cone ERG PST (c & d). The broken line on the lower two plots shows the pre-bleach focal cone ERG amplitude.

Table 7.3. Comparison of mean (\pm standard deviation) dark adaptation parameters in control and early AMD groups assessed using the optimal psychophysical protocol and the focal cone ERG PST. (* where there was no RCB within the recording time for an individual, 30 minutes was attributed as the time to RCB).

	Control	Early AMD	Univariate comparison
Pre-bleach ERG amplitude (μ V)	2.29 (0.84)	1.89 (0.98)	$p = 0.341$
Focal cone ERG PST: cone τ (mins)	2.78 (1.26)	8.68 (6.70)	$p = 0.017$
Psychophysics: cone τ (mins)	1.41 (0.74)	4.15 (2.93)	$p = 0.017$
Psychophysics: time to RCB (mins)*	8.18 (3.37)	21.82 (9.44)	$p = 0.001$

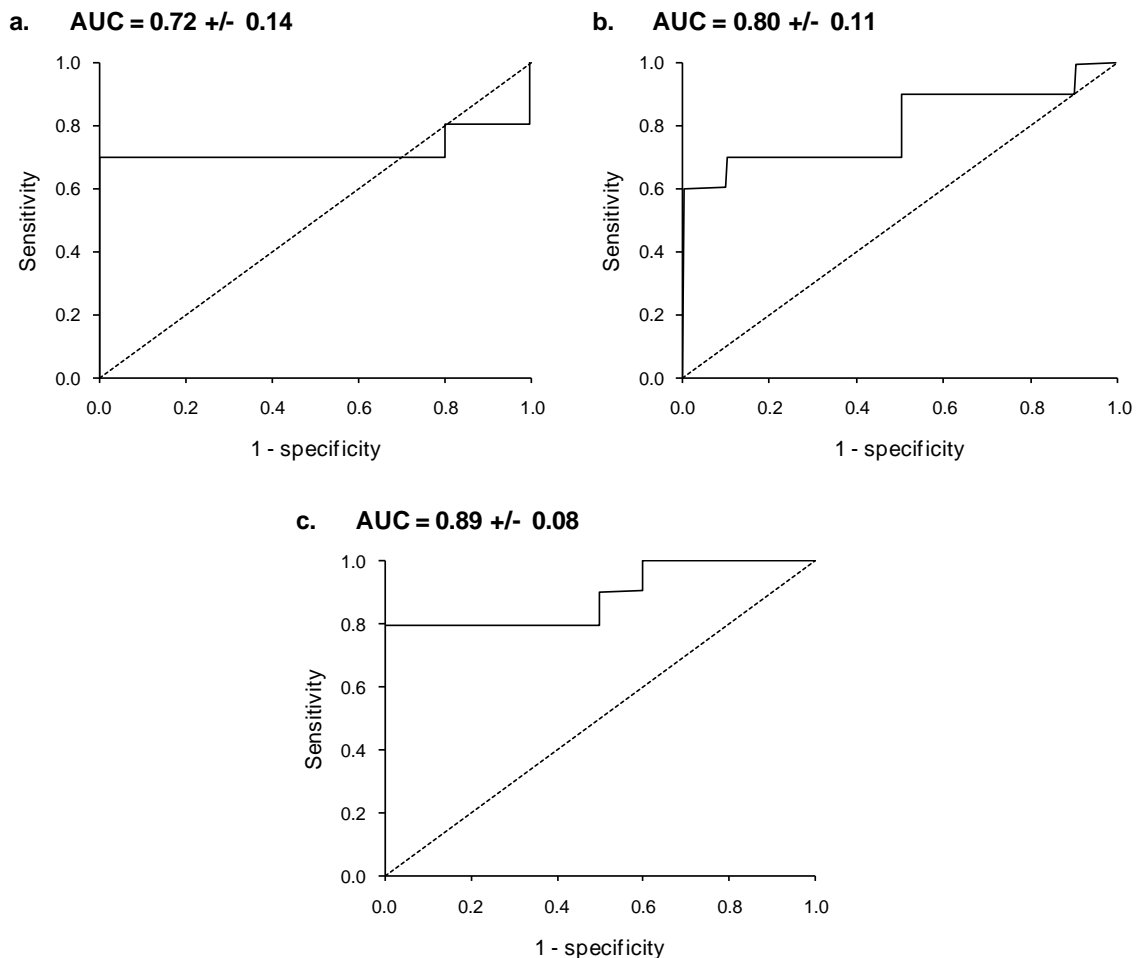


Figure 7.3. ROC curves for: cone τ measured using the focal cone ERG photostress test (a), psychophysical cone τ (b) and psychophysical time to RCB (c) after an 84% cone photopigment bleach. Each plot shows the sensitivity of the parameter to early AMD against the false detection rate (1 - specificity) for all 10 control and 10 early AMD participants.

Receiver operating characteristic curves for cone τ obtained using the focal cone ERG photostress test, psychophysical cone τ and psychophysical time to RCB are shown in Figure 7.3. The diagnostic capacity of each parameter is described by the area under the curve (AUC). Cone τ was highly diagnostic for early AMD using both techniques, yielding an area under the curve (AUC) of 0.80 +/- 0.11 for the psychophysical method and 0.72 +/- 0.14 for the focal cone ERG photostress test. The time to RCB, measured psychophysically, was also highly diagnostic for early AMD. There were no statistically significant differences in the AUC of the cone τ measured using the focal cone ERG PST and psychophysical cone τ and time to RCB ($z < 1.96$) (Hanley & McNeil, 1982; 1983).

7.5. Discussion

These results show that cone dark adaptation was significantly impaired in participants with early AMD. This is consistent with the results presented in the preceding chapters of this thesis (Chapters 4 and 5) and reports of delayed cone adaptation in early AMD in the literature (Phipps et al., 2003; Binns & Margrain, 2007; Dimitrov et al., 2008; 2011). Cone τ was highly diagnostic for early AMD when measured using the focal rod ERG photostress test and the psychophysical method, and both techniques yielded an AUC in excess of 0.72. In addition, the time to RCB, assessed psychophysically, was also highly diagnostic for early AMD (AUC = 0.89 +/- 0.08). There was no significant difference in the AUC for cone τ measured using the electrophysiological and psychophysical techniques. Consequently, although electrophysiological methods are more objective than psychophysical methods of dark adaptation measurement, both of the techniques can be used to identify patients with early AMD with similar sensitivity and specificity.

There are very few studies in the literature that have used both psychophysical and electrophysiological techniques to assess visual function in AMD. Most notably, Sandberg et al. (1998) evaluated a range of clinical tests, including visual acuity, macular visual field testing, psychophysical photostress recovery and the foveal ERG, in terms of their ability to predict the development of CNVM in the fellow eye of patients with unilateral neovascular AMD. Psychophysical photostress recovery and ERG implicit time both emerged as significant independent predictors for the development of CNVM. More recently, the multifocal ERG was compared to visual acuity and contrast sensitivity measurements as predictors of the outcome of photodynamic therapy in patients with

neovascular AMD (Mackay et al., 2008). A strong association was demonstrated between PDT outcome, contrast sensitivity and both the amplitude and latency of the multifocal ERG.

This is the first time that the focal cone ERG PST has been compared to a psychophysical method for the assessment of cone dark adaptation. Although the ERG technique was objective, its diagnostic ability was not superior to the psychophysical method. ERGs require specialist equipment and can be time consuming to set up and record, whereas computer controlled psychophysical methods require little input from the investigator. Consequently, psychophysical methods of cone dark adaptation measurement may be more clinically applicable for the assessment of cone dark adaptation in optometric practice. It is therefore reassuring that the diagnostic potential of that of the psychophysical technique is comparable to the focal cone ERG PST.

The diagnostic potential of the focal cone ERG PST in early AMD reported in this study was similar to the AUC of 0.74 obtained in a previous report that assessed cone dark adaptation using the focal cone ERG PST in a cohort of 31 participants with early AMD and 27 age-matched control participants (Binns & Margrain, 2007). The visual evoked potential (VEP) has also been used as an objective measure of photostress recovery, by monitoring the recovery of the amplitude of the PI component of the pattern VEP response after photopigment bleaching (Lovasik, 1983; Parisi & Bucci, 1992; Parisi et al., 1994; 1998; 2002). In the protocols described, full recovery of the VEP was shown to occur within one minute in healthy individuals (Lovasik, 1983; Parisi & Bucci, 1992). However, although recovery of the VEP has been shown to be prolonged in outer retinal disease (Paris et al., 2002), a similar effect has been documented in diseases of the retinal nerve fibres, such as multiple sclerosis (Parisi et al., 1998) and glaucoma (Parisi & Bucci, 1992). Consequently, the use of VEP recovery may be less specific for the detection of diseases like early AMD, which affect outer retinal function.

An additional advantage of using a psychophysical technique such as the one used in this study is that the RCB may also be used in the diagnosis of early AMD. This parameter was shown to be highly diagnostic for early AMD, yielding an AUC of 0.89 +/- 0.08. This is consistent with previous literature that reported delayed RCB in participants with early

AMD compared to control participants (Owsley et al., 2001; 2007; Dimitrov et al., 2008; 2011).

In conclusion, this study has emphasised the potential value of cone dark adaptation as a biomarker for early AMD. Although electrophysiological methods are more objective than psychophysical methods of dark adaptation measurement, the diagnostic potential of cone dark adaptation in early AMD was similar for both methods. Therefore we recommend the use of psychophysical methods for the assessment of dark adaptation in the clinic as they may be implemented with relative ease. This chapter has reinforced evidence from earlier chapters showing that cone dark adaptation is abnormal in early AMD. There is now an urgent need for longitudinal studies to clarify the value of dark adaptation as a biomarker for early AMD.

8. General discussion, conclusions and future directions

This thesis has demonstrated that delayed dark adaptation is highly diagnostic for early AMD. Assessment of parafoveal cone adaptation, using either electrophysiological or psychophysical techniques, allows rapid identification of those individuals at the earliest stages of disease presentation, with high sensitivity (70-100%) and specificity (90-100%).

8.1. Discussion

Age-related macular degeneration is the leading cause of visual impairment in the UK (Bunce and Wormald, 2008) and the developed world (Resnikoff et al., 2004). Until recently, treatment options for AMD were extremely limited, however, in the last two decades therapies have advanced extremely rapidly. The licensing of Ranibizumab for the treatment of wet AMD in the UK in 2008 (National Institute for Health and Clinical Excellence, 2008) was ground breaking as this antiVEGF agent was the first treatment to generate a clinically significant improvement in VA in patients with wet AMD (Brown et al., 2006; Rosenfeld et al., 2006; Brown et al., 2009). However, the average age of the population is forecast to increase in the UK and globally during the coming decades (Office for National Statistics, 2009; United Nations, 2009). Consequently, there is an urgent need for new treatments suitable for those with dry AMD, as well as wet, and for interventions that target the early stage of the disease, before sight loss has occurred. This necessitates the parallel development of tests that are sensitive to early visual dysfunction, in order to identify patients that are at an increased risk of developing AMD, to identify patients that are suitable for treatment, to assess the outcomes of that treatment and to evaluate emerging treatment strategies.

Dark adaptation is the gradual increase in visual sensitivity that occurs over time in the dark, following exposure to a bright adapting light source (Lamb & Pugh, 2004). As discussed in chapter 1, there is a body of evidence to suggest that dark adaptation is a sensitive functional biomarker for early AMD (Brown et al., 1983; Eisner et al., 1987a,

Eisner et al., 1991; Owsley et al., 2001; Phipps et al., 2003; Binns & Margrain, 2007; Owsley et al., 2007; Dimitrov et al., 2008; 2011). When measured alongside other visual functions, such as colour vision (Eisner et al., 1991) and flicker sensitivity (Phipps et al., 2003), dark adaptation abnormalities have emerged as the most sensitive marker for early AMD. Cone dark adaptation is particularly attractive to clinicians because of its ability to identify patients with early AMD in a relatively short recording period (Phipps et al., 2003, Dimitrov et al., 2008; 2011).

The primary aim of this thesis was to develop psychophysical and electrophysiological techniques for the assessment of dark adaptation in early AMD, with a particular emphasis on cone dark adaptation, in order to optimise their diagnostic potential.

Although psychophysical techniques have been used to quantify dark adaptation for many decades, there is little published literature regarding the most robust psychophysical procedure for monitoring the change in visual threshold over time in the dark. Consequently, the repeatability of a range of psychophysical methods of monitoring cone dark adaptation, including the Goldmann-Weekers adaptometer, was explored in Chapter 2. The Goldmann-Weekers adaptometer was once a commercially available instrument that was considered to be the ‘gold standard’ method for the measurement of dark adaptation. As new adaptometers are developed, it is useful to be able to compare their reliability to that of the current standard; therefore we assessed the Goldmann-Weekers to provide a benchmark for future technology. When the repeatability of the device was assessed in 31 healthy adults, it was capable of monitoring the rapid changes in visual threshold that occur during cone dark adaptation. A CoR of 1.32 +/- 0.25 minutes was obtained, which indicated that the adaptometer was insensitive to small changes in cone dark adaptation dynamics.

As discussed (Section 2.2.1, Page 76), adaptive psychophysical procedures may have advantages over the classical method of limits employed by the Goldmann-Weekers adaptometer. Consequently, in the second part of Chapter 2, the repeatability of the Goldmann-Weekers adaptometer was compared to three computer based methods of monitoring cone dark adaptation in a new cohort of 31 healthy adults. The computer based methods were, a hybrid adaptive stimulus presentation combined with a maximum likelihood calculation (Friedburg et al., 1998), a modified staircase procedure based on a

method previously used with the Humphrey Visual Field Analyser (Jackson et al., 1999) and a novel 10-alternative forced choice procedure. Contrary to expectations, the repeatability of the four methods was similar, with CoRs ranging between 1.18 +/- 0.22 minutes and 1.56 +/- 0.30 minutes, and therefore any of these techniques may be used to monitor cone dark adaptation in clinical practice. The modified staircase procedure was selected for use in the remaining investigations, as its simple algorithm facilitates rapid threshold measurement: a necessity for the assessment of cone dark adaptation.

Age-related macular degeneration is a disease of the ageing retina (Zarbin, 2004). Consequently, prior to examining the changes to dark adaptation that occur in AMD, it is important to consider the relationship between dark adaptation and age in the healthy eye. In Chapter 3, cone dark adaptation was assessed using a 4° diameter stimulus, centred on the fovea, in 41 healthy adults aged between 20 and 83 years. An increase in cone τ of 16.35 seconds/decade of life was recorded, which indicated a progressive slowing of cone dark adaptation kinetics throughout adulthood. Clearly, the sensitivity and specificity of cone dark adaptation as a biomarker for AMD may be improved by taking into account this significant age-related decline.

Chapter 4 began by comparing exponential and linear models as descriptions of cone and rod dark adaptation data. Traditionally, photopigment regeneration has been considered a 'first-order' process and threshold recovery data have therefore been summarised using an exponential function (Dowling, 1960; Rushton, 1961; Hollins & Alpern; 1973). More recently it has been proposed that threshold recovery during dark adaptation is 'rate-limited' and that a linear model would provide a more appropriate description of the data (Lamb, 1981; McGwin et al., 1999; Paupoo et al., 2000; Mahroo & Lamb, 2004). When exponential and linear models were applied to cone and rod threshold recovery data obtained from three highly experienced observers, at 5 retinal locations, the fit of the two models to the cone data was remarkably similar. There were no conclusive differences in RMS error or AIC values between the two models of cone recovery and therefore the exponential model, which contained fewer free parameters, was considered sufficient to describe the cone recovery data. In contrast, the linear model was shown to provide a marginally superior description of the rod recovery data. Consequently, an 'exponential-linear' model was applied to all psychophysical threshold recovery data in the investigations that followed.

As very few investigations have documented the effect of retinal location on the kinetics of dark adaptation in the healthy retina (Hecht et al., 1935; Wolf & Zigler, 1950; Dimitrov et al., 2008), the second aim of Chapter 4 was to quantify the dynamics of dark adaptation as a function of retinal location in three highly experienced observers. As the retinal eccentricity of the stimulus increased, a progressive acceleration of threshold recovery occurred, most markedly for rod-mediated dark adaptation. However, with respect to the rods, this was shown to be a function of the relationship between the rate of a linear model and reducing absolute threshold; rather than reflecting an actual increase in the rate of rod photopigment regeneration. Knowledge of this normal variation in dark adaptation parameters across the healthy retina is important when considering the changes to dark adaptation that occur in a disease such as AMD.

Although rod-mediated dark adaptation is widely agreed to be abnormal in early AMD (Brown & Lovie-Kitchin, 1983; Brown et al., 1986a, Steinmetz et al., 1993; Owsley et al., 2001; Owsley et al., 2007; Dimitrov et al., 2008; 2011), the evidence regarding changes to cone-mediated dark adaptation is equivocal (Brown et al., 1986b; Phipps et al., 2003; Binns & Margrain, 2007; Owsley et al., 2007; Dimitrov et al., 2008; 2011). One explanation for this conflicting evidence is that the cone dark adaptation deficit in early AMD is dependent on retinal location. Therefore, in the final part of Chapter 4 the diagnostic potential of cone dark adaptation and the time to RCB were assessed at four retinal locations: 0.5, 2, 7 and 12° from fixation in 10 participants with early AMD and 10 age-matched control participants. Cone τ and time to RCB were most diagnostic for early AMD at 12° from the fovea (the AUC was 0.99 +/- 0.02 for cone τ and 0.96 +/- 0.04 for time to RCB). This contradicted previous evidence to suggest that the dark adaptation deficit at this retinal location affected rods only (Owsley et al., 2007). Three related explanations, based on the well established rate-limiting step in dark adaptation: the local availability of 11-cis retinal (Lamb & Pugh, 2004), were proposed to explain the discrepancy between these results and those of previous studies.

Following the identification of the optimal retinal location for the detection of adaptational anomalies in early AMD, Chapter 5 assessed the diagnostic ability of cone dark adaptation and the time to RCB in early AMD as a function of the pre-adapting light intensity. Dark adaptation was measured in 10 participants with early AMD and 10 age-matched control

participants following exposure to three pre-adapting light intensities: 71%, 84% and 91% cone photopigment bleach. Cone τ and time to RCB emerged as highly diagnostic for early AMD at all of these pre-adapting intensities. Implementation of a low pre-adapting intensity for measurement of dark adaptation is attractive clinically as it expedites data collection. However, it is important that sufficient threshold recovery data are obtained to facilitate an accurate model fit, especially during the early stages of cone dark adaptation when threshold is changing most rapidly. Therefore, a pre-adapting intensity of 84% was considered optimal for the assessment of dark adaptation.

Although psychophysical methods have been widely used to assess dark adaptation, the data are highly subjective and may be considered unreliable in some participants. Consequently, objective methods for the assessment of retinal function, such as electroretinography, may be preferable. However, there are very few standardised protocols for the assessment of dark adaptation at the macula using the ERG. The focal cone ERG PST was developed previously to assess cone dark adaptation at the macula and has been shown to distinguish between patients with early AMD and healthy controls (Binns & Margrain, 2005; 2007; Wood et al., 2011a). The primary aim of Chapter 6 was to develop an equivalent technique for the assessment of rod dark adaptation, i.e. a focal rod ERG photostress test. The protocol was initially developed using a full field stimulus and was used to monitor dark adaptation in two highly experienced observers. After further optimisation of the stimulus parameters, a protocol using a focal stimulus was tested in two young experienced observers, followed by six older 'ERG naïve' participants: three participants with early AMD and three age-matched controls. Although the data obtained from the young experienced observers were reasonable, when the protocol was implemented in the older 'ERG naïve' participants, there was no meaningful recovery of ERG amplitude during the time in the dark, most likely due to intraocular light scatter leading to unfavourable SNR and high level of rejection of traces. Therefore, psychophysical methods appear to be a more reliable option for monitoring the changes in rod dark adaptation that occur at the macula in patients with early AMD.

Given the respective advantages and disadvantages of psychophysical and electrophysiological methods of cone dark adaptation assessment, Chapter 7 compared the diagnostic potential of the optimal computer based psychophysical procedure, developed in the preceding chapters, to the focal cone ERG PST in 10 participants with early AMD and

10 age-matched control participants. As expected, mean cone τ was significantly longer in the early AMD group when measured psychophysically and using the focal cone ERG PST. Both techniques were highly diagnostic for early AMD (the AUC was 0.80 +/- 0.11 for the psychophysical test and 0.72 +/- 0.14 for the focal cone ERG PST) and, with this sample size at least, no significant differences in the diagnostic potential of the two methods were observed. Therefore, despite the theoretical advantages of using an objective technique such as the focal cone ERG PST to assess cone dark adaptation in early AMD, the psychophysical method produced comparable results.

In summary, the main conclusions of this thesis are:

- A range of psychophysical methods may be used to monitor the rapid changes in threshold that occur during cone dark adaptation.
- Cone dark adaptation is a sensitive functional biomarker for early AMD.
- Consideration of the age-related changes in the dynamics of cone dark adaptation will improve the sensitivity and specificity of this parameter in early AMD.
- An annulus at 12° from fixation is the optimal psychophysical stimulus for the assessment cone dark adaptation in early AMD.
- A pre-adapting intensity of 84% cone photopigment allows cone dark adaptation data to be obtained in the shortest timeframe, without compromising the integrity of the data obtained.
- The time limitations imposed by the rapid rate at which threshold changes during dark adaptation rendered the protocol for recording the ‘focal rod ERG photostress’ test unsuitable for use in ‘ERG naïve’ participants.
- The optimal psychophysical method and the focal cone ERG PST are similarly diagnostic for early AMD despite the theoretical advantages of the objective ERG technique.

8.2. Future directions

The primary outcome of this thesis was the optimisation of cone dark adaptation protocols for the diagnosis of early AMD. However, cross-sectional studies are unable to determine the true diagnostic potential of a biomarker. In this study, individuals were classified as ‘early AMD’ or ‘control’ based on fundus appearance alone. Histological studies suggest

that changes to Bruch's membrane, such as basal laminar and linear deposition, occur before clinically visible signs present (Sarks, 1976, Sarks et al., 1999). On this basis, it is highly possible that some of the 'controls' were actually at a pre-clinical stage of early AMD. A longitudinal study, following up participants for months/years after baseline data collection, would allow a more comprehensive assessment of:

- i) the diagnostic potential of cone dark adaptation for early AMD and
- ii) the predictive value of the test in identifying those whose disease status is likely to progress.

There is currently a lack of comprehensive longitudinal data in the literature regarding the diagnostic and predictive power of cone dark adaptation and other functional biomarkers for the progression to late AMD (Hogg & Chakravarthy, 2006). Consequently there is an urgent need for follow up investigations to explore the long term potential of cone dark adaptation and other visual functions as biomarkers for the progression of AMD. The following sections describe several potential investigations.

8.2.1. Risk profiling for the development of wet AMD

As discussed, the average age of the UK population is forecast to increase during the next two decades (Office for National Statistics, 2009) and therefore the incidence of AMD will also increase. Although Ranibizumab injections can improve VA in patients with wet AMD (Brown et al., 2006; Rosenfeld et al., 2006; Brown et al., 2009), monthly follow up appointments are required to assess the need for retreatment. This places a huge pressure on limited healthcare resources, for example the estimated cost of Lucentis injections for a single patient is between £5,350 and £9,150 per year (National Institute for Health and Clinical Excellence, 2008). In addition, a recent meta-analysis of 4263 eyes with unilateral wet AMD showed that 26.8% of fellow eyes developed wet AMD within four years (Wong et al., 2008). The identification of biomarkers which are predictive of the occurrence and recurrence of neovascular events in patients with AMD would help to streamline the provision of these services in order to relieve the practical and economic burdens on the NHS, for example by structuring follow up intervals on the basis of the risk profile of the patient.

Aims: To identify biomarkers which are predictive of onset and recurrence of wet AMD by assessing the fellow eye of patients with unilateral wet AMD, in order to develop a 'risk profile' for:

- 1) the recurrence of wet AMD in an eye treated with Lucentis
- 2) the development of wet AMD in the fellow eye of an eye treated with Lucentis.

Preliminary design: The recruitment for this study would take place within hospital ophthalmology clinics, for example participants with unilateral wet AMD would be invited to take part in the study after receiving the third Ranibizumab injection, i.e. at the end of the loading phase. On enrolment into this study, each participant would undergo a 'biomarker assessment', including assessment of lifestyle factors (e.g. smoking, diet and body mass index (BMI), genetic and inflammatory markers, fundus appearance and visual functions (including VA, contrast sensitivity, dark adaptation, colour vision and visual field defects). Disease outcomes may be documented by consulting the medical records of the participants at the end of the study.

8.2.2. Investigation of risk factors for the development of early AMD

Treatment options for wet AMD have advanced rapidly during the last two decades and are constantly improving. However, the incidence of the development of early AMD in the general population has been estimated at 5.7-8.2% over 5 years (Klein et al., 1995) and the conversion from dry AMD to wet AMD between 7.1% and 14.5% over the same period (Klein et al., 1995; Smiddy & Fine, 1984). This means that substantial resources are currently being invested in the development of treatments for earlier stages of the disease (Pinilla et al., 2006; Lu et al., 2009; Miller 2010; Bull & Martin, 2011; Couch et al., 2011; Wang et al., 2011). As new therapies are developed for earlier stages of the disease, it becomes increasingly important to be able to identify those individuals that have a high risk of disease progression, to identify those individuals that may be suitable for treatment and to monitor the outcomes of that treatment. The identification of predictive biomarkers would be extremely valuable in these situations, to assess progression from 'normal' to early AMD, and early AMD to late AMD. Consequently, a longitudinal study of risk factors for the development and progression of AMD is required. This study would be based in optometric practices over approximately 5 years, examining similar biomarkers to the risk profiling study for wet AMD described above (Section 8.2.1). The cohort would

comprise two groups of participants: a group of participants with early AMD (unilateral or bilateral) and a group of age-matched control participants.

8.2.3. Development of a portable dark adaptometer

With the exception of the Goldmann-Weekers adaptometer, all of the psychophysical methods used to monitor dark adaptation during this thesis were implemented using a computer system. The pre-adapting ‘bleaching’ light was administered using a Maxwellian view optical system. Although these techniques demonstrated that psychophysical methods can be used to assess cone dark adaptation in AMD, they are not overly ‘user-friendly’. It has been suggested that one of the main barriers to the use of dark adaptation or photostress recovery by clinicians is the absence of a standardized recording protocol and the lack of normative data (Margrain & Thomson, 2002). The development of a portable dark adaptometer that is suitable for use in optometric practice is therefore fundamental to promoting the use of dark adaptation as a diagnostic tool in early AMD. During the first part of this study, a single unit comprising an integrated pre-adapting light and test stimulus would be developed, based on the findings of this thesis regarding the optimal parameters for assessment of early AMD. The second stage of the study would involve collection of data from an extensive cohort of healthy control participants using the device, in order to establish a normative database. Finally, the diagnostic ability of cone dark adaptation in early AMD measured using the device would be established in a cohort of participants with early AMD and a group of age-matched control participants.

References

Ahmed S S, Lott M G, and Marcus D M (2005) The macular xanthophylls. *Survey of Ophthalmology* 50: 183-193.

Aiello L P, Northrup J M, Keyt B A, Takagi H, and Iwamoto M A (1995) Hypoxic regulation of vascular endothelial growth factor in retinal cells. *Archives of Ophthalmology* 113: 1538-1544.

Akaike H (1974) A new look at statistical model identification. *IEEE Transactions on Automatic Control* AC19: 716-723.

Altman D G (1991) Practical statistics for medical research. London; New York: Chapman and Hall. pp. 277-324.

Altman D G, and Bland J M (1994) Diagnostic tests 3 - receiver operating characteristic plots 7. *British Medical Journal* 309: 188-188.

Amsler M (1953) Earliest symptoms of diseases of the macula. *British Journal of Ophthalmology* 37: 521-537.

Arden G B, and Wolf J E (2004) Colour vision testing as an aid to diagnosis and management of age related maculopathy. *British Journal of Ophthalmology* 88: 1180-1185.

AREDS (2001) The AREDS system for classifying age-related macular degeneration from stereoscopic color fundus photographs. AREDS Report No.6. *American Journal of Ophthalmology* 132: 668-681.

AREDS (2012) *Age-related eye disease study 2: The Lutein/Zeaxanthin and Omega-3 supplementation trial*. <http://www.areds2.org/> Accessed: 18th January 2012

Arnold J J, Sarks S H, Killingsworth M C, and Sarks J P (1995) Reticular pseudodrusen - a risk factor in age-related maculopathy. *Retina-the Journal of Retinal and Vitreous Diseases* 15: 183-191.

Asano K, Nomura H, Iwano M, Ando F, Niino N, Shimokata H, and Miyake Y (2005) Relationship between astigmatism and aging in middle-aged and elderly Japanese. *Japanese Journal of Ophthalmology* 49: 127-133.

Bamashmus M A, Matlhaga B, and Dutton G N (2004) Causes of blindness and visual impairment in the West of Scotland. *Eye* 18: 257-261.

Bartlett H, Davies L N, and Eperjesi F (2004) Reliability, normative data, and the effect of age-related macular disease on the Eger Macular Stressometer photostress recovery time. *Ophthalmic & Physiological Optics* 24: 594-599.

Beatty S, Koh H H, Henson D, and Boulton M (2000) The role of oxidative stress in the pathogenesis of age-related macular degeneration. *Survey of Ophthalmology* 45: 115-134.

Beirne R O, Hogg R E, Stevenson M R, Zlatkova M B, Chakravarthy U, and Anderson R S (2006) Severity staging by early features of age-related maculopathy exhibits weak relationships with functional deficits on SWS grating acuity. *Investigative Ophthalmology & Visual Science* 47: 4624-4631.

Bergeron-Sawitzke J, Gold B, Olsh A, Schlotterbeck S, Lemon K, Visvanathan K, Allikmets R et al. (2009) Multilocus analysis of age-related macular degeneration. *European Journal of Human Genetics* 17: 1190-1199.

Berninger T, and Schuurmans R P (1985) Spatial tuning of the pattern ERG across temporal frequency. *Documenta Ophthalmologica* 61: 17-25.

Berrow E J, Bartlett H E, Eperjesi F, and Gibson J M (2010) The electroretinogram: a useful tool for evaluating age-related macular disease? *Documenta Ophthalmologica* 121: 51-62.

Biarnes M, Mones J, Alonso J, and Arias L (2011) Update on Geographic Atrophy in Age-Related Macular Degeneration. *Optometry and Vision Science* 88: 881-889.

Binns A M, and Margrain T H (2005) Evaluation of retinal function using the dynamic focal cone ERG. *Ophthalmic and Physiological Optics* 25: 492-500.

Binns A, and Margrain T H (2006) Development of a technique for recording the focal rod ERG. *Ophthalmic & Physiological Optics* 26: 71-79.

Binns A M, and Margrain T H (2007) Evaluating retinal function in age-related maculopathy with the ERG photostress test. *Investigative Ophthalmology & Visual Science* 48: 2806-2813.

Bird A C (1992) Bruch's membrane change with age. *British Journal of Ophthalmology* 76: 166-168.

Bird A C, Bressler N M, Bressler S B, Chisholm I H, Coscas G, Davis M D et al. (1995) An international classification and grading system for age-related maculopathy and age-related macular degeneration. The International ARM Epidemiological Study Group. *Survey of Ophthalmology* 39: 367-374.

Birren J E, Bick M W, and Fox C (1948) Age changes in the light threshold of the dark adapted eye. *Journals of Gerontology* 3: 267-271.

Birren J E, Casperson R C, and Botwinick J (1950) Age changes in pupil size. *Journals of Gerontology* 5: 216-221.

Birren J E, and Shock N W (1950) Age changes in rate and level of visual dark adaptation. *Journal of Applied Physiology* 2: 407-411.

Blaauwgeers H G, Holtkamp G M, Rutten H, Witmer A N, Koolwijk P, Partanen T A et al. (1999) Polarized vascular endothelial growth factor secretion by human retinal pigment

epithelium and localization of vascular endothelial growth factor receptors on the inner choriocapillaris. Evidence for a trophic paracrine relation. *American Journal of Pathology* 155: 421-428.

Blakemore C B, and Rushton W A H (1965) Dark adaptation and increment threshold in a rod monochromat. *Journal of Physiology-London* 181: 612-628.

Bland J M, and Altman D G (1986) Statistical methods for assessing agreement between two methods of clinical measurement. *Lancet* 1: 307-310.

Blumenkranz M S, Bressler N M, Potter M J, Bressler S B, Mones J M, Harvey P, Singerman L J et al. (2001) Photodynamic therapy of subfoveal choroidal neovascularization in age-related macular degeneration with verteporfin - Two-year results of 2 randomized clinical trials - TAP report 2. *Archives of Ophthalmology* 119: 198-207.

Bok D (1993) The retinal pigment epithelium: a versatile partner in vision. *Journal of Cell Science (Supplement)* 17: 189-195.

Bolnick D A, Walter A E, and Sillman A J (1979) Barium suppresses slow PIII in perfused bullfrog retina. *Vision Research* 19: 1117-1119.

Bone R A, Brener B, and Gibert J C (2007) Macular pigment, photopigments, and melanin: Distributions in young subjects determined by four-wavelength reflectometry. *Vision Research* 47: 3259-3268.

Bone R A, Landrum J T, Mayne S T, Gomez C M, Tibor S E, and Twaroska E E (2001) Macular pigment in donor eyes with and without AMD: A case-control study. *Investigative Ophthalmology & Visual Science* 42: 235-240.

Bone R A, Landrum J T, and Tarsis S L (1985) Preliminary identification of the human macular pigment. *Vision Research* 25: 1531-1535.

Booij J C, Baas D C, Beisekeeva J, Gorgels T G, and Bergen A A (2010) The dynamic nature of Bruch's membrane. *Progress in Retinal Eye Research* 29: 1-18.

Boulton M, and Dayhaw-Barker P (2001) The role of the retinal pigment epithelium: topographical variation and ageing changes. *Eye (London)* 15: 384-389.

Boycott B B, and Wassle H (1991) Morphological Classification of Bipolar Cells of the Primate Retina. *European Journal of Neuroscience* 3: 1069-1088.

Brainard D, H., Pelli D, G., and Robson T (2001) Display Characterization. *IEEE Signal Processing Magazine* 18: 172-188.

Bressler N M (1999) Photodynamic therapy of subfoveal choroidal neovascularization in age-related macular degeneration with verteporfin - One-year results of 2 randomized clinical trials - TAP report 1. *Archives of Ophthalmology* 117: 1329-1345.

Bressler N M (2002) Verteporfin therapy for subfoveal choroidal neovascularization in age-related macular degeneration - Three-year results of an open-label extension of 2 randomized clinical trials - TAP report No. 5. *Archives of Ophthalmology* 120: 1307-1314.

Bressler N M, Bressler S B, West S K, Fine S L, and Taylor H R (1989) The grading and prevalence of macular degeneration in Chesapeake Bay watermen. *Archives of Ophthalmology* 107: 847-852.

Bressler N M, Silva J C, Bressler S B, Fine S L, and Green W R (1994) Clinicopathological correlation of drusen and retinal pigment epithelial abnormalities in age-related macular degeneration. *Retina-the Journal of Retinal and Vitreous Diseases* 14: 130-142.

Bringmann A, Pannicke T, Grosche J, Francke M, Wiedemann P, Skatchkov S N, Osborne N N et al. (2006) Muller cells in the healthy and diseased retina. *Progress in Retinal and Eye Research* 25: 397-424.

Bron A J, Vrensen G, Koretz J, Maraini G, and Harding J J (2000) The ageing lens. *Ophthalmologica* 214: 86-104.

Brown B, Adams A J, Coletta N J, and Haegerstromportnoy G (1986a) Dark-Adaptation in Age-Related Maculopathy. *Ophthalmic and Physiological Optics* 6: 81-84.

Brown B, and Lovie-Kitchin J L (1983) Dark adaptation and the acuity/luminance response in senile macular degeneration (SMD). *American Journal of Optometry & Physiological Optics* 60: 645-650.

Brown B, Tobin C, Roche N, and Wolanowski A (1986b) Cone adaptation in age-related maculopathy. *American Journal of Optometry & Physiological Optics* 63: 450-454.

Brown D M, Kaiser P K, Michels M, Soubrane G, Heier J S, Kim R Y et al. (2006) Ranibizumab versus verteporfin for neovascular age-related macular degeneration. *New England Journal of Medicine* 355: 1432-1444.

Brown D M, Michels M, Kaiser P K, Heier J S, Sy J P, and Ianchulev T (2009) Ranibizumab versus Verteporfin Photodynamic Therapy for Neovascular Age-Related Macular Degeneration: Two-Year Results of the ANCHOR Study. *Ophthalmology* 116: 57-65.

Brown K T, and Murakami M (1964) New receptor potential of monkey retina with no detectable latency. *Nature* 201: 626-628.

Buch H, Vinding T, la Cour M, Jensen G B, Prause J U, and Nielsen N V (2005) Risk factors for age-related maculopathy in a 14-year followup study: the Copenhagen City Eye Study. *Acta Ophthalmologica Scandinavica* 83: 409-418.

Bull N D, and Martin K R (2011) Concise Review: Toward Stem Cell-Based Therapies for Retinal Neurodegenerative Diseases. *Stem Cells* 29: 1170-1175.

Bunce C, and Wormald R (2008) Causes of blind certifications in England and Wales: April 1999 to March 2000. *Eye* 22: 905-911.

Burns M E, and Baylor D A (2001) Activation, deactivation, and adaptation in vertebrate, photoreceptor cells. *Annual Review of Neuroscience* 24: 779-805.

Buschini E, Piras A, Nuzzi R, and Vercelli A (2011) Age related macular degeneration and drusen: Neuroinflammation in the retina. *Progress in Neurobiology* 95: 14-25.

Bush R A, and Sieving P A (1994) A proximal retinal component in the primate photopic ERG a-wave. *Investigative Ophthalmology & Visual Science* 35: 635-645.

Bush R A, and Sieving P A (1996) Inner retinal contributions to the primate photopic fast flicker electroretinogram. *Journal of the Optical Society of America A - Optics Image Science and Vision* 13: 557-565.

Cameron A M, Mahroo O A, and Lamb T D (2006) Dark adaptation of human rod bipolar cells measured from the b-wave of the scotopic electroretinogram. *Journal of Physiology-London* 575: 507-526.

Cameron A M, Miao L, Ruseckaite R, Pianta M J, and Lamb T D (2008) Dark adaptation recovery of human rod bipolar cell response kinetics estimated from scotopic b-wave measurements. *Journal of Physiology-London* 586: 5419-5436.

Campbell F W, and Rushton W A (1955) Measurement of the scotopic pigment in the living human eye. *Journal of Physiology-London* 130: 131-147.

Chakravarthy U, Soubrane G, Bandello F, Chong V, Cruzot-Garcher C, Dimitrakos S A, et al. (2006) Evolving European guidance on the medical management of neovascular age related macular degeneration. *British Journal of Ophthalmology* 90: 1188-1196.

Chakravarthy U, Wong T Y, Fletcher A, Piauult E, Evans C, Zlateva G, Buggage R et al. (2010) Clinical risk factors for age-related macular degeneration: a systematic review and meta-analysis. *BMC Ophthalmology* 10.

Chang M A, Bressler S B, Munoz B, and West S K (2008) Racial differences and other risk factors for incidence and progression of age-related macular degeneration: Salisbury Eye Evaluation (SEE) project. *Investigative Ophthalmology & Visual Science* 49: 2395-2402.

Chen C, Wu L, Wu D, Huang S, Wen F, Luo G, and Long S (2004) The local cone and rod system function in early age-related macular degeneration. *Documenta Ophthalmologica* 109: 1-8.

Cheng A S, and Vingrys A J (1993) Visual losses in early age-related maculopathy. *Optometry and Vision Science* 70: 89-96.

Chew E Y, Lindblad A S, and Clemons T (2009) Summary results and recommendations from the age-related eye disease study. *Archives of Ophthalmology* 127: 1678-1679.

Choshi T, Matsumoto C S, and Nakatsuka K (2003) Rod-driven focal macular electroretinogram. *Japanese Journal of Ophthalmology* 47: 356-361.

Christen W G, Schaumberg D A, Glynn R J, and Buring J E (2011) Dietary omega-3 Fatty Acid and Fish Intake and Incident Age-Related Macular Degeneration in Women. *Archives of Ophthalmology* 129: 921-929.

Chung S E, Kang S W, Lee J H, and Kim Y T (2011) Choroidal Thickness in Polypoidal Choroidal Vasculopathy and Exudative Age-related Macular Degeneration. *Ophthalmology* 118: 840-845.

Chylack L T, Jr., Wolfe J K, Singer D M, Leske M C, Bullimore M A, Bailey I L, Friend J et al. (1993) The Lens Opacities Classification System III. The Longitudinal Study of Cataract Study Group. *Archives of Ophthalmology* 111: 831-836.

Cideciyan A V, Pugh E N, Lamb T D, Huang Y J, and Jacobson S G (1997) Plateaux during dark adaptation in Sorsby's fundus dystrophy and vitamin A deficiency. *Investigative Ophthalmology & Visual Science* 38: 1786-1794.

Ciulla T A, Danis R P, and Harris A (1998) Age-related macular degeneration: A review of experimental treatments. *Survey of Ophthalmology* 43: 134-146.

Ciulla T A, Harris A, Kagemann L, Danis R P, Pratt L M, Chung H S, Weinberger D et al. (2002) Choroidal perfusion perturbations in non-neovascular age related macular degeneration. *British Journal of Ophthalmology* 86: 209-213.

Coile D C, and Baker H D (1992) Foveal dark adaptation, photopigment regeneration, and aging. *Visual Neuroscience* 8: 27-39.

Coleman H R, Chan C C, Ferris F L, and Chew E Y (2008) Age-related macular degeneration. *Lancet* 372: 1835-1845.

Collins M (1989) The onset of prolonged glare recovery with age. *Ophthalmic and Physiological Optics* 9: 368-371.

Collins M, and Brown B (1989) Glare recovery and age-related maculopathy. *Clinical Vision Sciences* 4: 145-153.

Congdon N, O'Colmain B, Klaver C C W, Klein R, Munoz B, Friedman D S et al. (2004) Causes and prevalence of visual impairment among adults in the United States. *Archives of Ophthalmology* 122: 477-485.

Conner J D (1982) The temporal properties of rod vision. *Journal of Physiology-London* 332: 139-155.

Coral K, Raman R, Rathi S, Rajesh M, Sulochana K N, Angayarkanni N, Paul P G et al. (2006) Plasma homocysteine and total thiol content in patients with exudative age-related macular degeneration. *Eye* 20: 203-207.

Cornsweet T N (1962) Staircase-Method in Psychophysics. *American Journal of Psychology* 75: 485-491.

Couch S M, and Bakri S J (2011) Review of Combination Therapies for Neovascular Age-Related Macular Degeneration. *Seminars in Ophthalmology* 26: 114-120.

Coupland S G (2006) Electrodes for visual testing. In: Heckenlively, J R, and Arden, G B [eds.] *Principles and practice of clinical electrophysiology of vision*. (2nd edn.) London: MIT Press, pp. 245-254.

Cruess A F, Zlateva G, Pleil A M, and Wirostko B (2009) Photodynamic therapy with verteporfin in age-related macular degeneration: a systematic review of efficacy, safety, treatment modifications and pharmacoeconomic properties. *Acta Ophthalmologica* 87: 118-132.

Cruickshanks K J, Klein R, Klein B E K, and Nondahl D M (2001) Sunlight and the 5-year incidence of early age-related maculopathy - The Beaver Dam Eye Study. *Archives of Ophthalmology* 119: 246-250.

Curcio C A (2001) Photoreceptor topography in ageing and age-related maculopathy. *Eye* 15: 376-383.

Curcio C A, and Allen K A (1990) Topography of ganglion cells in human retina. *Journal of Comparative Neurology* 300: 5-25.

Curcio C A, Medeiros N E, and Millican C L (1996) Photoreceptor loss in age-related macular degeneration. *Investigative Ophthalmology & Visual Science* 37: 1236-1249.

Curcio C A, Millican C L, Allen K A, and Kalina R E (1993) Aging of the human photoreceptor mosaic - evidence for selective vulnerability of rods in central retina. *Investigative Ophthalmology & Visual Science* 34: 3278-3296.

Curcio C A, Sloan K R, Kalina R E, and Hendrickson A E (1990) Human photoreceptor topography. *The Journal of Comparative Neurology* 292: 497-523.

Dacey D M (1999) Primate retina: Cell types, circuits and color opponency. *Progress in Retinal and Eye Research* 18: 737-763.

Dacey D M, and Petersen M R (1992) Dendritic field size and morphology of midget and parasol ganglion cells of the human retina. *Proceedings of the National Academy of Sciences in the United States of America* 89: 9666-9670.

Das S R, Bhardwaj N, Kjeldbye H, and Gouras P (1992) Muller cells of the chicken retina synthesize 11-cis-retinol. *Biochemical Journal* 285: 907-913.

Davis M D, Gangnon R E, Lee L Y, Hubbard L D, Klein B E, Klein R, Ferris F L et al. (2005) The Age-Related Eye Disease Study severity scale for age-related macular degeneration: AREDS Report No. 17. *Archives of Ophthalmology* 123: 1484-1498.

Dawson W W, Trick G L, and Litzkow C A (1979) Improved electrode for electroretinography. *Investigative Ophthalmology & Visual Science* 18: 988-991.

Delcourt C, Carriere I, Delage M, Barberger-Gateau P, and Schalch W F (2006) Plasma lutein and zeaxanthin and other carotenoids as modifiable risk factors for age-related maculopathy and cataract: The POLA study. *Investigative Ophthalmology & Visual Science* 47: 2329-2335.

Delori F C, Fleckner M R, Goger D G, Weiter J J, and Dorey C K (2000) Autofluorescence distribution associated with drusen in age-related macular degeneration. *Investigative Ophthalmology & Visual Science* 41: 496-504.

Dieterle P, and Gordon E (1956) Standard curve and physiological limits of dark adaptation by means of the Goldmann-Weekers adaptometer. *British Journal of Ophthalmology* 40: 652-655.

Dimitrov P N, Guymer R H, Zele A J, Anderson A J, and Vingrys A J (2008) Measuring rod and cone dynamics in age-related maculopathy. *Investigative Ophthalmology and Visual Science* 49: 55-65.

Dimitrov P N, Robman L D, Varsamidis M, Aung K Z, Makeyeva G A, Guymer R H, and Vingrys A J (2011) Visual Function Tests as Potential Biomarkers in Age-Related Macular Degeneration. *Investigative Ophthalmology & Visual Science* 52: 9457-9469.

Donner K O, and Reuter T (1967) Dark adaptation processes in rhodopsin rods of frogs retina. *Vision Research* 7: 17-41.

Donoso L A, Kim D, Frost A, Callahan A, and Hageman G (2006) The role of inflammation in the pathogenesis of age-related macular degeneration. *Survey of Ophthalmology* 51: 137-152.

Dorey C K, Wu G, Ebenstein D, Garsd A, and Weiter J J (1989) Cell loss in the aging retina. Relationship to lipofuscin accumulation and macular degeneration. *Investigative Ophthalmology and Visual Science* 30: 1691-1699.

Dowling J E (1960) Chemistry of visual adaptation in the rat. *Nature* 188: 114-118.

Drasdo N, Aldebasi Y H, Chiti Z, Mortlock K E, Morgan J E, and North R V (2001) The s-cone PHNR and pattern ERG in primary open angle glaucoma. *Investigative Ophthalmology & Visual Science* 42: 1266-1272.

Drexler W, and Fujimoto J G (2008) State-of-the-art retinal optical coherence tomography. *Progress in Retinal and Eye Research* 27: 45-88.

Eisner A, Fleming S A, Klein M L, and Mauldin W M (1987a) Sensitivities in older eyes with good acuity: eyes whose fellow eye has exudative AMD. *Investigative Ophthalmology & Visual Science* 28: 1832-1837.

Eisner A, Fleming S A, Klein M L, and Mauldin W M (1987b) Sensitivities in older eyes with good acuity: cross-sectional norms. *Investigative Ophthalmology & Visual Science* 28: 1824-1831.

Eisner A, Klein M L, Zilis J D, and Watkins M D (1992) Visual Function and the Subsequent Development of Exudative Age-Related Macular Degeneration. *Investigative Ophthalmology & Visual Science* 33: 3091-3102.

Eisner A, Stoumbos V D, Klein M L, and Fleming S A (1991) Relations between Fundus Appearance and Function - Eyes Whose Fellow Eye Has Exudative Age-Related Macular Degeneration. *Investigative Ophthalmology & Visual Science* 32: 8-20.

Elliott D B, and Whitaker D (1991) Changes in macular function throughout adulthood. *Documenta Ophthalmologica* 76: 251-259.

Evans J (2008) Antioxidant supplements to prevent or slow down the progression of AMD: A systematic review and meta-analysis. *Eye* 22: 751-760.

Evans J R (2001) Risk factors for age-related macular degeneration. *Progress in Retinal and Eye Research* 20: 227-253.

Evans J R, Fletcher A E, and Wormald R P L (2004) Causes of visual impairment in people aged 75 years and older in Britain: an add-on study to the MRC Trial of Assessment and Management of Older People in the Community. *British Journal of Ophthalmology* 88: 365-370.

Evans J R, and Wormald R P L (1996) Is the incidence of registrable age-related macular degeneration increasing? *British Journal of Ophthalmology* 80: 9-14.

- Fain G L (2006) Early receptor potential. In: Heckenlively J R, and Arden G B [eds.] *Principles and practice of clinical electrophysiology of vision*. London: MIT Press, pp. 549-550.
- Falsini B, Serrao S, Fadda A, Iarossi G, Porrello G, Cocco F, and Merendino E (1999) Focal electroretinograms and fundus appearance in nonexudative age-related macular degeneration - Quantitative relationship between retinal morphology and function. *Graefes Archive for Clinical and Experimental Ophthalmology* 237: 193-200.
- Farwick A, Dasch B, Weber B H, Pauleikhoff D, Stoll M, and Hense H W (2009) Variations in five genes and the severity of age-related macular degeneration: results from the Muenster aging and retina study. *Eye* 23: 2238-2244.
- Feeneyburns L, and Ellersieck M R (1985) Age-Related-Changes in the Ultrastructure of Bruchs Membrane. *American Journal of Ophthalmology* 100: 686-697.
- Feigl B (2009) Age-related maculopathy - linking aetiology and pathophysiological changes to the ischaemia hypothesis. *Progress in Retina and Eye Research* 28: 63-86.
- Feigl B, Brown B, Love-Kitchin J, and Swann P (2005b) Cone- and rod-mediated multifocal electroretinogram in early age-related maculopathy. *Eye* 19: 431-441.
- Feigl B, Brown B, Lovie-Kitchin J, and Swann P (2005a) Monitoring retinal function in early age-related maculopathy: visual performance after 1 year. *Eye* 19: 1169-1177.
- Feigl B, Brown B, Lovie-Kitchin J, and Swann P (2006) The rod-mediated multifocal electroretinogram in aging and in early age-related maculopathy. *Current Eye Research* 31: 635-644.
- Ferris F L, Davis M D, Clemons T E, Lee L Y, Chew E Y, Lindblad A S, Milton R C et al. (2005) A simplified severity scale for age-related macular degeneration - AREDS report no. 18. *Archives of Ophthalmology* 123: 1570-1574.

Fletcher A E, Bentham G C, Agnew M, Young I S, Augood C, Chakravarthy U et al. (2008) Sunlight exposure, antioxidants, and age-related macular degeneration. *Archives of Ophthalmology* 126: 1396-1403.

Fletcher E C, and Chong N V (2008) Looking beyond Lucentis on the management of macular degeneration. *Eye* 22: 742-750.

Franze, K, Grosche J, Skatchkov S N, Schinkinger S, Foja C, Schlid D, et al. (2007) Muller cells are living optical fibers in the vertebrate retina. *Proceedings of the National Academy of Sciences of the United States of America* 104: 8287-8292.

Frennesson C, Nilsson U L, and Nilsson S E G (1995) Color contrast sensitivity in patients with soft drusen, an early stage of ARM. *Documenta Ophthalmologica* 90: 377-386.

Friedburg C, Sharpe L T, Beuel S, and Zrenner E (1998) A computer-controlled system for measuring dark adaptation and other psychophysical functions. *Graefes Archives of Clinical and Experimental Ophthalmology* 236: 31-40.

Frishman L J (2006) Origins of the electroretinogram. In: Heckenlively J R, and Arden G B [eds.] *Principles and practice of clinical electrophysiology of vision*. London: MIT Press, pp. 139-183.

Fry G A, and Bartley S H (1935) The relation of stray light in the eye to the retinal action potential. *American Journal of Physiology* 111: 335-340.

Fulton A B, and Rushton W A (1978) The human rod ERG: correlation with psychophysical responses in light and dark adaptation. *Vision Research* 18: 793-800.

Gaffney A J, Binns A, and Margrain T (2012) Aging and cone dark adaptation. *Optometry and Vision Science* 89 pp-pp.

Gaffney A J, Binns A M, and Margrain T H (2011a) The repeatability of the Goldmann-Weekers adaptometer for measuring cone adaptation. *Documenta Ophthalmologica* 122: 71-75.

Gaffney A J, Binns A M, and Margrain T H (2011b) The topography of cone dark adaptation deficits in age-related maculopathy. *Optometry and Vision Science* 88: 1080-1087.

Gale C R, Hall N F, Phillips D I W, and Martyn C N (2003) Lutein and zeaxanthin status and risk of age-related macular degeneration. *Investigative Ophthalmology & Visual Science* 44: 2461-2465.

Galloway N R (1967) Early receptor potential in human eye. *British Journal of Ophthalmology* 51: 261-264.

Gao H, and Hollyfield J G (1992) Aging of the human retina. Differential loss of neurons and retinal pigment epithelial cells. *Investigative Ophthalmology & Visual Science* 33: 1-17.

Gerth C (2009) The role of the ERG in the diagnosis and treatment of Age-Related Macular Degeneration. *Documenta Ophthalmologica* 118: 63-68.

Gescheider G, A. (1997) *Psychophysics: The Fundamentals*. 3rd ed. ed. Mahwah, New Jersey: Lawrence Erlbaum Associates, Inc.,

Glaser J S, Savino P J, Summers K D, McDonald S A, and Knighton R W (1977) Photo-Stress Recovery Test in Clinical-Assessment of Visual Function. *American Journal of Ophthalmology* 83: 255-260.

Goldstein E B (1970) Cone pigment regeneration in isolated frog retina. *Vision Research* 10: 1065-1068.

Goldstein E B (1975) Design for a dark adaptometer. *Behavior Research Methods & Instrumentation* 7: 277-280.

Gouras P (1984) Colour Vision. *Progress in Retinal and Eye Research* 3: 227-261.

Granit R (1933) The components of the retinal action potential in mammals and their relation to the discharge in the optic nerve. *Journal of Physiology-London* 77: 207-239.

Green D M, and Swets J A (1966) *Signal detection theory and psychophysics*. New York: Wiley.

Gregori G, Wang F H, Rosenfeld P J, Yehoshua Z, Gregori N Z, Lujan B J, Puliafito C A et al. (2011) Spectral Domain Optical Coherence Tomography Imaging of Drusen in Nonexudative Age-Related Macular Degeneration. *Ophthalmology* 118: 1373-1379.

Greve M D J, Hinz B J, Schulha M, Wakeman B, Colgon G, Schwanke B, Dalton K et al. (2005) Verteporfin therapy of subfoveal minimally classic choroidal neovascularization in age-related macular degeneration - 2-year results of a randomized clinical trial. *Archives of Ophthalmology* 123: 448-457.

Guymer R, Luthert P, and Bird A (1999) Changes in Bruch's membrane and related structures with age. *Progress in Retinal and Eye Research* 18: 59-90.

Hageman G S, Luthert P J, Victor Chong N H, Johnson L V, Anderson D H, and Mullins R F (2001) An integrated hypothesis that considers drusen as biomarkers of immune-mediated processes at the RPE-Bruch's membrane interface in aging and age-related macular degeneration. *Progress in Retinal Eye Research* 20: 705-732.

Hahn G A, Messias A, MacKeben M, Dietz K, Horwath K, Hyvarinen L, Leinonen M et al. (2009) Parafoveal letter recognition at reduced contrast in normal aging and in patients with risk factors for AMD. *Graefes Archive for Clinical and Experimental Ophthalmology* 247: 43-51.

Haig C (1941) The course of rod dark adaptation as influenced by the intensity and duration of pre-adaptation to light. *Journal of General Physiology* 24: 735-751.

Haig C, Hecht S, and Patek A J (1938) Vitamin A and rod-cone dark adaptation in cirrhosis of the liver. *Science* 87: 534-536.

Haimovici R, Owens S L, Fitzke F W, and Bird A C (2002) Dark adaptation in age-related macular degeneration: relationship to the fellow eye. *Graefes Archive for Clinical and Experimental Ophthalmology* 240: 90-95.

Hall J L (1981) Hybrid adaptive procedure for estimation of psychometric functions. *Journal of the Acoustical Society of America* 69: 1763-1769.

Hammond C J, Webster A R, Snieder H, Bird A C, Gilbert C E, and Spector T D (2002) Genetic influence on early age-related maculopathy - A twin study. *Ophthalmology* 109: 730-736.

Hanley J A, and McNeil B J (1982) The meaning and use of the area under a receiver operating characteristic (ROC) curve. *Radiology* 143: 29-36.

Hanley J A, and McNeil B J (1983) A method of comparing the areas under receiver operating characteristic curves derived from the same cases. *Radiology* 148: 839-843.

Harman A M, Fleming P A, Hoskins R V, and Moore S R (1997) Development and aging of cell topography in the human retinal pigment epithelium. *Investigative Ophthalmology & Visual Science* 38: 2016-2026.

Hawkins B S, and Fine S L (1993) Laser photocoagulation of subfoveal neovascular lesions of age-related macular degeneration - updated findings from 2 clinical trials. *Archives of Ophthalmology* 111: 1200-1209.

Hayhoe M M, and Chen B (1986) Temporal modulation sensitivity in cone dark adaptation. *Vision Research* 26: 1715-1725.

Hecht S (1937) Rods, cones, and the chemical basis of vision. *Physiological Reviews* 17: 239-290.

Hecht S, Haig C, and Chase A M (1937) The influence of light adaptation on subsequent dark adaptation of the eye. *Journal of General Physiology* 20: 831-850.

Hecht S, Haig C, and Wald G (1935) The Dark Adaptation of Retinal Fields of Different Size and Location. *Journal of General Physiology* 19: 321-337.

Hecht S, and Shlaer S (1936) Intermittent stimulation by light V. The relation between intensity and critical frequency for different parts of the spectrum. *Journal of General Physiology* 19: 965-977.

Hecht S, and Shlaer S (1938) An adaptometer for measuring human dark adaptation. *Journal of the Optical Society of America* 28: 269-275.

Heimes B, Lommatzsch A, Zeimer M, Gutfleisch M, Spital G, Bird A C, and Pauleikhoff D (2008) Foveal RPE autofluorescence as a prognostic factor for anti-VEGF therapy in exudative AMD. *Graefes Archive for Clinical and Experimental Ophthalmology* 246: 1229-1234.

Hendrickson A E (2005) Organization of the Adult Primate Fovea. In: Penfold, P L, and Provis, J M [eds.] *Macular Degeneration*. Heidelberg: Springer, pp. 1-20.

Henson D B, and Allen M J (1977) A new dark adaptometer. *American Journal of Optometry & Physiological Optics* 54: 641-644.

Heynen H, and Vannorren D (1985) Origin of the electroretinogram in the intact macaque eye. 2. Current source density analysis. *Vision Research* 25: 709-715.

Hibbs S P, Smith A, Chow L P, and Downes S M (2011) Colour photographs for screening in neovascular age-related macular degeneration: are they necessary? *Eye* 25: 917-920.

Ho L, van Leeuwen R, Witteman J C M, van Duijn C M, Uitterlinden A G, Hofman A, de Jong P et al. (2011) Reducing the Genetic Risk of Age-Related Macular Degeneration With Dietary Antioxidants, Zinc, and omega-3 Fatty Acids The Rotterdam Study. *Archives of Ophthalmology* 129: 757-765.

Hogg C, and Nusinowitz S (2006) Data acquisition systems for electrodiagnostic testing. In: Heckenlively, J R, and Arden, G B [eds.] *Principles and practice of clinical electrophysiology of vision*. (2nd edn.) London: MIT Press, pp. 237-244.

Hogg R E, and Chakravarthy U (2006) Visual function and dysfunction in early and late age-related maculopathy. *Progress in Retinal and Eye Research* 25: 249-276.

Hohberger B, Laemmer R, Adler W, Juenemann A G, and Horn F K (2007) Measuring contrast sensitivity in normal subjects with OPTEC 6500: influence of age and glare. *Graefes Archives for Clinical and Experimental Ophthalmology* 245: 1805-1814.

Holder G E, Brigell M G, Hawlina M, Meigen T, Vaegan, and Bach M (2007) ISCEV standard for clinical pattern electroretinography - 2007 update. *Documenta Ophthalmologica* 114: 111-116.

Holder G E, Votruba M, Carter A C, Bhattacharya S S, Fitzke F W, and Moore A T (1999) Electrophysiological findings in dominant optic atrophy (DOA) linking to the OPA1 locus on chromosome 3q 28-qter. *Documenta Ophthalmologica* 95: 217-228.

Hollins M, and Alpern M (1973) Dark adaptation and visual pigment regeneration in human cones. *Journal of General Physiology* 62: 430-447.

Holopigian K, Seiple W, Greenstein V, Kim D, and Carr R E (1997) Relative effects of aging and age-related macular degeneration on peripheral visual function. *Optometry and Vision Science* 74: 152-159.

Holz F G, Bellman C, Staudt S, Schutt F, and Volcker H E (2001) Fundus autofluorescence and development of geographic atrophy in age-related macular degeneration. *Investigative Ophthalmology & Visual Science* 42: 1051-1056.

Holz F G, Bindewald-Wittich A, Fleckenstein M, Dreyhaupt J, Scholl H P N, Schmitz-Valckenberg S, and Grp F A-S (2007) Progression of geographic atrophy and impact of fundus autofluorescence patterns in age-related macular degeneration. *American Journal of Ophthalmology* 143: 463-472.

Hong T, Tan A G, Mitchell P, and Wang J J A (2011) Review and Meta-analysis of the Association Between C-Reactive Protein and Age-related Macular Degeneration. *Survey of Ophthalmology* 56: 184-194.

Hood D C, Bach M, Brigell M, Keating D, Kondo M, Lyons J S, Marmor M F et al. (2011) ISCEV standard for clinical multifocal electroretinography (mfERG) (2011 edition). *Documenta Ophthalmologica*.

Hood D C, and Birch D G (1996) Assessing abnormal rod photoreceptor activity with the a-wave of the electroretinogram: Applications and methods. *Documenta Ophthalmologica* 92: 253-267.

Hood D C, and Birch D G (2006) Measuring the health of the human photoreceptors with the leading edge of the a-wave. In: Heckenlively J R, and Arden G B [eds.] *Principles and practice of clinical electrophysiology of vision*. (2nd edn.) London: MIT Press, pp. 487-501.

Hood D C, Frishman L J, Saszik S, and Viswanathan S (2002) Retinal origins of the primate multifocal ERG: Implications for the human response. *Investigative Ophthalmology & Visual Science* 43: 1673-1685.

Hood D C, and Hock P A (1973) Recovery of cone photoreceptor activity in frogs isolated retina. *Vision Research* 13: 1943-1951.

Hood D C, Wladis E J, Shady S, Holopigian K, Li J, and Seiple W (1998) Multifocal rod electroretinograms. *Investigative Ophthalmology & Visual Science* 39: 1152-1162.

Horiguchi M, Miyake Y, and Fujii Y (1991) Human Focal Rod ERG. *Investigative Ophthalmology & Visual Science* 32: 926-926.

Hu K G, and Marmor M F (1984) Selective actions of barium on the c-wave and slow negative potential of the rabbit eye. *Vision Research* 24: 1153-1156.

Huang S, Wu D, Jiang F, Ma J, Wu L, Liang J, and Luo G (2000) The multifocal electroretinogram in age-related maculopathies. *Documenta Ophthalmologica* 101: 115-124.

Inoue Y, Yanagi Y, Matsuura K, Takahashi H, Tamaki Y, and Araie M (2007) Expression of hypoxia-inducible factor 1 alpha and 2 alpha in choroidal neovascular membranes associated with age-related macular degeneration. *British Journal of Ophthalmology* 91: 1720-1721.

Ip M S, Scott I U, Brown G C, Brown M M, Ho A C, Huang S S, and Recchia F M (2008) Anti-vascular endothelial growth factor pharmacotherapy for age-related macular degeneration. *Ophthalmology* 115: 1837-1846.

Jackson G R, and Edwards J G (2008) A short-duration dark adaptation protocol for assessment of age-related maculopathy. *Journal of Ocular Biology, Diseases, and Informatics* 1: 7-11.

Jackson G R, Felix T, and Owsley C (2006b) The Scotopic Sensitivity Tester-1 and the detection of early age-related macular degeneration. *Ophthalmic and Physiological Optics* 26: 431-437.

Jackson G R, McGwin G, Phillips J M, Klein R, and Owsley C (2004) Impact of aging and age-related maculopathy on activation of the a-wave of the rod-mediated electroretinogram. *Investigative Ophthalmology & Visual Science* 45: 3271-3278.

Jackson G R, McGwin G, Jr., Phillips J M, Klein R, and Owsley C (2006a) Impact of aging and age-related maculopathy on inactivation of the a-wave of the rod-mediated electroretinogram. *Vision Research* 46: 1422-1431.

Jackson G R, Owsley C, Cordle E P, and Finley C D (1998) Aging and scotopic sensitivity. *Vision Research* 38: 3655-3662.

Jackson G R, Owsley C, and McGwin G (1999) Aging and dark adaptation. *Vision Research* 39: 3975-3982.

Jackson T L, and Kirkpatrick L (2011) Age-related macular degeneration: Cost comparison of ranibizumab and bevacizumab. *British Medical Journal* 343.

Jain S, Hamada S, Membrey W L, and Chong V (2006) Screening for age-related macular degeneration using nonstereo digital fundus photographs. *Eye* 20: 471-475.

Jampol L M, and Tielsch J (1992) Race, macular degeneration and the macular photocoagulation study. *Archives of Ophthalmology* 110: 1699-1700.

Jones G J, Crouch R K, Wiggert B, Cornwall M C, and Chader G J (1989) Retinoid requirements for recovery of sensitivity after visual pigment bleaching in isolated photoreceptors. *Proceedings of the National Academy of Sciences of the United States of America* 86: 9606-9610.

Kalloniatis M, and Luu C (2011) *Psychophysics of Vision*. <http://webvision.med.utah.edu/book/part-viii-gabac-receptors/psychophysics-of-vision/>
Accessed: 31st October 2011.

Kanda A, Abecasis G, and Swaroop A (2008) Inflammation in the pathogenesis of age-related macular degeneration. *British Journal of Ophthalmology* 92: 448-450.

Kannan R, Zhang N, Sreekumar P, Spee C, Rodriguez A, Barron E, and Hinton D (2006) Stimulation of apical and basolateral VEGF-A and VEGF-C secretion by oxidative stress in polarized retinal pigment epithelial cells. *Molecular Vision* 12: 1649-1659.

Karpe G, and Tansley K (1948) The relationship between the change in the electroretinogram and the subjective dark-adaptation curve. *Journal of Physiology-London* 107: 272-279.

Kassoff A, Kassoff J, Buehler J, Eglow M, Kaufman F, Mehu M et al. (2001) A randomized, placebo-controlled, clinical trial of high-dose supplementation with vitamins C and E, beta carotene, and zinc for age-related macular degeneration and vision loss - AREDS Report No. 8. *Archives of Ophthalmology* 119: 1417-1436.

Kelliher C, Kenny D, and O'Brien C (2006) Trends in blind registration in the adult population of the Republic of Ireland 1996-2003. *British Journal of Ophthalmology* 90: 367-371.

Kemp C M, Jacobson S G, Faulkner D J, and Walt R W (1988) Visual function and rhodopsin levels in humans with vitamin A deficiency. . *Experimental Eye Research* 46: 185-197.

Khan J C, Thurlby D A, Shahid H, Clayton D G, Yates J R W, Bradley M et al. (2006) Smoking and age related macular degeneration: the number of pack years of cigarette smoking is a major determinant of risk for both geographic atrophy and choroidal neovascularisation. *British Journal of Ophthalmology* 90: 75-80.

Khandhadia S, and Lotery A (2010) Oxidation and age-related macular degeneration: insights from molecular biology. *Expert Reviews in Molecular Medicine* 12.

Kiryu J, Asrani S, Shahidi M, Mori M, and Zeimer R (1995) Local response of the primate retinal microcirculation to increased metabolic demand induced by flicker. *Investigative Ophthalmology & Visual Science* 36: 1240-1246.

Klaver C C W, Assink J J M, van Leeuwen R, Wolfs R C W, Vingerling J R, Stijnen T, Hofman A et al. (2001) Incidence and progression rates of age-related maculopathy: The Rotterdam study. *Investigative Ophthalmology & Visual Science* 42: 2237-2241.

Klein B E K, Klein R, Lee K E, Moore E L, and Danforth L (2001) Risk of incident age-related eye diseases in people with an affected sibling - The Beaver Dam eye study. *American Journal of Epidemiology* 154: 207-211.

Klein R (2011) Race/Ethnicity and Age-Related Macular Degeneration. *American Journal of Ophthalmology* 152: 153-154.

Klein R, Chou C F, Klein B E K, Zhang X Z, Meuer S M, and Saaddine J B (2011) Prevalence of Age-Related Macular Degeneration in the US Population. *Archives of Ophthalmology* 129: 75-80.

Klein R, Davis M D, Magli Y L, Segal P, Klein B E K, and Hubbard L (1991a) The Wisconsin age-related maculopathy grading system. *Ophthalmology* 98: 1128-1134.

Klein R, Klein B E, and Lee K E (1996) Changes in visual acuity in a population. The Beaver Dam Eye Study. *Ophthalmology* 103: 1169-1178.

Klein R, Klein B E K, Jensen S C, and Meuer S M (1997) The five-year incidence and progression of age-related maculopathy - The Beaver Dam eye study. *Ophthalmology* 104: 7-21.

Klein R, Klein B E K, Knudtson M D, Meuer S M, Swift M, and Gangnon R E (2007) Fifteen-year cumulative incidence of age-related macular degeneration. *Ophthalmology* 114: 253-262

Klein R, Klein B E K, Knudtson M D, Wong T Y, Cotch M F, Liu K, Burke G et al. (2006) Prevalence of age-related macular degeneration in 4 racial/ethnic groups in the multi-ethnic study of atherosclerosis. *Ophthalmology* 113: 373-380.

Klein R, Klein B E K, Linton K L P, and Demets D L (1991b) The Beaver Dam Eye Study - Visual-Acuity. *Ophthalmology* 98: 1310-1315.

Klein R, Klein B E K, Marino E K, Kuller L H, Furberg C, Burke G L, and Hubbard L D (2003a) Early age-related maculopathy in the cardiovascular health study. *Ophthalmology* 110: 25-33.

Klein R, Klein B E K, Tomany S C, and Cruickshanks K (2003b) Association of emphysema, gout and inflammatory markers with long-term incidence of age-related maculopathy. *Archives of Ophthalmology* 121: 674-678.

Klein R, Wang Q, Klein B E, Moss S E, and Meuer S M (1995) The relationship of age-related maculopathy, cataract, and glaucoma to visual acuity. *Investigative Ophthalmology & Visual Science* 36: 182-191.

Klein R, Knudtson M D, Cruickshanks K J, and Klein B E K (2008b) Further observations on the association between smoking and the long-term incidence and progression of age-related macular degeneration. *Archives of Ophthalmology* 126: 115-121.

Klein R, Meuer S M, Knudtson M D, Iyengar S K, and Klein B E K (2008a) The epidemiology of retinal reticular drusen. *American Journal of Ophthalmology* 145: 317-326.

Kleiner R C, Enger C, Alexander M F, and Fine S L (1988) Contrast sensitivity in age-related macular degeneration. *Archives of Ophthalmology* 106: 55-57.

Kline D W, Kline T J B, Fozard J L, Kosnik W, Schieber F, and Sekuler R (1992) Vision, aging and driving - the problems of older drivers. *Journals of Gerontology* 47: 27-34.

Kolb H (1994) The architecture of functional neural circuits in the vertebrate retina - The Proctor Lecture. *Investigative Ophthalmology & Visual Science* 35: 2385-2404.

Kolb H (2001) The Outer Plexiform Layer. In: Kolb, H, Fernandez, E, and Nelson, R [eds.] *Webvision*, <http://webvision.med.utah.edu/>.

Kolb H (2003a) Simple anatomy of the retina. In: Kolb, H, Fernandez, E, and Nelson, R [eds.] *Webvision*, <http://webvision.med.utah.edu/>.

Kolb H (2003b) Morphology and Circuitry of Ganglion Cells. In: Kolb, H, Fernandez, E, and Nelson, R [eds.] *Webvision*, <http://webvision.med.utah.edu/>.

Kolb H, and Famiglietti E V (1974) Rod and cone pathways in the inner plexiform layer of cat retina. *Science* 186: 47-49.

Kolb H, Fernandez E, Schouten J, Ahnelt P, Linberg K A, and Fisher S K (1994) Are there 3 types of horizontal cell in the human retina? *Journal of Comparative Neurology* 343: 370-386.

Kolb H, Linberg K A, and Fisher S K (1992) Neurons of the human retina - a golgi study. *Journal of Comparative Neurology* 318: 147-187.

Kondo M, and Sieving P A (2002) Post-photoreceptor activity dominates primate photopic 32-Hz ERG for sine-, square-, and pulsed stimuli. *Investigative Ophthalmology and Visual Science* 43: 2500-2507.

Krishnadev N, Meleth A D, and Chew E Y (2010) Nutritional supplements for age-related macular degeneration. *Current Opinion in Ophthalmology* 21: 184-189.

Krueger D E, Milton R C, and Maunder L R (1980) The Framingham Eye Study - Introduction to the Monograph. *Survey of Ophthalmology* 24: 614-620.

Lachapelle P (2006) The oscillatory potentials of the electroretinogram. In: Heckenlively J R, and Arden G B [eds.] *Principles and practice of clinical electrophysiology of vision*. London: MIT Press, pp. 565-580.

Lamb T D (1981) The involvement of rod photoreceptors in dark adaptation. *Vision Research* 21: 1773-1782.

Lamb T D (1990) Dark adaptation: a re-examination. In: Hess, R, F, Sharpe, L, T, and Nordby, K [eds.] *Night vision: basic, clinical and applied aspects* Cambridge University Press, pp. 177-222.

Lamb T D, and Pugh E N, Jr. (2004) Dark adaptation and the retinoid cycle of vision. *Progress in Retinal Eye Research* 23: 307-380.

Le Goff M M, and Bishop P N (2008) Adult vitreous structure and postnatal changes. *Eye* 22: 1214-1222.

Lei B, and Perlman I (1999) The contributions of voltage- and time-dependent potassium conductances to the electroretinogram in rabbits. *Visual Neuroscience* 16: 743-754.

Leibrock C S, Reuter T, and Lamb T D (1998) Molecular basis of dark adaptation in rod photoreceptors. *Eye* 12 (Pt 3b): 511-520.

Li J, Tso M O M, and Lam T T (2001) Reduced amplitude and delayed latency in foveal response of multifocal electroretinogram in early age related macular degeneration. *British Journal of Ophthalmology* 85: 287-290.

Lim L S, Mitchell P, Seddon J M, Holz F G, and Wong T Y (2012) Age-related macular degeneration. *Lancet* 379: 1728-1738.

Lovasik J V (1983) An electrophysiological investigation of the macular photostress test. *Investigative Ophthalmology & Visual Science* 24: 437-441.

Lu B, Malcuit C, Wang S M, Girman S, Francis P, Lemieux L, Lanza R et al. (2009) Long-Term Safety and Function of RPE from Human Embryonic Stem Cells in Preclinical Models of Macular Degeneration. *Stem Cells* 27: 2126-2135.

Mackay A M, Brown M C, Grierson I, and Harding S P (2008) Multifocal electroretinography as a predictor of maintenance of vision after photodynamic therapy for neovascular age-related macular degeneration. *Documenta Ophthalmologica* 116: 13-18.

Maffei L, and Fiorentini A (1981) Electroretinographic responses to alternating gratings before and after section of the optic nerve. *Science* 211: 953-955.

Maffei L, Fiorentini A, Bisti S, and Hollander H (1985) Pattern ERG in the monkey after section of the optic nerve. *Experimental Brain Research* 59: 423-425.

Maguire M G, Klein M L, Olk J, Phillips D A, Alexander J, Javornik N B, et al. (1994) Persistent and recurrent neovascularisation after laser photocoagulation for subfoveal choroidal neovascularization of age-related macular degeneration. *Archives of Ophthalmology* 112: 489-499.

Mahroo O A, and Lamb T D (2004) Recovery of the human photopic electroretinogram after bleaching exposures: estimation of pigment regeneration kinetics. *Journal of Physiology-London* 554: 417-437.

Mantjarvi M (2001) Normal test scores in the Farnsworth-Munsell 100 hue test. *Documenta Ophthalmologica* 102: 73-80.

Margrain T H, and Thomson D (2002) Sources of variability in the clinical photostress test. *Ophthalmic and Physiological Optics* 22: 61-67.

Mariani A P (1984) Bipolar cells in monkey retina selective for the cones likely to be blue-sensitive. *Nature* 308: 184-186.

Mariani A P (1990) Amacrine cells of the rhesus monkey retina. *Journal of Comparative Neurology* 301: 382-400.

Marmor M F, Fulton A B, Holder G E, Miyake Y, Brigell M, and Bach M (2009) ISCEV Standard for full-field clinical electroretinography (2008 update). *Documenta Ophthalmologica* 118: 69-77.

Martin D F, Maguire M G, Ying G S, Grunwald J E, Fine S L, Jaffe G J, and Grp C R (2011) Ranibizumab and Bevacizumab for Neovascular Age-Related Macular Degeneration. The CATT Research Group. *New England Journal of Medicine* 364: 1897-1908.

Mata N L, Radu R A, Clemmons R C, and Travis G H (2002) Isomerization and oxidation of vitamin a in cone-dominant retinas: a novel pathway for visual-pigment regeneration in daylight. *Neuron* 36: 69-80.

Maturi R K, Bleau L A, and Wilson D L (2006) Electrophysiologic findings after intravitreal bevacizumab (Avastin) treatment. *Retina-the Journal of Retinal and Vitreous Diseases* 26: 270-274.

Mayer M J, Spiegler S J, Ward B, Glucs A, and Kim C B (1992) Mid-frequency loss of foveal flicker sensitivity in early stages of age-related maculopathy. *Investigative Ophthalmology & Visual Science* 33: 3136-3142.

Mayer M J, Ward B, Klein R, Talcott J B, Dougherty R F, and Glucs A (1994) Flicker sensitivity and fundus appearance in pre-exudative age-related maculopathy. *Investigative Ophthalmology & Visual Science* 35: 1138-1149.

McCulloch D L, Van Boemel G B, and Borchert M S (1997) Comparisons of contact lens, foil, fiber and skin electrodes for patterns electroretinograms. *Documenta Ophthalmologica* 94: 327-340.

McGregor L N, and Chaparro A (2005) Visual difficulties reported by low-vision and nonimpaired older adult drivers. *Human Factors* 47: 469-478.

McGwin G, Jr., Jackson G R, and Owsley C (1999) Using nonlinear regression to estimate parameters of dark adaptation. *Behaviour Research Methods, Instruments & Computers* 31: 712-717.

McMurdo M E T, and Gaskell A (1991) Dark adaptation and falls in the elderly. *Gerontology* 37: 221-224.

Mei M, and Leat S J (2007) Suprathreshold contrast matching in maculopathy. *Investigative Ophthalmology & Visual Science* 48: 3419-3424.

Meleth A D, Mettu P, Agron E, Chew E Y, Sadda S R, Ferris F L, and Wong W T (2011) Changes in Retinal Sensitivity in Geographic Atrophy Progression as Measured by Microperimetry. *Investigative Ophthalmology & Visual Science* 52: 1119-1126.

Merle B, Delyfer M N, Korobelnik J F, Rougier M B, Colin J, Malet F, Feart C et al. (2011) Dietary Omega-3 Fatty Acids and the Risk for Age-Related Maculopathy: The Alienor Study. *Investigative Ophthalmology & Visual Science* 52: 6004-6011.

Metha A B, Vingrys A J, and Badcock D R (1993) Calibration of a Color Monitor for Visual Psychophysics. *Behavior Research Methods Instruments & Computers* 25: 371-383.

Midena E, Angeli C D, Blarzino M C, Valenti M, and Segato T (1997) Macular function impairment in eyes with early age-related macular degeneration. *Investigative Ophthalmology & Visual Science* 38: 469-477.

Midena E, Segato T, Blarzino M C, and Angeli C D (1994) Macular drusen and the sensitivity of the central visual field. *Documenta Ophthalmologica* 88: 179-185.

Midena E, Vujosevic S, Convento E, Manfre A, Cavarzeran F, and Pilotto E (2007) Microperimetry and fundus autofluorescence in patients with early age-related macular degeneration. *British Journal of Ophthalmology* 91: 1499-1503.

Miller J W (2010) Treatment of Age-Related Macular Degeneration: Beyond VEGF. *Japanese Journal of Ophthalmology* 54: 523-528.

Miller R F, and Dowling J E (1970) Intracellular responses of the Muller (glial) cells of mudpuppy retina: their relation to b-wave of the electroretinogram. *Journal of Neurophysiology* 33: 323-341.

Minassian D C, Reidy A, Lightstone A, and Desai P (2011) Modelling the prevalence of age-related macular degeneration (2010-2020) in the UK: expected impact of anti-vascular endothelial growth factor (VEGF) therapy. *British Journal of Ophthalmology*.

Mitchell P (2011) A systematic review of the efficacy and safety outcomes of anti-VEGF agents used for treating neovascular age-related macular degeneration: comparison of ranibizumab and bevacizumab. *Current Medical Research and Opinion* 27: 1465-1475.

Mitchell P, Korobelnik J F, Lanzetta P, Holz F G, Prunte C, Schmidt-Erfurth U et al. (2010) Ranibizumab (Lucentis) in neovascular age-related macular degeneration: evidence from clinical trials. *British Journal of Ophthalmology* 94: 2-13.

Mitchell P, Wang J J, Foran S, and Smith W (2002) Five-year incidence of age-related maculopathy lesions - The Blue Mountains Eye Study. *Ophthalmology* 109: 1092-1097.

Moore A T, Fitzke F W, Kemp C M, Arden G B, Keen T J, Inglehearn C F, Bhattacharya S S et al. (1992) Abnormal dark adaptation kinetics in autosomal dominant sector retinitis pigmentosa due to rod opsin mutation. *British Journal of Ophthalmology* 76: 465-469.

Moore D J, Hussain A A, and Marshall J (1995) Age-related variation in the hydraulic conductivity of Bruch's membrane. *Investigative Ophthalmology and Visual Science* 36: 1290-1297.

Mote F A, and Riopelle A J (1951) The effect of varying the intensity and duration of pre-exposure upon foveal dark adaptation in the human eye *Journal of General Physiology* 34: 657-674.

Muller F L, Lustgarten M S, Jang Y, Richardson A, Van Remmen H (2007) Trends in oxidative aging theories. *Free Radical Biology and Medicine* 43: 477-503.

National Institute for Health and Clinical Excellence (2003) Guidance on the use of photodynamic therapy for age-related macular degeneration. http://www.nice.org.uk/nicemedia/pdf/68_PDTGuidance.pdf Accessed: 18th August 2009.

National Institute for Health and Clinical Excellence (2008) Ranibizumab and pegaptanib for the treatment of age-related macular degeneration. <http://www.nice.org.uk/nicemedia/pdf/TA155guidance.pdf> Accessed: 18th August 2009.

Neelam K, Hogg R E, Stevenson M R, Johnston E, Anderson R, Beatty S, and Chakravarthy U (2008) Carotenoids and Co-Antioxidants in Age-Related Maculopathy: Design and Methods. *Ophthalmic Epidemiology* 15: 389-401.

Neelam K, Nolan J, Chakravarthy U, and Beatty S (2009) Psychophysical function in age-related maculopathy. *Survey of Ophthalmology* 54: 167-210.

Newsome D A, and Negreiro M (2009) Reproducible Measurement of Macular Light Flash Recovery Time Using a Novel Device Can Indicate the Presence and Worsening of Macular Diseases. *Current Eye Research* 34: 162-170.

Nishikawa S, and Tamai M (2001) Muller cells in the human foveal region. *Current Eye Research* 22: 34-41.

Noell W K (1953) The origin of the electroretinogram. *American Journal of Ophthalmology* 38: 78-90.

Nomura H, Ando F, Niino N, Shimokata H, and Miyake Y (2003) Age-related change in contrast sensitivity among Japanese adults. *Japanese Journal of Ophthalmology* 47: 299-303.

- Nowak J Z (2006) Age-related macular degeneration (AMD): pathogenesis and therapy. *Pharmacological Reports* 58: 353-363.
- Oakley B, and Green D G (1976) Correlation of light-induced changes in retinal extracellular potassium concentration with c-wave of electroretinogram. *Journal of Neurophysiology* 39: 1117-1133.
- Office for National Statistics (2009) *National population projections release 2009: UK population projected to grow by 4 million over the next decade.* <http://www.statistics.gov.uk/statbase/Product.asp?vlnk=8519> Accessed: 4th June 2010.
- Oner A, Karakucuk S, Mirza E, and Erkilic K (2005) The changes of pattern electroretinography at the early stage of photodynamic therapy. *Documenta Ophthalmologica* 111: 107-112.
- Owen C G, Jarrar Z, Wormald R, Cook D G, Fletcher A E, and Rudnicka A R (2012) The estimated prevalence and incidence of late stage age related macular degeneration in the UK. *British Journal of Ophthalmology*.
- Owsley C (2003) Contrast sensitivity. *Ophthalmology Clinics of North America* 16: 171-177.
- Owsley C, Jackson G R, Cideciyan A V, Huang Y J, Fine S L, Ho A C, Maguire M G et al. (2000) Psychophysical evidence for rod vulnerability in age-related macular degeneration. *Investigative Ophthalmology & Visual Science* 41: 267-273.
- Owsley C, Jackson G R, White M, Feist R, and Edwards D (2001) Delays in rod-mediated dark adaptation in early age-related maculopathy. *Ophthalmology* 108: 1196-1202.
- Owsley C, McGwin G, Jr., Jackson G R, Kallies K, and Clark M (2007) Cone- and rod-mediated dark adaptation impairment in age-related maculopathy. *Ophthalmology* 114: 1728-1735.

Panda-Jonas S, Jonas J B, and JakobczykZmija M (1996) Retinal pigment epithelial cell count, distribution, and correlations in normal human eyes. *American Journal of Ophthalmology* 121: 181-189.

Parisi V, and Bucci M G (1992) Visual evoked potentials after photostress in patients with primary open angle glaucoma and ocular hypertension. *Investigative Ophthalmology & Visual Science* 33: 436-442.

Parisi V, Canu D, Iarossi G, Olzi D, and Falsini B (2002) Altered recovery of macular function after bleaching in Stargardt's disease-fundus flavimaculatus: Pattern VEP evidence. *Investigative Ophthalmology & Visual Science* 43: 2741-2748.

Parisi V, Pierelli F, Restuccia R, Spadaro M, Parisi L, Colacino G, and Bucci M G (1998) Impaired VEP after photostress response in multiple sclerosis patients previously affected by optic neuritis. *Evoked Potentials-Electroencephalography and Clinical Neurophysiology* 108: 73-79.

Parisi V, Uccioli L, Monticone G, Parisi L, Menzinger G, and Bucci M G (1994) Visual evoked potentials after photostress in insulin dependent diabetic patients with or without retinopathy. *Graefes Archive for Clinical and Experimental Ophthalmology* 232: 193-198.

Parravano M, Oddone F, Tedeschi M, Chiaravalloti A, Perillo L, Boccassini B, and Varano M (2010) Retinal functional changes measured by microperimetry in neovascular age-related macular degeneration treated with Ranibizumab: 24-Month Results. *Retina-the Journal of Retinal and Vitreous Diseases* 30: 1017-1024.

Pauleikhoff D, Loffert D, Spital G, Radermacher M, Dohrmann J, Lommatzsch A, and Bird A C (2002) Pigment epithelial detachment in the elderly - Clinical differentiation, natural course and pathogenetic implications. *Graefes Archive for Clinical and Experimental Ophthalmology* 240: 533-538.

Paupoo A A, Mahroo O A, Friedburg C, and Lamb T D (2000) Human cone photoreceptor responses measured by the electroretinogram [correction of electroretinogram] a-wave

during and after exposure to intense illumination. *Journal of Physiology-London* 529 Pt 2: 469-482.

Penn R D, and Hagins W A (1969) Signal transmission along retinal rods and origin of electroretinographic a-wave. *Nature* 223: 201-205.

Perry A, Rasmussen H, and Johnson E J (2009) Xanthophyll (lutein, zeaxanthin) content in fruits, vegetables and corn and egg products. *Journal of Food Composition and Analysis* 22: 9-15.

Perry V H, and Cowey A (1981) The morphological correlates of X-like and Y-like retinal ganglion cells in the retina of monkeys. *Experimental Brain Research* 43: 226-228.

Perry V H, and Cowey A (1984) Retinal ganglion cells that project to the superior colliculus and pretectum in the macaque monkey. *Neuroscience* 12: 1125-1137.

Perry V H, Oehler R, and Cowey A (1984) Retinal ganglion cells that project to the dorsal lateral geniculate nucleus in the macaque monkey. *Neuroscience* 12: 1101-1123.

Peters A Y, Locke K G, and Birch D G (2000) Comparison of the Goldmann-Weekers (TM) dark adaptometer and Scotopic Sensitivity Tester-1 (TM). *Investigative Ophthalmology & Visual Science* 40: 3763B3621.

Petzold A, and Plant G T (2006) Clinical disorders affecting mesopic vision. *Ophthalmic & Physiological Optics* 26: 326-341.

Phipps J A, Guymer R H, and Vingrys A J (2003) Loss of cone function in age-related maculopathy. *Investigative Ophthalmology & Visual Science* 44: 2277-2283.

Phipps J A, Yee P, Fletcher E L, and Vingrys A J (2006) Rod photoreceptor dysfunction in diabetes: Activation, deactivation, and dark adaptation. *Investigative Ophthalmology & Visual Science* 47: 3187-3194.

Pianta M J, and Kalloniatis M (2000) Characterisation of dark adaptation in human cone pathways: an application of the equivalent background hypothesis. *Journal of Physiology* 528: 591-608.

Piccardi M, Ziccardi L, Stifano G, Montrone L, Iarossi G, Minnella A, Fadda A et al. (2009) Regional Cone-Mediated Dysfunction in Age-Related Maculopathy Evaluated by Focal Electroretinograms: Relationship with Retinal Morphology and Perimetric Sensitivity. *Ophthalmic Research* 41: 194-202.

Pinilla I, Cuenca N, Sauve Y, Wang S M, and Lund R D (2007) Preservation of outer retina and its synaptic connectivity following subretinal injections of human RPE cells in the Royal College of Surgeons rat. *Experimental Eye Research* 85: 381-392.

Pirenne M H (1962) Directional sensitivity of the Rods and Cones. In: Davson H [ed.] *The Eye*. Vol. 2. New York: Academic Press, pp. 31-62.

Pugh E N (1975) Rushton's paradox: rod dark adaptation after flash photolysis. *Journal of Physiology-London* 248: 413-431.

Puntmann V O (2009) How-to guide on biomarkers: biomarker definitions, validation and applications with examples from cardiovascular disease. *Postgraduate Medical Journal* 85: 538-545.

Ramrattan R S, Vanderschaft T L, Mooy C M, Debruijn W C, Mulder P G H, and Dejong P (1994) Morphometric analysis of Bruch's membrane, the choriocapillaris and the choroid in aging. *Investigative Ophthalmology & Visual Science* 35: 2857-2864.

Redmond T M, Yu S, Lee E, Bok D, Hamasaki D, Chen N, Goletz P et al. (1998) Rpe65 is necessary for production of 11-cis-vitamin A in the retinal visual cycle. *Nature Genetics* 20: 344-351.

Rein D B, Wittenborn J S, Zhang X Z, Honeycutt A A, Lesesne S B, and Saaddine J (2009) Forecasting Age-Related Macular Degeneration Through the Year 2050 The Potential Impact of New Treatments. *Archives of Ophthalmology* 127: 533-540.

Remulla J F C, Gaudio A R, Miller S, and Sandberg M A (1995) Foveal electroretinograms and choroidal perfusion characteristics in fellow eyes of patients with unilateral neovascular age-related macular degeneration. *British Journal of Ophthalmology* 79: 558-561.

Resnikoff S, Pascolini D, Etya'ale D, Kocur I, Pararajasegaram R, Pokharel G P, and Mariotti S P (2004) Global data on visual impairment in the year 2002. *Bulletin of the World Health Organization* 82: 844-851.

Robertson G W, and Yudkin J (1944) Effect of age upon dark adaptation. *The Journal of Physiology* 103: 1-8.

Robinson R, Deutsch J, Jones H S, Youngsonreilly S, Hamlin D M, Dhurjon L, and Fielder A R (1994) Unrecognized and Unregistered Visual Impairment. *British Journal of Ophthalmology* 78: 736-740.

Robson J G, and Frishman L J (1999) Dissecting the dark-adapted electroretinogram. *Documenta Ophthalmologica* 95: 187-215.

Rochtchina E, Wang J J, Flood V M, and Mitchell P (2007) Elevated serum homocysteine, low serum vitamin B12, folate, and age-related macular degeneration: The Blue Mountains Eye Study. *American Journal of Ophthalmology* 143: 344-346.

Rodrigues E B (2007) Inflammation in dry age-related macular degeneration. *Ophthalmologica* 221: 143-152.

Rohrschneider K, Bultmann S, and Springer C (2008) Use of fundus perimetry (microperimetry) to quantify macular sensitivity. *Progress in Retinal and Eye Research* 27: 536-548.

Rosenfeld P J, Brown D M, Heier J S, Boyer D S, Kaiser P K, Chung C Y, and Kim R Y (2006) Ranibizumab for neovascular age-related macular degeneration. *New England Journal of Medicine* 355: 1419-1431.

Roth F, Bindewald A, and Holz F G (2004) Key pathophysiologic pathways in age-related macular disease. *Graefes Archive for Clinical and Experimental Ophthalmology* 42: 710-716.

Rushton W A (1961) Rhodopsin Measurement and Dark-Adaptation in a Subject Deficient in Cone Vision. *Journal of Physiology-London* 156: 193-205.

Rushton W A (1965) The Ferrier Lecture 1962: Visual Adaptation. *Proceedings of the Royal Society London B - Biological Sciences* 162: 20-46.

Rushton W A H (1972) Light and dark adaptation. *Investigative Ophthalmology* 11: 503-517.

Rushton W A, and Henry G H (1968) Bleaching and regeneration of cone pigments in man. *Vision Research* 8: 617-631.

Salvi S M, Akhtar S, and Currie Z (2006) Ageing changes in the eye. *Postgraduate Medical Journal* 82: 581-587.

Sandberg M A, and Gaudio A R (1995) Slow photostress recovery and disease severity in age-related macular degeneration. *Retina* 15: 407-412.

Sandberg M A, Miller S, and Gaudio A R (1993) Foveal cone ERGs in fellow eyes of patients with unilateral neovascular age-related macular degeneration. *Investigative Ophthalmology & Visual Science* 34: 3477-3480.

Sandberg M A, Pawlyk B S, and Berson E L (1996) Isolation of focal rod electroretinograms from the dark-adapted human eye. *Investigative Ophthalmology & Visual Science* 37: 930-934.

Sandberg M A, Pawlyk B S, and Berson E L (1999) Acuity recovery and cone pigment regeneration after a bleach in patients with retinitis pigmentosa and rhodopsin mutations. *Investigative Ophthalmology & Visual Science* 40: 2457-2461.

Sandberg M A, Weiner A, Miller S, and Gaudio A R (1998) High-risk characteristics of fellow eyes of patients with unilateral neovascular age-related macular degeneration. *Ophthalmology* 105: 441-447.

SanGiovanni J P, Agron E, Meleth A D, Reed G F, Sperduto R D, Clemons T E, and Chew E Y (2009) Omega-3 Long-chain polyunsaturated fatty acid intake and 12-y incidence of neovascular age-related macular degeneration and central geographic atrophy: AREDS report 30, a prospective cohort study from the Age-Related Eye Disease Study. *American Journal of Clinical Nutrition* 90: 1601-1607.

SanGiovanni J P, Chew E Y, Clemons T E, Ferris F L, Gensler G, Linblad A S, Milton R C et al. (2007) The relationship of dietary carotenoid and vitamin A, E, and C intake with age-related macular degeneration in a case-control study - AREDS Report no. 22. *Archives of Ophthalmology* 125: 1225-1232.

Sarks J P, Sarks S H, and Killingsworth M C (1994) Evolution of soft drusen in age-related macular degeneration. *Eye* 8: 269-283.

Sarks S H (1976) Ageing and degeneration in the macular region: a clinico-pathological study. *British Journal of Ophthalmology* 60: 324-341.

Sarks J, Arnold J, Ho I V, Sarks S, and Killingsworth M (2011) Evolution of reticular pseudodrusen. *British Journal of Ophthalmology* 95: 979-985.

Sarks S H, Arnold J J, Killingsworth M C, and Sarks J P (1999) Early drusen formation in the normal and aging eye and their relation to age related maculopathy: a clinicopathological study. *British Journal of Ophthalmology* 83: 358-368.

Schmitz-Valckenberg S, Alten F, Steinberg J S, Jaffe G J, Fleckenstein M, Mukesh B N, Hohman T C et al. (2011) Reticular Drusen Associated with Geographic Atrophy in Age-Related Macular Degeneration. *Investigative Ophthalmology & Visual Science* 52: 5009-5015.

Schmitz-Valckenberg S, Fleckenstein M, Scholl H P N, and Holz F G (2009) Fundus Autofluorescence and Progression of Age-related Macular Degeneration. *Survey of Ophthalmology* 54: 96-117.

Schmolesky M (2007) The Primary Visual Cortex. In: Kolb, H, Fernandez, E, and Nelson, R [eds.] *Webvision*, <http://webvision.med.utah.edu/>.

Schwartz S, H (2004) *Visual perception: a clinical orientation*. 3rd ed. New York: McGraw-Hill, Medical Publications Division.

Seddon J M, Gensler G, Klein M L, and Milton R C (2006) Evaluation of plasma homocysteine and risk of age-related macular degeneration. *American Journal of Ophthalmology* 141: 201-203.

Seddon J M, Reynolds R, Maller J, Fagerness J A, Daly M J, and Rosner B (2009) Prediction Model for Prevalence and Incidence of Advanced Age-Related Macular Degeneration Based on Genetic, Demographic, and Environmental Variables. *Investigative Ophthalmology & Visual Science* 50: 2044-2053.

Seiple W H, Siegel I M, Carr R E, and Mayron C (1986) Evaluating macular function using the focal ERG. *Investigative Ophthalmology & Visual Science* 27: 1123-1130.

Sekuler R, and Blake R (2006) *Perception*. 5th ed. London: McGraw-Hill.

Shankar A, Mitchell P, Rochtchina E, Tan J, and Wang J J (2007) Association between circulating white blood cell count and long-term incidence of age-related macular degeneration - The Blue Mountains eye study. *American Journal of Epidemiology* 165: 375-382.

Sharpe L T, Stockman A, and Macleod D I A (1989) Rod flicker perception - scotopic duality, phase lags and destructive interference. *Vision Research* 29: 1539-1559.

Sheridan C M, Pate S, Hiscott P, Wong D, Pattwell D M, and Kent D (2009) Expression of hypoxia-inducible factor-1 alpha and-2 alpha in human choroidal neovascular membranes. *Graefes Archive for Clinical and Experimental Ophthalmology* 247: 1361-1367.

Sieving P A, Frishman L J, and Steinberg R H (1986) Scotopic threshold response of proximal retina in cat. *Journal of Neurophysiology* 56: 1049-1061.

Sieving P A, and Nino C (1988) Scotopic threshold response (STR) of the human electroretinogram. *Investigative Ophthalmology & Visual Science* 29: 1608-1614.

Sillman A J, Ito H, and Tomita T (1969) Studies on the mass receptor potential of the isolated frog retina. I. General properties of the response. *Vision Research* 9: 1435-1442.

Silva R, Cachulo M L, Fonseca P, Bernardes R, Nunes S, Vilhena N, and de Abreu J R F (2011) Age-Related Macular Degeneration and Risk Factors for the Development of Choroidal Neovascularisation in the Fellow Eye: A 3-Year Follow-Up Study. *Ophthalmologica* 226.

Smiddy W E, and Fine S L (1984) Prognosis of patients with bilateral macular drusen. *Ophthalmology* 91: 271-277.

Smith W, Mitchell P, and Leeder S R (1996) Smoking and age-related maculopathy - The Blue Mountains Eye Study. *Archives of Ophthalmology* 114: 1518-1523.

Smith W, Mitchell P, Leeder S R, and Wang J J (1998) Plasma fibrinogen levels, other cardiovascular risk factors, and age-related maculopathy - The Blue Mountains Eye Study. *Archives of Ophthalmology* 116: 583-587.

Solomon S D, Jefferys J L, Hawkins B S, Bressler N M, Bressler S B, and Submacular Surgery Trials Research G (2009) Risk factors for second eye progression to advanced age-related macular degeneration: SST report No. 21 Submacular Surgery Trials Research Group. *Retina (Philadelphia, Pa.)* 29: 1080-1090.

Sommerburg O, Keunen J E E, Bird A C, and van Kuijk F (1998) Fruits and vegetables that are sources for lutein and zeaxanthin: the macular pigment in human eyes. *British Journal of Ophthalmology* 82: 907-910.

Spaide R F (2003) Fundus autofluorescence and age-related macular degeneration. *Ophthalmology* 110: 392-399.

Sperduto R D (1993) Antioxidant status and neovascular age-related macular degeneration. *Archives of Ophthalmology* 111: 104-109.

Stangos N, Voutas S, Topouzis F, and Karampatakis V (1995) Contrast sensitivity evaluation in eyes predisposed to age-related macular degeneration and presenting normal visual acuity. *Ophthalmologica* 209: 194-198.

Stefansson E, Geirsdottir A, and Sigurdsson H (2011) Metabolic physiology in age related macular degeneration. *Progress in Retinal and Eye Research* 30: 72-80.

Steinmetz R L, Haimovici R, Jubb C, Fitzke F W, and Bird A C (1993) Symptomatic abnormalities of dark adaptation in patients with age-related Bruch's membrane change. *British Journal of Ophthalmology* 77: 549-554.

Steven D M (1946) Relation between dark adaptation and age. *Nature* 157: 376-377.

Stiles W S, and Crawford B H (1932) Equivalent adaptational levels in localized retinal areas. In: Stiles, W S [ed.] *Mechanisms of colour vision: selected papers of W.S.Stiles with a new introductory essay*. London: Academic Press.

Stiles W S, and Crawford B H (1933) The luminous efficiency of rays entering the eye pupil at different points. *Proceedings of the Royal Society of London Series B-Containing Papers of a Biological Character* 112: 428-450.

Stockton R A, and Slaughter M M (1989) B-wave of the electroretinogram. A reflection of ON bipolar cell activity. *Journal of General Physiology* 93: 101-122.

Strauss O (2005) The retinal pigment epithelium in visual function. *Physiological Reviews* 85: 845-881.

Stroud K A (1986) *Further engineering mathematics*. Basingstoke: Palgrave, pp. 953-964.

Sturr J F, Zhang L, Taub H A, Hannon D J, and Jackowski M M (1997) Psychophysical evidence for losses in rod sensitivity in the aging visual system. *Vision Research* 37: 475-481.

Sunness J S, Massof R W, Johnson M A, Finkelstein D, and Fine S L (1985) Peripheral retinal function in age-related macular degeneration. *Archives of Ophthalmology* 103: 811-816.

Sunness J S, Rubin G S, Zuckerbrod A, and Applegate C A (2008) Foveal-Sparing Scotomas in Advanced Dry Age-Related Macular Degeneration. *Journal of Visual Impairment & Blindness* 102: 600-610.

Sutter E E, and Tran D (1992) The field topography of ERG components in man. 1. The photopic luminance response. *Vision Research* 32: 433-446.

Takamine Y, Shiraki K, Moriwaki M, Yasunari T, and Miki T (1998) Retinal sensitivity measurement over drusen using scanning laser ophthalmoscope microperimetry. *Graefes Archive for Clinical and Experimental Ophthalmology* 236: 285-290.

Tamada K, Machida S, Oikawa T, Miyamoto H, Nishimura T, and Kurosaka D (2010) Correlation between Photopic Negative Response of Focal Electroretinograms and Local Loss of Retinal Neurons in Glaucoma. *Current Eye Research* 35: 155-164.

Tan J S L, Wang J J, Flood V, and Mitchell P (2009) Dietary Fatty Acids and the 10-Year Incidence of Age-Related Macular Degeneration The Blue Mountains Eye Study. *Archives of Ophthalmology* 127: 656-665.

Tan J S L, Wang J J, Flood V, Rochtchina E, Smith W, and Mitchell P (2008) Dietary antioxidants and the long-term incidence of age-related macular degeneration - The Blue Mountains Eye Study. *Ophthalmology* 115: 334-341.

Tanner W P, and Swets J A (1954) A decision-making theory of visual detection. *Psychological Review* 61: 401-409.

Taylor M M, and Creelman C D (1967) PEST - efficient estimates on probability functions. *Journal of the Acoustical Society of America* 41: 782-787.

Thomas M M, and Lamb T D (1999) Light adaptation and dark adaptation of human rod photoreceptors measured from the a-wave of the electroretinogram. *Journal of Physiology-London* 518 (Pt 2): 479-496.

Thornton J, Edwards R, Mitchell P, Harrison R A, Buchan I, and Kelly S P (2005) Smoking and age-related macular degeneration: a review of association. *Eye* 19: 935-944.

Ting A Y C, Lee T K M, and MacDonald I M (2009) Genetics of age-related macular degeneration. *Current Opinion in Ophthalmology* 20: 369-376.

Tomany S C, Cruickshanks K J, Klein R, Klein B E K, and Knudtson M D (2004) Sunlight and the 10-year incidence of age-related maculopathy - The Beaver Dam eye study. *Archives of Ophthalmology* 122: 750-757.

Topuz H, Ozdemir M, Cinal A, and Gumusalan Y (2004) Age-related differences in normal corneal topography. *Ophthalmic surgery, lasers & imaging : the official journal of the International Society for Imaging in the Eye*. 35: 298-303.

Tornow R P, Beuel S, and Zrenner E (1997) Modifying a Rodenstock scanning laser ophthalmoscope for imaging densitometry. *Applied Optics* 36: 5621-5629.

Tornow R P, and Stilling R (1998) Variation in sensitivity, absorption and density of the central rod distribution with eccentricity. *Acta Anatomica* 162: 163-168.

Treutwein B (1995) Adaptive psychophysical procedures. *Vision Research* 35: 2503-2522.

United Nations (2009) *Population prospects: 2008 revision* [Online]. Available at: http://www.un.org/esa/population/publications/wpp2008/wpp2008_highlights.pdf [Accessed: 18th July 2011].

van der Pols J C, Bates C J, McGraw P V, Thompson J R, Reacher M, Prentice A, and Finch S (2000) Visual acuity measurements in a national sample of British elderly people. *British Journal of Ophthalmology* 84: 165-170.

VanderBeek B L, Zacks D N, Talwar N, Nan B, Musch D C, and Stein J D (2011) Racial Differences in Age-Related Macular Degeneration Rates in the United States: A Longitudinal Analysis of a Managed Care Network. *American Journal of Ophthalmology* 152: 273-282.

Varma R, Foong A W P, Lai M Y, Choudhury F, Klein R, Azen S P, and Los Angeles Latino Eye Study G (2010) Four-Year Incidence and Progression of Age-Related Macular Degeneration: The Los Angeles Latino Eye Study. *American Journal of Ophthalmology* 149: 741-751.

Virgili G, and Bini A (2007) Laser photocoagulation for neovascular age-related macular degeneration. *Cochrane Database of Systematic Reviews*.

Viswanathan S, Frishman L J, and Robson J G (2000) The uniform field and pattern ERG in macaques with experimental glaucoma: Removal of spiking activity. *Investigative Ophthalmology & Visual Science* 41: 2797-2810.

Viswanathan S, Frishman L J, Robson J G, Harwerth R S, and Smith E L (1999) The photopic negative response of the macaque electroretinogram: Reduction by experimental glaucoma. *Investigative Ophthalmology & Visual Science* 40: 1124-1136.

Viswanathan S, Frishman L J, Robson J G, and Walters J W (2001) The photopic negative response of the flash electroretinogram in primary open angle glaucoma. *Investigative Ophthalmology & Visual Science* 42: 514-522.

vonRuckmann A, Fitzke F W, and Bird A C (1997) Fundus autofluorescence in age-related macular disease imaged with a laser scanning ophthalmoscope. *Investigative Ophthalmology & Visual Science* 38: 478-486.

Wakabayashi K, Gieser J, and Sieving P A (1988) Aspartate separation of the scotopic threshold response (STR) from the photoreceptor a-wave of the cat and monkey ERG. *Investigative Ophthalmology & Visual Science* 29: 1615-1622.

Wald G, and Clark A B (1937) Visual adaptation and chemistry of the rods. *Journal of General Physiology* 21: 93-105.

Walter P, Widder R A, Luke C, Konigsfeld P, and Brunner R (1999) Electrophysiological abnormalities in age-related macular degeneration. *Graefes Archive for Clinical and Experimental Ophthalmology* 237: 962-968.

Wang J S, and Kefalov V J (2009) An alternative pathway mediates the mouse and human cone visual cycle. *Current Biology* 19: 1665-1669.

Wang J S, and Kefalov V J (2011) The cone-specific visual cycle. *Progress in Retinal Eye Research* 30: 115-128.

Wang Y, Wang V M, and Chan C C (2011) The role of anti-inflammatory agents in age-related macular degeneration (AMD) treatment. *Eye* 25: 127-139.

Wangsa-Wirawan N D, and Linsenmeier R A (2003) Retinal oxygen - Fundamental and clinical aspects. *Archives of Ophthalmology* 121: 547-557.

Weale R A (1963) *The ageing eye*. London: H. K. Lewis.

Weisinger H S, Vingrys A J, and Sinclair A J (1996) Electrodiagnostic methods in vision. Part 1: Clinical application and measurement. *Clinical and Experimental Optometry* 79: 50-61.

West S K, Munoz B, Rubin G S, Schein O D, Bandeen-Roche K, Zeger S, German S et al. (1997) Function and visual impairment in a population-based study of older adults. The SEE project. Salisbury Eye Evaluation. *Investigative Ophthalmology and Visual Science* 38: 72-82.

Winsor C P, and Clark A B (1936) Dark adaptation after varying degrees of light adaptation. *Proceedings of the National Academy of Sciences of the United States of America* 22: 400-404.

Witkovsky P, Nelson J, and Ripps H (1973) Action spectra and adaptation properties of carp photoreceptors. *Journal of General Physiology* 61: 401-423.

Wolf E, and Zigler M J (1950) Dark adaptation level and size of testfield. *Journal of the Optical Society of America* 40: 211-218.

Wolf G (2003) Lipofuscin and macular degeneration. *Nutrition Reviews* 61: 342-346.

Wolffsohn J S, Anderson S J, Mitchell J, Woodcock A, Rubinstein M, Ffytche T, Browning A et al. (2006) Effect of age related macular degeneration on the Eger macular stressometer photostress recovery time. *British Journal of Ophthalmology* 90: 432-434.

Wong T Y, Chakravarthy U, Klein R, Mitchell P, Zlateva G, Buggage R, Fahrback K et al. (2008) The natural history and prognosis of neovascular age-related macular degeneration: a systematic review of the literature and meta-analysis. *Ophthalmology* 115: 116-126.

Wood A, Binns A, Margrain T, Drexler W, Povazay B, Esmaelpour M, and Sheen N (2011a) Retinal and Choroidal Thickness in Early Age-Related Macular Degeneration. *American Journal of Ophthalmology* 152: 1030-1038.

Wood A, Margrain T, and Binns A (2011b) The effect of bleach duration and age on the ERG photostress test. *Graefes Archive for Clinical and Experimental Ophthalmology* 249: 1359-1365.

Wu G, Weiter J J, Santos S, Ginsburg L, and Villalobos R (1990) The macular photostress test in diabetic retinopathy and age-related macular degeneration. *Archives of Ophthalmology* 108: 1556-1558.

Wyszecki G, and Stiles W S (1982) *Color Science: Concepts and Methods, Quantitative Data and Formulae*. 2nd ed. New York: John Wiley & Sons, Inc.

Xu X, and Karwoski C J (1994) Current source density analysis of retinal field potentials. II. Pharmacological analysis of the b-wave and M-wave. *Journal of Neurophysiology* 72: 96-105.

Yannuzzi L A (2011) Indocyanine Green Angiography: A Perspective on Use in the Clinical Setting. *American Journal of Ophthalmology* 151: 745-751.

Yasuda M, Kiyohara Y, Hata Y, Arakawa S, Yonemoto K, Doi Y, Iida M et al. (2009) Nine-Year Incidence and Risk Factors for Age-Related Macular Degeneration in a Defined Japanese Population The Hisayama Study. *Ophthalmology* 116: 2135-2140.

Yasuno Y, Miura M, Kawana K, Makita S, Sato M, Okamoto F, Yamanari M et al. (2009) Visualization of Sub-retinal Pigment Epithelium Morphologies of Exudative Macular Diseases by High-Penetration Optical Coherence Tomography. *Investigative Ophthalmology & Visual Science* 50: 405-413.

Yehoshua Z, Wang F H, Rosenfeld P J, Penha F M, Feuer W J, and Gregori G (2011) Natural History of Drusen Morphology in Age-Related Macular Degeneration Using Spectral Domain Optical Coherence Tomography. *Ophthalmology* 118: 2434-2441.

Young R W (1969) A difference between rods and cones in the renewal of outer segment protein. *Investigative Ophthalmology* 8: 222-231.

Young R W (1970) Visual cells. *Scientific American* 223: 80-91.

Zarbin M A (2004) Current concepts in the pathogenesis of age-related macular degeneration. *Archives of Ophthalmology* 122: 598-614.

Zayit-Soudry S, Moroz I, and Loewenstein A (2007) Retinal pigment epithelial detachment. *Survey of Ophthalmology* 52: 227-243.

Zhou J L, Jang Y P, Kim S R, and Sparrow J R (2006) Complement activation by photooxidation products of A2E, a lipofuscin constituent of the retinal pigment epithelium. *Proceedings of the National Academy of Sciences of the United States of America* 103: 16182-16187.

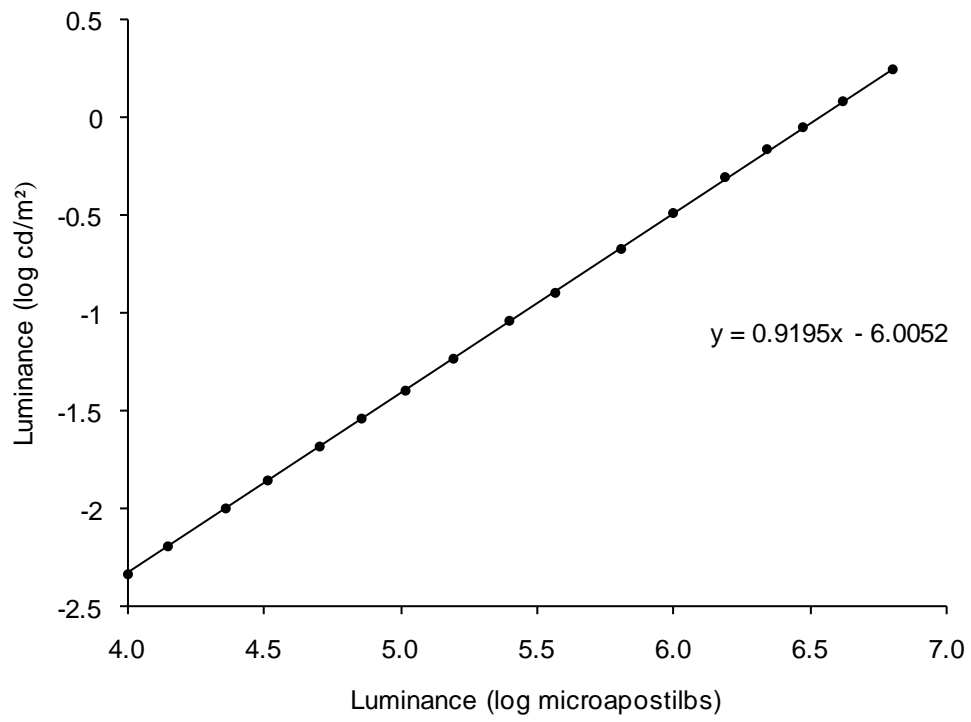
Zweifel S A, Imamura Y, Spaide T C, Fujiwara T, and Spaide R F (2010) Prevalence and Significance of Subretinal Drusenoid Deposits (Reticular Pseudodrusen) in Age-Related Macular Degeneration. *Ophthalmology* 117: 1775-1781.

Appendix I. Calibration of the Goldmann-Weekers adaptometer

Luminance of the stimulus presented by the Goldmann-Weekers adaptometer calibrated using a photometer (LS-110; Konica Minolta, Osaka, Japan)

Luminance (log microapostilbs)	Measured luminance (average of 3)	
	(cd/m²)	(log cd/m²)
6.80	1.762	0.24
6.62	1.202	0.08
6.47	0.893	-0.05
6.34	0.682	-0.17
6.19	0.494	-0.31
6.00	0.327	-0.48
5.81	0.211	-0.68
5.57	0.128	-0.89
5.40	0.091	-1.04
5.19	0.059	-1.22
5.02	0.040	-1.40
4.86	0.029	-1.54
4.71	0.021	-1.68
4.51	0.014	-1.85
4.36	0.010	-2.00
4.14	0.006	-1.19
4.00	0.005	-2.33

Measured luminance of the stimulus presented by the Goldmann-Weekers adaptometer (log cd/m²) plotted as a function of presented luminance (log microapostilbs).



Appendix II. Matlab code for psychophysical dark adaptation programs

Hybrid adaptive procedure

```

clearall
KbName('UnifyKeyNames');
%The Try, Catch, End commands will respond to bugs / problems
try
%First set up all the parameters
whichScreen = 0;
window = Screen(whichScreen, 'OpenWindow');
white = WhiteIndex(window); % pixel value for white
black = BlackIndex(window); % pixel value for black
gray = (white+black)/2;
inc = white-gray;

% And, set the parameters of the spot
offsetCenteredspotRect = [569 441 711 583]; %size and position of spot
SurroundRectInner = [498 370 782 654]; % size and position of annulus
SurroundRectOuter = [496 368 784 656];

% Set up the sounds for correct and incorrect responses
correctSound = sin(2*pi*100*[0:0.00125:2.0]);
incorrectSound = sin(2*pi*40*[0:0.00125:2.0]);
NewFilterSound = sin (2*pi*200*[0:0.00125:10.0]);

% Set up various flags
response = 0;
responseCounter = 0;
reversalCounter = 1;% counts reversals (reset after each threshold)
DarkAdptCounter = 0; % counts number of thresholds recorded
presentationCounter = 0;
dataCounter=1;% counts ALL reversals
AdjustmentFilter1 = 1.2;% optical density of first ND filter
AdjustmentFilter2 = 0;% optical density of second ND filter

% Clear arrays that contain data
SecondNDFilterFlag = 0; % flag to stop luminance being raised if the spot
luminance hits it's lowest level a second time after 2nd filter added)
BreakFlag = 0;
resultTime = 1;
resultThreshold = 1;
resultSeenOrNot = 1;
resultsDetails = [0 00];

% Set keys up.
rightKey = KbName('RightArrow');
leftKey = KbName('LeftArrow');
escapeKey = KbName('ESCAPE');

% This screen can be used to write instructions
Screen(window, 'FillRect', 0);
Screen('DrawText', window, 'DARK ADAPTATION VERSION 30/09/10', 300, 200, white);
Screen('DrawText', window, 'Hit any key to start experiment', 300, 400, white);
Screen(window, 'Flip');
Kbwait;% duration of instruction presentation

% Set up the timer.

```

```

startTime = now;
durationInSeconds = 300;
durationEachThreshold = 1;
numberOfSecondsRemaining = durationInSeconds;
SecondsRemaining = durationEachThreshold;

%Calibration variables
MinScreenLum = 0.12; % Kept contrast = 100 & brightness = 63
GammaFunc = 2.15;
MaxScreenLum = 122.5;

% Now start the experiment loop.
fprintf('Experiment started'),
StartExptSecs = GetSecs; % this times the whole experiment

while GetSecs - StartExptSecs < durationInSeconds % Keep experiment running

% Set up flags etc to re enter the threshold loop
stopRule = 1; % keeps loop running till stop rules met, then =0
stopRuleCounter1 = 0; % reset threshold loop depending on presentations
stopRuleCounter2 = 0; % reset threshold loop depending on reversals
lastFlag = 0; % used to determine if a reversal was present
thisFlag = 0;

while stopRule > 0 % Keep experiment running
stopRuleCounter1 = stopRuleCounter1 + 1; % for stopRule 1

GammaCorrectSpotLum = 255 * ((10^SpotLuminance) -
MinScreenLum) / (MaxScreenLum)^(1/GammaFunc)

Screen('DrawText', window, ['GammaCorr: ' num2str(GammaCorrectSpotLum,4)], 1020,
1000, [0,0,40]);

% Present stimulus
Screen('DrawLine', window, [white], 640, 335, 640, 689,18);
Screen('DrawLine', window, [white], 463, 512, 817, 512,18);
Screen('FillOval', window, [0 00], SurroundRectInner);
Screen('FillOval', window,
[GammaCorrectSpotLum GammaCorrectSpotLum GammaCorrectSpotLum],
offsetCenteredSpotRect);
Screen(window, 'Flip');
WaitSecs (0.2); % presentation time

% Remove stimulus
Screen('DrawLine', window, [white], 640, 335, 640, 689,18);
Screen('DrawLine', window, [white], 463, 512, 817, 512,18);
Screen('FillOval', window, [0 00], SurroundRectInner);
Screen('DrawText', window, ['GammaCorr: ' num2str(GammaCorrectSpotLum,4)], 1020,
1000, [0,0,40]);
Screen(window, 'Flip');
ResponseSecs = GetSecs;

% Wait for a response
while 1
[ keyIsDown, timeSecs, keyCode ] = KbCheck;
if keyIsDown

if keyCode(escapeKey) % exit loop
BreakFlag=1;
break
end
if (timeSecs - ResponseSecs) < 0.6;
response = 1; % correct response
responseCounter = responseCounter + 1;
else
response = -1; % incorrect response (too slow)
responseCounter = responseCounter - 1;

```

```

sound (incorrectSound)
break
end

whileKbCheck; end% this avoids KbCheck reporting multiple events
break
end

% Now, if no button push + long wait, time is up!
SecsNow = GetSecs;
timeSincePresentation = (SecsNow - ResponseSecs);
iftimeSincePresentation > 1+rand(1);
response = -1; % incorrect response (missed)
responseCounter = responseCounter - 1;
break
end
end

ifBreakFlag==1 % exit loop
break
end

%Now adjust next stimulus increment on the basis of the response
if response > 0;% correct
sound(correctSound)
thisFlag = 1;% flag for reversal checking
ifresponseCounter> 1; % correct twice
incrementStep = incrementStep*2;
end
WaitSecs (0.5 + rand(1))
end

if response < 0;% incorrect
thisFlag = 0;% flag for reversal checking
ifresponseCounter< -1; % incorrect twice
incrementStep = incrementStep*2;

%Now limit max step size
ifincrementStep>0.5
incrementStep =0.5;
end
end
end

%Now record each presentation.
presentationCounter = presentationCounter + 1;
presentationTime(presentationCounter)= (GetSecs - StartExptSecs);
presentationThreshold(presentationCounter)=SpotLuminance-AdjustmentFilter1-
AdjustmentFilter2;

%Now check if the last response was a reversal
iflastFlag == thisFlag; %this was not a reversal

else % this must have been a reversal
resultTime (reversalCounter) = (GetSecs - StartExptSecs);
resultThreshold (reversalCounter) = SpotLuminance-AdjustmentFilter1-
AdjustmentFilter2;
resultSeenOrNot (reversalCounter) = thisFlag;
reversalCounter = reversalCounter + 1;

%Now log all the reversals
reversalThreshold(dataCounter) = SpotLuminance-AdjustmentFilter1-
AdjustmentFilter2;
reversalTime(dataCounter)=(GetSecs - StartExptSecs);
dataCounter = dataCounter+1;
incrementStep = incrementStep * 0.6;
ifincrementStep<0.07

```

```

incrementStep=0.07;
end

response = 0; % reset response flag
responseCounter = 0; %reset response counter
stopRuleCounter2 = stopRuleCounter2 +1;

end

% Now alter stimulus for next presentation
ifthisFlag == 1;
SpotLuminance =SpotLuminance - incrementStep;
End

ifthisFlag == 0;
SpotLuminance = SpotLuminance + incrementStep;
%Now limit max spot luminance
ifSpotLuminance > 2.0
SpotLuminance = 2.0; %limits maximum spot luminance
end
end

% Now reset the stimulus intensity when the minimum luminance is reached
ifSpotLuminance < -0.9;
sound (NewFilterSound) % insert new filter
AdjustmentFilter2 = 2.1;
LineThickness = 10;
ifSecondNDFilterFlag < 1
WaitSecs (5.0)
SpotLuminance = 1.1; % resets stimulus intensity to the maximum brightness
SecondNDFilterFlag = 2;
end
end

lastFlag = thisFlag;

% Now see if stopRule needs to be evoked
if stopRuleCounter1 >12
stopRule = 0;%this will stop the threshold loop
end
if stopRuleCounter2 >5
stopRule = 0;
end

end% this ends the search for a threshold
beep

ifBreakFlag==1 % exit loop
break
end

% Now display the results
resultTime = resultTime(:);% changes format to column vectors
resultThreshold = resultThreshold(:);
resultSeenOrNot = resultSeenOrNot(:);
plot(resultTime, resultThreshold,':ko')
hold on
plot(presentationTime, presentationThreshold,'b*')
xlabel('Time(s)')
ylabel('Log Threshold')
AXIS ([0 300 -1.5 2.5])

% Now, together with the function 'myfit' fits a FOC curve.
DarkAdptCounter = DarkAdptCounter + 1;
thresholdEstimate = 10.^(mean (resultThreshold));% this estimates threshold
Starting = [thresholdEstimate,27];
options=optimset('Display','off');% if set 'off' to 'iter' will see iterations

```

```

resultThresholdNotLog = 10.^(resultThreshold);

Estimates=fminsearch(@myfitWeibull,Starting,options,resultThresholdNotLog,resultS
eenOrNot);
alpha(DarkAdptCounter) = Estimates(1);
beta(DarkAdptCounter) = Estimates(2);
% Now determine threshold at 50% probability
FOCThresholdNotLog(DarkAdptCounter) =
log(2).^(1./beta(DarkAdptCounter))*alpha(DarkAdptCounter);
DarkAdptTime(DarkAdptCounter) = (GetSecs - StartExptSecs);
plot(DarkAdptTime, log10(FOCThresholdNotLog), 'ro', 'MarkerFaceColor', 'r')

% Clear resultThreshold,resultSeenOrNot arrays in preparation for next loop
resultTime = 1;
resultThreshold = 1;
resultSeenOrNot = 1;
resultsDetails = [0 00];
reversalCounter = 1;

% Now adjust spot parameters for next threshold measurement
incrementStep = incrementStep * 2.5;
SpotLuminance = SpotLuminance * 0.8;
end% Now go back and collect data for the next threshold point

%Now fit the final exponential curve
Starting = [1.2,5,40];
options=optimset('Display','off');% if set 'off' to 'iter' will see iterations
logFOCThreshold=log10(FOCThresholdNotLog);
Estimates=fminsearch(@myfitExp,Starting,options,DarkAdptTime,logFOCThreshold);
fT = Estimates(1)
iT = Estimates(2)
Tau = Estimates(3)
% Now plot this curve
ExpFitTime = 0:2.0:300;% now create some x-axis data at 1.0 steps
ExpFitThreshold = Estimates(1)+((Estimates(2)-Estimates(1))*exp(-
ExpFitTime./Estimates(3)));
plot(ExpFitTime, ExpFitThreshold, 'r-', 'LineWidth',2)

Screen('CloseAll');

%Now output all the data to Excel spreadsheet
presentationTime = presentationTime(:);
presentationThreshold = presentationThreshold(:);
presentationData = [presentationTime, presentationThreshold]
reversalTime = reversalTime(:);
reversalThreshold = reversalThreshold(:);
reversalData = [reversalTime, reversalThreshold]
logFOCThreshold = log10(FOCThresholdNotLog);
logFOCThreshold = logFOCThreshold(:);
DarkAdptTime = DarkAdptTime(:);
FOCData = [DarkAdptTime, logFOCThreshold]
ExpFitTime = ExpFitTime(:);
ExpFitThreshold = ExpFitThreshold(:);
curveFit = [ExpFitTime, ExpFitThreshold]
xlswrite('d:\Repeatability\Data\Results\TopographyDAresults.xls',
presentationData, 'Model', 'A14');
xlswrite('d:\Repeatability\Data\Results\TopographyDAresults.xls',
reversalData, 'Model', 'D14');
xlswrite('d:\Repeatability\Data\Results\TopographyDAresults.xls',
FOCData, 'Model', 'K14');
catch
Screen('CloseAll');
rethrow(lasterror);
psychrethrow(psychlasterror);
end

```

Modified staircase procedure

```

clearall
KbName('UnifyKeyNames');
%The Try, Catch, End commands will respond to bugs / problems
try
%First set up all the parameters
whichScreen = 0;
window = Screen(whichScreen, 'OpenWindow');
white = WhiteIndex(window); % pixel value for white
black = BlackIndex(window); % pixel value for black
gray = (white+black)/2;
inc = white-gray;

% And, set the parameters of the spot
offsetCenteredspotRect = [569 441 711 583]; %size and position of spot
SurroundRectInner = [498 370 782 654]; % size and position of annulus
SurroundRectOuter = [496 368 784 656];

% Set up the sounds for correct and incorrect responses
correctSound = sin(2*pi*100*[0:0.00125:2.0]);
incorrectSound = sin(2*pi*40*[0:0.00125:2.0]);
NewFilterSound = sin(2*pi*200*[0:0.00125:10.0]);

% Set up various flags
response = 0;
responseCounter = 0;
reversalCounter = 1;% counts reversals (reset after each threshold)
DarkAdptCounter = 0; % counts the number thresholds recorded
presentationCounter = 1; % counts all presentations
dataCounter=1;% counts ALL reversals
thresholdCounter = 1;% counts the no. of threshold points
AdjustmentFilter1 = 1.2;% optical density of first ND filter
AdjustmentFilter2 = 0;% optical density of second ND filter

% Clear arrays that contain data
SecondNDFilterFlag = 0; % flag to stop luminance being raised if the spot
luminance hits it's
lowest level a second time (after the 2nd filter added)
resultTime = 1;
resultThreshold = 1;
BreakFlag = 0;

% Set keys up.
rightKey = KbName('RightArrow');
leftKey = KbName('LeftArrow');
escapeKey = KbName('ESCAPE');

% This screen can be used to write instructions
Screen(window, 'FillRect', 0);
Screen('DrawText', window, 'DARK ADAPTATION VERSION 30/09/10', 300, 200, white);
Screen('DrawText', window, 'Hit any key to start experiment', 300, 400, white);
Screen(window, 'Flip');
Kbwait;% duration of instruction presentation

% Set up the timer.
startTime = now;
durationInSeconds = 300;
durationEachThreshold = 1;
numberOfSecondsRemaining = durationInSeconds;
SecondsRemaining = durationEachThreshold;

%Calibration variables
MinScreenLum = 0.12; % Kept contrast = 100 & brightness = 63
GammaFunc = 2.15;
MaxScreenLum = 122.5;

```

```

% Now start the experiment loop.
fprintf('Experiment started'),
StartExptSecs = GetSecs; % this times the whole experiment

while GetSecs - StartExptSecs < durationInSeconds % Keep experiment running

% Set up flags etc to re enter the threshold loop
stopRule = 1; % keeps loop running till stop rules met, then = 0

while stopRule > 0 % Keep looking for threshold

GammaCorrectSpotLum = 255 * ((10^SpotLuminance) -
MinScreenLum) / (MaxScreenLum - 1) / GammaFunc
% This calculates the grey scale required for desired luminance

Screen('DrawText', window, ['GammaCorr: ' num2str(GammaCorrectSpotLum, 4)], 1020,
1000, [0, 0, 40]);

% Present stimulus
Screen('DrawLine', window, [white], 640, 335, 640, 689, 18);
Screen('DrawLine', window, [white], 463, 512, 817, 512, 18);
Screen('FillOval', window, [0 0], SurroundRectInner);
Screen('FillOval', window, [GammaCorrectSpotLum GammaCorrectSpotLum
GammaCorrectSpotLum], offsetCenteredSpotRect);
Screen(window, 'Flip');
WaitSecs (0.2); % presentation time

% Remove stimulus
Screen('DrawLine', window, [white], 640, 335, 640, 689, 18);
Screen('DrawLine', window, [white], 463, 512, 817, 512, 18);
Screen('FillOval', window, [0 0], SurroundRectInner);
Screen('DrawText', window, ['GammaCorr: ' num2str(GammaCorrectSpotLum, 4)], 1020,
1000, [0, 0, 40]);
Screen(window, 'Flip');
ResponseSecs = GetSecs;

% Wait for a response
while 1
[ keyIsDown, timeSecs, keyCode ] = KbCheck;
if keyIsDown

if keyCode(escapeKey) % exit loop
BreakFlag = 1;
break
end

if (timeSecs - ResponseSecs) < 0.6;
response = 1; % correct response
sound(correctSound)
else
response = -1; % incorrect response (too slow)
sound(incorrectSound)
break
end

while KbCheck; end % avoids KbCheck noting mutile events
break
end

% Now, if no button push + long wait, time is up!
SecsNow = GetSecs;
timeSincePresentation = (SecsNow - ResponseSecs);
if timeSincePresentation > 1 + rand(1);
response = -1; % incorrect response (missed)
break
end

```

```

end

ifBreakFlag==1% exit loop
break
end

%Now record each presentation.
presentationTime(presentationCounter)= (GetSecs - StartExptSecs);
presentationThreshold(presentationCounter)= SpotLuminance-AdjustmentFilter1-
AdjustmentFilter2;
presentationCounter = presentationCounter + 1;

%Now adjust next stimulus increment on the basis of the response
if response > 0;% correct

ifincrementStep > 0.0; % luminance increased = threshold
resultTime (thresholdCounter) = (GetSecs - StartExptSecs);
resultThreshold (thresholdCounter) = SpotLuminance-AdjustmentFilter1-
AdjustmentFilter2;
thresholdCounter = thresholdCounter + 1;
stopRule = -1;
end

incrementStep = -0.3;% next increment = 0.3 log unit decrease
WaitSecs (0.5 + rand(1.5))
end

if response < 0;% incorrect
incrementStep = 0.1;
WaitSecs (rand(1.0))
end

% Now alter stimulus for next presentation
SpotLuminance = SpotLuminance + incrementStep;
ifSpotLuminance > 2
SpotLuminance = 2;
end

% Now reset stimulus intensity when minimum luminance reached
ifSpotLuminance < -0.9;
sound (NewFilterSound) % insert a new filter
AdjustmentFilter2 = 2.1;
LineThickness = 10;
ifSecondNDFilterFlag < 1
WaitSecs (5.0)
SpotLuminance = 1.1; % intensity reset to maximum brightness
SecondNDFilterFlag = 2;
end
end

end% ends search for a threshold
beep

ifBreakFlag==1 % exit loop
break
end

end% Returns to collect data for the next threshold point

% Now display the results
presentationTime = presentationTime (:);% converts row to column
presentationThreshold = presentationThreshold (:); %converts to column
plot(presentationTime, presentationThreshold, 'b*')%plots every presentation
xlabel('Time(s)')
ylabel('Log Threshold')
AXIS ([0 300 -1.5 2.5])

```

```

hold on

resultTime = resultTime(:);% changes format to column vectors
resultThreshold = resultThreshold(:);
plot(resultTime, resultThreshold,':ko')% plots the thresholds

%Now fit the final exponential curve
Starting = [1.2,5,40];
options=optimset('Display','off');% if set 'off' to 'iter' will see iterations
Estimates=fminsearch(@myfitExp,Starting,options,resultTime,resultThreshold);
fT = Estimates(1)
iT = Estimates(2)
Tau = Estimates(3)
% Now plot this curve
ExpFitTime = 0:2.0:300;% now create some x-axis data at 1.0 steps
ExpFitThreshold = Estimates(1)+((Estimates(2)-
Estimates(1))*exp(ExpFitTime./Estimates(3)));
plot(ExpFitTime, ExpFitThreshold,'r-','LineWidth',2)

Screen('CloseAll');

%Now output all the data to Excel spreadsheet
presentationData = [presentationTime, presentationThreshold]
thresholdData = [resultTime, resultThreshold]
ExpFitTime = ExpFitTime(:);
ExpFitThreshold = ExpFitThreshold(:);
curveFit = [ExpFitTime, ExpFitThreshold]
xlswrite('d:\Repeatability\Data\Results\TopographyDAresults.xls',
presentationData,'Model','A14');
xlswrite('d:\Repeatability\Data\Results\TopographyDAresults.xls',
thresholdData,'Model','D14');
catch
Screen('CloseAll');
rethrow(lasterror);
psychrethrow(psychlasterror);
end

```

10-alternative forced choice procedure

```

clearall
KbName('UnifyKeyNames');

try%The Try, Catch, End commands will respond to bugs / problems
%First set up all the parameters
whichScreen = 0;
window = Screen(whichScreen, 'OpenWindow');
white = WhiteIndex(window); % pixel value for white
black = BlackIndex(window); % pixel value for black
gray = (white+black)/2;
inc = white-gray;

% And, set the parameters of the spot
offsetCenteredspotRect = [569 441 711 583]; %size and position of
SurroundRectInner = [498 370 782 654]; % size and position of annulus
SurroundRectOuter = [496 368 784 656];

% Set up the sounds for correct and incorrect responses
correctSound = sin(2*pi*70*[0:0.00125:2.0]);
incorrectSound = sin(2*pi*30*[0:0.00125:2.0]);
presentationSound = sin(2*pi*50*[0:0.00125:3.0]);
NewFilterSound = sin(2*pi*200*[0:0.00125:10.0]);

% Set up various flags
response = 0;

```

```

responseCounter = 0;
reversalCounter = 1;% counts reversals (reset after each threshold)
DarkAdptCounter = 0; % counts the number of thresholds recorded.
presentationCounter=1; %counts all presentations
dataCounter = 1;% counts ALL reversals
thresholdCounter = 1;% counts the no. of threshold points
AdjustmentFilter1 = 1.2;% optical density of first ND filter
AdjustmentFilter2 = 0;% optical density of second ND filter

% Clear arrays that contain data
SecondNDFilterFlag = 0; % flag to stop luminance being raised if the spot
luminance hits it's lowest level a second time (after the 2nd ND filter added)
resultTime = 1;
resultThreshold = 1;
BreakFlag = 0;

% Set keys up.
rightKey = KbName('RightArrow');
leftKey = KbName('LeftArrow');
escapeKey = KbName('ESCAPE');

% This screen can be used to write instructions
Screen(window, 'FillRect', 0);
Screen('DrawText', window, 'DARK ADAPTATION VERSION 30/09/10', 300, 200, white);
Screen('DrawText', window, 'Hit any key to start experiment', 300, 400, white);
Screen(window, 'Flip');
Kbwait;% duration of instruction presentation

% Set up the timer.
startTime = now;
durationInSeconds = 300;
durationEachThreshold = 1;
numberOfSecondsRemaining = durationInSeconds;
SecondsRemaining = durationEachThreshold;

%Calibration variables
MinScreenLum = 0.12; % Kept contrast = 100 & brightness = 63
GammaFunc = 2.15;
MaxScreenLum = 122.5;

% Now start the experiment loop.
fprintf('Experiment started'),
StartExptSecs = GetSecs; % this times the whole experiment
WaitSecs (0.5);

whileGetSecs - StartExptSecs<durationInSeconds% Keep experiment running

stopRule = 1;%keeps loop running till stop rules met, then =0

RandomNumber = 9*rand; % random number 0 to 1
PresentationNumber = round(RandomNumber); % returns integer between 1-10
sound(presentationSound)
WaitSecs (0.2); % allow 200ms before presentation

GammaCorrectSpotLum = 255*((10^SpotLuminance)-
MinScreenLum)/MaxScreenLum)^(1/GammaFunc);

Screen('DrawText', window, ['GammaCorr: ' num2str(GammaCorrectSpotLum,4)], 1020,
1000, [0,0,40]);

% Present stimulus
Screen('TextFont',window, 'Ariel');
Screen('TextSize', window, 156);
Screen('DrawLine', window, [white], 640, 335, 640, 689,18);
Screen('DrawLine', window, [white], 463, 512, 817, 512,18);
Screen('FillOval', window, [0 00], SurroundRectInner);

```

```

Screen('DrawText', window, num2str(PresentationNumber),580, 395,
[GammaCorrectSpotLumGammaCorrectSpotLumGammaCorrectSpotLum]);
Screen(window, 'Flip');
WaitSecs (0.2); % presentation time

%Remove stimulus
Screen('DrawLine', window, [white], 640, 335, 640, 689,18);
Screen('DrawLine', window, [white], 463, 512, 817, 512,18);
Screen('FillOval', window, [0 00], SurroundRectInner);
Screen('DrawText', window, ['GammaCorr: ' num2str(GammaCorrectSpotLum,4)], 1020,
1000, [0,0,40]);
Screen(window, 'Flip');
ResponseSecs = GetSecs;

% record time of presentation
presentationTime(presentationCounter)= (GetSecs - StartExptSecs);
presentationThreshold(presentationCounter)= SpotLuminance-AdjustmentFilter1-
AdjustmentFilter2;

% Wait for a response from keyboard
escapeKey = KbName('ESCAPE');
whileKbCheck; end% Wait until all keys are released.

while 1
% Check the state of the keyboard.
[ keyIsDown, seconds, keyCode ] = KbCheck;
% If key is pressed, display its code number and name.
ifkeyIsDown

ifkeyCode(escapeKey)% exit loop
BreakFlag = 1;
break
end

whileKbCheck; end
break
end
end

UserResponse = find(keyCode);% 'keyCode' is a big array, the 'find' command gets
the keys number e.g. 1=49
ifPresentationNumber==(UserResponse-48) % i.e. correct response
sound(correctSound)
response = 1; % correct response
incrementStep = -0.3;
%next lines record a 'threshold'
resultTime (thresholdCounter) = presentationTime(presentationCounter);
resultThreshold (thresholdCounter) = SpotLuminance-AdjustmentFilter1-
AdjustmentFilter2;;
thresholdCounter = thresholdCounter + 1;
else
sound (incorrectSound)
response = -1; % incorrect response
incrementStep = 0.1;
end

presentationCounter = presentationCounter + 1;

% Now alter stimulus for next presentation
SpotLuminance = SpotLuminance + incrementStep;
ifSpotLuminance > 2
SpotLuminance = 2;
end

% Now reset stimulus intensity when minimumluminance reached
ifSpotLuminance < -0.9;
sound (NewFilterSound) % insert a new filter

```

```

AdjustmentFilter2 = 2.1;
LineThickness = 10;
ifSecondNDFilterFlag < 1
WaitSecs (5.0)
SpotLuminance = 1.1; % intensity reset to maximum brightness
SecondNDFilterFlag = 2;
end
end

WaitSecs (1);

ifBreakFlag==1 % exit loop
break
end

end% Returns to collect data for the next threshold point

% Now display the results
presentationTime = presentationTime (:);% converts row to column
presentationThreshold = presentationThreshold (:); %converts row to column
plot(presentationTime, presentationThreshold, 'b*')% plots every presentation
xlabel('Time(s)')
ylabel('Log Threshold')
AXIS ([0 300 -1.5 2.5])
Hold on

resultTime = resultTime(:);% changes format to column vectors
resultThreshold = resultThreshold(:);
plot(resultTime, resultThreshold, ':ko')% plots the thresholds

%Now fit the final exponential curve
Starting = [1.2,5,40];
options=optimset('Display','off');% if set 'off' to 'iter' will see iterations
Estimates=fminsearch(@myfitExp,Starting,options,resultTime,resultThreshold);
fT = Estimates(1)
iT = Estimates(2)
Tau = Estimates(3)
% Now plot this curve
ExpFitTime = 0:2.0:300;% now create some x-axis data at 1.0 steps
ExpFitThreshold = Estimates(1)+((Estimates(2)-Estimates(1))*exp(-
ExpFitTime./Estimates(3)));
plot(ExpFitTime, ExpFitThreshold, 'r-', 'LineWidth', 2)

Screen('CloseAll');

%Now output all the data to Excel spreadsheet
presentationData = [presentationTime, presentationThreshold]
thresholdData = [resultTime, resultThreshold]
ExpFitTime = ExpFitTime(:);
ExpFitThreshold = ExpFitThreshold(:);
curveFit = [ExpFitTime, ExpFitThreshold]
xlswrite('d:\Repeatability\Data\Results\TopographyDAresults.xls',
presentationData, 'Model', 'A14');
xlswrite('d:\Repeatability\Data\Results\TopographyDAresults.xls',
thresholdData, 'Model', 'D14');
catch
Screen('CloseAll');
rethrow(lasterror);
psychrethrow(psychlasterror);
end

```

Retinal eccentricity procedure

```

clearall

% Input co ordinates and sizes for cross and spot
HorizontalLocation = input('Horizontal location in degrees? ');
VerticalLocation = input('Vertical location in degrees? ');
SpotSize = input('Spot size in degrees?')*17.5; % size of spot in pixels
ifSpotSize < 9*17.5; OutsideLineSize=100; InsideLineSize=40; end
ifSpotSize > 9*17.5; OutsideLineSize=0; InsideLineSize=175; end
LineThickness = 4; % thickness of the fixation cross
LineSize = SpotSize+OutsideLineSize; % length of the cross in pixels
InnerLineSize = SpotSize-InsideLineSize;
% NOTE assumes a 55 cm viewing distance!

KbName('UnifyKeyNames');
% The Try, Catch, End commands will respond to bugs / problems
try
% First set up all the parameters
whichScreen = 0;
window = Screen(whichScreen, 'OpenWindow');
white = WhiteIndex(window); % pixel value for white
black = BlackIndex(window); % pixel value for black
gray = (white+black)/2;
inc = white-gray;

% And, set the parameters of the spot
offsetCenteredspotRect = [640-SpotSize 512-SpotSize 640+SpotSize 512+SpotSize];
offsetCenteredspotRect2 = [640-SpotSize+17.5 512-SpotSize+17.5 640+SpotSize-17.5
512+SpotSize-17.5];
SurroundRectInner = [640-SpotSize-10 512-SpotSize-10 640+SpotSize+10
512+SpotSize+10]; % size and position of annulus
SurroundRectOuter = [496 368 784 656];

% Set up the sounds for correct/incorrect responses and to indicate that new ND
filter is required
correctSound = sin(2*pi*100*[0:0.00125:2.0]);
incorrectSound = sin(2*pi*40*[0:0.00125:2.0]);
NewFilterSound = sin (2*pi*200*[0:0.00125:10.0]);

% Set up various flags
response = 0;
responseCounter = 0;
reversalCounter = 1;% counts reversals (reset after each threshold)
DarkAdptCounter = 0; % counts the number of thresholds recorded
presentationCounter = 1; % counts all presentations
dataCounter = 1;% counts ALL reversals
thresholdCounter = 1;% counts no. of threshold points
AdjustmentFilter1 = 1.2;% optical density of first ND filter
AdjustmentFilter2 = 0;% optical density of second ND filter

% Clear arrays that contain data
SecondNDFilterFlag = 0; % flag to stop luminance being raised if spot luminance
hits it's lowest level a second time (after ND filterhas been added)
resultTime = 1;
resultThreshold = 1;
BreakFlag = 0;

% Set keys up.
rightKey = KbName('RightArrow');
leftKey = KbName('LeftArrow');
escapeKey = KbName('ESCAPE');

% This screen can be used to write instructions
Screen(window, 'FillRect', 0);
Screen('DrawText', window, 'DARK ADAPTATION VERSION 6/5/10', 300, 200, white);

```

```

Screen('DrawText', window, 'Hit any key to start experiment', 300, 400, white);
Screen(window, 'Flip');
Kbwait;% duration of instruction presentation

% Set up the timer.
startTime = now;
durationInSeconds = 1500;
durationEachThreshold = 1;
numberOfSecondsRemaining = durationInSeconds;
SecondsRemaining = durationEachThreshold;

% Calibration variables
MinScreenLum = 0.12; % Keep: contrast = 100 & brightness = 63
GammaFunc = 2.15;
MaxScreenLum = 122.5;

% Now start the experiment loop.
fprintf('Experiment started'),
StartExptSecs = GetSecs; % this times the whole experiment

while GetSecs - StartExptSecs < durationInSeconds % Keep experiment running

% Set up flags etc to re enter the threshold loop
stopRule = 1; % keeps loop running till stop rules met, then =0

while stopRule > 0 % Keep looking for threshold i.e. experiment running.

GammaCorrectSpotLum = 255*((10^SpotLuminance)-
MinScreenLum)/MaxScreenLum)^(1/GammaFunc)

Screen('DrawText', window, ['GammaCorr: ' num2str(SpotLuminance,4)], 970, 940,
[0,0,240]);
if InnerLineSize < 0 % invoked if small spot presented to avoid interference with
cross
InnerLineSize = 0;
End

% Present stimulus
Screen('DrawLine', window, [white], 640+(HorizontalLocation*35), 512
(VerticalLocation*35)-LineSize, 640+(HorizontalLocation*35), 512-
(VerticalLocation*35)+LineSize, LineThickness); % presents peripheral fixation
markers
Screen('DrawLine', window, [white], 640+(HorizontalLocation*35)-LineSize, 512-
(VerticalLocation*35), 640+(HorizontalLocation*35)+LineSize, 512-
(VerticalLocation*35), LineThickness);
Screen('FillOval', window, [0 0], SurroundRectInner);
Screen('FillOval', window,
[GammaCorrectSpotLum GammaCorrectSpotLum GammaCorrectSpotLum],
offsetCenteredspotRect);
Screen('FillOval', window, [0 0], offsetCenteredspotRect2); % draws black spot
Screen('DrawLine', window, [white], 640+(HorizontalLocation*35), 512-
(VerticalLocation*35)-InnerLineSize, 640+(HorizontalLocation*35), 512-
(VerticalLocation*35)+InnerLineSize, LineThickness); % presents peripheral
fixation markers
Screen('DrawLine', window, [white], 640+(HorizontalLocation*35)-InnerLineSize,
512-(VerticalLocation*35), 640+(HorizontalLocation*35)+InnerLineSize, 512-
(VerticalLocation*35), LineThickness);
Screen(window, 'Flip');
WaitSecs (0.2); % presentation time

% Remove stimulus
Screen('DrawText', window, ['GammaCorr: ' num2str(SpotLuminance,4)], 970, 940,
[0,0,240]);
Screen('DrawLine', window, [white], 640+(HorizontalLocation*35), 512-
(VerticalLocation*35)-LineSize, 640+(HorizontalLocation*35), 512-
(VerticalLocation*35)+LineSize, LineThickness);

```

```

Screen('DrawLine', window, [white], 640+(HorizontalLocation*35)-LineSize, 512-
(VerticalLocation*35), 640+(HorizontalLocation*35)+LineSize, 512-
(VerticalLocation*35),LineThickness);
Screen('FillOval', window, [0 0], SurroundRectInner);
Screen('DrawLine', window, [white], 640+(HorizontalLocation*35), 512-
(VerticalLocation*35)-InnerLineSize, 640+(HorizontalLocation*35), 512-
(VerticalLocation*35)+InnerLineSize,LineThickness); % presents peripheral
fixation markers
Screen('DrawLine', window, [white], 640+(HorizontalLocation*35)-InnerLineSize,
512-(VerticalLocation*35), 640+(HorizontalLocation*35)+InnerLineSize, 512-
(VerticalLocation*35),LineThickness);
Screen(window, 'Flip');
ResponseSecs = GetSecs;

% Wait for a response
while 1
[ keyIsDown, timeSecs, keyCode ] = KbCheck;
ifkeyIsDown

ifkeyCode(escapeKey)% exit loop
BreakFlag=1;
break
end

if (timeSecs - ResponseSecs)<0.6;
response = 1; % correct response
sound(correctSound)
else
response = -1; % incorrect response (too slow)
sound (incorrectSound)
break
end

whileKbCheck; end% this avoids KbCheck reporting multiple events
break
end

% Now, if no button push + long wait, time is up!
SecsNow = GetSecs;
timeSincePresentation = (SecsNow - ResponseSecs);
iftimeSincePresentation> 1;
response = -1; % incorrect response (missed)
break
end
end

ifBreakFlag==1% exit loop
break
end

%Now record each presentation.
presentationTime(presentationCounter)= (GetSecs - StartExptSecs);
presentationThreshold(presentationCounter)= SpotLuminance-AdjustmentFilter1-
AdjustmentFilter2;
presentationCounter = presentationCounter + 1;

%Now adjust next stimulus increment on the basis of the response
if response > 0; % correct response

ifincrementStep> 0.0; % intensity increased on last step so this must be a
threshold
resultTime (thresholdCounter) = (GetSecs - StartExptSecs);
resultThreshold (thresholdCounter) = SpotLuminance-AdjustmentFilter1-
AdjustmentFilter2;
thresholdCounter = thresholdCounter + 1;
stopRule = -1; % notes that a threshold has been recorded
end

```

```

incrementStep = -0.3;% next presentation = 0.3 log units decrease
WaitSecs (0.5 + rand(1.5))
end

if response < 0;% incorrect response
incrementStep = 0.1;
WaitSecs (rand(1.0))
end

% Now alter stimulus for next presentation
SpotLuminance = SpotLuminance + incrementStep;
ifSpotLuminance > 2
SpotLuminance = 2;
end

% Now reset the stimulus intensity when the minimum luminance is reached
ifSpotLuminance < -0.9;
SecondNDFilterFlag = SecondNDFilterFlag + 1; %This counter determines adjustments
that are made for ND filter put on the screen
sound (NewFilterSound) % insert a new filter
ifSecondNDFilterFlag == 1 % 1st loop i.e. 1st time the subject reaches -llog
cd/m2
                AdjustmentFilter2 = 2.1;
LineThickness = 10;
WaitSecs (5.0)
SpotLuminance = 1.1; % resets stimulus intensity to maximum brightness
end
ifSecondNDFilterFlag == 2 % 2nd loop i.e. 2nd time the subject reaches -llog
cd/m2
                AdjustmentFilter2 = 3.0;
WaitSecs (5.0)
SpotLuminance = -0.1; % resets stimulus intensity to maximum brightness
end
end

end% this ends the search for a threshold
beep

ifBreakFlag==1 % exit loop
break
end

end% Now go back and collect data for the next threshold point

% Now display the results
presentationTime = presentationTime (:);% converts row to column
presentationThreshold = presentationThreshold (:); %converts row to column
plot(presentationTime, presentationThreshold, 'b*')% plots every presentation
xlabel('Time(s)')
ylabel('Log Threshold')
AXIS ([0 300 -1.5 2.5])
Hold on

resultTime = resultTime(:);% changes format to column vectors
resultThreshold = resultThreshold(:);
plot(resultTime, resultThreshold, ':ko')% plots thresholds

% Now fit the final exponential curve
Starting = [1.2,5,40];
Options = optimset('Display','off');% if set 'off' to 'iter' will see iterations
Estimates = fminsearch(@myfitExp,Starting,options,resultTime,resultThreshold);
fT = Estimates(1)
iT = Estimates(2)
Tau = Estimates(3)
% Now plot this curve
ExpFitTime = 0:2.0:300;% now create some x-axis data at 1.0 steps

```

```

ExpFitThreshold = Estimates(1)+((Estimates(2)-Estimates(1))*exp(-
ExpFitTime./Estimates(3)));
plot(ExpFitTime, ExpFitThreshold,'r-','LineWidth',2)

Screen('CloseAll');

%Now output all the data to Excel spreadsheet
presentationData = [presentationTime, presentationThreshold]
thresholdData = [resultTime, resultThreshold]
ExpFitTime = ExpFitTime(:);
ExpFitThreshold = ExpFitThreshold(:);
curveFit = [ExpFitTime, ExpFitThreshold]
xlswrite('c:\Data\Results\TopographyDAresults.xls',
presentationData,'Model','A14');
xlswrite('c:\Data\Results\TopographyDAresults.xls', thresholdData,'Model','D14');
catch
Screen('CloseAll');
rethrow(lasterror);
psychrethrow(psychlasterror);
end

```

Bleaching intensity procedure

```

clear all

% Input co ordinates and sizes for cross and spot
HorizontalLocation = input('Horizontal location in degrees? ');
VerticalLocation = input('Vertical location in degrees? ');
SpotSize = input('Spot size in degrees?')*17.5; % size of spot in pixels
if SpotSize < 9*17.5; OutsideLineSize=100; InsideLineSize=40; end
if SpotSize == 24*17.5; OutsideLineSize=0; InsideLineSize=350; end
LineThickness = 5; % this is the thickness of the fixation cross
LineSize = SpotSize+OutsideLineSize; % this is the length of the cross line in
pixels
InnerLineSize = SpotSize-InsideLineSize;
% NOTE assumes a 55 cm viewing distance!
LineColour = 1; %this is the colour of the cross at the start of the program

KbName('UnifyKeyNames');
% The Try, Catch, End commands will respond to bugs / problems
try
% First set up all the parameters
whichScreen = 0;
window = Screen(whichScreen, 'OpenWindow');
white = WhiteIndex(window); % pixel value for white
black = BlackIndex(window); % pixel value for black
gray = (white+black)/2;
inc = white-gray;

% And, set the parameters of the spot, 1st and 3rd numbers give the horizontal
position
% the 2nd and 4th give the vertical, the spot is stretched inbetween.
% SpotSize = 35/2; % This is the size of the spot in pixels
offsetCenteredspotRect = [640-SpotSize 512-SpotSize 640+SpotSize 512+SpotSize]; %
size and position of spot on screen
offsetCenteredspotRect2 = [640-SpotSize+17.5 512-SpotSize+17.5 640+SpotSize-17.5
512+SpotSize-17.5];
SurroundRectInner = [640-SpotSize-10 512-SpotSize-10 640+SpotSize+10
512+SpotSize+10]; % size and position of annulus
SurroundRectOuter = [496 368 784 656];

% Set up the sounds for correct and incorrect responses and to indicate
% that a new neutral density filter is required

```

```

correctSound = sin(2*pi*100*[0:0.00125:2.0]);
incorrectSound = sin(2*pi*40*[0:0.00125:2.0]);
NewFilterSound = sin (2*pi*200*[0:0.00125:10.0]);

% Set up various flags
response = 0;
responseCounter = 0;
reversalCounter = 1;%this counts reversals but is reset after each threshold
DarkAdptCounter = 0; % counts the number of times a dark adptn threshold is
recorded.
presentationCounter=1; %counts all presentations, used in Humphrey version
dataCounter=1;%this is the reversal counter, it counts all reversals
thresholdCounter = 1;% this counter is for the Humphrey version i.e. it counts
the no. of threshold points
AdjustmentFilter1 = 2.1;% this is the optical density of the first ND filter
AdjustmentFilter2 = 0;% this is the optical density of the second ND filter -
which is not yet in place!!!
% Clear arrays that contain data
SecondNDFilterFlag = 0; % this line is used as a flag to stop the luminance being
raised if the spot luminance hits it's lowest level a second time i.e. after the
2.1 ND filter has been added
resultTime = 1;
resultThreshold = 1;
BreakFlag = 0;

% Set keys up.
rightKey = KbName('RightArrow');
leftKey = KbName('LeftArrow');
escapeKey = KbName('ESCAPE');

% This screen can be used to write instructions
Screen(window, 'FillRect', 0);
Screen('DrawText', window, 'DARK ADAPTATION VERSION 6/5/10', 300, 200, white);
Screen('DrawText', window, 'Hit any key to start experiment', 300, 400, white);
Screen(window, 'Flip');
Kbwait;% duration of instruction presentation

% Set up the timer.
startTime = now;
durationInSeconds = 1800;
durationEachThreshold = 1;
numberOfSecondsRemaining = durationInSeconds;
SecondsRemaining = durationEachThreshold;

% Calibration variables
MinScreenLum = 0.12; % Keep: contrast = 100 & brightness = 63
GammaFunc = 2.15;
MaxScreenLum = 122.5;

% Now start the experiment loop.
fprintf('Experiment started'),
StartExptSecs = GetSecs; % this times the whole dark adaptation expt

while GetSecs - StartExptSecs < durationInSeconds% Keep experiment running

% Set up flags etc to re enter the threshold loop
stopRule = 1;%keeps loop running till stop rules met, then =0

while stopRule > 0 % Keep looking for threshold i.e. expt running.

GammaCorrectSpotLum = 255*((10^SpotLuminance)-
MinScreenLum)/MaxScreenLum)^(1/GammaFunc)
%This calculates the grey scale required for desired luminance
%SpotLuminance raised to power of 10 to 'un-log' the number

```

```

Screen('DrawText', window, ['GammaCorr: ' num2str(SpotLuminance,4)], 970, 940,
[0,0,240]);
if InnerLineSize < 0 % this line stops the central cross going ' funny' if we are
presenting a small spot.
InnerLineSize = 0;
end
if LineColour == 1
LineSpectrum = [256 256 0]; % this is the colour of the cross line at the start
of the program i.e. blue gun off
end
if LineColour > 1
LineSpectrum = [white]; % this is the colour of the cross line when the filter
comes down, i.e. white
end
Screen('DrawLine', window, [LineSpectrum], 640+(HorizontalLocation*35), 512-
(VerticalLocation*35)-LineSize, 640+(HorizontalLocation*35), 512-
(VerticalLocation*35)+LineSize, LineThickness); % presents peripheral fixation
markers
Screen('DrawLine', window, [LineSpectrum], 640+(HorizontalLocation*35)-LineSize,
512-(VerticalLocation*35), 640+(HorizontalLocation*35)+LineSize, 512-
(VerticalLocation*35), LineThickness);
Screen('FillOval', window, [0 0 0], SurroundRectInner); % draws invisible spot
i.e. surround
Screen('FillOval', window, [GammaCorrectSpotLum GammaCorrectSpotLum 0],
offsetCenteredspotRect); % draws white spot
Screen('FillOval', window, [0 0 0], offsetCenteredspotRect2); % draws black spot
Screen('DrawLine', window, [LineSpectrum], 640+(HorizontalLocation*35), 512-
(VerticalLocation*35)-InnerLineSize, 640+(HorizontalLocation*35), 512-
(VerticalLocation*35)+InnerLineSize, LineThickness); % presents peripheral
fixation markers
Screen('DrawLine', window, [LineSpectrum], 640+(HorizontalLocation*35)-
InnerLineSize, 512-(VerticalLocation*35),
640+(HorizontalLocation*35)+InnerLineSize, 512-
(VerticalLocation*35), LineThickness);
Screen(window, 'Flip'); % presents test
WaitSecs (0.2); % presentation time

%Remove stimulus
%Screen('DrawText', window, sprintf('%i seconds remaining...',
numberOfSecondsRemaining), 20, 60, white);
Screen('DrawText', window, ['GammaCorr: ' num2str(SpotLuminance,4)], 970, 940,
[0,0,240]);
Screen('DrawLine', window, [LineSpectrum], 640+(HorizontalLocation*35), 512-
(VerticalLocation*35)-LineSize, 640+(HorizontalLocation*35), 512-
(VerticalLocation*35)+LineSize, LineThickness);
Screen('DrawLine', window, [LineSpectrum], 640+(HorizontalLocation*35)-LineSize,
512-(VerticalLocation*35), 640+(HorizontalLocation*35)+LineSize, 512-
(VerticalLocation*35), LineThickness);
Screen('FillOval', window, [0 0 0], SurroundRectInner); % draws large spot i.e.
surround
Screen('DrawLine', window, [LineSpectrum], 640+(HorizontalLocation*35), 512-
(VerticalLocation*35)-InnerLineSize, 640+(HorizontalLocation*35), 512
(VerticalLocation*35)+InnerLineSize, LineThickness); % presents peripheral
fixation markers
Screen('DrawLine', window, [LineSpectrum], 640+(HorizontalLocation*35)-
InnerLineSize, 512-(VerticalLocation*35),
640+(HorizontalLocation*35)+InnerLineSize, 512-
(VerticalLocation*35), LineThickness);
Screen(window, 'Flip'); % blanks out test
ResponseSecs = GetSecs;% gets the time the stimulus was flipped out

% Wait for a response
while 1
[ keyIsDown, timeSecs, keyCode ] = KbCheck;
if keyIsDown

```

```

if keyCode(escapeKey)% this small loop helps stop the programme after the ESC key
is pushed.
BreakFlag=1;
break
end
fprintf('"%s" typed at time %.3f seconds\n', KbName(keyCode), timeSecs -
ResponseSecs);
if (timeSecs - ResponseSecs)<0.6;
    response = 1; %this means the response was correct
    sound(correctSound)
else
    response = -1; %this means the response was incorrect (in this case too slow)
    sound (incorrectSound)
    break
end

while KbCheck; end % this avoids KbCheck reporting multiple events
break
end

% Now, if no button push + long wait, time is up!
SecsNow = GetSecs;
timeSincePresentation = (SecsNow - ResponseSecs);
if timeSincePresentation > 1;
response = -1; %this means the response was incorrect (in this case completely
missed)
break
end
end % waiting for response or time up

if BreakFlag==1% this small loop helps stop the programme after the ESC key is
pushed.
break
end

%Now record each presentation.
presentationTime(presentationCounter)= (GetSecs - StartExptSecs);
presentationThreshold(presentationCounter)= SpotLuminance-AdjustmentFilter1-
AdjustmentFilter2;
presentationCounter = presentationCounter + 1;

%Now adjust next stimulus increment on the basis of the response
if response > 0;% that is, correct
if incrementStep > 0.0; % that is, threshold was raised up on the last step, this
must be a threshold
resultTime (thresholdCounter) = (GetSecs - StartExptSecs);
resultThreshold (thresholdCounter) = SpotLuminance-AdjustmentFilter1-
AdjustmentFilter2;
thresholdCounter = thresholdCounter + 1;
    stopRule = -1; % this should make the programme realise that a threshold has
been recorded
end

incrementStep = -0.3;% now ensure that the next step is down 0.3 log units
WaitSecs (0.5 + rand(1.5))
end

if response < 0;% that is, incorrect
incrementStep = 0.1;
WaitSecs (rand(1.0))
end

% Now alter stimulus for next presentation
SpotLuminance = SpotLuminance + incrementStep;
if SpotLuminance > 2
SpotLuminance = 2;
end

```

```

% Now reset the stimulus intensity when the minimum luminance is reached
if SpotLuminance < -0.6;
SecondNDFilterFlag = SecondNDFilterFlag + 1; %This is the counter that determines
which adjustments are made for a ND filter put on the screen
sound (NewFilterSound) % makes a beep to tell the investigator to insert a new
filter
if SecondNDFilterFlag == 1 % This is the 1st loop i.e. the 1st time the subject
reaches -1log cd/m2
AdjustmentFilter2 = 2.1;
LineThickness = 10;
LineColour = LineColour + 1; % resets the colour of the cross to white
WaitSecs (5.0)
SpotLuminance = SpotLuminance + AdjustmentFilter2; % resets the stimulus
intensity to the maximum brightness
end
if SecondNDFilterFlag == 2 % This is the 2nd loop i.e. the 2nd time the subject
reaches -1log cd/m2
AdjustmentFilter2 = 3.0;
WaitSecs (5.0)
SpotLuminance = SpotLuminance + AdjustmentFilter2; % resets the stimulus
intensity to the maximum brightness
end
end

end % this ends the search for a threshold
beep

if BreakFlag==1 % this small loop helps stop the programme after the ESC key is
pushed.
break
end

end % Now go back and collect data for the next threshold point

% Now display the results
presentationTime = presentationTime (:);% converts row of presentation time into
column
presentationThreshold = presentationThreshold (:); %converts row of presentation
threshold to column
plot(presentationTime, presentationThreshold, 'b*')%this should plot every
presentation
xlabel('Time(s)')
ylabel('Log Threshold')
AXIS ([0 300 -1.5 2.5])
hold on

resultTime = resultTime(:);% This changes format to column vectors
resultThreshold = resultThreshold(:);
plot(resultTime, resultThreshold, ':ko')% this should plot the thresholds

% Now fit the final exponential curve
Starting = [1.2,5,40];
Options = optimset('Display','off');% if set 'off' to 'iter' will see iterations
Estimates=fminsearch(@myfitExp,Starting,options,resultTime,resultThreshold);
fT = Estimates(1)
iT = Estimates(2)
Tau = Estimates(3)
% Now plot this curve
ExpFitTime = 0:2.0:300;% now create some x-axis data at 1.0 steps
ExpFitThreshold = Estimates(1)+((Estimates(2)-Estimates(1))*exp(-
ExpFitTime./Estimates(3)));
plot(ExpFitTime, ExpFitThreshold, 'r-', 'LineWidth', 2)

Screen('CloseAll');

%Now output all the data to Excel spreadsheet

```

```
presentationData = [presentationTime, presentationThreshold]
thresholdData = [resultTime, resultThreshold]
ExpFitTime = ExpFitTime(:);
ExpFitThreshold = ExpFitThreshold(:);
curveFit = [ExpFitTime, ExpFitThreshold]
xlswrite('c:\Data\Results\TopographyDAresults.xls',
presentationData, 'Model', 'A14');
xlswrite('c:\Data\Results\TopographyDAresults.xls', thresholdData, 'Model', 'D14');
catch
Screen('CloseAll');
rethrow(lasterror);
psychrethrow(psychlasterror);
end
```

Appendix III. Peer reviewed papers and supporting publications

Peer reviewed papers

Page 263: Gaffney A J, Binns A M, and Margrain T H (2011a) The repeatability of the Goldmann-Weekers adaptometer for measuring cone adaptation. *Documenta Ophthalmologica* 122: 71-75.

Page 268: Gaffney A J, Binns A M, and Margrain T H (2011b) The topography of cone dark adaptation deficits in age-related maculopathy. *Optometry and Vision Science* 88: 1080-1087.

Page 276: Gaffney A J, Binns A M, and Margrain T H (2012) Aging and cone dark adaptation. *Optometry and Vision Science* In Press.

Conference abstracts

Page 282: Gaffney A J, Binns A M, and Margrain T H (September 2009) A comparison of objective and subjective measures of dark adaptation. BriSCEV, Sheffield.

Page 284: Gaffney A J, Margrain T H, and Binns A M (April 2010) A comparison of four psychophysical methods of monitoring dark adaptation. Optometry Tomorrow, College of Optometrists, York.

Page 286: Gaffney A J, Margrain T H, and Binns A M (March 2012 and May 2011) The topography of cone-mediated dark adaptation in AMD. Optometry Tomorrow, College of Optometrists, Liverpool and ARVO annual meeting, Fort Lauderdale, Florida.

Page 288: Gaffney A J, Margrain T H, and Binns A M (March 2012 and May 2012) A comparison of psychophysical and electrophysiological methods of assessing cone dark adaptation in ARM. Optometry Tomorrow, College of Optometrists, Brighton and ARVO annual meeting, Fort Lauderdale, Florida.

The repeatability of the Goldmann-Weekers adaptometer for measuring cone adaptation

Allannah J. Gaffney · Alison M. Binns ·
Tom H. Margrain

Received: 19 October 2010 / Accepted: 13 January 2011 / Published online: 29 January 2011
© Springer-Verlag 2011

Abstract To assess the inter-session repeatability of the Goldmann-Weekers adaptometer for the measurement of cone dark adaptation in a population of healthy subjects. Data were obtained from 31 healthy adults (mean age 21.5 ± 2.5) on 2 days. At each visit, pupils were dilated and a 96% bleach of cone photopigment was administered to the test eye before threshold was monitored continuously for 5 min in the dark using the Goldmann-Weekers adaptometer. A single exponential function was fitted to the threshold recovery data on a least squares basis. The coefficient of repeatability (CoR) was calculated to assess the repeatability of the time constant of recovery (τ), initial threshold and final threshold. Cone dark adaptation functions were successfully recorded from all subjects on both visits. The CoR was 79.48 s for τ , $0.71 \log \text{cdm}^{-2}$ for the initial threshold, and $0.58 \log \text{cdm}^{-2}$ for the final threshold. Paired samples t-tests showed that there were no significant differences between visits for any of the parameters assessed. Although the Goldmann-Weekers adaptometer was capable of monitoring the rapid changes in threshold that occur during cone dark adaptation, the CoR for τ was relatively large compared to the mean recovery time constants (126.48 ± 40.33 and 119.94 ± 33.25 s at the first

and second visits, respectively). This indicates that the Goldmann-Weekers adaptometer is unlikely to be a useful instrument to chart changes in an individual's vision over time.

Keywords Goldmann-Weekers adaptometer · Cone dark adaptation · Repeatability

Introduction

Abnormal dark adaptation kinetics are diagnostic of a range of conditions, including retinitis pigmentosa [1, 2], age-related macular degeneration (AMD) [3–6], diabetic retinopathy [7, 8] and vitamin A deficiency [9, 10]. Recently there has been renewed interest in cone dark adaptation because of its ability to identify people with early AMD and the relative speed with which it can be recorded [6].

Although dark adaptation functions have been recorded using several custom made dark adaptometers [6, 11–15], few are available commercially [16, 17]. However, given the diagnostic potential of dark adaptometry in AMD, the largest cause of blindness in the developed world [18], it seems likely that the number of commercially available dark adaptometers is set to grow. Knowledge about the performance of these new devices, and in particular their repeatability, will be important. Ideally, the repeatability of emerging technologies will be superior to that obtained with existing clinical equipment.

A. J. Gaffney · A. M. Binns · T. H. Margrain (✉)
School of Optometry and Vision Sciences, Cardiff
University, Maindy Road, Cathays,
Cardiff CF24 4LU, UK
e-mail: margrainth@cf.ac.uk

For several decades the Goldmann-Weekers adaptometer was considered the ‘gold standard’ method used to measure dark adaptation. Once a commercially available instrument, it uses an operator controlled method of ascending limits to determine the visual threshold and each threshold measurement is recorded directly onto logarithmic paper [19]. However, despite its widespread use, there is little information about the performance of this device, and remarkably, no published data regarding its repeatability for the assessment of the kinetics of dark adaptation.

In this brief report we describe the inter-session repeatability of the Goldmann-Weekers adaptometer for the measurement of cone dark adaptation in a population of healthy subjects. The data may be used as a benchmark for future comparisons.

Methods

Subjects

Thirty-one healthy adults, aged 19–30 years (mean age 21.5 ± 2.5) were recruited to the study and visited the laboratory on 2 days. All subjects had a corrected visual acuity of 6/6 or better, clear ocular media, normal retinal appearance and no history of ocular or systemic disease. The subjects provided informed consent and all procedures adhered to the tenets of the Declaration of Helsinki.

Experimental procedure

At each visit, subjects were dilated with one drop of 1.0% Tropicamide in each eye. After a short familiarisation trial, dark adaptation was monitored in the right eye of all subjects (the left eye was occluded). Refractive correction was worn if required.

In order to have precise control over photopigment bleaching, a Maxwellian view optical system was used to bleach 96% of cone photopigment in the central 44° of the test eye [20]. Upon cessation of the bleach, the subject turned to fixate the stimulus in the bowl of the Goldmann-Weekers adaptometer within 3 s, and cone dark adaptation was monitored continuously for 5 min using the Goldmann-Weekers adaptometer. The adaptometer’s stimulus, viewed centrally, was a 4° diameter achromatic spot presented for 1 s once every 2 s (i.e. 0.5 Hz).

The luminance of the Goldmann-Weekers stimulus was under direct control of the investigator who employed the method of ascending limits to record the dark adaptation function. That is, the investigator manually increased the intensity of the stimulus until the subject reported that it was just seen. Threshold was recorded using the logarithmic paper provided, before the stimulus intensity was reduced and the procedure repeated. This continued throughout the recording period. Subsequently, the marks on the recording paper were digitised (DigitizeIt Ver 1.5) and transferred to a spreadsheet for analysis.

Calibration

The Goldmann-Weekers adaptometer recorded luminance in units of log microapostilbs, rather than the more contemporary unit of luminance, cdm^{-2} . Therefore, in order to ensure that the values recorded were accurately converted to $\log \text{cdm}^{-2}$ the luminance of the stimulus was calibrated using a photometer (LS-110; Konica Minolta, Osaka, Japan).

Statistical analysis

The time constant of recovery (τ) was determined by fitting a single exponential function (Eq. 1), on a least squares basis, to the threshold recovery data, using Microsoft Excel.

$$a = fT + (iT - fT)e^{(-T/\tau)} \quad (1)$$

where a is the threshold at time T after the bleach, fT is the final dark adapted threshold, iT is the threshold immediately after cessation of the bleach and τ is the time constant of cone recovery.

The repeatability of τ , initial threshold and final threshold measurements was assessed using established statistical techniques [21], including by calculating the coefficient of repeatability (CoR).

Results

Cone dark adaptation functions were successfully recorded from all 31 subjects on two occasions. The dark adaptation functions recorded from a typical subject (SH) at each visit are shown in Fig. 1.

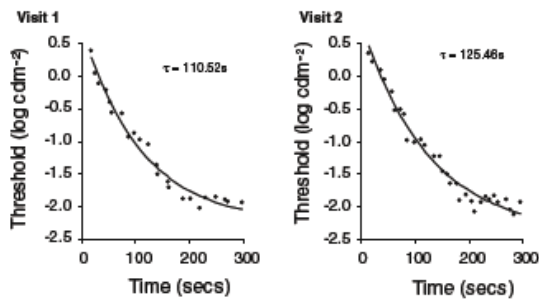


Fig. 1 Cone dark adaptation for subject SH, recorded using the Goldmann-Weekers adaptometer at visit 1 (*left panel*) and 2 (*right panel*). Shown with the time constant of recovery (τ) in seconds

The difference between τ recorded at visit one and visit two is plotted as a function of the mean τ , together with the 95% limits of agreement, for all 31 subjects in the Bland-Altman plot shown in Fig. 2a. Similar plots for the initial and final threshold data are shown in Figs. 2b and c. In each plot the dashed horizontal lines indicate the limits of agreement i.e. the coefficient of repeatability (CoR) and the solid line the bias i.e. the absolute difference observed between visits. The CoR for τ was 79.48 s, for the initial threshold 0.71 log cdm⁻² and final threshold 0.58 log cdm⁻².

The mean (\pm standard deviation) for all of the dark adaptation parameters assessed at the two visits are described in Table 1. Paired samples *t*-testing showed that there was no significant difference in cone τ , initial threshold or final threshold between the two visits.

Discussion

Despite being the default clinical instrument for the measurement of dark adaptation for many decades, until now there has been no published data on the repeatability of kinetic measurement of dark adaptation with the Goldmann-Weekers adaptometer. The repeatability data presented here may be used as a benchmark comparison for other contemporary adaptometers, such as LKC Technologies' SST-1 [16, 17], Roland Consult's dark adaptometer and Apeliotus Vision Science's AdaptDx.

The Goldmann-Weekers adaptometer was capable of monitoring the rapid changes in threshold that

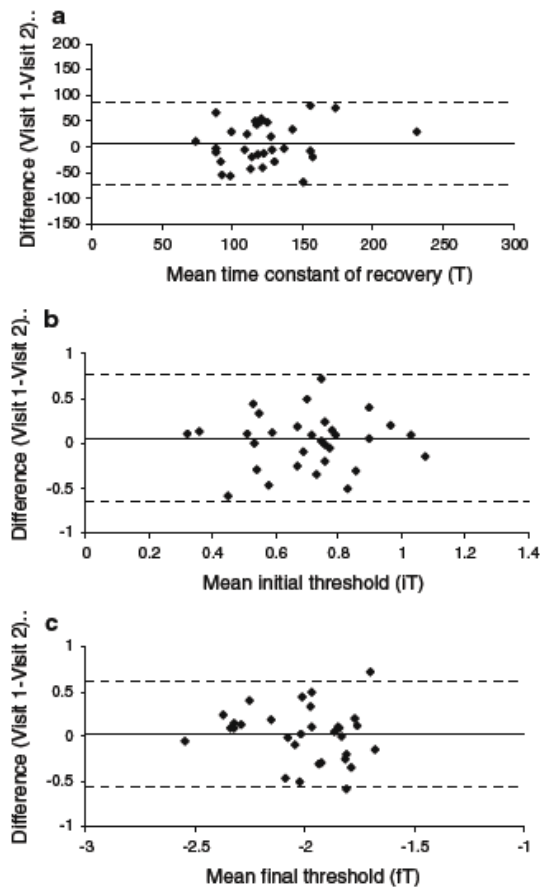


Fig. 2 Bland-Altman plots for cone τ (a), initial threshold (b) and final threshold (c). The difference between the value recorded at visit 1 and visit 2 is plotted as a function of the mean value for all 31 subjects and is shown with the bias (*solid line*) and 95% limits of agreement (*dashed lines*)

occur during cone dark adaptation and data was successfully recorded from all subjects on both occasions. The CoR is important when a technique is evaluated for clinical use, as it indicates the extent of inherent variability, and so the smallest change which may be considered to be clinically significant. In order to be confident that the rate of dark adaptation has changed from one visit to the next, clinicians must ensure that a difference equal to or greater than the CoR is measured.

This study employed a Maxwellian view optical system to deliver a standardised bleach of known intensity. Although the Goldmann-Weekers adaptometer may be used to deliver a continuous background

Table 1 Summary of parameters assessed at visit one and visit two

	Mean (\pm standard deviation)		P-value
	Visit 1	Visit 2	
Cone τ (seconds)	126.48 (\pm 40.33)	119.94 (\pm 33.25)	0.376
Initial threshold (log cdm ⁻²)	0.73 (\pm 0.25)	0.68 (\pm 0.25)	0.443
Final threshold (log cdm ⁻²)	-1.99 (\pm 0.25)	-2.02 (\pm 0.29)	0.652

bleach, the bleach delivered is not consistent between instruments because it depends on the wattage of the bulb used. Hence, repeatability may differ between units but it is unlikely that the performance will be better than that reported here where results were obtained under optimal control of bleach conditions.

A recording time of 300 s was selected in order to assess cone dark adaptation measurement using a clinically applicable (short) protocol. Over this period threshold fell on average by 2.5 log units, but by only 0.08 log units in the last minute. This suggests that the cone plateau had been reached by the end of the recording period.

Of the three parameters of cone dark adaptation studied here, it is the time constant of recovery, τ , that has particular diagnostic significance for conditions such as AMD [3–6]. Relative to the mean recovery time constants observed (126.48 ± 40.33 and 119.94 ± 33.25 s at the first and second visits, respectively) the CoR (79.48 ± 14.86 s) is large i.e. the adaptometer is not capable of identifying differences in cone tau of less than 79.48 s.

To conclude, the results of this study suggest that the adaptometer is insensitive to small to moderate changes in cone dark adaptation.

Acknowledgments This study was funded by a research grant from The College of Optometrists, UK. We would like to thank Katie Kenny for her help with data collection.

References

- Moore AT, Fitzke FW, Kemp CM, Arden GB, Keen TJ, Inglehearn CF, Bhattacharya SS et al (1992) Abnormal dark adaptation kinetics in autosomal dominant sector retinitis pigmentosa due to rod opsin mutation. *Br J Ophthalmol* 76:465–469
- Sandberg MA, Pawlyk BS, Berson EL (1999) Acuity recovery and cone pigment regeneration after a bleach in patients with retinitis pigmentosa and rhodopsin mutations. *Invest Ophthalmol Vis Sci* 40:2457–2461

- Phipps JA, Guymer RH, Vingrys AJ (2003) Loss of cone function in age-related maculopathy. *Invest Ophthalmol Vis Sci* 44:2277–2283
- Binns AM, Margrain TH (2007) Evaluating retinal function in age-related maculopathy with the ERG photostress test. *Invest Ophthalmol Vis Sci* 48:2806–2813
- Owsley C, McGwin G Jr, Jackson GR, Kallies K, Clark M (2007) Cone- and rod-mediated dark adaptation impairment in age-related maculopathy. *Ophthalmol* 114:1728–1735
- Dimitrov PN, Guymer RH, Zele AJ, Anderson AJ, Vingrys AJ (2008) Measuring rod and cone dynamics in age-related maculopathy. *Invest Ophthalmol Vis Sci* 49:55–65
- Phipps JA, Yee P, Fletcher EL, Vingrys AJ (2006) Rod photoreceptor dysfunction in diabetes: Activation, deactivation, and dark adaptation. *Invest Ophthalmol Vis Sci* 47:3187–3194
- Newsome DA, Negreiros M (2009) Reproducible measurement of macular light flash recovery time using a novel device can indicate the presence and worsening of macular diseases. *Curr Eye Res* 34:162–170
- Kemp CM, Jacobson SG, Faulkner DJ, Walt RW (1988) Visual function and rhodopsin levels in humans with vitamin A deficiency. *Exp Eye Res* 46:185–197
- Cideciyan AV, Pugh EN, Lamb TD, Huang YJ, Jacobson SG (1997) Plateaux during dark adaptation in Sorsby's fundus dystrophy and vitamin A deficiency. *Invest Ophthalmol Vis Sci* 38:1786–1794
- Hecht S, Shlaer S (1938) An adaptometer for measuring human dark adaptation. *J Opt Soc Am* 28:269–275
- Goldstein EB (1975) Design for a dark adaptometer. *Behav Res Methods Instrum* 7:277–280
- Henson DB, Allen MJ (1977) A new dark adaptometer. *Am J Opt Physiol Opt* 54:641–644
- Friedburg C, Sharpe LT, Beuel S, Zrenner E (1998) A computer-controlled system for measuring dark adaptation and other psychophysical functions. *Graefes Arch Clin Exp Ophthalmol* 236:31–40
- Jackson GR, Owsley C, McGwin G (1999) Aging and dark adaptation. *Vis Res* 39:3975–3982
- Peters AY, Locke KG, Birch DG (2000) Comparison of the Goldmann-Weekers (TM) dark adaptometer and Scotopic Sensitivity Tester-1 (TM). *Invest Ophthalmol Vis Sci* 40:3763B3621
- Jackson GR, Felix T, Owsley C (2006) The Scotopic Sensitivity Tester-1 and the detection of early age-related macular degeneration. *Ophthalmic Physiol Opt* 26:431–437
- Resnikoff S, Pascolini D, Etya'ale D, Kocur I, Pararajasegaram R, Pokharel GP, Mariotti SP (2004) Global data on visual impairment in the year 2002. *Bull WHO* 82:844–851

19. Dieterle P, Gordon E (1956) Standard curve and physiological limits of dark adaptation by means of the Goldmann-Weekers adaptometer. *Br J Ophthalmol* 40:652–655
20. Hollins M, Alpern M (1973) Dark adaptation and visual pigment regeneration in human cones. *J Gen Physiol* 62:430–447
21. Bland JM, Altman DG (1986) Statistical methods for assessing agreement between two methods of clinical measurement. *Lancet* 1:307–310

ORIGINAL ARTICLE

Topography of Cone Dark Adaptation Deficits in Age-Related Maculopathy

Allannah J. Gaffney*, Alison M. Binns†, and Tom H. Margrain†

ABSTRACT

Purpose. Despite widespread agreement that dark adaptation is abnormal in age-related maculopathy (ARM), the optimal retinal location for detection of this deficit is unclear. We quantified the diagnostic potential of cone dark adaptation as a function of retinal eccentricity and compared this with the diagnostic potential of the time to the rod-cone-break (RCB).

Methods. Cone dark adaptation was monitored after an 80% cone photopigment bleach in 10 subjects with ARM and 10 age-matched controls, using four achromatic annuli (0.5, 2, 7, and 12° radius) centered on the fovea. Threshold recovery data were modeled and the time constant of cone recovery (τ), final cone threshold, and time to RCB were determined. Diagnostic potential was evaluated by constructing receiver operating characteristic curves for these parameters.

Results. Cone τ was significantly longer for the ARM group at 2, 7, and 12°. The greatest difference between groups was observed at 12° from fixation. At this location, the mean τ was 3.49 (± 2.02) min and 0.64 (± 0.38) min for ARM and control subjects, respectively ($p = 0.002$), and time to RCB was 17.68 (± 5.37) min and 9.05 (± 2.11) min for ARM and control subjects, respectively ($p = 0.001$). Correspondingly, receiver operating characteristic curves showed that the diagnostic potential of dark adaptometry is greatest for stimuli presented 12° from fixation; for cone τ , the area under the curve = 0.99 ± 0.02 and for time to RCB, area under the curve = 0.96 ± 0.04 .

Conclusions. This study has shown cone-mediated dark adaptation to be significantly impaired in ARM. Our results provide compelling evidence in support of the diagnostic potential of cone dark adaptation and the use of annular stimuli at 12°. The observation that cone τ is highly diagnostic at this eccentricity is significant clinically because this parameter may be quantified within a few minutes.

(Optom Vis Sci 2011;88:1080-1087)

Key Words: age-related maculopathy, dark adaptation, retinal eccentricity, diagnostic potential, psychophysics

Age-related macular degeneration (AMD) is the primary cause of irreversible vision loss in the developed world.¹ It is a degenerative disease of the central retina that typically presents after 50 years of age and affects the photoreceptors, retinal pigment epithelium (RPE), Bruch's membrane, and choriocapillaris. The early stage of the disease, before the development of noticeable vision loss, is known as age-related maculopathy (ARM).²

Current treatment strategies, such as photodynamic therapy³ and anti-vascular endothelial growth factor (anti-VEGF) therapy,^{4,5} target only the exudative form of the disease. There is as yet no effective therapy for the treatment of atrophic AMD. However, the development of tests sensitive to early macular changes and capable of monitoring subtle changes in visual function would help

to expedite the development of new interventions and to monitor outcomes.

Color vision,⁶ flicker sensitivity,⁷ temporal thresholds,⁸⁻¹⁰ and dark adaptation^{7,11-14} abnormalities have all been reported to precede the loss of visual acuity and the appearance of retinal abnormalities in people developing AMD. In the few studies that have measured more than one of these parameters in people with AMD,^{6,7,14} dark adaptation abnormalities appear to be the single most sensitive markers for the condition. For example, an evaluation of the data presented in Fig. 2 of Eisner et al.⁶ shows that while both color vision and dark adaptation parameters provided 100% specificity in AMD, the sensitivity of photopic dark adaptation (65%) was superior to that of the color matching (48%). Similarly, Owsley et al.¹⁴ and Phipps et al.⁷ found dark adaptation kinetics to be more sensitive to AMD than steady state measures of visual function.

However, although many studies have reported dark adaptation deficits in people with AMD, the literature is not entirely consis-

*BSc (Hons)

†PhD

School of Optometry and Vision Sciences, Cardiff University, Cardiff, United Kingdom.

tent. For example, although there is a clear consensus that dark adaptation is delayed in rods,^{14–18} evidence for abnormal cone dark adaptation is equivocal.^{17,18} More specifically, while Dimitrov et al.¹⁸ reported significant delays in cone-mediated dark adaptation in people with AMD, Owsley et al.¹⁷ found no such difference in their study of a similar patient group.

One explanation for the contradictory evidence regarding cone dark adaptation in ARM is that the cone dark adaptation deficit in ARM is dependent on retinal location. The observation that delays in cone adaptation have been reported for stimuli centered on the fovea^{7,18,19} but not for small spot stimuli presented at more eccentric retinal locations¹⁷ leads to the hypothesis that cone dark adaptation deficits in ARM are greatest for centrally presented stimuli.

A number of studies have examined the effect of retinal location on rod and cone thresholds in ARM.^{16,20–23} These studies tend to show a modest reduction in threshold at peripheral locations and a larger deficit in the macular region. However, only one study has systematically described the topographical variation in dark adaptation kinetics in the disease.²⁰ In this study, Brown et al.²⁰ monitored cone dark adaptation at four locations in the central 40° of visual field, in six patients with geographic atrophy and six healthy controls. However, while cone threshold was elevated at all retinal locations in the subjects with geographic atrophy, there were no significant differences in the rate of cone dark adaptation between groups at any of the locations studied.

Clearly, there is ambiguity surrounding the extent to which cone photoreceptors are affected by ARM and the effect, if any, of the retinal location at which dark adaptation is measured. The current study aims to quantify any topographical differences in cone dark adaptation between people with ARM and healthy controls. More specifically, this study determines the diagnostic potential of cone dark adaptation as a function of retinal eccentricity and compares this with the diagnostic potential of the time to rod-cone-break (RCB), the aspect of rod recovery that can be obtained most rapidly in the clinic.

METHODS

Participants

Twenty subjects (10 people with ARM and 10 healthy controls) were recruited. All participants were aged at least 55 years, had a corrected visual acuity of 6/9 or better in the test eye and none had a history of systemic disease or medication known to affect visual function, or significant media opacity.

Participants with ARM were recruited from the Eye Unit at the University Hospital of Wales, Cardiff, and the Eye Clinic at Cardiff University and had a diagnosis of ARM according to the Age-Related Eye Disease Study severity scale,² in the absence of any co-existing ocular or fundus abnormality. The assessment of fundus status was based on 37° fundus photographs (Canon CR-DGi Camera) obtained at the baseline examination. Ten age-matched control subjects were recruited from the Eye Clinic at Cardiff University. All had a normal retinal appearance in both eyes.

All subjects provided informed written consent before participation. The study was approved by the South East Wales Research Ethics Committee and all procedures adhered to the tenets of the Declaration of Helsinki.

Apparatus and Psychophysical Methods

All stimuli were presented on a calibrated, high-resolution CRT monitor (Iiyama LS 902UT) driven by an 8-bit (nVIDIA Geforce 9) graphics board under software control (Matlab). The luminance output of the monitor was γ -corrected^{24,25} and modified by neutral density filters mounted on the screen to expose the full range of recovery. The background luminance of the CRT was $-0.85 \log \text{cd/m}^2$, which was further attenuated by a 1.2 ND filter that was in place throughout all recordings. The computer emitted a sound to signal that the lower end of the luminance range was approaching, at which point an additional 2.1 ND filter was added to further attenuate the luminance. Although the γ -corrected monitor generated a linear output over a 3 log unit range, only 2.1 log units of this range were used during testing.

Thresholds were recorded in response to a foveal spot (radius 0.5°) and three achromatic annuli (2, 7, and 12° in radius), all 0.5° wide, centered on the fovea (Fig. 1). Subjects were instructed to fixate the center of the screen, marked by a fixation cross, and to indicate perception of the stimulus using the computer keyboard.

Dark adaptation was monitored using a psychophysical method, which was previously implemented by Jackson et al.²⁶ using a modified Humphrey perimeter. The stimulus was presented for 200 ms, followed by a 600 ms response window and then a randomly determined interstimulus delay of 0.9 to 2.4 s. This procedure generated a stimulus, on average, every 2.25 s. If the subject responded to the stimulus within 600 ms, the luminance was reduced by 0.3 log units for the next presentation. Conversely, if the subject took longer than 600 ms to respond to the stimulus, or failed to respond at all the intensity was increased by 0.1 log units on each of the following presentations. Threshold was recorded when the stimulus first became visible on an ascending staircase. Using this method, recovery was sampled approximately every 7.2 s on average.

Experimental Procedures

Participants attended the laboratory on 2 days. Baseline examinations, including patient history, logMAR visual acuity (Early Treatment Diabetic Retinopathy Study), central visual field screening (C-40, Humphrey Field Analyzer), stereoscopic fundus examination, fundus photography (Canon CR-DGi Camera), and media opacity grading²⁷ were completed at the start of the first visit.

Before dark adaptation, subjects' eyes were dilated with one drop of 1.0% Tropicamide in each eye. The eye selected for testing was the eye with ARM, or the eye with the better visual acuity in bilateral ARM or control subjects. The contralateral eye was occluded and refractive correction was worn if required.

Each subject was instructed how to use the dark adaptation program, before undergoing a 5-min practice recording session. This was repeated until subjects produced consistent thresholds and the investigator considered the subject to be competent with the procedure.

A Maxwellian view optical system was used to deliver an 80% bleach (5.1 log phot. Td for 120 s) of cone photopigment²⁸ to the central 43.6° of the test eye. On cessation of the bleach, subjects placed their chin on the rest in front of the computer screen and the computer program commenced immediately. Dark adaptation was monitored in response to one of the four stimuli, selected at random, until the

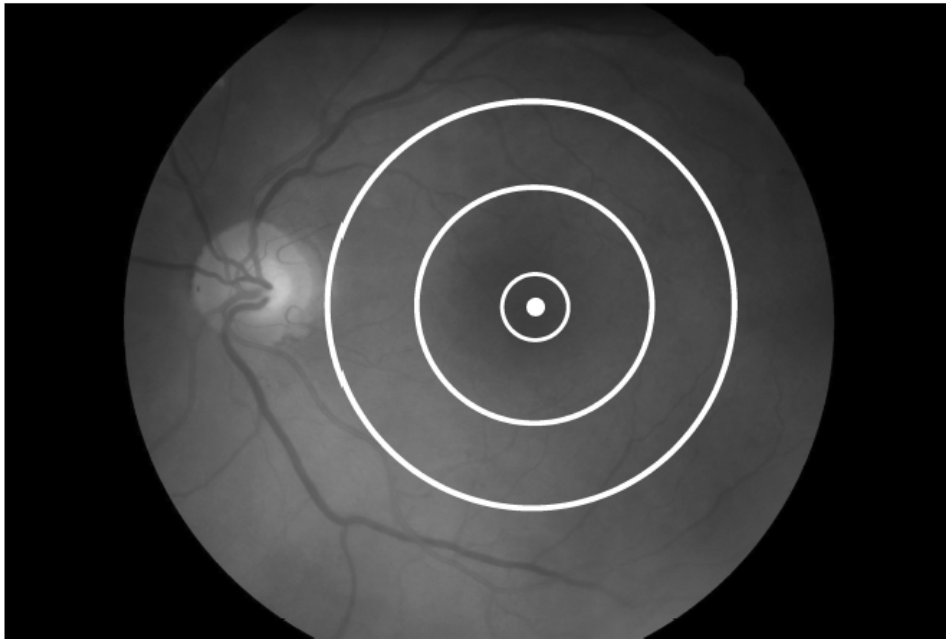


FIGURE 1.

Diagrammatic representation of the spot stimulus and the three annular stimuli superimposed on the macular of a healthy subject. In order of increasing size, the radii of the stimuli were 0.5, 2, 7, and 12° from fixation. Each annulus was 0.5° wide. A color version of this figure is available online at www.optvissci.com.

RCB occurred or for 25 min. The investigator deemed the RCB to have occurred when threshold fell by at least 1 log unit below the cone plateau. For the 0.5° stimulus, recovery was only monitored for 10 min, as no RCB was expected for a small stimulus, presented to the rod-free fovea. This procedure was repeated for each of the remaining stimuli. Generally, two stimulus sizes were completed at each session, with a washout period of an hour between bleaches. In addition, as the study used a long duration adapting light, sufficient to produce an equilibrium level of bleach,²⁸ all individuals should have reached the same level of photopigment bleach regardless of any small differences in prebleach adaptational status.

Statistical Analysis

The dynamics of cone recovery and the time to RCB were determined by fitting an exponential model of dark adaptation to the cone threshold recovery data and a linear model to any rod threshold recovery data, after McGwin et al.²⁹ (Eq. 1), on a least squares basis, using Microsoft Excel. Threshold was recorded when the stimulus first became visible on an ascending staircase. An alternative rate-based model of cone recovery^{18,30} was also evaluated, but was rejected in favor of the exponential model²⁹ because although the rate-based model is theoretically superior, it did not fit the data and the exponential one.

$$T(t) = (a + (b * \exp^{-t/\tau})) + (c * (\max[t - rcb, 0])) \quad (1)$$

where T is the threshold ($\log \text{cd/m}^2$) at time t after cessation of the bleach, a is the final cone threshold, b is the change in cone thresh-

old from $t = 0$, τ is the time constant of cone recovery, c is the slope of the second component of rod recovery, \max is a logic statement, and rcb denotes the time from bleach offset to the RCB. Although the RCB was the only aspect of rod recovery assessed during the analysis, the second component of rod recovery was modeled to identify the time to RCB.

The parameters of interest were cone τ , the final cone threshold, and the time to RCB. The mean (\pm SD) was calculated for each parameter, before independent sample t tests were used to make comparisons between ARM and control groups. Receiver operating characteristic curves were constructed using statistical software (SPSS, version 16.0) to assess the diagnostic potential of the parameters that showed a statistically significant difference between groups.

RESULTS

The clinical characteristics of the ARM group are shown in Table 1. There were no significant differences in age between ARM (mean age = 68.3 ± 7.3 SD years) and control (mean age = 70.0 ± 4.7 SD years) groups ($p = 0.54$). Fifty percent of ARM subjects had ARM in their fellow eye and the remaining 50% had exudative changes. There were no significant differences in logMAR acuity between the test eyes of ARM and control groups (mean acuity = 0.09 ± 0.11 SD logMAR for ARM subjects and -0.002 ± 0.10 SD logMAR for control subjects; $p = 0.11$).

Fig. 2A shows the time course of dark adaptation for a typical control subject, in response to the four stimuli. An example of the dark adaptation curves for an ARM subject is shown in Fig. 2B.

TABLE 1.
Visual acuity and fundus appearance in the ARM group

Subject	Age (yr)	Gender	Test eye			Fellow eye		
			Eye	logMAR VA	ARM status	Eye	logMAR VA	ARM status
1	80	M	L	0.12	Early	R	0.02	Early
2	65	F	R	0.02	Early	L	0.18	Advanced
3	65	F	L	0.0	Intermediate	R	0.2	Advanced
4	68	F	L	0.0	Early	R	0.02	Early
5	73	M	L	0.24	Early	R	0.26	Advanced
6	67	F	R	-0.1	Intermediate	L	0.06	Advanced
7	57	M	L	0.0	Early	R	0.0	Early
8	59	M	L	0.1	Early	R	0.02	Early
9	75	M	R	0.2	Early	L	0.54	Advanced
10	74	F	R	0.2	Early	L	0.04	Early

ARM status according to the Age-Related Eye Disease Study severity scale,² where normal retinal aging = step 1; early ARM = steps 2–6; intermediate ARM = steps 7–9; and advanced ARM = steps 10–11.

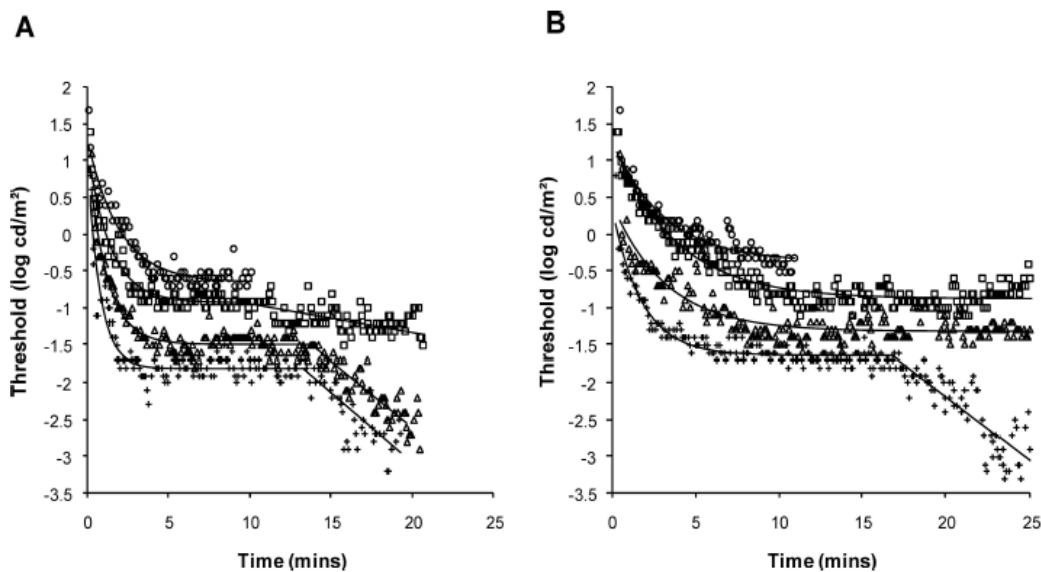


FIGURE 2.
Dark adaptation curves recorded in response to all four stimulus sizes for a typical control subject (A) and a subject with ARM (B). For each stimulus size, the raw data are shown with the best fitting model of dark adaptation given by Eq. 1 (circles = 0.5°, squares = 2°, triangles = 7°, and crosses = 12°). The 12° data are correctly placed with respect to the y-axis. All other data are displaced upward by an additional 0.3 log units from the previous (larger) stimulus to aid visualization.

This ARM subject had prolonged cone adaptation and only displayed a RCB within 25 min for the 12° stimulus.

The mean dark adaptation parameters for each group are summarized in Table 2. Where there was no RCB within 25 min, the RCB was given as 25 min. This means a conservative estimate of the delay in rod adaptation was included in all statistics. There were no significant differences in final cone threshold between control and ARM groups for any of the locations studied. In contrast, there were significant differences in the cone time constant of recovery (τ) between groups for stimuli located 2, 7, and 12° from fixation (all $p < 0.05$). In addition, there was a significant difference in the time to RCB at 12° ($p < 0.001$) between groups. The mean τ , final cone

threshold, and time to RCB for control and ARM groups at each retinal location are summarized in Fig. 3. Although it can be seen that the greatest absolute difference in recovery rate (Fig. 3A) between those with ARM and healthy controls was observed for the central stimulus, this difference failed to reach significance because of the variability in the data obtained at this location. The most significant difference between groups was observed for the stimulus located at 12° where the variability in the data set was minimal.

Equation 1 fitted the data well as exemplified by the RMS error, which was 0.140, 0.146, 0.146, and 0.178, for stimuli located at 0.5, 2, 7, and 12° for the ARM group and 0.152, 0.157, 0.180, and 0.216, for those without ARM at the same locations.

1084 Cone Dark Adaptation Deficits in Age-Related Maculopathy—Gaffney et al.

TABLE 2.
Comparison of mean (\pm SD) dark adaptation parameters in control and ARM groups

	Control	ARM	Univariate comparison
Cone τ (min)			
0.5°	2.08 (1.29)	10.09 (15.61)	p = 0.123
2°	2.07 (0.81)	6.44 (4.95)	p = 0.021
7°	1.28 (0.77)	4.47 (3.13)	p = 0.011
12°	0.64 (0.38)	3.49 (2.02)	p = 0.002
Final cone threshold (log cd/m²)			
0.5°	-1.47 (0.28)	-1.77 (0.50)	p = 0.111
2°	-1.92 (0.34)	-1.94 (0.57)	p = 0.918
7°	-1.93 (0.30)	-1.96 (0.48)	p = 0.856
12°	-1.78 (0.30)	-1.92 (0.40)	p = 0.400
Time to RCB (min)^a			
2°	16.99 (5.91)	20.39 (6.04)	p = 0.221
7°	14.03 (3.01)	18.76 (6.62)	p = 0.061
12°	9.05 (2.11)	17.68 (5.37)	p = 0.001

^aWhere there was no RCB within the recording time, 25 min was given as the time to RCB.

Fig. 4 shows the receiver operating characteristic curves for all the parameters that differed significantly between groups on univariate analysis. The diagnostic capacity of each parameter is expressed as the area under the curve (AUC). The 12° annulus was the best stimulus for discriminating subjects with ARM from healthy controls, yielding an AUC of 0.99 ± 0.02 for cone τ and 0.96 ± 0.04 for time to RCB, respectively. This equates to 100% sensitivity and 90% specificity for a cone τ of 1.04 min and 90% sensitivity and 90% specificity for a RCB of 11.98 min.

Table 3 shows that the sensitivity and specificity of the parameters differed significantly on univariate analysis according to the

normal reference range (defined as two standard deviations around the mean of the control group). This further supports the high diagnostic ability of the 12° stimulus, which showed 90% sensitivity and 90% specificity for cone τ .

A separate analysis was undertaken to check for test order effects (Table 4). There were no significant differences in dark adaptation parameters recorded for the first and second bleaches within a single session. This analysis indicates that there is no learning, fatigue, or bleach carry-over effects within the dataset.

DISCUSSION

Contrary to expectations, these results show that cone τ and time to the RCB are highly diagnostic for ARM for stimuli located 12° from the fovea, with cone τ discriminating participants with ARM from healthy controls with 100% sensitivity and 90% specificity. To a lesser extent, cone τ was also diagnostic for ARM for stimuli located at 2 and 7°. Interestingly, although the greatest absolute difference in mean cone τ between the groups was observed at the fovea, a finding consistent with previous reports,^{7,18,19} this difference failed to reach significance because of the variability of the data at this retinal location (see size of 95% CI in Fig. 3A). Consequently, in terms of diagnostic potential, the functional deficit at 12° from fixation provides the best separation between groups.

Although a previous study reported that dark adaptation was impaired at 12° in ARM, the impairment was thought to affect rods only.¹⁷ In contrast, this study has shown that cone dark adaptation is also highly abnormal at this location. This has significant clinical implications because in the clinic, “time is of the essence” and cone dark adaptation may generally be assessed in less time than rod adaptation.

What then explains the discrepancies between the current study and the results of previous investigations?

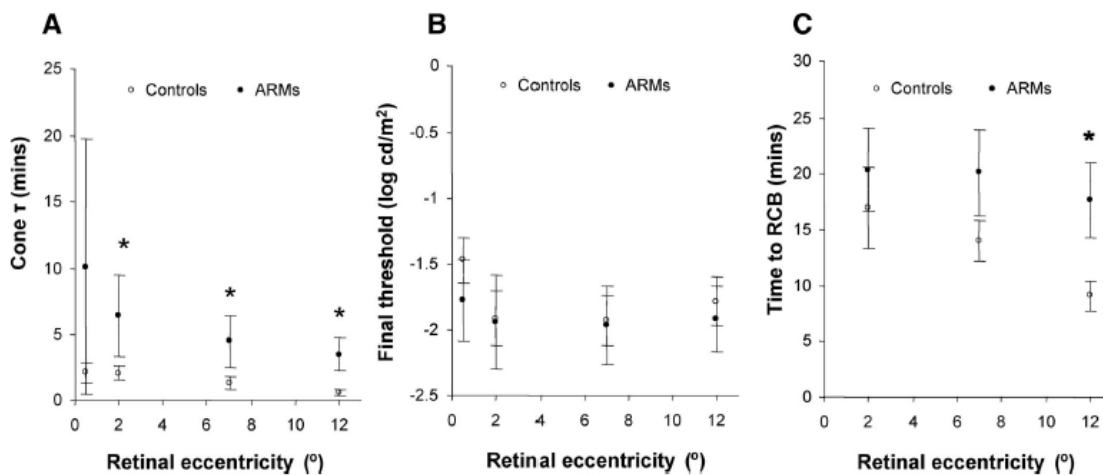


FIGURE 3.

Summary of mean cone τ (A), cone final threshold (B), and time to RCB (C) at each retinal eccentricity, shown with 95% confidence intervals. Filled symbols represent the ARM group and open symbols the control group. * indicates the parameters that demonstrate a significant difference between groups.

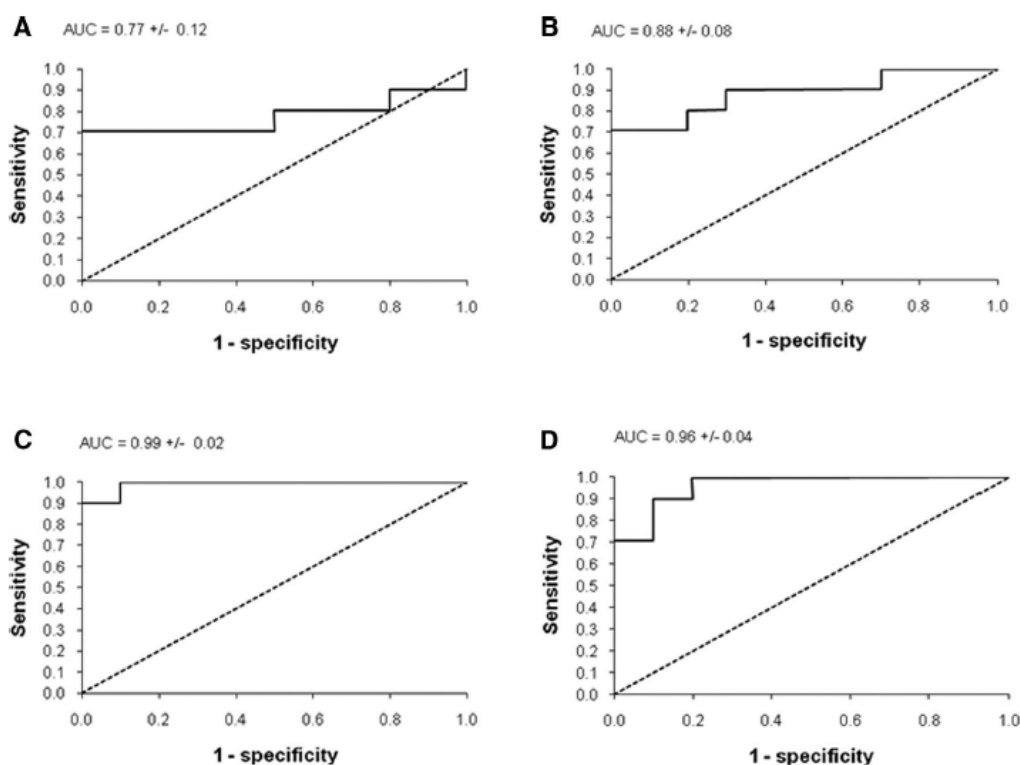


FIGURE 4.

Receiver operating characteristic curves for cone τ at 2° (A), 7° (B), and 12° (C), and time to RCB at 12° (D). Each plot shows the sensitivity of the parameter to ARM against the false detection rate (1 – specificity) for all 10 control and 10 ARM subjects.

TABLE 3.

Sensitivity and specificity of the dark adaptation parameters that differed significantly on univariate analysis, calculated according to the normal reference range (two standard deviations around the mean of the control group)

Parameter	Sensitivity (%)	Specificity (%)
Cone τ at 2°	70	100
Cone τ at 7°	70	90
Cone τ at 12°	90	90
RCB at 12°	70	90

The following paragraphs provide three related explanations based on the well-established rate-limiting step in dark adaptation, that is, the local availability of 11-cis retinal.³¹

The first explanation relates to the bleaching method used (photoflash vs. steady state bleach) and its effect on the rate of cone dark adaptation in people with AMD. Both rods and cones need 11-cis retinal to regenerate visual pigment but while rods can only obtain that supply from the RPE, there is good evidence to suggest that cones have access to a secondary supply, derived from Müller cells.^{32–34} Rods and cones compete for RPE-derived 11-cis retinal but the additional Müller cell pathway provides cones with an exclusive secondary source that helps them regenerate photopig-

ment much more rapidly than rods. Unlike photoflashes, steady state bleaches involve both sustained phototransduction and activation of the visual cycle. If this sustained metabolic activity adversely affected the Müller cell retinoid recycling pathway, cone photopigment regeneration following a long duration bleach would be relatively slow and more dependent on RPE derived 11-cis-retinal, that is, the part of the retina that is abnormal in ARM. Any impairment to cone-mediated dark adaptation in ARM would therefore be more likely to manifest under the conditions used here than following the 11 ms bleach used previously.¹⁷

The second explanation provides a physiologically plausible rationale for the cone dark adaptation deficit at 12°. As discussed, the long duration adapting light makes both rods and cones reliant on the RPE for regeneration of 11-cis retinal, that is, any deficit in RPE function or in the local supply of retinoid is likely to affect both rod and cone adaptation. Rod photoreceptor density reaches a peak of about 150,000 cells/mm² about 12° from the fovea,³⁵ and it has previously been shown that rod adaptation is significantly impaired at this eccentricity.^{14,17} Direct competition between the rods and cones for the same limited supply of retinoid will be greatest at this location and therefore, providing the cones' intraretinal source of 11-cis-retinal is deficient following a long duration bleach, cone recovery at this site would also be expected to

TABLE 4.
Comparison of mean (\pm SD) dark adaptation parameters obtained during the first and second test within a single recording session

	1st test	2nd test	Univariate comparison
Cone τ (min)			
0.5°	7.64 (16.23)	4.54 (3.48)	$p = 0.586$
2°	3.99 (4.55)	4.51 (3.86)	$p = 0.734$
7°	2.63 (2.61)	3.13 (3.02)	$p = 0.733$
12°	2.47 (2.40)	1.65 (1.60)	$p = 0.350$
Final cone threshold (log cd/m²)			
0.5°	-1.48 (0.35)	-1.76 (0.45)	$p = 0.065$
2°	-2.03 (0.49)	-1.82 (0.42)	$p = 0.367$
7°	-1.97 (0.34)	-1.92 (0.45)	$p = 0.814$
12°	-1.76 (0.40)	-1.94 (0.29)	$p = 0.329$
Time to RCB (min)^a			
2°	17.82 (6.40)	19.57 (5.93)	$p = 0.174$
7°	16.54 (5.30)	17.62 (6.38)	$p = 0.745$
12°	14.37 (6.77)	12.36 (5.15)	$p = 0.286$

^aWhere there was no RCB within the recording time, 25-mins was given as the time to RCB.

be highly abnormal. That is, the important topographical parameter in ARM is not photoreceptor type but the local availability of 11-cis-retinal on which both rods and cones are dependent.

The third explanation relates to the size of the stimuli used to track dark adaptation and its effect on variability and the results we obtained at the fovea. Cone density peaks at the fovea (200,000 cells/mm²⁵⁵); hence, competition for 11-cis-retinal will be relatively high and, as we observed, recovery was particularly slow at this retinal location for those with ARM. However, small spot stimuli sample the retina at a precise location. If the disease being investigated is characterized by localized abnormalities (i.e., it is heterogeneous), then the results obtained with small spots will be influenced by chance, that is, the chance that the stimulus is located on a healthy or unhealthy part of the retina. Conversely, thresholds obtained in response to large annuli will be determined by the part of the retina that is most functional/healthy because small areas of abnormality will not contribute to the threshold measured. Hence, we might expect large annuli to produce relatively consistent results based on the functional ability of the retina at a given eccentricity and spots to produce more variable data based on their "hit or miss" sampling of heterogeneous retina. This is exemplified in Table 2, where the standard deviations reported for the ARM group are relatively small for our largest annuli, for example, the standard deviation was on average only 0.57 times the size of the mean recovery time. This contrasts sharply with the data reported by Owsley et al.¹⁷ who sampled the retina at the same distance from the fovea (12° in the inferior visual field) but who used a spot stimulus (1.7° diameter). They reported standard deviations that were more than twice the value of the mean cone τ for their "intermediate" ARM group. This hypothesis appears to provide an explanation for the relatively increased variability observed for the 0.5° data reported here and may have also contributed to the variability observed in other studies that used relatively small spot stimuli.^{14,17}

The heterogeneity argument proposed above may also explain why Dimitrov et al.¹⁸ found cone dark adaptation to be highly diagnostic for ARM (AUC = 0.98). They also used a large (area = 12.6 deg²) stimulus that would have been relatively unaffected by focal abnormalities and reported relatively little variability in their dataset (the standard deviation of their recovery rate was only 0.35 of the mean value).¹⁸ Taken together with the current findings, this suggests that the size of the stimulus may be just as important as location because larger stimuli are associated with reduced variability and hence better diagnostic power.

Previously, Brown et al.²⁰ reported no differences in cone dark adaptation dynamics within the central 40° of visual field between control subjects and those with geographic atrophy. However, that patient group had end-stage AMD and was very different from those studied here.

A group of eight individuals with ARM failed to reach a RCB within the 25 min recording period for one or more of the experimental stimuli. This group included all five of the participants diagnosed with exudative disease in their fellow eye. It is known that there is a higher incidence of choroidal neovascularization in the fellow eyes of patients with unilateral exudative AMD.³⁶⁻³⁸ Therefore, the results support evidence to suggest that dark adaptation is more severely impaired in eyes with an increased risk of exudative changes.⁶

We collected data over a maximum recording period of 25 min. This time constraint was implemented to evaluate the diagnostic potential of cone dark adaptation and the time to RCB within a clinically viable time frame. Although rod dark adaptation can be assessed in as little as 20 min using an alternative protocol,³⁹ the results presented here are particularly significant because cone τ is highly diagnostic for ARM and may be quantified in as little as 10 min.

A limitation of our rod parameter, time to RCB, is that it is dependent not only on the rate of rod adaptation but also on changes in cone final threshold. Therefore, it cannot be considered to be a pure measure of rod adaptation. However, this study showed no evidence of elevation in the cone plateau of participants with early ARM, therefore the finding of a significantly delayed RCB is likely to be attributable to delayed rod adaptation in these individuals.

Although our sample size ($n = 20$) is modest, our primary interest was in distinguishing those with early ARM from healthy controls, that is, detecting clinically significant differences, rather than identifying small differences in mean values. Even with a relatively modest sample size, there was a marked separation of participants with ARM and controls in the cone recovery and RCB data.

In conclusion, this study has demonstrated the diagnostic potential of cone dark adaptation in the detection of ARM and the effect of the retinal location at which dark adaptation is measured. Our results provide compelling evidence supporting the use of cone dark adaptation and the use of large, annular stimuli at 12° in the diagnosis of ARM.

ACKNOWLEDGMENTS

This study was funded by a research grant from the College of Optometrists, UK. Received January 10, 2011; accepted April 15, 2011.

REFERENCES

- Resnikoff S, Pascolini D, Etya'ale D, Kocur I, Pararajasegaram R, Pokharel GP, Mariotti SP. Global data on visual impairment in the year 2002. *Bull World Health Organ* 2004;82:844–51.
- Davis MD, Gangnon RE, Lee LY, Hubbard LD, Klein BE, Klein R, Ferris FL, III, Bressler SB, Milton RC. The Age-Related Eye Disease Study severity scale for age-related macular degeneration: AREDS Report No. 17. *Arch Ophthalmol* 2005;123:1484–98.
- Bressler NM, Bressler SB. Photodynamic therapy with verteporfin (Visudyne): impact on ophthalmology and visual sciences. *Invest Ophthalmol Vis Sci* 2000;41:624–8.
- Brown DM, Michels M, Kaiser PK, Heier JS, Sy JP, Ianchulev T. Ranibizumab versus verteporfin photodynamic therapy for neovascular age-related macular degeneration: two-year results of the ANCHOR study. *Ophthalmology* 2009;116:57–65.
- Mitchell P, Korobelnik JF, Lanzetta P, Holz FG, Prunte C, Schmidt-Erfurth U, Tano Y, Wolf S. Ranibizumab (Lucentis) in neovascular age-related macular degeneration: evidence from clinical trials. *Br J Ophthalmol* 2010;94:2–13.
- Eisner A, Stoumbos VD, Klein ML, Fleming SA. Relations between fundus appearance and function. Eyes whose fellow eye has exudative age-related macular degeneration. *Invest Ophthalmol Vis Sci* 1991;32:8–20.
- Phipps JA, Guymer RH, Vingrys AJ. Loss of cone function in age-related maculopathy. *Invest Ophthalmol Vis Sci* 2003;44:2277–83.
- Mayer MJ, Spiegler SJ, Ward B, Glucs A, Kim CB. Mid-frequency loss of foveal flicker sensitivity in early stages of age-related maculopathy. *Invest Ophthalmol Vis Sci* 1992;33:3136–42.
- Mayer MJ, Spiegler SJ, Ward B, Glucs A, Kim CB. Foveal flicker sensitivity discriminates ARM-risk from healthy eyes. *Invest Ophthalmol Vis Sci* 1992;33:3143–9.
- Mayer MJ, Spiegler SJ, Ward B, Glucs A, Kim CB. Preliminary evaluation of flicker sensitivity as a predictive test for exudative age-related maculopathy. *Invest Ophthalmol Vis Sci* 1992;33:3150–5.
- Collins M, Brown B. Glare recovery and age-related maculopathy. *Clin Vis Sci* 1989;4:145–53.
- Sandberg MA, Gaudio AR. Slow photostress recovery and disease severity in age-related macular degeneration. *Retina* 1995;15:407–12.
- Midena E, Degli Angeli C, Blarmino MC, Valenti M, Segato T. Macular function impairment in eyes with early age-related macular degeneration. *Invest Ophthalmol Vis Sci* 1997;38:469–77.
- Owsley C, Jackson GR, White M, Feist R, Edwards D. Delays in rod-mediated dark adaptation in early age-related maculopathy. *Ophthalmology* 2001;108:1196–202.
- Brown B, Kitchin JL. Dark adaptation and the acuity/luminance response in senile macular degeneration (SMD). *Am J Optom Physiol Opt* 1983;60:645–50.
- Brown B, Adams AJ, Coletta NJ, Haegerstrom-Portnoy G. Dark adaptation in age-related maculopathy. *Ophthalm Physiol Opt* 1986;6:81–4.
- Owsley C, McGwin G, Jr., Jackson GR, Kallies K, Clark M. Cone- and rod-mediated dark adaptation impairment in age-related maculopathy. *Ophthalmology* 2007;114:1728–35.
- Dimitrov PN, Guymer RH, Zele AJ, Anderson AJ, Vingrys AJ. Measuring rod and cone dynamics in age-related maculopathy. *Invest Ophthalmol Vis Sci* 2008;49:55–65.
- Binns AM, Margrain TH. Evaluating retinal function in age-related maculopathy with the ERG photostress test. *Invest Ophthalmol Vis Sci* 2007;48:2806–13.
- Brown B, Tobin C, Roche N, Wolanowski A. Cone adaptation in age-related maculopathy. *Am J Optom Physiol Opt* 1986;63:450–4.
- Steinmetz RL, Haimovici R, Jubb C, Fitzke FW, Bird AC. Symptomatic abnormalities of dark adaptation in patients with age-related Bruch's membrane change. *Br J Ophthalmol* 1993;77:549–54.
- Owsley C, Jackson GR, Cideciyan AV, Huang Y, Fine SL, Ho AC, Maguire MG, Lolley V, Jacobson SG. Psychophysical evidence for rod vulnerability in age-related macular degeneration. *Invest Ophthalmol Vis Sci* 2000;41:267–73.
- Zele AJ, Dang TM, O'Loughlin RK, Guymer RH, Harper A, Vingrys AJ. Adaptation mechanisms, eccentricity profiles, and clinical implementation of red-on-white perimetry. *Optom Vis Sci* 2008;85:309–17.
- Metha AB, Vingrys AJ, Badcock DR. Calibration of a color monitor for visual psychophysics. *Behav Res Method Instrum Comput* 1993;25:371–83.
- Brainard DH, Pelli DG, Robson T. Display characterization. In: Hornak J, ed. *The Encyclopaedia of Imaging Science and Technology*, vol 18. Hoboken, NJ: Wiley; 2001:172–88.
- Jackson GR, Owsley C, McGwin G. Aging and dark adaptation. *Vision Res* 1999;39:3975–82.
- Chylack LT, Jr., Wolfe JK, Singer DM, Leske MC, Bullimore MA, Bailey IL, Friend J, McCarthy D, Wu SY. The Lens Opacities Classification System III. The Longitudinal Study of Cataract Study Group. *Arch Ophthalmol* 1993;111:831–6.
- Hollins M, Alpern M. Dark adaptation and visual pigment regeneration in human cones. *J Gen Physiol* 1973;62:430–47.
- McGwin G, Jr., Jackson GR, Owsley C. Using nonlinear regression to estimate parameters of dark adaptation. *Behav Res Methods Instrum Comput* 1999;31:712–7.
- Pianta MJ, Kalloniatis M. Characterisation of dark adaptation in human cone pathways: an application of the equivalent background hypothesis. *J Physiol* 2000;528:591–608.
- Lamb TD, Pugh EN, Jr. Dark adaptation and the retinoid cycle of vision. *Prog Retin Eye Res* 2004;23:307–80.
- Mata NL, Radu RA, Clemmons RC, Travis GH. Isomerization and oxidation of vitamin a in cone-dominant retinas: a novel pathway for visual-pigment regeneration in daylight. *Neuron* 2002;36:69–80.
- Wang JS, Kefalov VJ. An alternative pathway mediates the mouse and human cone visual cycle. *Curr Biol* 2009;19:1665–9.
- Wang JS, Kefalov VJ. The cone-specific visual cycle. *Prog Retin Eye Res* 2011;30:115–28.
- Curcio CA, Sloan KR, Kalina RE, Hendrickson AE. Human photoreceptor topography. *J Comp Neurol* 1990;292:497–523.
- Klaver CC, Assink JJ, van Leeuwen R, Wolfs RC, Vingerling JR, Stijnen T, Hofman A, de Jong PT. Incidence and progression rates of age-related maculopathy: the Rotterdam Study. *Invest Ophthalmol Vis Sci* 2001;42:2237–41.
- Mitchell P, Wang JJ, Foran S, Smith W. Five-year incidence of age-related maculopathy lesions: the Blue Mountains Eye Study. *Ophthalmology* 2002;109:1092–7.
- Klein R, Klein BE, Knudson MD, Meuer SM, Swift M, Gangnon RE. Fifteen-year cumulative incidence of age-related macular degeneration: the Beaver Dam Eye Study. *Ophthalmology* 2007;114:253–62.
- Jackson GR, Edwards JG. A short-duration dark adaptation protocol for assessment of age-related maculopathy. *J Ocul Biol Dis Infor* 2008;1:7–11.

Tom H. Margrain

School of Optometry and Vision Sciences

Cardiff University

Maindy Road

Cathays, Cardiff, CF24 4LU, United Kingdom

e-mail: margrainth@cf.ac.uk

ORIGINAL ARTICLE

Aging and Cone Dark Adaptation

Allannah J. Gaffney*, Alison M. Binns†, and Tom H. Margrain†

ABSTRACT

Purpose. Following exposure to a bright light that bleaches a significant portion of photopigment, the eyes take several minutes to regain sensitivity. This slow process, known as dark adaptation, is impaired in patients with age-related macular degeneration and is an important candidate biomarker for this disease. The aim of this study was to evaluate the effect of age on cone dark adaptation.

Methods. Data were obtained from 41 healthy adults aged between 20 and 83 years. Pupils were dilated and 96% of cone photopigment was "bleached," before threshold was monitored continuously for 5 min in the dark, using a 4° diameter achromatic spot centered on the fovea. Threshold recovery data were modeled, and the time constant of cone recovery (τ), initial cone thresholds, and final cone thresholds were determined. Regression analysis was used to determine the relationship between age and cone dark adaptation parameters.

Results. Cone τ increased by 16.4 s/decade of life, indicating a progressive slowing of dark adaptation with increasing age. This change in cone τ throughout adulthood was significant ($p < 0.0005$). There was no significant relationship between increasing age and initial cone threshold ($p = 0.84$) or final cone threshold ($p = 0.82$).

Conclusions. Our results provide evidence for age-related slowing of cone dark adaptation after a full bleach in healthy adults, which is likely to contribute to visual difficulties when moving from bright to dim photopic light levels. We propose that the sensitivity and specificity of cone τ as a biomarker for early age-related macular disease could be improved by taking into account the significant age-related decline in this parameter.

(Optom Vis Sci 2012;89:1-●●●)

Key Words: aging, dark adaptation, cones, age-related macular degeneration, biomarker

Visual difficulties in low illumination are frequently reported by elderly adults in the absence of ocular pathology^{1,2} and have been identified as a cause of trips and falls in these individuals.³ Correspondingly, a reduction in both photopic and scotopic visual sensitivity with age has been demonstrated.⁴⁻⁹ This may partially be attributed to the increased optical density of the ocular media and pupillary miosis that occur with increasing age, causing a reduction in the amount of light reaching the retina.^{10,11} However, when the effects of these pre-retinal factors are controlled for, a reduction in scotopic sensitivity with increasing age is still evident.⁹ This indicates that retinal factors are also likely to contribute to diminishing visual sensitivity,^{12,13} and this may be related to the age-related reduction reported in the density of rod photoreceptors,¹³ or may be due to retinal ganglion cell loss.^{12,14}

Although reduced sensitivity to light is a well-documented feature of aging, the effect of age on the rate at which the eye can adapt

to a change in ambient illumination is less clear. Dark adaptation classically refers to the relatively slow recovery of visual threshold that occurs in the dark after exposure to a bright light that bleaches a significant portion of photopigment. Visual threshold during dark adaptation is initially mediated by the cones, and subsequently by the rods. In addition to reductions in dark-adapted retinal sensitivity,⁴⁻⁹ contemporary investigations have demonstrated an age-related decline in the rate of rod-mediated dark adaptation.¹⁵ However, data regarding the relationship between age and cone dark adaptation are sparse. Prolonged photostress or "glare recovery" with increasing age has been reported.¹⁶⁻²⁰ However, only three studies have specifically examined the changes in cone dark adaptation dynamics with increasing age.^{7,8,21} Eisner et al. found the rate of dark adaptation, measured using a two-channel Maxwellian view device, to be independent of age in 122 subjects aged between 60 and 90 years.⁸ This finding was supported by earlier work, using the Hecht-Shlaer adaptometer, in 91 male subjects aged between 40 and 83 years.⁷ In contrast, Coile and Baker demonstrated a reduction in the rate of cone dark adaptation with increasing age in a cohort of 58 subjects aged between 10 and 78 years, using a modified retinal densitometer.²¹

*BSc (Hons)

†PhD

School of Optometry and Vision Sciences, Cardiff University, Cardiff, Wales, United Kingdom (all authors).

2 Aging and Cone Dark Adaptation—Gaffney et al.

The clinical significance of dark adaptation measurement is growing because there is an emerging body of evidence to suggest that it is a sensitive biomarker for age-related macular degeneration (AMD), the leading cause of visual impairment in the developed world.^{22–31} Recent studies that have examined the diagnostic potential of cone dark adaptation in participants with early AMD reported an area under the receiver operating characteristic curve in excess of 0.90.^{29–31} When measured alongside visual functions, such as color vision,^{24,30} flicker sensitivity,^{26,30} contrast sensitivity, and photopic and scotopic thresholds,^{25,30} dark adaptation appears to be the single most sensitive marker for AMD. In addition, cone dark adaptation may be measured in <10 min, making it particularly attractive to clinicians.

In light of the limited and seemingly contradictory evidence regarding the relationship between the dynamics of cone dark adaptation and age and the potential value of cone dark adaptation as a biomarker for AMD,^{26,29–31} this study aimed to explore the effect of age on cone dark adaptation in healthy adults.

METHODS

Participants

Cone dark adaptation was recorded in 41 healthy adults aged between 20 and 83 years. The subjects provided informed written consent before participation, and all procedures adhered to the tenets of the Declaration of Helsinki. The study was approved by the South East Wales Research Ethics Committee.

Baseline examinations were completed at the start of the visit. These included patient history, visual acuity testing (Snellen), media opacity grading,³² and a binocular indirect fundus examination. All subjects included in the study had corrected visual acuity of 6/6 or better in the test eye, clear ocular media, normal retinal appearance, and no history of ocular or systemic disease known to affect visual function, such as diabetes or uncontrolled hypertension.

Apparatus and Psychophysical Methods

All stimuli were presented on a calibrated, high resolution computer monitor (Iiyama LS 902UT) driven by an 8-bit (nVIDIA GeForce 9) graphics board under software control (Matlab, Mathworks, Cambridge, UK). The luminance output of the monitor was γ -corrected^{33,34} and modified by a 1.2 log neutral density filter mounted on the screen to expose the full range of cone adaptation.

Dark adaptation was monitored using a psychophysical method, which was previously implemented by Jackson et al. (1999) using a modified Humphrey perimeter.¹⁵ The 4° white (9300K) stimulus was presented to the fovea for 200 ms, followed by a 600 ms response window, and then a randomly determined interstimulus delay of 0.9 to 2.4 s. If the subject responded to the stimulus within 600 ms, the luminance was reduced by 0.3 log units for the next presentation. Conversely, if the subject took longer than 600 ms to respond to the stimulus, or failed to respond at all, the intensity was increased by 0.1 log units for the following presentation. Threshold was recorded, approximately every 6.5 s, when the stimulus first became visible on an ascending staircase.

Experimental Procedures

Before dark adaptation, subjects were dilated with one drop of 1.0% tropicamide in each eye. After a short familiarization trial, dark adaptation was monitored in the right eye of all subjects (the left eye was occluded). Participants viewed the computer screen at a distance of 55 cm, wearing their distance refractive correction.

A Maxwellian view optical system was used to deliver a 95% “bleach” (white, 5.78 log phot.Td for 60 s) of cone photopigment³⁵ to the central 43.6° of the test eye. During light adaptation, the subject’s head position was monitored by the examiner to ensure accurate fixation. In addition, the long duration adapting light was sufficient to produce an equilibrium level of cone photopigment bleach, which meant that all individuals should have reached the same level of photopigment bleach regardless of any momentary fixation losses. On cessation of the bleach, subjects placed their chin on the rest in front of the computer screen within 3 s; the computer program commenced immediately, and dark adaptation was monitored continuously for 5 min. Subjects were instructed to fixate the center of the computer monitor, marked by an achromatic fixation cross (0.8 log cd/m²), and to indicate perception of the stimulus via the computer keyboard.

Statistical Analysis

The time constant of recovery (τ), initial cone thresholds, and final cone thresholds were determined by fitting a single exponential function (Eq. 1), on a least squares basis, to the threshold recovery data obtained from each participant, using Microsoft Excel (Redmond, WA).

$$T(t) = F + (I - F) \cdot e^{(-t/\tau)} \quad (1)$$

where T is the threshold at time t after the bleach, F is the final dark adapted threshold, I is the initial threshold immediately after the cessation of the bleach, and τ is the time constant of recovery. Linear regression was performed to assess the relationship between age and the parameters of cone dark adaptation.

RESULTS

Cone dark adaptation functions were successfully recorded from all 41 subjects. Fig. 1 shows dark adaptation data obtained from typical subjects aged 23, 45, 65, and 83 years. A general trend toward slower dark adaptation with increasing age, but relatively stable final thresholds, can be observed.

Linear regression was used to evaluate the change in the parameters of cone dark adaptation with age (Fig. 2). There was no relationship between increasing age and initial threshold ($p = 0.84$) or final threshold ($p = 0.82$). In contrast, cone τ became significantly larger with increasing age ($p < 0.0005$), confirming that cone dark adaptation becomes progressively slower with advancing age (Fig. 2C). These data suggest that approximately half of the variation in cone τ measured here may be explained by this single parameter ($R^2 = 0.50$). Cone τ increased by 16.4 s/decade of life.

DISCUSSION

The results show that cone dark adaptation kinetics become progressively slower throughout adulthood. Adults aged 20 to 30

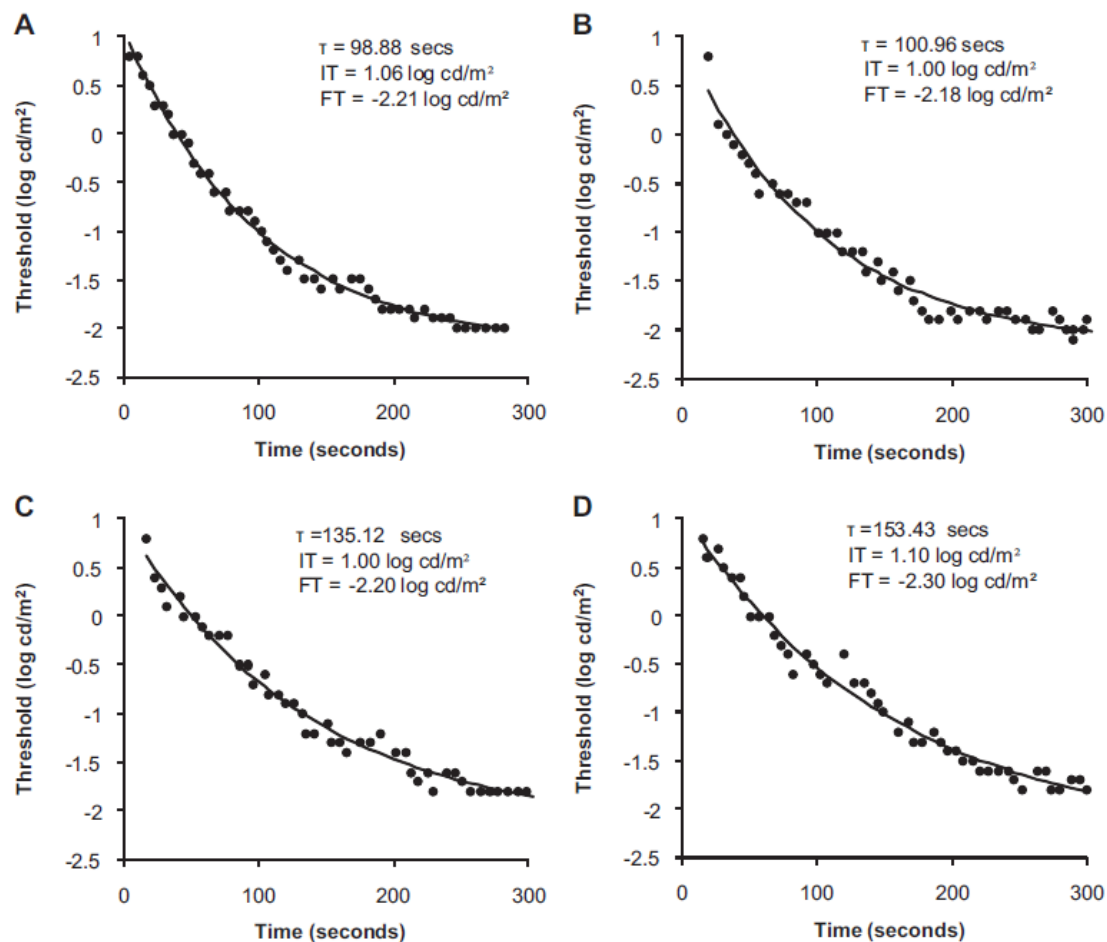


FIGURE 1.

Cone dark adaptation data for typical subjects aged 23 (A), 45 (B), 65 (C), and 83 years (D). Each plot is shown with the time constant of cone recovery (τ), initial cone threshold (I), and final cone threshold (F).

years displayed an average cone τ that was approximately half that of adults aged >70 years. This indicates that older adults require substantially more time to adjust to darkness than their younger counterparts. These findings suggest that the performance of older individuals may be impaired during routine visual tasks that take them from very bright to dim lighting.

The increase in cone τ of 16.4 s/decade of life found here agrees with the increase in cone τ of 12.6 s/decade reported by Coile and Baker.²¹ The differences between these results and those of early work, in which no association between cone dark adaptation and age was reported,^{7,8} are likely to result from methodological differences. The key methodological differences are shown in Table 1. Notably, Eisner et al. measured cone dark adaptation after exposure to a pre-adapting light of markedly lower intensity to that used by the other investigators, and this may have contributed to the variability in their Fig. 3 data.⁸ The 20,000 phot.td bleach used in that study would have bleached only about 37% of cone photopig-

ment. Although the use of a relatively modest bleach should not influence the measured exponential time constant, it does reduce the extent to which threshold is initially raised, and this may have made modeling an individual's recovery data more challenging.³⁵ In addition, the effects of low intensity pre-adapting lights on the fraction of pigment bleached are more dependent on media changes than more substantial ones. For example, early media changes that reduce the retinal illuminance by a factor of 2 from 20,000 to 10,000 phot.td would reduce the percentage of photopigment bleached from 37% to just 22%, a 15% reduction. In contrast, in this study, the same media change would have reduced the percentage of photopigment bleach from 95% to 91%, a 4% reduction. Perhaps, just as importantly, Eisner et al.⁸ only studied older adults with a limited age range. That is, of the 122 subjects studied, all but five were in their 60s and 70s. Therefore, it is possible that over the limited age range studied, any effects of age were masked by variability in the data set.

4 Aging and Cone Dark Adaptation—Gaffney et al.

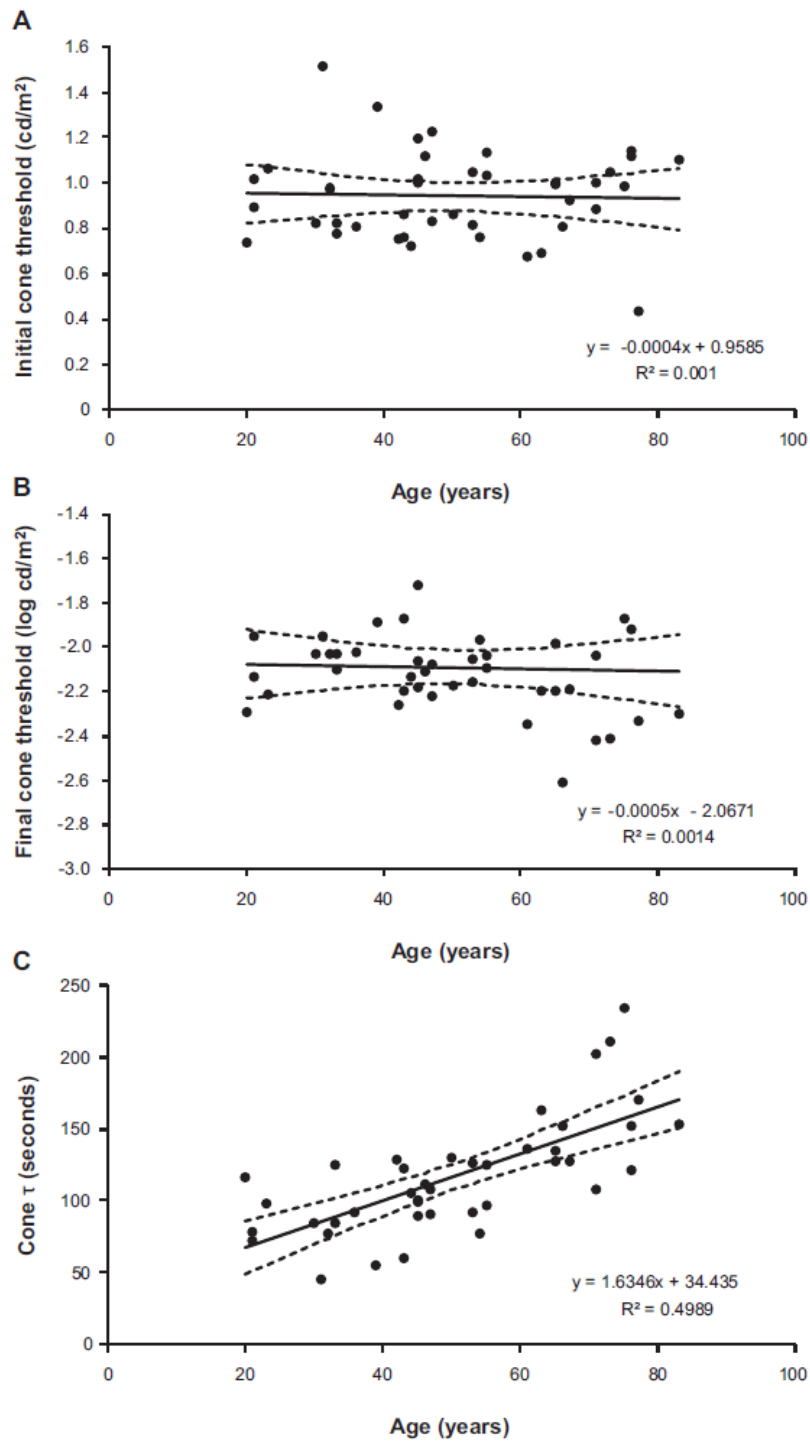


FIGURE 2.

Dark adaptation as a function of age for initial threshold (A), final threshold (B), and cone τ (C). In each case, the solid line is the regression line, and the dashed lines indicate the 95% confidence interval for the regression line. The equation for the regression line is displayed on each plot.

Optometry and Vision Science, Vol. 89, No. 8, August 2012

Copyright © American Academy of Optometry. Unauthorized reproduction of this article is prohibited.

TABLE 1.

Summary of previous studies that have examined the relationship between cone dark adaptation and age in healthy participants

Parameter	Birren and Shock (1950) ⁷	Eisner et al. (1987) ⁸	Coile and Baker (1992) ²⁰
Participants	91	122	58
Age range	40–83 years	60–90 years	10–78 years
Bleach intensity	5.5 log.Td	3.4 log.Td	5.8 log.Td
Bleach duration	3 min	3 min	1 min
Bleach λ	^a	580 nm	white
Stimulus size	3° \emptyset	3° \emptyset	1° \emptyset
Stimulus location	7.5° nasal to fixation	Fovea	Fovea
Stimulus λ	<460 nm	660 nm	589 nm
Psychophysical equipment	Hecht-Shlaer adaptometer	Two-channel Maxwellian view	Modified photon counting retinal densitometer
Psychophysical method	Method of limits	Method of limits	Method of adjustment
Threshold interval	1 min for initial 10 min and 2 mins thereafter	Variable	10 sec for initial 4 min and 1 min thereafter

^aThe information was not stated by the authors.

Although the methodology used here minimized the impact of pre-retinal factors on the results, achromatic stimuli, such as those used in this study, are generally not well suited to the study of psychophysical thresholds in older participants because of age-related media changes. However, there are several reasons why media changes cannot explain the findings reported here. First, to obtain a good view of the retina, to rule out any pathology, we chose to include only those with “clear” ocular media (grade 3 or lower, LOCS-III³²). Second, any reduction in retinal illuminance caused by media opacities would be unlikely to alter the cone dark adaptation time constant because, where “bleaches” are relatively substantial, recovery is independent of the fraction of pigment bleached. For example, Hollins and Alpern showed that 30%, 50%, 70%, and 100% cone pigment bleaches resulted in recoveries that had the same exponential time constant in one experienced observer.³⁵ Third, although age-related media changes are associated with elevated visual thresholds, the vertical translation of threshold data that may result has no effect on the “shape” of the recovery, and hence no effect on dark adaptation time constant.³⁵ Histological studies have shown that aging causes RPE cell loss and thickening of Bruch’s membrane.^{12,36} These changes might be expected to impair photopigment regeneration, and are therefore likely to contribute to delays in cone dark adaptation observed here.

There was no evidence of a relationship between age and final cone threshold within these data. This contrasts with previous work in which a modest increment in absolute cone threshold with increasing age (0.09 to 0.37 log cd/m²/decade) has been reported.^{7,8,21} However, unlike the current study, in which only participants classified as having “clear” ocular media (grade 3 or lower, LOCS-III³²) were included in the sample, these studies did not use such criteria. Consequently, the changes in visual threshold reported previously may be attributed, at least in part, to age-related changes in the density of the ocular media.¹¹ This notion is supported by Weale who showed that when cone threshold data collected from participants aged between 15 and 85 years were adjusted for age-related changes in lenticular absorption, there was no increment in cone threshold with increasing age.³⁷ Additionally, histological evidence has shown that although there is a reduc-

tion in rod photoreceptor density throughout life,¹³ foveal cone density remains relatively stable throughout life.¹³ Although retinal ganglion cell density declines with increasing age,^{12,38–42} it has been suggested that large achromatic stimuli are relatively insensitive to this age-related neuronal loss.¹⁴ Consequently, there is no histological premise for a change in cone thresholds with advancing age, using the 4° diameter white stimulus used in this study.

Knowledge about the relationship between cone dark adaptation and age is clinically important because cone τ is potentially an important biomarker for early macular disease.^{22–31} Our observation that about 50% of the variance in cone τ may be attributed to age alone ($R^2 = 0.50$) for our experimental conditions, suggests that the sensitivity and specificity of this biomarker could be improved by taking into account the significant age-related decline. To determine whether an individual’s cone τ falls within the normal reference range for their age, it should be compared with the upper 95% prediction interval for the regression line, that is, $(1.6346^{\text{age}}) + 90.41$. A cone τ that is greater than this value is therefore “outside normal limits.”

In conclusion, this study has examined the relationship between age and the time course of cone dark adaptation in healthy adults and has provided evidence in support of an age-related slowing of cone dark adaptation after a full bleach. Older adults require up to twice as long to adapt to darkness as younger adults. Investigators proposing to use cone dark adaptation as a biomarker for AMD could optimize its diagnostic potential by comparing the results from individuals with age-adjusted norms.

ACKNOWLEDGMENTS

This study was funded by a research grant from the College of Optometrists, United Kingdom. We would like to thank Bryn Jones for his help with data collection. Received November 7, 2011; accepted April 9, 2012.

REFERENCES

1. Kline DW, Kline TJ, Fozard JL, Kosnik W, Schieber F, Sekuler R. Vision, aging, and driving: the problems of older drivers. *J Gerontol* 1992;47:P27–34.

- 6 Aging and Cone Dark Adaptation—Gaffney et al.
2. McGregor LN, Chaparro A. Visual difficulties reported by low-vision and nonimpaired older adult drivers. *Hum Factors* 2005;47:469–78.
 3. McMurdo ME, Gaskell A. Dark adaptation and falls in the elderly. *Gerontology* 1991;37:221–4.
 4. Robertson GW, Yudkin J. Effect of age upon dark adaptation. *J Physiol* 1944;103:1–8.
 5. Steven DM. Relation between dark adaptation and age. *Nature* 1946;157:376.
 6. Birren JE, Bick MW, Fox C. Age changes in the light threshold of the dark adapted eye. *J Gerontol* 1948;3:267–71.
 7. Birren JE, Shock NW. Age changes in rate and level of visual dark adaptation. *J Appl Physiol* 1950;2:407–11.
 8. Eisner A, Fleming SA, Klein ML, Mauldin WM. Sensitivities in older eyes with good acuity: cross-sectional norms. *Invest Ophthalmol Vis Sci* 1987;28:1824–31.
 9. Jackson GR, Owsley C, Cordle EP, Finley CD. Aging and scotopic sensitivity. *Vision Res* 1998;38:3655–62.
 10. Birren JE, Casperson RC, Botwinick J. Age changes in pupil size. *J Gerontol* 1950;5:216–21.
 11. Bron AJ, Vrensen GF, Koretz J, Maraini G, Harding JJ. The ageing lens. *Ophthalmologica* 2000;214:86–104.
 12. Gao H, Hollyfield JG. Aging of the human retina. Differential loss of neurons and retinal pigment epithelial cells. *Invest Ophthalmol Vis Sci* 1992;33:1–17.
 13. Curcio CA, Millican CL, Allen KA, Kalina RE. Aging of the human photoreceptor mosaic: evidence for selective vulnerability of rods in central retina. *Invest Ophthalmol Vis Sci* 1993;34:3278–96.
 14. Pearson PM, Schmidt LA, Ly-Schroeder E, Swanson WH. Ganglion cell loss and age-related visual loss: a cortical pooling analysis. *Optom Vis Sci* 2006;83:444–54.
 15. Jackson GR, Owsley C, McGwin G. Aging and dark adaptation. *Vision Res* 1999;39:3975–82.
 16. Collins M. The onset of prolonged glare recovery with age. *Ophthalm Physiol Opt* 1989;9:368–71.
 17. Elliott DB, Whitaker D. Changes in macular function throughout adulthood. *Doc Ophthalmol* 1990;76:251–9.
 18. Margrain TH, Thomson D. Sources of variability in the clinical photostress test. *Ophthalm Physiol Opt* 2002;22:61–7.
 19. Newsome DA, Negreiros M. Reproducible measurement of macular light flash recovery time using a novel device can indicate the presence and worsening of macular diseases. *Curr Eye Res* 2009;34:162–70.
 20. Wood A, Margrain T, Binns A. The effect of bleach duration and age on the ERG photostress test. *Graefes Arch Clin Exp Ophthalmol* 2011;249:1359–65.
 21. Coile DC, Baker HD. Foveal dark adaptation, photopigment regeneration, and aging. *Vis Neurosci* 1992;8:27–39.
 22. Brown B, Kitchin JL. Dark adaptation and the acuity/luminance response in senile macular degeneration (SMD). *Am J Optom Physiol Opt* 1983;60:645–50.
 23. Eisner A, Fleming SA, Klein ML, Mauldin WM. Sensitivities in older eyes with good acuity: eyes whose fellow eye has exudative AMD. *Invest Ophthalmol Vis Sci* 1987;28:1832–7.
 24. Eisner A, Stoumbos VD, Klein ML, Fleming SA. Relations between fundus appearance and function. Eyes whose fellow eye has exudative age-related macular degeneration. *Invest Ophthalmol Vis Sci* 1991;32:8–20.
 25. Owsley C, Jackson GR, White M, Feist R, Edwards D. Delays in rod-mediated dark adaptation in early age-related maculopathy. *Ophthalmology* 2001;108:1196–202.
 26. Phipps JA, Guymer RH, Vingrys AJ. Loss of cone function in age-related maculopathy. *Invest Ophthalmol Vis Sci* 2003;44:2277–83.
 27. Binns AM, Margrain TH. Evaluating retinal function in age-related maculopathy with the ERG photostress test. *Invest Ophthalmol Vis Sci* 2007;48:2806–13.
 28. Owsley C, McGwin G, Jr, Jackson GR, Kallies K, Clark M. Cone- and rod-mediated dark adaptation impairment in age-related maculopathy. *Ophthalmology* 2007;114:1728–35.
 29. Dimitrov PN, Guymer RH, Zele AJ, Anderson AJ, Vingrys AJ. Measuring rod and cone dynamics in age-related maculopathy. *Invest Ophthalmol Vis Sci* 2008;49:55–65.
 30. Dimitrov PN, Robman LD, Varsamidis M, Aung KZ, Makeyeva GA, Guymer RH, Vingrys AJ. Visual function tests as potential biomarkers in age-related macular degeneration. *Invest Ophthalmol Vis Sci* 2011;52:9457–69.
 31. Gaffney AJ, Binns AM, Margrain TH. Topography of cone dark adaptation deficits in age-related maculopathy. *Optom Vis Sci* 2011;88:1080–7.
 32. Chylack LT, Jr, Wolfe JK, Singer DM, Leske MC, Bullimore MA, Bailey IL, Friend J, McCarthy D, Wu SY. The lens opacities classification system III. The longitudinal study of cataract study group. *Arch Ophthalmol* 1993;111:831–6.
 33. Metha AM, Vingrys AJ, Badcock DR. Calibration of a color monitor for visual psychophysics. *Behav Res Methods Instrum Comput* 1993;25:371–83.
 34. Brainard DH, Pelli DG, Robson T. Display characterization. In: Hornak JP, ed. *The Encyclopaedia of Imaging Science and Technology*, vol 18. New York: Wiley; 2001:172–88.
 35. Hollins M, Alpern M. Dark adaptation and visual pigment regeneration in human cones. *J Gen Physiol* 1973;62:430–47.
 36. Sarks SH. Ageing and degeneration in the macular region: a clinicopathological study. *Br J Ophthalmol* 1976;60:324–41.
 37. Weale RA. *The Senescence of Human Vision*. Oxford: Oxford University Press; 1992.
 38. Balazsi AG, Rootman J, Drance SM, Schulzer M, Douglas GR. The effect of age on the nerve fiber population of the human optic nerve. *Am J Ophthalmol* 1984;97:760–6.
 39. Johnson BM, Miao M, Sadun AA. Age-related decline of human optic nerve axon populations. *Age* 1987;10:5–9.
 40. Curcio CA, Drucker DN. Retinal ganglion cells in Alzheimer's disease and aging. *Ann Neurol* 1993;33:248–57.
 41. Harman A, Abrahams B, Moore S, Hoskins R. Neuronal density in the human retinal ganglion cell layer from 16–77 years. *Anat Rec* 2000;260:124–31.
 42. Lovasik JV, Kergoat MJ, Justino L, Kergoat H. Neuroretinal basis of visual impairment in the very elderly. *Graefes Arch Clin Exp Ophthalmol* 2003;241:48–55.

Tom H. Margrain

*School of Optometry and Vision Sciences
Cardiff University, Maindy Road
Cathays, Cardiff CF24 4LU
United Kingdom
e-mail: margrainth@cf.ac.uk*

A comparison of the parameters of objective and subjective measures of dark adaptation

Gaffney A J, Margrain T H, and Binns A M

British Society for Clinical Electrophysiology of Vision, Sheffield: September 2009

Purpose

Current methods of monitoring dark adaptation are primarily based around subjective psychophysical procedures. A comparison of the parameters of photostress recovery using psychophysical and electrophysiological techniques will demonstrate the viability of objective methods as an alternative measure of dark adaptation.

Method

Photostress recovery after a 99% bleach of rod and cone photopigment was monitored in two normal subjects (AB and AG) using two electrophysiological and one psychophysical method. All electrophysiological stimuli were generated by a light emitting diode (LED) miniature ganzfeld stimulator held at the eye. Signals were amplified, bandpass filtered (1-100Hz) and averaged using a Medelec Synergy EP system.

Full field cone flicker electroretinograms (ERGs) were recorded in response to an amber ($\lambda_{\max} = 595\text{nm}$, half-height bandwidth = 17nm) square wave flickering (41Hz) stimulus, with a time-averaged illuminance of 1500phot.td. Four pre-bleach ERGs were recorded as a baseline measure. Post-bleach ERGs were recorded every 20 secs for 5 mins, with 100 responses averaged on each trace. The amplitude of the first harmonic was plotted as a function of time after the bleach.

Full field rod ERGs were recorded in response to a blue ($\lambda_{\max} = 454\text{nm}$, half-height bandwidth = 67nm) 5scot.td.s flash, duration 5ms, at a temporal frequency of 0.5Hz. Post-bleach ERGs were recorded at 2 minute intervals for 35 mins. 30 responses were averaged on each trace and b-wave amplitude was plotted as a function of time after the bleach, after removal of high frequency noise (>45Hz).

Finally, the Goldmann-Weekers adaptometer was used to measure dark adaptation psychophysically using a method of ascending limits. The stimulus subtended 6.6° at the eye and was located at 11.8° in the inferior field.

Recovery data was fitted, using a least squares paradigm, with an exponential model and the time to half recovery assessed.

Results

An exponential model provided a good fit to the rod and cone ERG and psychophysical recovery data. The times to half recovery (given for subjects AB and AG) for photopic ERG amplitudes were 1.22 and 0.96 mins, and for scotopic ERG amplitudes were 19 and 10 mins. For the Goldmann-Weekers adaptometer, times to half recovery for the cone branch were 1.46 and 1.12 mins, and for the rod branch were 14.45 and 13.1 mins.

Conclusion

The ERG can be used as a simple objective measure of rod and cone dark adaptation. An exponential model provided a good fit to all recovery data. The times to half recovery were comparable to those obtained using a psychophysical technique. This indicates that the ERG provides a potential clinical means of assessing dark adaptation, which avoids the problems inherent in subjective psychophysical strategies.

A comparison of four psychophysical methods of monitoring dark adaptation

Gaffney A J, Binns A M, and Margrain T H

Optometry Tomorrow, York: April 2010

Purpose

Dark adaptometry has an important role in the detection of early age-related macular degeneration (AMD). However, measuring threshold with robust, criteria free, psychophysical techniques is problematic due to the speed with which threshold changes. To identify the most robust, clinically applicable technique we assessed the repeatability and agreement of four different psychophysical methods of dark adaptation measurement.

Methods

The methods used were: a) the Goldmann-Weekers adaptometer, b) a hybrid adaptive threshold procedure based on a series of decision criteria (Friedburg et al., 1998), c) a computerised 3-down 1-up modified staircase procedure (Jackson et al., 1999) and d) a novel method based on a 10-alternative forced choice procedure. With the exception of the Goldmann-Weekers method, all stimuli were presented on a calibrated, high resolution cathode ray tube (CRT) monitor (Iiyama LS902UT) driven by an 8-bit (nVIDIA Geforce9) graphics board under software control (Matlab).

Data were obtained from 31 adults on two occasions. At each visit pupils were dilated with tropicamide (1%) and 98% of cone photopigment was bleached using a Maxwellian view optical system, before threshold was monitored in the dark using one of the four techniques, chosen at random. This procedure was repeated for each of the remaining methods. A 5 minute 'wash out' period was interleaved between successive dark adaptation measurements.

Results

The time constant of recovery (τ) was determined by fitting a single exponential function, on a least squares basis, to the threshold recovery data. The methods described by Bland and Altman (1986) were used to establish the repeatability and agreement of the methods. For all subjects and methods, the time constant of recovery ranged from 25 to 86 seconds. The coefficient of repeatability was typically 39 seconds but varied between methods.

Conclusions

All four techniques were clinically viable and capable of following the rapid changes in threshold observed during cone dark adaptation. We identify the most repeatable, clinically applicable method and highlight the ability of a novel 10-alternative forced choice technique that can measure dark adaptation whilst avoiding the potentially distorting effects of subjective ‘criteria’.

The topography of cone-mediated dark adaptation deficits in age-related maculopathy

Gaffney A J, Binns A M, and Margrain T H

Optometry Tomorrow, Liverpool: March 2011; and ARVO annual meeting, Fort Lauderdale: May 2011

Purpose

Despite widespread agreement that dark adaptation is abnormal in age-related maculopathy (ARM), the optimal retinal location for detection of this deficit is unclear. The purpose of this study was to evaluate the effect of retinal location on the diagnostic potential of cone dark adaptation parameters. The time to the rod-cone-break (RCB) was also assessed as an indicator of rod adaptation kinetics.

Methods

Cone dark adaptation was monitored in 10 subjects with ARM and 10 age-matched controls, using four achromatic annuli (1, 4, 14 and 24° diameter) centred on the fovea.

Following pupil dilation (tropicamide 1%), 80% of cone photopigment was bleached using a Maxwellian view optical system. Subsequently, threshold was monitored in the dark, using one of the stimuli, selected at random, until the RCB occurred, or for a maximum of 25 minutes. This procedure was repeated for each of the four stimuli. A 15 minute 'wash out' period was interleaved between successive trials.

Threshold recovery data were modelled and the time constant of cone recovery (τ), final cone threshold and time to RCB determined. Diagnostic potential was evaluated by constructing receiver operating characteristic (ROC) curves for these parameters.

Results

Cone τ was significantly longer for the ARM group at 2, 7 and 12°. The greatest difference between groups was observed at 12° from fixation. At this location, the mean τ was 3.49 (+/-2.02) and 0.64 (+/-0.38) minutes for ARM and control subjects respectively ($p=0.002$) and time to RCB was 17.68 (+/-5.37) minutes for ARM subjects and 9.05 (+/-2.11) minutes for control subjects ($p=0.001$). Correspondingly, ROC curves showed that the

diagnostic potential of dark adaptometry is greatest for stimuli presented 12° from fixation; for cone τ the area under the curve (AUC)=0.99+/-0.02 and for time to RCB AUC=0.96+/-0.04.

Conclusions

This study has shown cone-mediated dark adaptation to be significantly impaired in ARM. The diagnostic potential of dark adaptation may be enhanced by measuring thresholds at an eccentricity of 12°. The observation that cone τ is highly diagnostic at this eccentricity is clinically significant, because this parameter may be quantified in as little as 10 minutes.

A comparison of psychophysical & electrophysiological methods for assessment of cone dark adaptation in ARM

Gaffney A J, Margrain T H, and Binns A M

Optometry Tomorrow, Brighton: March 2012; and ARVO annual meeting, Fort Lauderdale, Florida: May 2012

Purpose

Dark adaptation is an important clinical tool for the diagnosis of age-related maculopathy (ARM). Cone dark adaptation is particularly attractive because it can identify people with ARM in a relatively short recording period. We compared the diagnostic potential of established electrophysiological & psychophysical techniques for measuring cone dark adaptation in ARM.

Methods

Cone dark adaptation was measured in 10 subjects with ARM & 10 age-matched controls on two days. Prior to dark adaptation, subjects' pupils were dilated (1.0% tropicamide) & an 84% cone photopigment bleach (5.20 log phot.td for 120secs) administered to the test eye.

At the first visit, threshold was monitored continuously for 30mins using an automated psychophysical method of limits. The stimulus was a 12° diameter achromatic annulus, centred on the fovea.

At the second visit, cone dark adaptation was assessed using the focal cone electroretinogram (ERG) photostress test. Focal cone ERGs were recorded using a central 20° diameter, amber ($\lambda_{\max} = 595\text{nm}$, half-height bandwidth = 17nm), square wave 41Hz stimulus, with a time-averaged illuminance of 1500 phot.td). Eight pre-bleach ERGs were recorded as a baseline. Post-bleach ERGs were recorded every 20secs for 5mins.

Recovery data (psychophysical thresholds & first harmonic of ERG responses) were plotted as a function of time after the bleach & modelled using an exponential function. Receiver operating characteristic (ROC) curves were used to compare the diagnostic potential of the time constant of cone recovery (τ).

Results

Cone τ was significantly longer in the ARM group for psychophysical & electrophysiological ($p < 0.02$) methods. Both techniques were highly diagnostic for ARM: area under the curve (AUC) = 0.80 +/- 0.11 for the psychophysical test & 0.72 +/- 0.14 for the focal cone ERG photostress test. There was no statistically significant difference in the AUC of the two techniques.

Conclusions

Consistent with previous reports, cone dark adaptation was significantly impaired in ARM. Although electrophysiological methods are more objective than psychophysical methods of dark adaptation measurement, the diagnostic potential of cone dark adaptation in ARM was similar for both methods. There is now an urgent need for longitudinal studies to clarify the value of dark adaptation as a biomarker for ARM.